frontiers | Research Topics

Frontiers in astronomy and space sciences: a decade of discovery and advancement - 10th anniversary conference

Edited by
Julio Navarro, Alberto Fairén, Joseph E. Borovsky, Cristina Puzzarini, Didier Fraix-Burnet, Miriam Rengel, Paola Marziani and Steve B. Howell

Published in
Frontiers in Astronomy and Space Sciences

FRONTIERS EBOOK COPYRIGHT STATEMENT

The copyright in the text of individual articles in this ebook is the property of their respective authors or their respective institutions or funders. The copyright in graphics and images within each article may be subject to copyright of other parties. In both cases this is subject to a license granted to Frontiers.

The compilation of articles constituting this ebook is the property of Frontiers.

Each article within this ebook, and the ebook itself, are published under the most recent version of the Creative Commons CC-BY licence. The version current at the date of publication of this ebook is CC-BY 4.0. If the CC-BY licence is updated, the licence granted by Frontiers is automatically updated to the new version.

When exercising any right under the CC-BY licence, Frontiers must be attributed as the original publisher of the article or ebook, as applicable.

Authors have the responsibility of ensuring that any graphics or other materials which are the property of others may be included in the CC-BY licence, but this should be checked before relying on the CC-BY licence to reproduce those materials. Any copyright notices relating to those materials must be complied with.

Copyright and source acknowledgement notices may not be removed and must be displayed in any copy, derivative work or partial copy which includes the elements in question.

All copyright, and all rights therein, are protected by national and international copyright laws. The above represents a summary only. For further information please read Frontiers' Conditions for Website Use and Copyright Statement, and the applicable CC-BY licence.

ISSN 1664-8714
ISBN 978-2-8325-6259-8
DOI 10.3389/978-2-8325-6259-8

About Frontiers

Frontiers is more than just an open access publisher of scholarly articles: it is a pioneering approach to the world of academia, radically improving the way scholarly research is managed. The grand vision of Frontiers is a world where all people have an equal opportunity to seek, share and generate knowledge. Frontiers provides immediate and permanent online open access to all its publications, but this alone is not enough to realize our grand goals.

Frontiers journal series

The Frontiers journal series is a multi-tier and interdisciplinary set of open-access, online journals, promising a paradigm shift from the current review, selection and dissemination processes in academic publishing. All Frontiers journals are driven by researchers for researchers; therefore, they constitute a service to the scholarly community. At the same time, the *Frontiers journal series* operates on a revolutionary invention, the tiered publishing system, initially addressing specific communities of scholars, and gradually climbing up to broader public understanding, thus serving the interests of the lay society, too.

Dedication to quality

Each Frontiers article is a landmark of the highest quality, thanks to genuinely collaborative interactions between authors and review editors, who include some of the world's best academicians. Research must be certified by peers before entering a stream of knowledge that may eventually reach the public - and shape society; therefore, Frontiers only applies the most rigorous and unbiased reviews. Frontiers revolutionizes research publishing by freely delivering the most outstanding research, evaluated with no bias from both the academic and social point of view. By applying the most advanced information technologies, Frontiers is catapulting scholarly publishing into a new generation.

What are Frontiers Research Topics?

Frontiers Research Topics are very popular trademarks of the *Frontiers journals series*: they are collections of at least ten articles, all centered on a particular subject. With their unique mix of varied contributions from Original Research to Review Articles, Frontiers Research Topics unify the most influential researchers, the latest key findings and historical advances in a hot research area.

Find out more on how to host your own Frontiers Research Topic or contribute to one as an author by contacting the Frontiers editorial office: frontiersin.org/about/contact

Frontiers in astronomy and space sciences: a decade of discovery and advancement - 10th anniversary conference

Topic editors

Julio Navarro — University of Victoria, Canada
Alberto Fairén — Center for Astrobiology (CAB), CSIC-INTA, Spain
Joseph E. Borovsky — Space Science Institute (SSI), United States
Cristina Puzzarini — University of Bologna, Italy
Didier Fraix-Burnet — UMR5274 Institut de Planétologie et d'Astrophysique de Grenoble (IPAG), France
Miriam Rengel — Max Planck Institute for Solar System Research, Germany
Paola Marziani — Osservatorio Astronomico di Padova (INAF), Italy
Steve B. Howell — Ames Research Center, National Aeronautics and Space Administration, United States

Citation

Navarro, J., Fairén, A., Borovsky, J. E., Puzzarini, C., Fraix-Burnet, D., Rengel, M., Marziani, P., Howell, S. B., eds. (2025). *Frontiers in astronomy and space sciences: a decade of discovery and advancement - 10th anniversary conference*. Lausanne: Frontiers Media SA. doi: 10.3389/978-2-8325-6259-8

Table of contents

frontiers | Frontiers in Astronomy and Space Sciences

TYPE Editorial
PUBLISHED 08 April 2025
DOI 10.3389/fspas.2025.1599964

Check for updates

OPEN ACCESS

EDITED AND REVIEWED BY
Scott William McIntosh,
Lynker Technologies LLC, United States

*CORRESPONDENCE
Julio Navarro,
jfn@uvic.ca

RECEIVED 25 March 2025
ACCEPTED 31 March 2025
PUBLISHED 08 April 2025

CITATION
Navarro J, Fairén AG, Fraix-Burnet D, Howell SB, Marziani P, Puzzarini C and Rengel M (2025) Editorial: Frontiers in astronomy and space sciences: a decade of discovery and advancement-10th anniversary conference.
Front. Astron. Space Sci. 12:1599964.
doi: 10.3389/fspas.2025.1599964

COPYRIGHT
© 2025 Navarro, Fairén, Fraix-Burnet, Howell, Marziani, Puzzarini and Rengel. This is an open-access article distributed under the terms of the Creative Commons Attribution License (CC BY). The use, distribution or reproduction in other forums is permitted, provided the original author(s) and the copyright owner(s) are credited and that the original publication in this journal is cited, in accordance with accepted academic practice. No use, distribution or reproduction is permitted which does not comply with these terms.

Editorial: Frontiers in astronomy and space sciences: a decade of discovery and advancement-10th anniversary conference

Julio Navarro[1]*, Alberto G. Fairén[2,3], Didier Fraix-Burnet[4], Steve B. Howell[5], Paola Marziani[6], Cristina Puzzarini[7] and Miriam Rengel[8]

[1]Department of Physics and Astronomy, University of Victoria, Victoria, BC, Canada, [2]Centro de Astrobiología (CAB), CSIC-INTA, Madrid, Spain, [3]Department of Astronomy, Cornell University, Ithaca, NY, United States, [4]CNRS, IPAG, University Grenoble Alpes, Grenoble, France, [5]NASA Ames Research Center, Moffett Field, CA, United States, [6]INAF, Astronomical Observatory of Padova, Padova, Italy, [7]ROT&Comp Lab, Department of Chemistry "Giacomo Ciamician", University of Bologna, Bologna, Italy, [8]Max-Planck-Institut für Sonnensystemforschung, Göttingen, Germany

KEYWORDS

astrobiology, astrochemistry, astronomical instrumentation, astrostatistics, cosmology, exoplanets, extragalactic astronomy, planetary science

Editorial on the Research Topic
Frontiers in astronomy and space sciences: a decade of discovery and advancement-10th anniversary conference

The Research Topic you are reading highlights the breadth and cross disciplinary nature of Astronomy and Space Physics. The papers contained here feature research efforts spanning the wide range of research topics covered by this Journal, from our Solar System to Relativity theory, and even to ourselves as scientists. Close to home, new research on space weathering and its relation to rubble pile asteroids, geomagnetic storms, and Saturn's magnetosphere is brought into view. Looking outward, the role of dust throughout the universe is examined and related to the current results contributed by the James Webb Space Telescope. Active galaxies are discussed in two contexts; one regarding the modeling of reflections produced by spinning supermassive black holes, the other about how the quasar main sequence is revealed. Relativity is also scrutinized, as the constancy of the speed of light is examined over cosmic time. Finally, we come back home and take a look at the topic of equity in our science practices.

Danehkar's contribution "Relativistic Reflection Modeling in AGN and Related Variability from PCA: A Brief Review" provides a comprehensive yet concise overview and a handy reference of how relativistic reflection signatures—such as broadened iron Kα emission lines and Compton reflection humps—are shaped by the strong gravitational fields of spinning supermassive black holes. One of the most remarkable aspects of this work is the application of principal component analysis (PCA) to analyze X-ray variability in AGNs, which has provided significant insights into the separation of spectral components contributing to the observed variability. The discussion on PCA results from several AGN

X-ray spectra shows that the relativistic reflection component remains nearly constant while the power-law continuum varies significantly, reinforcing the idea that reflection originates from stable inner accretion flows near the event horizon. The review by Danehkar also offers an excellent synthesis of recent developments in relativistic disk models, covering spectral fitting techniques that incorporate the Kerr metric to extract black hole spin parameters.

The Panda mini-review provides a comprehensive synthesis of three decades of research on the quasar main sequence (MS). By drawing an analogy with the Hertzsprung-Russell diagram for stars, the paper presents how the Eigenvector 1 scheme has revolutionized our understanding of the diverse population of Type-1 AGNs, linking key spectral properties such as the full width at half-maximum (FWHM) of the Hβ emission line and the strength of Fe II emission to physical parameters such as Eddington ratio and black hole mass. The author not only revisits the foundational work of Boroson and Green (1992) and Sulentic et al. (2000), but also contextualizes large spectroscopic surveys, such as the Sloan Digital Sky Survey (SDSS), and multi-epoch spectroscopic studies of changing-look AGNs through the MS. The discussion on quasars as potential standard candles for cosmology is particularly thought-provoking, as it underscores the role of MS in refining the radius-luminosity relation and its implications for high-redshift distance measurements. Overall, this paper stands out as a must-read for anyone interested in the physics of AGNs.

The astrochemistry contribution "Nanosilicates and molecular silicate dust species: properties and observational prospects" of Bromley to this Research Topic highlights the importance of molecular silicates and nanosilicates in the formation and processing of larger silicate dust grains. Nucleation processes and growth of silicate dust grains in circumstellar environments are reviewed. When fully formed, silicate grains (~0.1 μm diameter) enter the interstellar medium (ISM), where they are expected to play an important role from both physical and chemical points of view. Then, supernova shockwaves, through collision-induced shattering, redistribute a significant proportion of the silicate dust mass into a huge number of nanosilicates. In this paper, their properties have been reviewed with a particular focus on insights arising from bottom-up atomistic computational modeling, also reviewing the energetic and chemical processing of silicate dust. Attention has also been paid to the unique potential of this modeling in predicting spectral features of nanosilicates that may be detectable using the James Webb Space Telescope. Figure 1 of Bromley provides a good example in this regard, as it shows the structural evolution from molecular silicates containing ~10 atoms (< 1 nm diameter) to small nanosilicates containing hundreds of atoms (~1 nm diameter) and then to systems of thousands of atoms (~3 nm diameter). The representative structures of these silicate species are accompanied by their calculated absorption infrared spectra and microwave emission spectra. To conclude, the contribution of Bromley suggests that the combination of computational modeling and observational data will enable confirmation of the presence of nanosilicates and the assessment of their abundance in the ISM and other astrophysical environments.

The planetary science contribution "Evaluation of simulated space weathering based meteorite alteration and potential influence on mechanical deformation of rubble pile asteroids" by Kereszturi et al to this Research Topic investigates the effects of space weathering on meteorites and the implications of radiation-induced changes in the mineral composition and structure of small rubble-pile asteroids. The authors discuss much of what we know about the infrared spectral characteristics of meteorites induced by laboratory-based artificial irradiation simulating space weathering. Through laboratory simulations of solar wind exposure, the study reveals key mineralogical changes, such as decreasing magnesium content in olivine, water loss-induced mineral transformations, and lattice amorphization. These surface alterations, though limited to a thin layer of asteroid grains, may influence the mechanical behavior of small asteroids by affecting grain migration, surface mixing, and granular cohesion, potentially modulated by the Yarkovsky–O'Keefe–Radzievskii–Paddack (YORP) effect. Understanding the influence of space weathering on the internal properties and joint behavior of grain within rubble pile asteroids, how we have acquired information about it, and its relevance to assessing the mechanical behavior of debris asteroids, is of paramount importance for the future of Planetary Science, with significant implications in planetary defense.

Wing et al reviews an intriguing topic in our understanding of the Saturnian magnetosphere, namely, the radially inward transport of plasma, or plasma injections. This contribution highlights the role played by plasma originating from one of Saturn's moons (Enceladus), and by Saturn's rapid rotation, with an emphasis on how effective gravity and flux tube entropy affect Saturnian plasma injections.

Closer to home, Khabarova and Price report on space weather forecasts of geomagnetic storms, a central research topic of solar-terrestrial studies. These forecasts are important, as even storms of moderate intensity can lead to power outages as severe as those caused by extreme storms. This publication reviews geomagnetic storm statistics and discusses recent advances in storm prediction.

At the other end of the scale, Lee scrutinizes the role that the assumption of a constant speed of light plays in our current paradigm for structure formation in the Universe, the ΛCDM model. It makes the intriguing case that models where the speed of light varies with cosmic time, such as the "minimally extended varying speed of light model" (or meVSL), are also consistent with current data, so it will be up to future observations to come up with tests that could probe one of the basic tenets of our cosmological understanding.

Finally, Liemohn examines steps that may be taken to mitigate issues of inequity, inclusion, and lack of diversity in Space Physics. In particular, this contribution highlights key advice and practical actions, as compiled in a recent Research Topic. Although some are specific to Space Physics, other recommendations are likely to prove useful to other scientific communities dealing with similar issues.

Author contributions

JN: Writing – original draft, Writing – review and editing. AF: Writing – review and editing. DF-B: Writing – review and editing. SH: Writing – review and editing. PM: Writing – review and editing. CP: Writing – review and editing. MR: Writing – review and editing.

Funding

The author(s) declare that no financial support was received for the research and/or publication of this article.

Acknowledgments

The Editors wish to thank all the authors and reviewers of the papers submitted to this Research Topic for their time, their careful work and their patience. The authors appreciate the assistance of the staff in the Frontiers Editorial Office.

Conflict of interest

The authors declare that the research was conducted in the absence of any commercial or financial relationships that could be construed as a potential conflict of interest.

The author(s) declared that they were an editorial board member of Frontiers, at the time of submission. This had no impact on the peer review process and the final decision.

Generative AI statement

The authors declare that no Generative AI was used in the creation of this manuscript.

Publisher's note

All claims expressed in this article are solely those of the authors and do not necessarily represent those of their affiliated organizations, or those of the publisher, the editors and the reviewers. Any product that may be evaluated in this article, or claim that may be made by its manufacturer, is not guaranteed or endorsed by the publisher.

References

Boroson, T. A., and Green, R. F. (1992). The emission-line properties of low-redshift quasi-stellar objects. *Astrophysical J. Suppl. Ser.* 80, 109. doi:10.1086/191661

Sulentic, J. W., Marziani, P., and Dultzin-Hacyan, D. (2000). Phenomenology of broad emission lines in active galactic nuclei. *Annu. Rev. Astronomy Astrophysics* 38, 521–571. doi:10.1146/annurev.astro.38.1.521

frontiers | Frontiers in Astronomy and Space Sciences

TYPE Mini Review
PUBLISHED 02 August 2024
DOI 10.3389/fspas.2024.1453806

Check for updates

OPEN ACCESS

EDITED BY
Julio Navarro,
University of Victoria, Canada

REVIEWED BY
Elmo Benedetto,
University of Salerno, Italy

*CORRESPONDENCE
Seokcheon Lee,
skylee@skku.edu

RECEIVED 24 June 2024
ACCEPTED 09 July 2024
PUBLISHED 02 August 2024

CITATION
Lee S (2024), Constraining the minimally extended varying speed of light model using time dilations.
Front. Astron. Space Sci. 11:1453806.
doi: 10.3389/fspas.2024.1453806

COPYRIGHT
© 2024 Lee. This is an open-access article distributed under the terms of the Creative Commons Attribution License (CC BY). The use, distribution or reproduction in other forums is permitted, provided the original author(s) and the copyright owner(s) are credited and that the original publication in this journal is cited, in accordance with accepted academic practice. No use, distribution or reproduction is permitted which does not comply with these terms.

Constraining the minimally extended varying speed of light model using time dilations

Seokcheon Lee*

Department of Physics, Institute of Basic Science, Sungkyunkwan University, Suwon, Republic of Korea

The Robertson–Walker (RW) metric, derived from the cosmological principle and Weyl's postulate, characterizes the ΛCDM cosmological model. Traditionally, in this framework, the assumption of a constant speed of light leads to specific cosmological time dilation (TD). However, because the Robertson–Walker metric lacks a way to define time dilation, the speed of light, like wavelength and temperature, may vary with cosmic time. The minimally extended varying speed of light (meVSL) model fits standard cosmological observations while considering the evolution of physical constants. One model-independent test for the meVSL model is cosmological time dilation. However, current data cannot distinguish between the meVSL model and the standard model.

KEYWORDS

varying speed of light, cosmological time dilation, supernovae, cosmological redshift, standard model cosmology

1 Introduction

The contemporary ΛCDM model, based on the Robertson–Walker (RW) metric, assumes large-scale spatial homogeneity and isotropy, supported by the uniformity of the cosmic microwave background (CMB) (Hinshaw et al., 2013; Aghanim et al., 2020) and large-scale structures (Guzzo et al.; Cawthon et al., 2022). This model describes an expanding universe, evidenced by the redshift of light from distant galaxies, where the redshift indicates the stretching of photon wavelengths due to space expansion (Weinberg, 2008).

The traditional RW metric can derive a specific relationship regarding cosmological time dilation (TD) based on the postulate of a constant speed of light. However, it is not directly derived from the metric's fundamental principles. Various projects using supernova light curves (Leibundgut et al., 1996; Riess et al., 1997; Foley et al., 2005; Blondin and Tonry, 2007; Blondin et al., 2008; White et al.), gamma-ray bursts (Band, 1994; Norris et al., 1994; Wijers and Paczynski, 1994; Meszaros and Meszaros, 1996; Lee and Petrosian, 1997; Chang, 2001; Crawford; Zhang et al., 2013; Singh and Desai, 2022), and quasars (Hawkins, 2001; Dai et al., 2012; Lewis and Brewer, 2023) have attempted to measure cosmological TD, but conflicting results have prevented convincing detection. The speed of light in the RW metric might change with cosmic time without clear rules determining TD, just like other physical parameters like temperature and mass density. This variation supports the hypothesis of a varying speed of light (VSL) (Lee, 2021; Lee, 2023a; Lee, 2023b; Lee, 2024). In the RW universe, a hypersurface of specific time defines uniform physical quantities such as temperature or density, and these quantities are cosmologically redshifted due to the universe's expansion.

One can rewrite the RW metric with the possibility of the VSL as follows:

$$\begin{aligned} ds^2 &= -c(t)^2 dt^2 + a(t)^2 \frac{dr^2}{1-Kr^2} + r^2 d\theta^2 + \sin^2\theta d\phi^2 \\ &\equiv -c(t)^2\, dt^2 + a(t)^2 dl_{3D}^2. \end{aligned} \tag{1}$$

Physical quantities like the scale factor $a(t)$, density $\rho(t)$, pressure $P(t)$, temperature $T(t)$, and $c(t)$ evolve over cosmic time, governed by solutions from Einstein's field equations and Bianchi's identity, accounting for fluid equations of state. Redshift calculation involves using the geodesic equation in co-moving coordinates, ensuring the consistency of radial light signals dl_{3D}:

$$\begin{aligned} dl_{3D} = \frac{c(t_i)\,dt_i}{a(t_i)} \quad &: \quad \frac{c_1 dt_1}{a_1} \\ = \frac{c_2 dt_2}{a_2} \Rightarrow &\begin{cases} c_1 = c_2 = c & \text{if} \quad \dfrac{dt_1}{a_1} = \dfrac{dt_2}{a_2} \quad \text{SMC} \\ c_1 = \left(\dfrac{a_1}{a_2}\right)^{\frac{b}{4}} c_2 & \text{if} \quad \dfrac{dt_1}{a_1^{1-\frac{b}{4}}} = \dfrac{dt_2}{a_2^{1-\frac{b}{4}}} \quad \text{meVSL} \end{cases}, \end{aligned} \tag{2}$$

where SMC stands for the standard model cosmology and $dt_i = 1/\nu(t_i)$ represents the time interval between successive crests of light at t_i (i.e., the inverse of the frequency ν_i at t_i). This expresses the TD in the meVSL model as $T_0 = (1+z)^{1-b/4}T$ (i.e., the present time is dilated by a factor $(1+z)^{1-b/4}$).

2 Methods

In an expanding universe described by the RW metric, galaxies uniformly recede from each other, and TD affects clocks differently depending on the distance. Whether the speed of light is constant or not influences local clock rates, thus playing a crucial role in understanding TD. Therefore, it is important to obtain the precise relationship of TD by comparing observational data such as distant Type Ia supernovae (SNeIa) light curves and spectral evolution.

Supernova light curves (LCs) track brightness changes over time, crucial for understanding their evolution and properties, especially for SNeIa used as cosmological standard candles. Comparing LCs across different distances reveals TD effects due to cosmic expansion, indicating the stretching of distant LCs compared to nearby LCs. The spectral evolution of SNeIa provides a reliable method to measure aging and confirm TD, offering insights into the Universe's expansion rate and dark energy dynamics.

We present aging rate measurements of 13 high-redshift SNeIa data provided in Blondin et al. (2008), as shown in Table 1. These data are derived from a sample of 35 spectra of 13 SNeIa in the redshift range $0.28 \le z \le 0.62$, comparing the differences between observer- and rest-frame ages.

We perform a least-square fit to the data using the SMC and meVSL model predictions. The fitting is given by

$$\chi^2 = \sum_{i=1}^{13} \frac{\left((1+z_i)^{-1}_{\rm obs} - (1+z_i)^{-1+b/4}\right)^2}{\sigma_i^2}, \tag{3}$$

TABLE 1 Aging rate measurements from SNeIa observation (Blondin et al., 2008).

SN	z	$1/(1+z)$	Aging rate (error)
1996bj	0.574	0.635	0.527 (0.369)
1997ex	0.361	0.735	0.745 (0.076)
2001go	0.552	0.644	0.652 (0.062)
2002iz	0.427	0.701	0.655 (0.089)
b027	0.315	0.760	0.823 (0.092)
2003js	0.363	0.734	0.718 (0.082)
04D2an	0.621	0.617	0.567 (0.341)
2006mk	0.475	0.678	0.753 (0.060)
2006sc	0.357	0.737	0.619 (0.121)
2006tk	0.312	0.762	0.835 (0.181)
2007tg	0.502	0.666	0.687 (0.102)
2007tt	0.374	0.728	0.718 (0.108)
2007un	0.283	0.779	0.759 (0.135)

TABLE 2 A simple χ^2 analysis for both the SM and meVSL model using TD data (Blondin et al., 2008). The best-fit value for the b exponent is $b = 0.198$ with 0.415 for the 1-σ confidence interval.

Model	χ^2/dof	$\bar{b}$	1-σ	GoF (%)
$(1+z)^{-1}$	3.6/13	0	0	99.5
$(1+z)^{-1+b/4}$	3.4/12	0.198	0.415	99.2

where $(1+z_i)^{-1}_{\rm obs}$ corresponds to the 13 data points and σ_i represents their errors, as listed in Table 1.

3 Results

The aging rate analysis based on the SMC, using $1/(1+z)$, achieves a good fit to the data with $\chi^2 = 3.6$ for 13 degrees of freedom (d.o.f), indicating a high goodness-of-fit (GoF) of 99.5%. Conversely, applying the meVSL model yields a best-fit parameter value of $b = 0.198$ with a 1-σ error interval of ± 0.415. The minimum χ^2 value obtained is 3.4, with 12 d.o.f, corresponding to a GoF of 99.3%. Detailed results are summarized in Table 2 and illustrated in Figure 1, where vertical lines represent the 13 data points along with their measurement errors. The dashed line illustrates the SMC prediction of the aging rate $1/(1+z)$, while the solid line with shaded regions depicts the meVSL model within its 1-σ confidence interval. These findings suggest that the current observational data do not conclusively distinguish between the predictions of the meVSL model and those of the SMC.

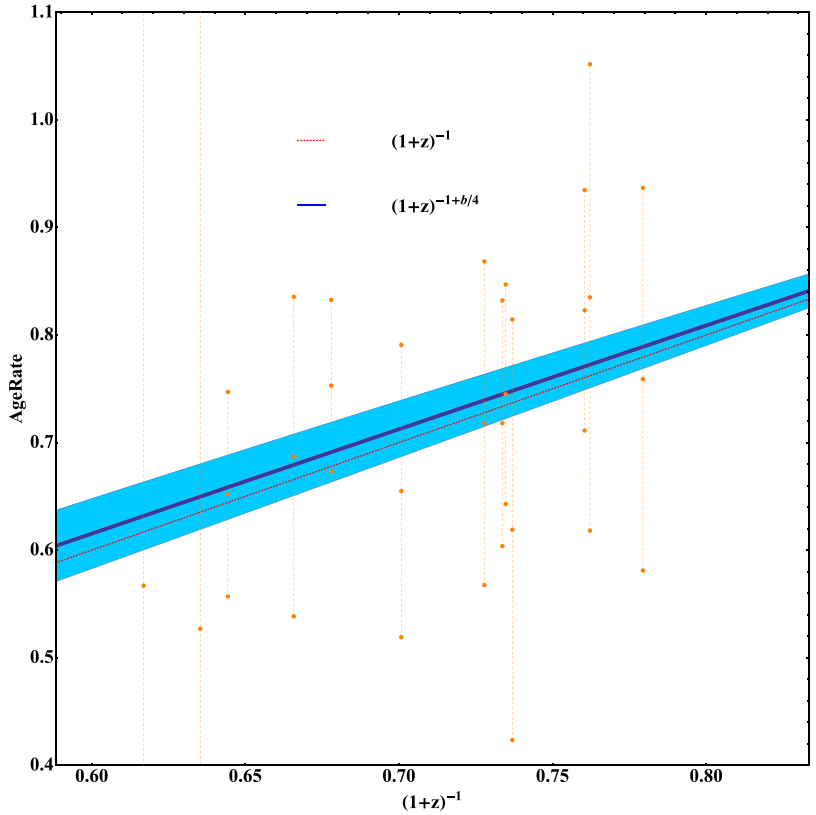

FIGURE 1
Time dilation for two models with data points. The dashed line depicts the SC prediction of TD. The thick solid line represents the best-fit value predicted TD of the meVSL model. The shaded region represents the 1-σ confidence interval region.

4 Discussion

We derived the time dilation formula in the minimally extended varying speed of light model as $T(z) = T_0(1+z)^{1-b/4}$. Analyzing data from 13 high-redshift SNeIa, we found $b = 0.198 \pm 0.415$ at the 1-σ confidence level, less precise than cosmological chronometers (Lee, 2023c). Using (H_0, Ω_{m0}) values from Planck18 (Aghanim et al., 2020) and Pantheon22 (Brout et al., 2022), we obtained optimal b fits of -0.105 ± 0.178 and 0.584 ± 0.184, respectively. These results align with the standard model cosmology and the meVSL model, reflecting data from SNe where distinguishing between models remains inconclusive. Recent Dark Energy Survey results also support the standard model of cosmology (White et al.). Time dilation data from gamma-ray bursts are sparse (Singh and Desai, 2022), but a study of 190 quasars confirmed cosmic time dilation (Lewis and Brewer, 2023), detecting redshift-dependent effects with $n \equiv (1 - b/4) = 1.28^{+0.28}_{-0.29}$. Challenges in previous quasar studies highlight the need for larger, diverse samples to detect time dilation effects across various redshifts. Future observations may clarify model distinctions as data accrues. A study exploring an Einstein–de Sitter cosmological model that generalizes the redshift-time dilation relation demonstrates that this model can fit the data from 1,048 supernovae comparably to the standard model (Benedetto et al., 2024). The authors propose this intriguing formalism as an alternative to the standard cosmological model without the need for dark energy. This study appears to be another interesting research using time dilation.

Author contributions

SL: conceptualization, data curation, formal analysis, funding acquisition, investigation, methodology, project administration, resources, validation, visualization, writing–original draft, and writing–review and editing.

Funding

The author(s) declare that financial support was received for the research, authorship, and/or publication of this article. This research was funded by the National Research Foundation of Korea (NRF), funded both by the Ministry of Science, ICT, and Future Planning (grant no. NRF-2019R1A6A1A10073079) and the Ministry of Education (grant no. NRF-RS202300243411).

Acknowledgments

The author is grateful for the invitation to present at the ‘Frontiers in Astronomy and Space Sciences: A Decade of Discovery and Advancement, 10th Anniversary Conference’. Additionally, the

author would like to express his gratitude to the editor, who requested a mini-review related to this presentation.

Conflict of interest

The author declares that the research was conducted in the absence of any commercial or financial relationships that could be construed as a potential conflict of interest.

Publisher's note

All claims expressed in this article are solely those of the authors and do not necessarily represent those of their affiliated organizations, or those of the publisher, the editors, and the reviewers. Any product that may be evaluated in this article, or claim that may be made by its manufacturer, is not guaranteed or endorsed by the publisher.

References

Aghanim, N., Akrami, Y., Arroja, F., Ashdown, M., Aumont, J., Baccigalupi, C., et al. (2020). *Planck*2018 results: I. Overview and the cosmological legacy of*Planck*. *Astron. Astrophys.* 641, A1. arXiv:1807.06205 [astro-ph.CO]]. doi:10.1051/0004-6361/201833880

Band, D. (1994). *Astrophys. J. Lett.* 432, L23. [astro-ph]. doi:10.1086/187502

Benedetto, E., D'Errico, L., and Feoli, A. (2024). An evolution of the universe based on a modified time-redshift relation can avoid the introduction of a cosmological constant. *Astrophys. Space Sci.* 369 (4), 37. doi:10.1007/s10509-024-04301-x

Blondin, S., Davis, T. M., Krisciunas, K., Schmidt, B. P., Sollerman, J., Wood-Vasey, W. M., et al. (2008). Time dilation in Type Ia supernova spectra at high redshift. *Astrophys. J.* 682, 724–736. [astro-ph]]. doi:10.1086/589568

Blondin, S., and Tonry, J. L. (2007). Determining the Type, redshift, and age of a supernova spectrum. *Astrophys. J.* 666, 1024–1047. arXiv:0709.4488 [astro-ph]. doi:10.1086/520494

Brout, D., Scolnic, D., Popovic, B., Riess, A. G., Zuntz, J., Kessler, R., et al. (2022). The Pantheon+ analysis: cosmological constraints. *Astrophys. J.* 938 (2), 110. arXiv:2202.04077 [astro-ph.CO]]. doi:10.3847/1538-4357/ac8e04

Cawthon, R., Elvin-Poole, J., Porredon, A., Crocce, M., Giannini, G., Gatti, M., et al. (2022). Dark Energy Survey Year 3 results: calibration of lens sample redshift distributions using clustering redshifts with BOSS/eBOSS. *Mon. Not. Roy. Astron. Soc.* 513, 5517–5539. [astro-ph.CO]. doi:10.1093/mnras/stac1160

Chang, H. Y. (2001). Fourier analysis of gamma-ray burst light curves: searching for a direct signature of cosmological time dilation. *Astrophys. J. Lett.* 557, L85–L88. [astro-ph]. doi:10.1086/323331

Crawford, D. F., [arXiv:0901.4169 [astro-ph.CO]].

Dai, D. C., Starkman, G. D., Stojkovic, B., Stojkovic, D., and Weltman, A. (2012). Using quasars as standard clocks for measuring cosmological redshift. *Phys. Rev. Lett.* 108, 231302. arXiv:1204.5191 [astro-ph.CO]]. doi:10.1103/PhysRevLett.108.231302

Foley, R. J., Filippenko, A. V., Leonard, D. C., Riess, A. G., Nugent, P., and Perlmutter, S. (2005). A definitive measurement of time dilation in the spectral evolution of the moderate-redshift Type Ia supernova 1997ex. *Astrophys. J. Lett.* 626, L11–L14. [astro-ph]. doi:10.1086/431241

Guzzo, L., Bel, J., Bianchi, D., Carbone, C., Granett, B. R., Hawken, A. J., et al. doi:10.1007/978-3-030-01629-6_1[arXiv:1803.10814 [astro-ph.CO]]

Hawkins, M. R. S. (2001). Time dilation and quasar variability. *Astrophys. J. Lett.* 553, L97–L100. [astro-ph]. doi:10.1086/320683

Hinshaw, G., Larson, D., Komatsu, E., Spergel, D. N., Bennett, C. L., Dunkley, J., et al. (2013). *Astrophys. J. Suppl. Ser.* 208, 20. arXiv:1212.5226 [astro-ph.CO]]. doi:10.1088/0067-0049/208/2/19

Lee, S. (2021). JCAP **08**. *J. Cosmol. Astropart. Phys.* 2021, 054. arXiv:2011.09274 [astro-ph.CO]]. doi:10.1088/1475-7516/2021/08/054

Lee, S. (2023a). The cosmological evolution condition of the Planck constant in the varying speed of light models through adiabatic expansion. *Phys. Dark Univ.* 42, 101286. arXiv:2212.03728 [astro-ph.CO]]. doi:10.1016/j.dark.2023.101286

Lee, S. (2023b). A viable varying speed of light model in the RW metric. *Phys.* 53, 40. arXiv:2303.13772 [physics.gen-ph]]. doi:10.1007/s10701-023-00682-1

Lee, S. (2023c). Constraining minimally extended varying speed of light by cosmological chronometers. *Mon. Not. Roy. Astron. Soc.* 522 (3), 3248–3255. arXiv:2301.06947 [astro-ph.CO]]. doi:10.1093/mnras/stad1190

Lee, S. (2024). Review on minimally extended varying speed of light model. *Particles* 7, 309–326. arXiv:2406.02556 [physics.gen-ph]]. doi:10.3390/particles7020019

Lee, T. T., and Petrosian, V. (1997). Time dilation of BATSE gamma-ray bursts. *Astrophys. J.* 474, 37–46. [astro-ph]. doi:10.1086/303458

Leibundgut, B., Schommer, R., Phillips, M., Riess, A., Schmidt, B., Spyromilio, J., et al. (1996). Time dilation in the light curve of the distant Type Ia supernova SN 1995K. *Astrophys. J. Lett.* 466, L21–L24. [astro-ph]. doi:10.1086/310164

Lewis, G. F., and Brewer, B. J. (2023). Detection of the cosmological time dilation of high-redshift quasars. *Nat. Astron* 7 (10), 1265–1269. arXiv:2306.04053 [astro-ph.CO]]. doi:10.1038/s41550-023-02029-2

Meszaros, A., and Meszaros, P. (1996). Cosmological evolution and luminosity function effects on number counts, redshift, and time dilation of bursting sources. *Astrophys. J.* 466, 29. [astro-ph]. doi:10.1086/177491

Norris, J. P., Nemiroff, R. J., Scargle, J. D., Kouveliotou, C., Fishman, G. J., Meegan, C. A., et al. (1994). Detection of signature consistent with cosmological time dilation in gamma-ray bursts. *Astrophys. J.* 424, 540. [astro-ph]]. doi:10.1086/173912

Riess, A. G., Filippenko, A. V., Leonard, D. C., Schmidt, B. P., Suntzeff, N., Phillips, M. M., et al. (1997). Time dilation from spectral feature age measurements of Type IA supernovae. *Astron. J.* 114, 722. [astro-ph]. doi:10.1086/118506

Singh, A., and Desai, S. (2022). JCAP **02**. *J. Cosmol. Astropart. Phys.* 2022 (02), 010. arXiv:2108.00395 [astro-ph.HE]]. doi:10.1088/1475-7516/2022/02/010

Weinberg, S. (2008). *Cosmology*. Oxford University Press.

White, R. M. T., Davis, T. M., Lewis, G. F., Lidman, C., Shah, P., Abbott, T. M. C., et al. *[DES]*. [arXiv:2406.05050 [astro-ph.CO]].

Wijers, R. A. M. J., and Paczynski, B. (1994). On the nature of gamma-ray burst time dilations. *Astrophys. J. Lett.* 437, L107. [astro-ph]. doi:10.1086/187694

Zhang, F. W., Fan, Y. Z., Shao, L., and Wei, D. M. (2013). Cosmological time dilation in durations of *swift* long gamma-ray burstS. *Astrophys. J. Lett.* 778, L11. arXiv:1309.5612 [astro-ph.HE]]. doi:10.1088/2041-8205/778/1/L11

frontiers | Frontiers in Astronomy and Space Sciences

TYPE Mini Review
PUBLISHED 09 August 2024
DOI 10.3389/fspas.2024.1425500

Check for updates

OPEN ACCESS

EDITED BY
Joseph E. Borovsky,
Space Science Institute (SSI), United States

REVIEWED BY
Olga V. Khabarova,
Tel Aviv University, Israel
Fran Bagenal,
University of Colorado Boulder, United States
Larry Lyons,
University of California, Los Angeles, United States
Michelle Thomsen,
Planetary Science Institute, United States

*CORRESPONDENCE
Michael W. Liemohn,
liemohn@umich.edu

RECEIVED 29 April 2024
ACCEPTED 24 July 2024
PUBLISHED 09 August 2024

CITATION
Liemohn MW (2024) Practical actions towards equity in space physics.
Front. Astron. Space Sci. 11:1425500.
doi: 10.3389/fspas.2024.1425500

COPYRIGHT
© 2024 Liemohn. This is an open-access article distributed under the terms of the Creative Commons Attribution License (CC BY). The use, distribution or reproduction in other forums is permitted, provided the original author(s) and the copyright owner(s) are credited and that the original publication in this journal is cited, in accordance with accepted academic practice. No use, distribution or reproduction is permitted which does not comply with these terms.

Practical actions towards equity in space physics

Michael W. Liemohn*

Department of Climate and Space Sciences and Engineering, University of Michigan, Ann Arbor, MI, United States

To mitigate the issues of inequity, exclusion, and a lack of diversity in the solar and space physics research community, a Research Topic collection gathered articles of how scientists in this discipline are taking strides to make this community more welcoming. This review summarizes the key advice from those articles and offers practical actions for both immediate and long-term implementation. There are six major topical categories into which the collection's article can be grouped: early-year improvements (pre-college and undergraduate); inclusive project teams; diversity in awards; equity in hiring and promotion; leadership development; and the workplace environment. The scope of suggestions ranges from the very localized, such as the language choices we make in everyday conversations, to the institutional, such as the establishment of codes of conduct with a definition and enforcement of consequences for inappropriate behavior regarding inclusion and equity issues. It is hoped that the recommendations are applicable not only to the space physics community but also to others.

KEYWORDS

space physics, diversity, equity, inclusion, demographics, recommendations

1 Introduction

There are compelling reasons to support diversity, equity, inclusion, accessibility, and justice (DEIAJ) action. The first and foremost is that it is considerate, polite, and thoughtful workplace behavior and policy. In addition, it is worthwhile to combat the long-lasting and still-prevalent systemic biases of centuries of marginalization and disadvantage for certain identities (e.g., Elphick and Fredrickson, 1983; Haacker et al., 2022). There is also the well-established case that diverse teams lead to better outcomes. Specifically in scientific collaboration, the review by Nielsen et al. (2018) documents that gender diversity leads to better science, and AlShebli et al. (2018) detail how ethnic diversity yields better scientific results.

Whenever a demographics survey of solar and space physics is conducted, however, it has consistently found that the field is dominated by white men (e.g., Jones and Maute, 2022; Liemohn et al., 2023a; Bagenal, 2023; Yalim et al., 2023). As stated by Liemohn et al. (2023a), the Space Physics and Aeronomy section of the American Geophysical Union (AGU) has a student population with twice as many men as women (and gets worse with seniority), and the percentage of Latine and Black people within the American Astronomical Society is four to six times lower than the US population (see their Tables 1, 2). The student gender gap of space physics is similar to other areas of science, technology, engineering, and mathematics (STEM), as exemplified by the 2-to-1 men-women ratio found among STEM students at a multi-campus university in Mexico (Ortiz-Martínez et al., 2023).

While this indicates a "pipeline" issue in the education years, there is also an issue in the STEM workplace. Marin-Spiotta et al. (2020) note that a hostile work environment contributes to a lack of diversity in the geosciences. Ford et al. (2018), Ford et al. (2019) conducted an analysis of presentations at the annual meetings of AGU, finding large disparities in both gender and race among those invited and those given the prized oral session slots. In a large survey of Earth and space scientists, Popp et al. (2019) found that women face twice as much negative gender bias acts as their male colleagues (e.g., in the style of supervision, promotion and pay, support of mentors, selection for presentations, and awards). An analysis of acceptance rates in Earth and space science journals (Lerback et al., 2020) discovered that racially diverse coauthor teams have a lower overall acceptance rate. An assessment of scientist participation in competed space missions (Centrella et al., 2019) found that the teams are far less diverse than the research community. Studies have routinely shown that white, able-bodied, heterosexual men have intersectional privilege in STEM (e.g., Cech, 2022). In short, systemic biases against nondominant cultural groups–women; black, indigenous, and people of color (BIPOC); and lesbian, gay, bisexual, transgender, and queer (LGBTQ+), to name a few–exist in our community. The field of solar and space physics is not diverse and there are large structural issues that lead to slow progress on this issue. The net result is that two people with the same scholarly record might have gotten there through very different lived experiences.

To raise awareness of DEIAJ action in the space science research community, a special collection in Frontiers in Astronomy and Space Sciences was organized (Liemohn et al., 2023b). These articles were by space scientists writing about their DEIAJ work. This review summarizes a few key findings from the collection, focusing on the practical actions that individuals can take to make the research community and work environment more diverse, equitable, inclusive, accessible, and just. These recommendations are hopefully applicable not only to the space physics research community but also to many other scientific disciplines.

2 Practical actions for equity

The six major categories into which the collection's articles are grouped below cover the Research Topic collection but additional content has been added throughout this discussion for supplementary context.

2.1 Early-year improvements

Gallagher Dunn et al. (2023) addresses the issue of maintaining interest in STEM across a diverse student body within the pre-college years. One key point they make is to drop the strict disciplinarian mindset because a positive teacher-student relationship serves the students better (e.g., Rivas-Drake et al., 2014). This is evidenced by the concept of stereotype threat (Steele, 1997; Lewis et al., 2016), in which the judgment of other people negatively influences the performance of those in marginalized groups. Another conclusion to highlight from this article is the need for long-term mentorship, which has significant positive impacts (e.g., Hund et al., 2018). Scientists should serve as role models for the next-generation of scholars.

Because the STEM workplace is not fully inclusive of women (e.g., Settles and O'Connor, 2014), Lin et al. (2023) founded a program for undergraduate and graduate students focusing on marginalized genders in STEM fields, the HUG Initiative–Historically marginalized and Underrepresented Genders. The HUG initiative instituted a three-pronged approach to inclusion (e.g., Grogan, 2019): building the career skillset; building community and networks; and building awareness of policy issues. They created an impressive action list of sponsored workshops, seminars by alumni, fellowship activities, and a campus peer mentoring program.

Following the advice of Lopatto (2007) that undergraduate research experiences support science career decisions, Yalim et al. (2023) describe their summer programs in plasma physics and technology. About 50 undergraduate students, mostly from marginalized demographic groups, get to work on a science or engineering project and gain valuable life skills. This takes a concerted effort; it is a continual process to get buy-in from departmental colleagues to participate in these programs.

Bagenal (2023) synthesized several national reports on pre-college and undergraduate engagement in STEM. Higher education should be accessible for everyone (McNutt, 2022), and there are specific actions that can be taken to make this a reality. One finding is a pinch point of participation in the early college years. The recommendations to alleviate this are to improve teaching in those first-year courses, especially getting rid of the "weed-out" mentality. This is the mindset in which instructors intentionally make it difficult to get a high grade in these courses, advantaging those with prior knowledge of the subject. It is a practice that disproportionately discourages students from underrepresented groups from continuing in STEM (e.g., Bradforth et al., 2015). Also, undergrad research experiences are powerful motivators towards STEM disciplines (e.g., Russell et al., 2007).

2.2 Actions for inclusive project teams

In 2020, NASA's Heliophysics Division created a new research and analysis program: the DRIVE (Diversity, Realize, Integrate, Venture, Educate) Science Centers. One of the projects is SHIELD (Solar wind with Hydrogen Ion charge Exchange and Large-Scale Dynamics), focusing on the edge of the solar system where the charged gases from the Sun interact with the local interstellar medium. As described by Buxner et al. (2023), the team embraces the cross-disciplinary nature of their work. Knowing that scientists from historically excluded groups face hostile environments (e.g., Berhe et al., 2022), the SHIELD project created a seminar series on DEIAJ topics, covering mental health awareness, outreach activities, and LGBTQ+ issues. The SHIELD project is also collecting individual testimonials; inspiring personal interviews allowing everyone–from a very broad range of backgrounds–to see themselves within the research community.

Another group fostering an inclusive atmosphere is the mission team for MAVEN (Mars Atmospheric and Volatile EvolutioN), as detailed by Curry (2023). When she became leader of this

mission to Mars, she undertook DEIAJ as a priority, amplifying existing actions and instituting new ones. Adopting the findings of Fernando et al. (2022), they have included early career researchers in leadership positions. Following Davies et al. (2021), they work to change the discriminatory reward system in STEM fields (e.g., gender and racial bias in citation metrics (Nielsen and Andersen, 2021), course evaluations (Madera et al., 2019), and letters of recommendation (El-Alayli et al., 2018)). Another key practice is the rules of the road document for team meetings, which sets the tone for group cultural expectations. As Cortina and Areguin (2021) discuss, Codes of Conduct should go well beyond overt harassment (e.g., assault or coercion) and also address microaggressions (like insults and rudeness). The MAVEN team does many small actions, accumulating to substantial change.

2.3 Improving diversity in awards

Within the annual AGU Fellows process, the Space Physics and Aeronomy (SPA) section usually gets 15–20 nominations. In 2017, no women were nominated for Fellow in the SPA section. Seeing this problem, Dr. Liz MacDonald formed the Nomination Task Force (NTF) to proactively submit nominations of senior women colleagues (Keesee et al., 2022). Part of the success of the NTF is to get the nominations fully drafted a month early, and then review each other's packages. This pre-submission review better highlights the strength of each nomination.

Soon after the NTF formed, a similar group in the UK followed (Walach et al., 2022). One big recommendation for the community is that awards are highly competitive; even a strong candidate needs a strong nomination to be selected. Another suggestion is for transparency in the selection criteria and process. Another proposition: take the risk of nominating your peers.

On the concern from Walach et al. (2022) of wanting more transparency in the selection process, Halford et al. (2022) detail the actions of the SPA Fellows selection committee for the year they served. They note that there are multiple paths to selection for this honor, and the community should take advantage of these options. A decision they made was to deemphasize metrics and instead focus on the nominee's story of significance. This is because there is a first-author gender gap in the geosciences (Pico et al., 2020), and use of the h-index without context and adjustment leads to a negative impact on diversity (Chapman et al., 2019).

2.4 Fostering equity in hiring and promotion

A large part of the hiring and promotion process is the letter of recommendation. Studies have shown, though, that academics are biased. Earth and space scientists are biased in how letters of recommendation are written, with stronger letters for white men on average (Dutt et al., 2016). There is help out there, though, as described by Burrell et al. (2023). This article details best practices for how to write a strong letter. In addition, the group provides a service, reading draft letters and offering suggestions to remove bias and better highlight aspects of the person's record that best addresses the specific evaluation criteria.

DEIAJ best practices in hiring and promotion is the primary focus of Liemohn et al. (2023a). It has been demonstrated that workshops to equip faculty to conduct an equitable search are quite effective at achieving this objective (Sekaquaptewa et al., 2019). One key piece of advice is, early in the hiring process, to develop a holistic set of job-relevant criteria that expands the definition of excellence beyond the standard metrics (c.f., Stewart et al., 2016). Then, during the process, recenter these holistic criteria. Standard metrics are often biased towards white men, like citations in high impact journals (Chatterjee and Werner, 2021). Another significant recommendation is the use of equity checkpoints (O'Meara, 2021). These are intentional pauses in the search and applicant evaluation process to specifically refocus DEIAJ and consider if any adjustments to the workflow are needed to ensure equity.

2.5 Equipping ourselves for leadership

Leading a spaceflight mission proposal is an enormous task, posing a major learning curve for those unfamiliar with the process. Seeing that this disadvantages newcomers, the NASA PI Launchpad Workshop was created (Hamden et al., 2022). This event equips scientists with the skills and contacts to get through that barrier to being a principal investigator of a spaceflight mission. One of the significant tasks is to learn the mission-proposal-specific method of writing the science story, which is quite different from a standard research and analysis proposal (Wessen et al., 2022).

Another path to leadership is serving as an editor of a peer-reviewed journal. Liemohn (2022) documents the DEIAJ lessons learned over 6 years as Editor in Chief of the Journal of Geophysical Research Space Physics. A strong suggestion is to stop assuming that anonymous reviewers of manuscripts are men. This assumption is offensively sexist (e.g., Atherton et al., 2016). Instead, use "they" when gender is unknown. Also, do a thorough literature review instead of only including those papers from your close-friend group; expansive searches lead to a more diverse reference list. Finally, the prevalence of colorblindness, particularly in men, means that certain color maps cause confusion (Moreland, 2016). In particular, avoid the rainbow scale; there are much better ones that support accessibility and readability.

Research community leadership also includes conference organization. Jones and Maute (2022) are part of the steering committee for an annual upper atmospheric physics conference and, after a demographics survey quantified the prevalence of white men, the organizing committee created a DEI Task Force. Their recommendations build on the inclusive meetings guidelines of Pendergrass et al. (2019) and an updated version of this guide is now available (Jack-Scott et al., 2023). This research community now has events during the workshop week as well as monthly virtual events. They also offer childcare grants to make attendance more accessible for scientists who are also parents. A key point they make is that this work takes time and that it is beneficial to develop systems and norms to reward those that conduct DEIAJ work. This reward system should acknowledge not only the visible DEIAJ work of leaders and committees but also the invisible service workload (Daniels, 1987) in supporting underrepresented students, a task that systematically burdens those from marginalized

groups, especially BIPOC scientists (e.g., Jimenez et al., 2019; Gewin, 2020).

Similarly, Smith-Keiling and Keiling (2023) note that conferences often have a less-than-positive climate for women [e.g., overt sexist attitudes, as well as condescending remarks, flirtatiousness, or exclusion from discussions, (Biggs et al., 2018)]. They focus on the value of building a diverse organizing team and emphasize the importance of personal interactions at creating a positive culture for inclusion of all, not only at the conference but also in the planning meetings. That is, listening fosters cultural wellness, so the organizing committee should go beyond introductions and the members should get to know each other more deeply (Smith-Keiling et al., 2020).

2.6 Research workplace recommendations

While it is true that the lack of diversity in the field is a "pipeline" issue because women and BIPOC leave STEM during their schooling, another major reason for a lack of diversity is that they leave due to toxic and hostile work environments [e.g., words or behavior than denigrate an individual based on their sex (Cortina et al., 2022)]. One example is described by Settles et al. (2018), who found that faculty of color experience both invisibility (with respect to leadership and recognition) and hypervisibility (with respect to interpersonal interactions and evaluations). Unfortunately, a racial bias against BIPOC faculty still persists in the academic workplace, and this was amplified by the antiscience rhetoric that arose during the Trump presidency and the extraordinary burdens of the pandemic (McGee et al., 2021). The situation is worse for those with multiple marginalized identities because intersectionality compounds the inequalities (e.g., Clancy et al., 2017; Kozlowski et al., 2022). Following the ten simple rules towards healthier research labs of Maestre (2019), Halford et al. (2023) give many ways in which space scientists can improve the workplace. This includes thinking beyond our normal close-knit colleagues when forming a new team. It also means designing the workplace for universal accessibility, including access to affordable childcare, a family task that still disproportionately burdens women. When running hybrid meetings, establish norms that foster connection between the local and remote participants. Finally, it is recommended to develop policies with consequences for inappropriate behavior.

Turner and Smith (2023) address the topic of neurodiversity in space physics. One significant point made by Turner and Smith (2023) is that word choice matters. Table 1 offers a quick guide to neurodiversity-affirming language and some key phrases to avoid. When pathologizing language is noted, politely take correction and learn to use more inclusive words. Taboas et al. (2022) found that autistic adults prefer to be called autistic rather than "having autism." This is akin to being left handed, for which we would never refer to someone as "having lefthandedness." Furthermore, avoid moralizing about neurodivergent behavior; people work differently and we should accept these styles rather than conform to past standards. Finally, we should move past compliance and towards supportive caring and universal accessibility.

Nikoukar et al. (2023) raise awareness of mental health issues in the space physics community. The pandemic was a stressor (Gewin, 2021), but not the only one (Evans et al., 2018; Wong et al., 2019). STEM scientists experience isolation, burnout, poor-work-life balance, endure a toxic research culture, and suffer the negative consequences of our hierarchical institutional structures (e.g., Hall, 2023). Furthermore, there is a stigma against openly talking about this topic. Nikoukar et al. (2023) recommend the development of programs that foster good stress management to build resilience to stressors. Also, mental health should be included in surveys to better understand the scope.

TABLE 1 A brief language guide for more inclusive conversations with and about neurodiverse colleagues and students (from Turner and Smith, 2023).

Use this (neurodiversity-affirming language)	Avoid this (pathologizing language)
Autistic person	"Person with autism"
Autism	Autism spectrum disorder (ASD)
Traits	Symptoms
Identification	Diagnosis
Neurotype	Disorder
Co-occurring	Comorbid
Passions or interests	"Restricted interests"
Typical	Normal
Naming specific supports or accommodations	Functioning levels (e.g., high-functioning or low-functioning)

Burt et al. (2022) detail findings from surveys conducted of alumni of the Advanced Studies Program (ASP) at this institution. There are two main motivations as to why people become engaged in DEIAJ work. One is the business case: many studies show that diverse teams lead to more creativity and productivity. Another is the moral case: historical marginalization has been going on for centuries, and there is an ethical and social responsibility to take part in dismantling those policies and practices. Burt et al. (2022) found that these ASP alumni resonate more with the moral case than with the business case. Also, as shown in Figure 1, young researchers are stepping up and getting engaged, with 87% of ASP alumni doing some form of DEIAJ work–many of them engaging in multiple forms–at their new institutions.

3 Conclusion

Below are a dozen recommendations to implement across the solar and space physics research community. While these recommendations are distilled from actions within this particular scientific community, they are hopefully applicable across all STEM research fields.

First, immediate actions to create a more inclusive culture:

- Make kinder and more respectful language choices
- Speak up and intervene when you see or hear racism, sexism, prejudice, and harassment

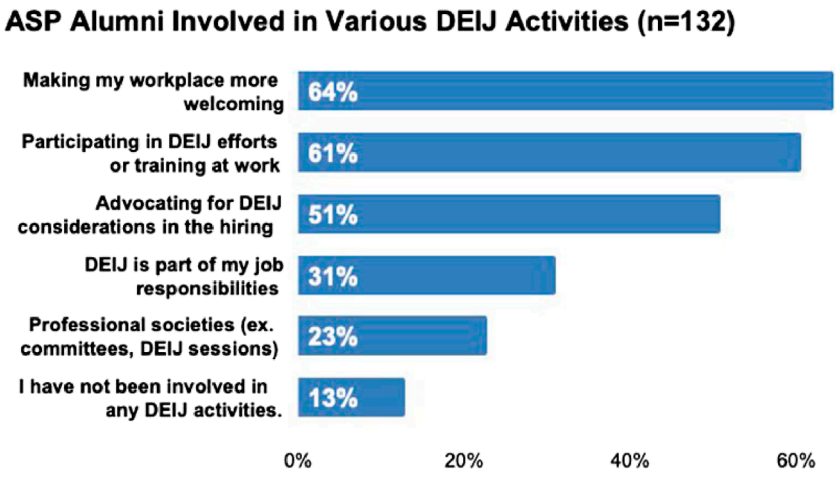

FIGURE 1
Involvement of ASP alumni in DEIAJ activities at their new institutions. From Burt et al., 2022.

- Make space for the voices of those from marginalized identities
- Take correction from others with humility rather than getting defensive

Second, additional actions towards equity as the situation arises:

- Adopt positive teacher-student interactions, especially in introductory STEM courses
- Mentor pre-college and undergraduate researchers
- Take the risk to nominate your peers for awards and proactively strengthen the nomination
- Expand your definition of excellence when evaluating other scientists for hiring, promotion, and awards

Third, some policy changes to enact to make the workplace better for all:

- Proactively plan for universal accessibility
- Develop codes of conduct and safety protocols for the lab, group meetings, and field work
- Establish processes to acknowledge DEIAJ work, especially the invisible service of helping students and colleagues through difficult situations
- Introduce and enforce appropriate consequences for the full range of workplace inclusivity offenses

DEIAJ action is about treating others with decency and respect. Systemic racism, sexism, and inequality still exist in our workplace culture and these reinforce individual biases and stereotypes. We should work to break this cycle, so that, some day, equity and equality might mean the same thing.

This work is for all of us to do. Inequity and exclusion negatively influence everyone, in particular those from marginalized groups, and those in the current dominant cultural group in solar and space physics–white men–should use their privilege to address it. Whichever of the various motivations for engaging in DEIAJ work best appeals to you, you are strongly urged to get involved.

Author contributions

ML: Conceptualization, Funding acquisition, Resources, Writing–original draft, Writing–review and editing.

Funding

The author(s) declare that financial support was received for the research, authorship, and/or publication of this article. The author would like to thank the University of Michigan for its financial support, as well as the US government, in particular research grants from NASA (80NSSC23M0040, 80NSSC19K0077, 80NSSC21K1127, and 80NSSC21K1405) and NSF (AGS-1414517).

Acknowledgments

Soon after Dr. Joe Borovsky became the Topical Chief Editor for Space Physics for Frontiers in Astronomy and Space Sciences, he asked me to lead a special collection on diversity issues in the field. Thank you, Joe, for spotlighting this matter. I also thank him for the invitation to give a plenary session presentation at the celebratory conference, "A decade of discovery and advancement–10th anniversary conference of Frontiers in Astronomy and Space Sciences," and thank all of those at "Frontiers In" that made that conference possible. This review is based on that presentation. I would especially like to thank my co-editors on this Research Topic–Drs. Xochitl Blanco-Cano, Chigomezyo Ngwira, John Coxon, Alexa Halford, and McArthur Jones Jr.–without whom this collection would not have happened. I am very grateful to all–editors, reviewers, authors, and staff–who invested time and effort on that Research Topic. I am also grateful for my opportunities to be involved in DEIAJ work at the University of Michigan, including my role as an Associate Director of the U-M ADVANCE Program. Finally, I would also like to state that the University of Michigan is located on land obtained from indigenous peoples through unjust treaties. While I cannot change the past, I can work

towards a more equitable and sustainable future. Please support indigenous nation sovereignty.

Conflict of interest

The author declares that the research was conducted in the absence of any commercial or financial relationships that could be construed as a potential conflict of interest.

Publisher's note

All claims expressed in this article are solely those of the authors and do not necessarily represent those of their affiliated organizations, or those of the publisher, the editors and the reviewers. Any product that may be evaluated in this article, or claim that may be made by its manufacturer, is not guaranteed or endorsed by the publisher.

References

AlShebli, B. K., Rahwan, T., and Woon, W. L. (2018). The preeminence of ethnic diversity in scientific collaboration. *Nat. Commun.* 9, 5163. doi:10.1038/s41467-018-07634-8

Atherton, T. J., Barthelemy, R. S., Deconinck, W., Falk, M. L., Garmon, S., Long, E., et al. (2016). *LGBT climate in physics: building an inclusive community*. College Park, MD: American Physical Society.

Bagenal, F. (2023). Enhancing demographics and career pathways of the space physics workforce in the US. *Front. Astronomy Space Sci.* 10, 1130803. doi:10.3389/fspas.2023.1130803

Berhe, A. A., Barnes, R. T., Hastings, M. G., Mattheis, A., Schneider, B., Williams, B. M., et al. (2022). Scientists from historically excluded groups face a hostile obstacle course. *Nat. Geosci.* 15, 2–4. doi:10.1038/s41561-021-00868-0

Biggs, J., Hawley, P. H., and Biernat, M. (2018). The academic conference as a chilly climate for women: effects of gender representation on experiences of sexism, coping responses, and career intentions. *Sex. Roles* 78 (5–6), 394–408. doi:10.1007/s11199-017-0800-9

Bradforth, S. E., Miller, E. R., Dichtel, W. R., Leibovich, A. K., Feig, A. L., Martin, J. D., et al. (2015). University learning: improve undergraduate science education. *Nature* 523, 282–284. doi:10.1038/523282a

Burrell, A. G., Jones, M., Zawdie, K. A., Coxon, J. C., and Halford, A. J. (2023). Tips for writing a good recommendation letter. *Front. Astronomy Space Sci.* 10, 1114821. doi:10.3389/fspas.2023.1114821

Burt, M. A., Haacker, R., Montaño, P., Vara, M., and Sloan, V. (2022). The ethics of diversity, equity, inclusion, and justice in the earth system sciences. *Front. Phys.* 10, 1085789. doi:10.3389/fphy.2022.1085789

Buxner, S., Gross, N., Opher, M., Wong, J., and Richardson, J. (2023). SHIELD DRIVE Science Center: efforts in diversification and inclusion in heliophysics. *Front. Astronomy Space Sci.* 10, 1155843. doi:10.3389/fspas.2023.1155843

Cech, E. A. (2022). The intersectional privilege of white able-bodied heterosexual men in STEM. *Sci. Adv.* 8 (24), eabo1558. doi:10.1126/sciadv.abo1558

Centrella, J., New, M., and Thompson, M. (2019). Leadership and participation in NASA's astrophysics explorer-class missions. *Bull. Am. Astron. Soc.* 51, 290. doi:10.48550/arXiv.1909.10314

Chapman, C. A., Bicca-Marques, J. C., Calvignac-Spencer, S., Fan, P., Fashing, P. J., Gogarten, J., et al. (2019). Games academics play and their consequences: how authorship, h-index and journal impact factors are shaping the future of academia. *Proc. R. Soc. B* 286, 20192047. doi:10.1098/rspb.2019.2047

Chatterjee, P., and Werner, R. M. (2021). Gender disparity in citations in high-impact journal articles. *JAMA Netw. Open* 4, e2114509. doi:10.1001/jamanetworkopen.2021.14509

Clancy, K. B. H., Lee, K. M. N., Rodgers, E. M., and Richey, C. (2017). Double jeopardy in astronomy and planetary science: women of color face greater risks of gendered and racial harassment. *J. Geophys. Res. Planets* 122, 1610–1623. doi:10.1002/2017JE005256

Cortina, L. M., and Areguin, M. A. (2021). Putting people down and pushing them out: sexual harassment in the workplace. *Annu. Rev. Organ. Psychol. Organ. Behav.* 8, 285–309. doi:10.1146/annurev-orgpsych-012420-055606

Cortina, L. M., Sandy Hershcovis, M., and Clancy, K. B. H. (2022). The embodiment of insult: a theory of biobehavioral response to workplace incivility. *J. Manag.* 48 (3), 738–763. doi:10.1177/0149206321989798

Curry, S. (2023). MAVEN mission perspectives and approaches to inclusion. *Front. Astronomy Space Sci.* 10, 1162107. doi:10.3389/fspas.2023.1162107

Daniels, A. K. (1987). Invisible work. *Soc. Probl.* 34 (5), 403–415. doi:10.2307/800538

Davies, S. W., Putnam, H. M., Ainsworth, T., Baum, J. K., Bove, C. B., Crosby, S. C., et al. (2021). Promoting inclusive metrics of success and impact to dismantle a discriminatory reward system in science. *PLOS Biol.* 19 (6), e3001282. doi:10.1371/journal.pbio.3001282

Dutt, K., Pfaff, D. L., Bernstein, A. F., Dillard, J. S., and Block, C. J. (2016). Gender differences in recommendation letters for postdoctoral fellowships in geoscience. *Nat. Geosci.* 9, 805–808. doi:10.1038/ngeo2819

El-Alayli, A., Hansen-Brown, A. A., and Ceynar, M. (2018). Dancing backwards in high heels: female professors experience more work demands and special favor requests, particularly from academically entitled students. *Sex. roles* 79, 136–150. doi:10.1007/s11199-017-0872-6

Elphick, R., and Fredrickson, G. M. (1983). A comparative history of white supremacy. *J. Interdiscip. Hist.* 13 (3), 503–513. doi:10.2307/202948

Evans, T., Bira, L., Gastelum, J., Weiss, L., and Vanderford, N. (2018). Evidence for a mental health crisis in graduate education. *Nat. Biotechnol.* 36, 282–284. doi:10.1038/nbt.4089

Fernando, B., Daubar, I. J., Irving, J. C. E., Johnson, C. L., Marusiak, A. G., Baker, M. M., et al. (2022). Inclusion of early-career researchers in space missions. *Nat. Astron* 6, 1339–1341. doi:10.1038/s41550-022-01861-2

Ford, H. L., Brick, C., Azmitia, M., Blaufuss, K., and Dekens, P. (2019). Women from some under-represented minorities are given too few talks at world's largest Earth science conference. *Nature* 576, 32–35. doi:10.1038/d41586-019-03688-w

Ford, H. L., Brick, C., Blaufuss, K., and Dekens, P. S. (2018). Gender inequity in speaking opportunities at the American geophysical union fall meeting. *Nat. Commun.* 9 (1), 1358–1366. doi:10.1038/s41467-018-03809-5

Gallagher Dunn, S. L., Haviland, H. F., and Gallagher, D. L. (2023). The importance of local long-duration STEM mentorship as a global mechanism for increasing diversity at all levels of education. *Front. Astronomy Space Sci.* 10, 1134836. doi:10.3389/fspas.2023.1134836

Gewin, V. (2020). The time tax put on scientists of colour. *Nature* 583, 479–481. doi:10.1038/d41586-020-01920-6

Gewin, V. (2021). Pandemic burnout is rampant in academia. *Nature* 591, 489–491. doi:10.1038/d41586-021-00663-2

Grogan, K. E. (2019). How the entire scientific community can confront gender bias in the workplace. *Nat. Ecol. Evol.* 3, 3–6. doi:10.1038/s41559-018-0747-4

Haacker, R., Burt, M., and Vara, M. (2022). Moving beyond the business case for diversity. *Eos*, 103. doi:10.1029/2022eo220080

Halford, A. J., Bard, C., Burrell, A. G., McGranaghan, R., Wilson, L. B., Jones, M., Jr., et al. (2023). The importance of recruitment and retention in heliophysics: it's not just a pipeline problem. *Front. Astronomy Space Sci.* 10, 1216449. doi:10.3389/fspas.2023.1216449

Halford, A. J., Burrell, A. G., Yizengaw, E., Bothmer, V., Carter, B. A., Raymond, J. C., et al. (2022). Thoughts from a past AGU SPA fellows committee. *Front. Astron. Space Sci.* 9, 1054343. doi:10.3389/fspas.2022.1054343

Hall, S. (2023). A mental-health crisis is gripping science -toxic research culture is to blame. *Nature* 617, 666–668. doi:10.1038/d41586-023-01708-4

Hamden, E., New, M. H., Pugel, B., Liemohn, M. W., Wessen, R., Quinn, R., et al. (2022). The PI Launchpad: expanding the base of potential principal investigators across space sciences. *Front. Astronomy Space Sci.* 9, 1048644. doi:10.3389/fspas.2022.1048644

Hund, A. K., Churchill, A. C., Faist, A. M., Havrilla, C. A., McCreery, H. F., Ng, J., et al. (2018). Transforming mentorship in STEM by training scientists to be better leaders. *Ecol. Evol.* 8 (20), 9962–9974. doi:10.1002/ece3.4527

Jack-Scott, E., Aponte, K. L., Bhatia, R., Behl, M., Burke, J., Burt, M., et al. (2023). *Inclusive scientific meetings: where to begin*. Boulder, CO: 500 Women Scientists. Available at: https://500womenscientists.org/inclusive-scientific-meetings (Accessed April 23, 2024).

Jimenez, M. F., Laverty, T. M., Bombaci, S. P., Wilkins, K., Bennett, D. E., and Pejchar, L. (2019). Underrepresented faculty play a disproportionate role in advancing diversity and inclusion. *Nat. Ecol. Evol.* 3, 1030–1033. doi:10.1038/s41559-019-0911-5

Jones, Jr. M., and Maute, A. (2022). Assessing the demographics of the 2021 and 2022 CEDAR workshop. *Front. Astron. Space Sci.* 9, 1074460. doi:10.3389/fspas.2022.1074460

Keesee, A. M., Claudepierre, S. G., Bashier, M. F., Hartinger, M. D., MacDonald, E. A., and Jaynes, A. N. (2022). Increasing recognition of historically marginalized scientists: lessons learned from the Nomination Task Force. *Front. Astronomy Space Sci.* 9, 1032486. doi:10.3389/fspas.2022.1032486

Kozlowski, D., Lariviere, V., Sugimoto, C. R., and Monroe-White, T. (2022). Intersectional inequalities in science. *Proc. Natl. Acad. Sci.* 119 (2), e2113067119. doi:10.1073/pnas.2113067119

Lerback, J. C., Hanson, B., and Wooden, P. (2020). Association between author diversity and acceptance rates and citations in peer-reviewed Earth science manuscripts. *Earth Space Sci.* 7, e2019EA000946. doi:10.1029/2019ea000946

Lewis, N., and Sekaquaptewa, D. (2016). Beyond test performance: a broader view of stereotype threat. *Curr. Opin. Psychol.* 11, 40–43. doi:10.1016/j.copsyc.2016.05.002

Liemohn, M. W. (2022). Use singular they – and other lessons learned from editing JGR-Space. *Eos Trans. AGU.* 9, 1018099. doi:10.3389/fspas.2022.1018099

Liemohn, M. W., Linderman, J. L., and Settles, I. H. (2023a). Space Physics Guide to STRIDE: strategies and tactics for recruiting to improve diversity and excellence. *Front. Astronomy Space Sci.* 10, 1152567. doi:10.3389/fspas.2023.1152567

Liemohn, M. W., McArthur, J., Halford, A. J., Coxon, J. C., Ngwira, C. M., and Blanco-Cano, X. (2023b). Editorial: driving towards a more diverse space physics research community – perspectives, initiatives, strategies, and actions. *Front. Astronomy Space Sci.* 10, 1292058. doi:10.3389/fspas.2023.1292058

Lin, M.-Y., Chen, H., and Golecki, H. (2023). HUG initiative: overcoming roadblocks on a research career roadmap of individuals from historically marginalized or underrepresented genders. *Front. Astronomy Space Sci.* 10, 1134327. doi:10.3389/fspas.2023.1134327

Lopatto, D. (2007). Undergraduate research experiences support science career decisions and active learning. *CBE—Life Sci. Educ.* 6 (4), 297–306. doi:10.1187/cbe.07-06-0039

Madera, J. M., Hebl, M. R., Dial, H., Martin, R., and Valian, V. (2019). Raising doubt in letters of recommendation for academia: gender differences and their impact. *J. Bus. Psychol.* 34, 287–303. doi:10.1007/s10869-018-9541-1

Maestre, F. T. (2019). Ten simple rules towards healthier research labs. *PLOS Comput. Biol.* 15, e1006914. doi:10.1371/journal.pcbi.1006914

Marín-Spiotta, E., Barnes, R. T., Berhe, A. A., Hastings, M. G., Mattheis, A., Schneider, B., et al. (2020). Hostile climates are barriers to diversifying the geosciences. *Adv. Geosci.* 53, 117–127. doi:10.5194/adgeo-53-117-2020

McGee, E., Fang, Y., Ni, Y., and Monroe-White, T. (2021). How an antiscience president and the COVID-19 pandemic altered the career trajectories of STEM PhD students of color. *AERA Open* 7, 233285842110392. doi:10.1177/23328584211039217

McNutt, M. (2022). Higher education for all. *Science* 378 (6620), 579. doi:10.1126/science.adf6263

Moreland, K. (2016). Why we use bad color maps and what you can do about it. *Electron. Imaging* 16, 1–6. doi:10.2352/ISSN.2470-1173.2016.16.HVEI-133

Nielsen, M. W., and Andersen, J. P. (2021). Global citation inequality is on the rise. *Proc. Natl. Acad. Sci.* 118, e2012208118. doi:10.1073/pnas.2012208118

Nielsen, M. W., Bloch, C. W., and Schiebinger, L. (2018). Making gender diversity work for scientific discovery and innovation. *Nat. Hum. Behav.* 2 (10), 726–734. doi:10.1038/s41562-018-0433-1

Nikoukar, R., Regoli, L., Halford, A. J., Zettergren, M. D., Dialynas, K., and Filwett, R. (2023). Raising awareness on mental health in the heliophysics community. *Front. Phys.* 11, 1237166. doi:10.3389/fphy.2023.1237166

O'Meara, K. (2021). Leveraging, checking, and structuring faculty discretion to advance full participation. *Rev. High. Educ.* 44 (4), 555–585. doi:10.1353/rhe.2021.0012

Ortiz-Martínez, G., Vázquez-Villegas, P., Ruiz-Cantisani, M. I., Delgado-Fabián, M., Conejo-Márquez, D. A., and Membrillo-Hernández, J. (2023). Analysis of the retention of women in higher education STEM programs. *Humanit. Soc. Sci. Commun.* 10, 101. doi:10.1057/s41599-023-01588-z

Pendergrass, A., Zelikova, J., Arnott, J., Bain, H., Barnes, R., Baron, J., et al. (2019). *Inclusive scientific meetings: where to start*. Boulder, CO: 500 Women Scientists.

Pico, T., Bierman, P., Doyle, K., and Richardson, S. (2020). First authorship gender gap in the geosciences. *Earth Space Sci.* 7, e2020EA001203. doi:10.1029/2020ea001203

Popp, A. L., Lutz, S. R., Khatami, S., van Emmerik, T., and Knoben, W. J. M. (2019). A global survey on the perceptions and impacts of gender inequality in the Earth and space sciences. *Earth Space Sci.* 6, 1460–1468. doi:10.1029/2019EA000706

Rivas-Drake, D., Syed, M., Umaña-Taylor, A., Markstrom, C., French, S., Schwartz, S. J., et al. (2014). Feeling good, happy, and proud: a meta-analysis of positive ethnic–racial affect and adjustment. *Child. Dev.* 85, 77–102. doi:10.1111/cdev.12175

Russell, S. H., Hanckock, M. P., and McCullough, J. (2007). Benefits of undergraduate research experiences. *Science* 316, 548–549. doi:10.1126/science.1140384

Sekaquaptewa, D., Takahashi, K., Malley, J., Herzog, K., and Bliss, S. (2019). An evidence-based faculty recruitment workshop influences departmental hiring practice perceptions among university faculty. *Equal. Divers. Inclusion* 38 (2), 188–210. doi:10.1108/EDI-11-2018-0215

Settles, I. H., and O'Connor, R. C. (2014). Incivility at academic conferences: Gender differences and the mediating role of climate. *Sex Roles* 71, 71–82. doi:10.1007/s11199-014-0355-y

Settles, I. H., Buchanan, N. T., and Dotson, K. (2018). Scrutinized but not recognized: (In) visibility and hypervisibility experiences of faculty of color. *J. Vocat. Behav.* 113, 62–74. doi:10.1016/j.jvb.2018.06.003

Smith-Keiling, B. L., and Keiling, A. (2023). Perspectives of interpersonal interventions at conferences to promote broader inclusion. *Front. Astronomy Space Sci.* 10, 1154793. doi:10.3389/fspas.2023.1154793

Smith-Keiling, B. L., Sharma, A., Fagbodun, S. M., Chahal, H. K., Singleton, K., Gopalakrishnan, H., et al. (2020). Starting the conversation: initial listening and identity approaches to community cultural wellness. *J. Microbiol. Biol. Educ.* 21 (1), 21.1.33–33. doi:10.1128/jmbe.v21i1.2073

Steele, C. (1997). A threat in the air: how stereotypes shape intellectual identity and performance. *Am. Psych.* 52, 613–629. doi:10.1037/0003-066X.52.6.613

Stewart, A. J., Malley, J. E., and Herzog, K. A. (2016). Increasing the representation of women faculty in STEM departments: what makes a difference? *J. Women Minor. Sci. Eng.* 22, 23–47. doi:10.1615/JWomenMinorScienEng.2016014785

Taboas, A., Doepke, K., and Zimmerman, C. (2022). Preferences for identity-first versus person-first language in a US sample of autism stakeholders. *Autism* 27, 565–570. doi:10.1177/13623613221130845

Turner, N. E., and Smith, H. H. (2023). Supporting neurodivergent talent: ADHD, autism, and dyslexia in physics and space sciences. *Front. Phys.* 11, 1223966. doi:10.3389/fphy.2023.1223966

Walach, M.-T., Agiwal, O., Allanson, O., Owens, M. J., Rae, I. J., Sandhu, J. K., et al. (2022). UK magnetosphere, ionosphere and solar-terrestrial (MIST) awards taskforce: a perspective. *Front. Astron. Space Sci.* 9, 1011839. doi:10.3389/fspas.2022.1011839

Wessen, R. R., Propster, P., Cable, M., Case, K., Guethe, C., Matousek, S., et al. (2022). Developing compelling and science-focused mission concepts for NASA competed mission proposals. *Acta Astronaut.* 191, 502–509. doi:10.1016/j.actaastro.2021.12.002

Wong, K., Chan, A., and Ngan, S. (2019). The effect of long working hours and overtime on occupational health: a meta-analysis of evidence from 1998 to 2018. *Int. J. Environ. Res. Public Health* 16, 2102–2134. doi:10.3390/ijerph16122102

Yalim, M. S., Zank, G. P., Provenzani, L., Spencer, D., and Howatson, K. (2023). Diversity in the space physics community: an overview of collaborative efforts led by the University of Alabama in Huntsville. *Front. Astronomy Space Sci.* 10, 1155972. doi:10.3389/fspas.2023.1155972

frontiers | Frontiers in Astronomy and Space Sciences

TYPE Mini Review
PUBLISHED 19 September 2024
DOI 10.3389/fspas.2024.1479874

Check for updates

OPEN ACCESS

EDITED BY
Didier Fraix-Burnet,
UMR5274 Institut de Planétologie et d'Astrophysique de Grenoble (IPAG), France

REVIEWED BY
Pu Du,
Chinese Academy of Sciences (CAS), China

*CORRESPONDENCE
Swayamtrupta Panda,
swayamtrupta.panda@noirlab.edu

†Gemini Science Fellow

RECEIVED 12 August 2024
ACCEPTED 09 September 2024
PUBLISHED 19 September 2024

CITATION
Panda S (2024) Unveiling the quasar main sequence: illuminating the complexity of active galactic nuclei and their evolution. *Front. Astron. Space Sci.* 11:1479874. doi: 10.3389/fspas.2024.1479874

COPYRIGHT
© 2024 Panda. This is an open-access article distributed under the terms of the Creative Commons Attribution License (CC BY). The use, distribution or reproduction in other forums is permitted, provided the original author(s) and the copyright owner(s) are credited and that the original publication in this journal is cited, in accordance with accepted academic practice. No use, distribution or reproduction is permitted which does not comply with these terms.

Unveiling the quasar main sequence: illuminating the complexity of active galactic nuclei and their evolution

Swayamtrupta Panda[1,2]*†

[1]International Gemini Observatory/NSF NOIRLab, La Serena, Chile, [2]Laboratório Nacional de Astrofísica - MCTI, Itajubá, Brazil

The Eigenvector 1 schema, or the main sequence of quasars, was introduced as an analogous scheme to the HR diagram that would allow us to understand the more complex, extended sources - active galactic nuclei (AGNs) that harbor accreting supermassive black holes. The study has spanned more than three decades and has advanced our knowledge of the diversity of Type-1 AGNs from both observational and theoretical aspects. The quasar main sequence, in its simplest form, is the plane between the FWHM of the broad Hβ emission line and the strength of the optical Fe II emission to the Hβ. While the former allows the estimation of the black hole mass, the latter enables direct measurement of the metal content and traces the accretion rate of the AGN. Together, they allow us to track the evolution of AGN in terms of the activity of the central nuclei, its effect on the line-emitting regions surrounding the AGN, and their diversity making them suitable distance indicators to study the expansion of our Universe. This mini-review aims to provide (i) a brief history leading up to the present day in the study of the quasar main sequence, (ii) introduce us to the many possibilities to study AGNs with the main sequence as a guiding tool, and (iii) highlight some recent, exciting lines of researches at the frontier of this ever-growing field.

KEYWORDS

active galactic nuclei, quasars, seyfert galaxies, emission lines, AGN variability, changing-look AGNs, accretion disks

1 What is the quasar main sequence? - a brief history

More than three decades ago, Boroson and Green (1992) put forward the idea of a main sequence of quasars - an analogous schema to the Hertzsprung-Russel (HR) diagram (Hertzsprung, 1911; Russell, 1914) that has allowed us to track the evolution of stars of varied ages and diverse properties utilizing the classification based on their color and magnitude. Akin to the HR diagram, the quasar main sequence (QMS) was envisioned to help put together the diverse population of Type-1, unobscured active galactic nuclei (AGNs) through the compilation of spectral properties from the broad- and narrow line-emitting regions of a sample of nearby, bright AGNs.

Before diving into the recent advances, we would like to reflect on the importance of Boroson and Green's work with a brief account of the procedure carried out to realize the first results that laid the foundations of the Quasar Main Sequence.

1.1 The inception of the main sequence of quasars

Boroson and Green conducted their study within the low-redshift range ($z < 0.5$), analyzing 87 sources from the Bright Quasar Survey (Schmidt and Green, 1983). Their primary finding from optical spectra analysis of these quasars was that the Fe II line equivalent width consistently matched that of Hβ, indicating that Fe II emission originates from the same broad-line region (BLR) clouds as Hβ. Additionally, they compiled optical spectral properties for each source. They integrated these with data from other spectral regions from previous studies, creating a 17-parameter correlation matrix for emission lines and continuum properties. Using principal component analysis (PCA, Francis and Wills, 1999) on this matrix to identify meaningful correlations, they focused on 13 key properties including M_V (V-band magnitude), $\log R$ (radio-to-optical spectral index, Kellermann et al., 1989), α_{ox} (optical-to-X-ray spectral index, Tananbaum et al., 1986), EW(Hβ), [O III]λ5,007 strength, He IIλ4,686 strength, Fe II (4434-4684 Å) strength (see also left panel of Figure 1), [O III]λ5,007/Hβ peak height ratio, FWHM(Hβ), Hβ profile shift, shape, asymmetry, and $M_{[Oiii]}$. They determined that the primary eigenvector (Eigenvector 1 or EV1) derived from these properties was primarily characterized by the anti-correlation between Fe II strength (specifically R_{FeII}, the ratio of EW(Fe II) for the 4434-4684 Å blend to EW(Hβ) and [O III]λ5,007 strength. EV1 also showed significant correlations ($> |0.5|$) with $\log R$, FWHM(Hβ), and Hβ profile asymmetry.

To interpret the PCA results, the authors identified several key parameters that could influence the observed properties: (1) the mass accretion rate, (2) the black hole (BH) mass, (3) the covering factor of the BLR clouds, (4) the degree of anisotropy in the emitted radiation from the continuum source, (5) the orientation of the source to the observer, (6) the velocity distribution of the BLR clouds, and (7) the ionization parameter.

To summarize, the paper by Boroson and Green (1992) is fundamental for two main reasons:

1. It is one of the first publications in AGN research to use principal component analysis (PCA) to explore the connections between the observed properties of quasars, particularly in the study of the Quasar Main Sequence (see right panel of Figure 1 for a recent rendition). This sequence unifies the diverse group of AGNs through Eigenvectors, specifically, Eigenvector 1, which shows an anti-correlation between the width of the optical Fe II blend (4434-4684 Å) and the peak intensity of the forbidden [OIII]λ5,007 Å line. The study also established a connection between the width of the broad Hβ emission and this eigenvector, forming the well-known "Quasar Main Sequence", primarily driven by the Eddington ratio among other physical properties (e.g., Sulentic et al., 2000; Shen and Ho, 2014; Marziani et al., 2018; Panda et al., 2019c, and references therein).
2. For the first time, the paper constructed the Fe II pseudo-continuum template from the optical spectrum of I Zw 1. This template has become widely used in analyzing the optical spectra of AGNs, facilitating the study of the Fe II complex (Phillips, 1978a) both theoretically and observationally. It helped understand the excitation mechanisms (Phillips, 1978b; Verner et al., 1999) behind the thousands of spectral transitions from the UV to the NIR, transforming Fe II from being considered a spectral contaminant to an evolution tracer and fundamental component of the BLR in AGNs (Marinello et al., 2016; Marziani et al., 2018; Panda et al., 2019c; Martínez-Aldama et al., 2021b; Panda, 2022).

1.2 The broad contextualization in the form of 4D Eigenvector 1

An advanced version of the Eigenvector 1 (EV1) schema was introduced by Sulentic et al. (2000), incorporating additional parameters beyond the initial (1) FWHM of the broad component of Hβ and (2) the equivalent width ratio of the optical Fe II blend (4,434–4,684 Å) to broad Hβ (R_{FeII}). These new parameters include (3) the centroid shift at FWHM of the high ionization line C IV λ1,549, c(1/2), and (4) the soft X-ray photon index (Γ_{soft}). Simplified, these measures: (1) the extent of virialized motions in a low-ionization line-emitting accretion disk or a flattened cloud distribution, acting as a virial estimator of black hole mass (e.g., Collin-Souffrin et al., 1988; Dultzin-Hacyan et al., 1999; Joly et al., 2008) (2) the ionization and size of the BLR cloud, with the Fe II emission strength (R_{FeII}) suggesting its origin near the accretion disk; (3) indicators of winds/outflows in high ionization broad line gas; and (4) thermal emission related to the accretion disk and SMBH accretion state (e.g., Mineshige et al., 2000; Done et al., 2012). We refer the readers to a comprehensive summary in Marziani et al. (2018).

Accumulating evidence from subsequent studies, following Boroson and Green (1992), indicates that EV1 correlations involve at least two principal independent parameters: (1) the source's bolometric luminosity (L_{bol}) and its black hole mass (M_{BH}), convolved with source orientation (Marziani et al., 2001; Panda et al., 2019c). These two parameters are succinctly expressed as the Eddington ratio (L_{bol}/L_{Edd}).

1.3 Getting the "bigger" picture

The onset of the new century saw the rise of large spectroscopic surveys, such as the Sloan Digital Sky Survey (SDSS, York et al., 2000; Shen et al., 2011). These surveys revitalized EV1 studies and extended their applicability to much larger samples. Shen and Ho (2014) made significant strides with their seminal paper, utilizing data from over 20,000 spectroscopically observed SDSS quasars, analyzed using an automated spectral fitting pipeline (Shen et al., 2011). This study provided spectral parameters for a wide range of emission lines, as well as estimates for black hole masses and Eddington ratios. Leveraging this comprehensive dataset, Shen and

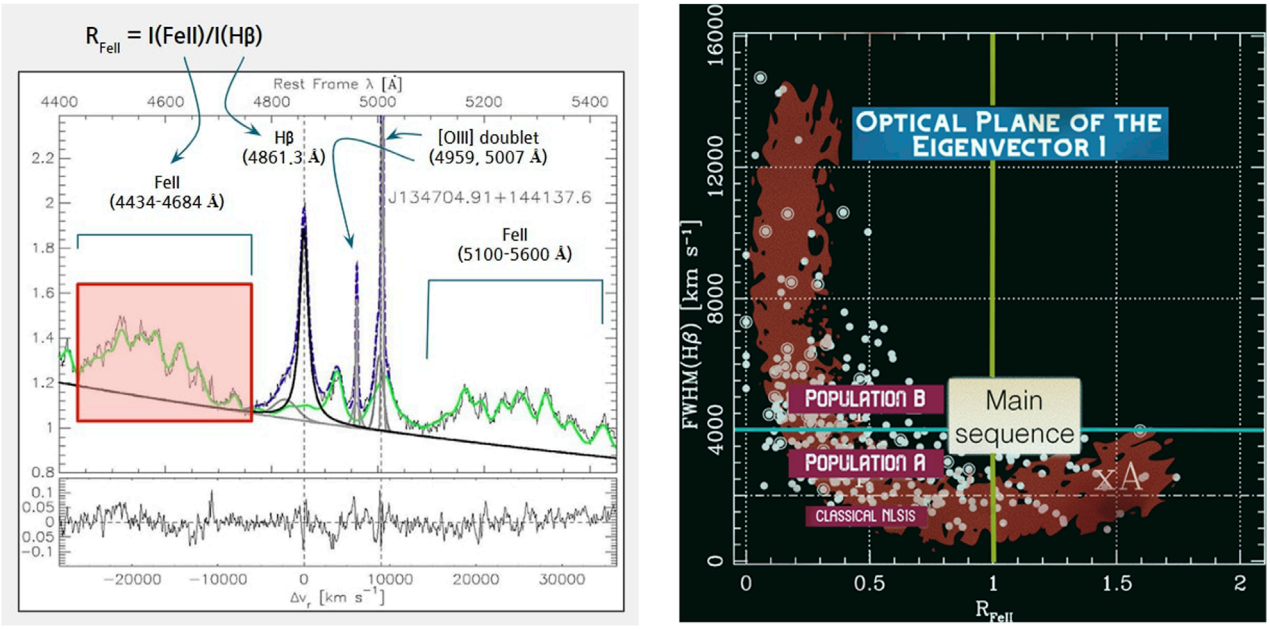

FIGURE 1
Left: Spectral decomposition (optical region) of a Type-1 Narrow-line Seyfert (NLS1) galaxy, SDSS J134704.91 + 144137.6. The original spectrum is shown in light gray, the Hβ profile is fit with a Lorentzian function (solid black) and a blue-shifted outflowing component (solid grey), the fit to the Hβ-[O III] complex is shown in dashed gray, and in green the Fe II pseudocontinuum fit is shown. The shaded region highlights the Fe II blend within 4,434–4,684 Å used to estimate the Fe II strength (wrt broad Hβ), i.e., R_{FeII}. The residua from the fit is shown in the bottom panel. Credit: Negrete et al. (2017); Right: A Schematic diagram of the optical plane of Eigenvector 1. The solid horizontal line (turquoise) represents the threshold in FWHM(Hβ) at 4,000 km s^{-1}, which distinguishes between Population A and Population B sources (Marziani et al., 2018). The "classical" NLS1s are situated below the FWHM(Hβ) $\lesssim$ 2,000 km s^{-1} mark (indicated by the dotted-dashed line). The vertical green line marks the boundary for R_{FeII} = 1, which separates weak from strong Fe II emitters, also known as xA sources. Credit: Panda et al. (2024a), Marziani et al. (2018).

Ho redefined the main sequence of quasars and concluded that (1) the average Eddington ratio increases from left to right on the sequence, and (2) the dispersion in FWHM(Hβ) at a fixed R_{FeII} is largely due to orientation effects (see also Sun and Shen, 2015). They proposed that quasar properties correlated with EV1 can be unified by variations in the average Eddington ratio of the accreting black hole, driven by systematic changes in the shape of the accretion disk continuum and its role in photoionizing the line-emitting regions.

More recently, the exploration of large samples has been extended to include sources from the Southern Hemisphere (Chen et al., 2018, and references therein), and the number of Type-1 AGNs, including strong Fe II-emitting ones, has grown many folds with deeper surveys extending to fainter magnitudes (Rakshit et al., 2020; Wu and Shen, 2022; Paliya et al., 2024; Panda et al., 2024a). We are now at a stage where AGNs are frequently revisited and thus we also have a wealth of multi-epoch, multi-wavelength data for samples of AGNs. This has greatly helped to build samples of AGNs that demonstrate changes in their continuum and emission line properties - the Changing-Look AGNs (see recent compilations in Panda and Śniegowska, 2024; Guo et al., 2024; Zeltyn et al., 2024, and references therein), especially investigating the changes in the Fe II emission in the context of the quasar main sequence (Panda and Śniegowska, 2024).

The paper is organized as follows: In Section 2, we highlight some recent advances in the last decade on the studies with the quasar main sequence - Fe II template creation and improvements, theoretical predictions, and advancements in photoionization modeling including some direct confirmations of long-standing hypotheses. We discuss the connection of the main sequence with one of the fundamental properties demonstrated by AGNs - Variability in Section 3, especially in advancing our knowledge through techniques like reverberation mapping (RM), and the renewed interest in Changing-look/Changing-state AGNs. We then give a brief account of the present-day scenario of incorporating AGNs (and quasars) as *standard(izable)* candles and touch upon some relevant studies that have progressed in this direction. Finally, we conclude this mini-review with some closing remarks and perspective for the future in Section 4 with up-and-coming massive, multiplex surveys that will make things more intriguing.

2 Quasar main sequence - current state and advances

In this section, we touch upon a few of the ongoing, interesting lines of research to improve our understanding of the main sequence of quasars.

2.1 Generating Fe II templates

Owing to its complexity and uncertainties in transition probabilities and excitation mechanisms, the most successful

approach to model the Fe II emission in AGNs consists of deriving empirical templates from observations and supplementing the missing transitions with state-of-the-art radiative transfer models, e.g., CLOUDY (Ferland et al., 2017; Chatzikos et al., 2023). The templates thus derived using this methodology are referred to as semi-empirical. The work of Kovačević et al. (2010) is seminal in this regard who provided the AGN community with an interface[1] to create Fe II templates by combining the Fe II transitions from theoretical expectations and those revealed in the spectrum of the prototypical Fe II-emitter, I Zw 1. Their methodology involves the knowledge of the temperature of the ionized cloud responsible for the Fe II emission, information on the dynamics of the Fe II profile in the observed spectrum, and intensities of the strongest Fe II multiplets collected in three groups (b^4 F, a^6 S, and a^4 G). Their semi-empirical templates have been applied to large samples of AGNs, and demonstrated to provide convincing results. All except one went back to the I Zw 1 - in the optical (e.g., Véron-Cetty et al., 2004; Marziani et al., 2021a), in the UV (e.g., Vestergaard and Wilkes, 2001; Bruhweiler and Verner, 2008; Tsuzuki et al., 2006). The exception happened more recently with the HST/STIS observations for Mrk 493 (Park et al., 2022) which has narrower lines, lower reddening, and a less extreme Eddington ratio value than I Zw 1, therefore, can be applied to a larger population of Type-1 AGNs with intrinsically lower Fe II emission (Shen and Ho, 2014; Panda et al., 2018). These templates also allow us to infer the velocity information of the Fe II emission, a key aspect constraining the geometry and kinematics of the Fe II emitting region in the BLR. Studies (Hu et al., 2008; Ferland et al., 2009; Kovacevic-Dojcinovic and Popovic, 2015) have suggested that the Fe II emission originates from a location different from, and most likely exterior to, the region that produces most of Hβ. These observational findings were confirmed through the analysis of emissivity profiles of AGNs using photoionization modeling (Panda et al., 2018; Sniegowska et al., 2020) and studies of Fe II time-lags relative to the Hβ in samples of AGNs using reverberation mapping (Barth et al., 2013; Gaskell et al., 2022).

In recent years, there has been noteworthy development to improve the atomic datasets available for iron emission, with updated radiative and electron collisional rates, and include higher levels (up to 716) and energies as high as 26.4 eV. We refer the readers to Sarkar et al. (2021) for an overview of these datasets and their performance within the spectral synthesis code, CLOUDY.

2.2 Fe II spectral synthesis and inferring the BLR cloud properties

Over the years after Boroson and Green put forward their findings from the Eigenvector 1, the expected parameters that should influence the observed correlation in the quasar main sequence have been looked at, albeit separately. Notable among them are (i) the Fe II emission model developed in Verner et al. (1999) with 371 atomic levels producing 13,157 (permitted) emission lines with the highest energy level of ~11.6 eV; (ii) study by Baldwin et al. (2004) which were among the first to suggest the importance of microturbulence ($\gtrsim$100 km s^{-1})- the intra-cloud pressure broadening in the broad-line emitting region (BELR) clouds, to explain both the observed shape and equivalent width of the Fe II emission. We note that the findings in Baldwin et al. were confined to the UV regime to recover the 2,200–2,800 Å Fe II bump feature. They also suggested the need to include higher metal abundances in the BELR clouds to recover the observed Fe II intensities, confirming the earlier results from observations by, e.g., Hamann and Ferland (1993), (1999); Dietrich et al. (2003); (iii) the need to have higher mean densities and column densities in the BELR clouds via numerical modeling to recover the Fe II pseudocontinuum behavior, still in the UV regime, was suggested in the paper by Bruhweiler and Verner, who re-affirmed the importance of the microturbulence in the BELR.

In more recent years, a clearer picture of the Fe II emission, especially in the optical region, linking to the quasar main sequence has been achieved. There is a growing consensus that the main sequence of quasars, earlier thought to be primarily driven by the Eddington ratio, is in reality, dependent on a combination of parameters of the underlying accretion disk and the BELR clouds Panda et al. (2018), 2019a,c. These parameters are: (1) Eddington ratio, (2) BH mass; (3) shape of the ionizing continuum (SED); (4) BLR density; (5) BLR metallicity; (6) velocity distribution of the BLR clouds (including microturbulence); (7) source's orientation; and (8) BLR cloud sizes (see Panda, 2021a). The 8-dimensional parameter space was first presented by Panda et al. (2019c), and extended by Panda et al. (2020b) wherein through large grids of photoionization models with CLOUDY and massive observational spectroscopic catalogs (Shen et al., 2011; Rakshit et al., 2020) the inherent trends along the main sequence have been confirmed. This almost completes the circle initiated with the hypotheses in Boroson and Green (1992) although more progress is needed, from observational and theoretical aspects. This multi-dimensional parameterization includes the viewing angle to the source (or orientation), which is constrained for a small fraction of the AGNs, especially those that show strong radio "jetted" emissions (see, e.g., Padovani et al., 2017, for an overview) or strong water masers (Neufeld et al., 1994; Greenhill et al., 2003). For the remaining sources, the viewing angle is estimated indirectly - through dynamical modeling (Pancoast et al., 2011; Li et al., 2013; Williams et al., 2018; Li et al., 2024), through polarization studies of the emission lines (Savić et al., 2018; Jiang et al., 2021; Śniegowska et al., 2023; Jose et al., 2024), or broad-band SED modeling (Yang et al., 2020; Martínez-Ramírez et al., 2024). The knowledge of the viewing angle is crucial since it can be combined with the spatial and velocity distribution of BELR clouds and their location from the central ionizing source, to estimate the black hole mass of the source. The methodology presented by Panda et al. (2020b) is powerful and acts in dual-purpose - for sources with known orientation and spectroscopically measured Fe II emission, it can allow to constrain the BLR density and metallicity. On the other hand, through observed UV diagnostics if the BLR density and metallicity can be inferred (in addition to the Fe II emission), one can recover the orientation angle of the source. The methodology, at present, includes the state-of-the-art broad-band SEDs presented in Panda et al. (2019c) and Ferland et al. (2020), while the BH mass, Eddington ratio, velocity distributions and line intensities are from the SDSS QSO catalogs (Shen et al., 2011; Rakshit et al.,

1 http://servo.aob.rs/FeII_AGN/

2020) for observed AGNs, and can be refined with future multi-wavelength campaigns. Recent works by Pandey et al. (2023, 2024) have extended these results with new, and up-to-date Fe II atomic datasets and accounting for dust within the BLR. Additionally, using these new datasets, Dias dos Santos et al. (2023, 2024) have probed into the Fe II emission in the NIR regime with the added advantage of transitions being isolated and less in number relative to the optical and UV.

In another recent work (Floris et al., 2024), we performed a multi-component analysis on the strongest UV and optical emission lines and using ~10 metal content diagnostic ratios that reveal a systematic progression in metallicity, ranging from sub-solar values to several times higher than solar values. This notable finding was a result of a series of papers (Śniegowska et al., 2021; Garnica et al., 2022; Marziani et al., 2024) wherein a robust recipe of estimating metallicity and other physical parameters in highly-accreting Type-1 AGNs were developed. These results confirm the theoretical predictions made by Panda et al. (2019c) where the increase in the metal content was noted as a key factor that proportionally led to an increase in the Fe II emission along the main sequence.

There are multiple studies predating the aforementioned papers that have paved the way to our current understanding of the Fe II emission and we recommend the readers to the detailed accounts by, e.g., Sulentic et al. (2000); Marziani et al. (2001); Zamfir et al. (2010); D'Onofrio et al. (2012); Shen and Ho (2014); Sulentic and Marziani (2015); Marziani et al. (2018); Gaskell et al. (2022); Panda and Marziani (2023a).

2.3 Developing AGN SEDs along the main sequence

The shape of the ionizing continuum has been an integral part of the main sequence of quasars studies. Around the same time as Boroson and Green, researchers were already developing mean AGN SEDs (Vanden Berk et al., 2001; Richards et al., 2006), be it to distinguish the sources based on radio dichotomy (Laor et al., 1997) and more recently in Marziani et al. (2021a) or to reveal the prominence of the big blue bump feature in typical Type-1 AGNs (Mathews and Ferland, 1987; Korista et al., 1997). With the advent of large spectroscopic surveys spearheaded by SDSS (York et al., 2000; Shen et al., 2011) AGNs exhibiting stronger Fe II emission alike I Zw 1 were being consistently discovered and led to the creation of a mean SED representing Narrow-line Seyfert 1 galaxies (Marziani and Sulentic, 2014). We now have broad-band mean SEDs grouped in Eddington ratios ranging from sub-to super-Eddington limits (Jin et al., 2012; 2017; Ferland et al., 2020). Although these mean SEDs have helped provide statistical inferences on the role of AGN SED in the main sequence trends, having broad-band SED for individual AGNs is a much more recent endeavor that has seen growth. With the increase in simultaneous observations across multiple spectral regimes and the development of self-consistent AGN SED models (Done et al., 2012; Kubota and Done, 2018; 2019; Hagen and Done, 2023), the number of individual sources with broad-band SEDs is growing at a rapid pace, especially for sources demonstrating the most intense Fe II emission (Marinello et al., 2020; Jin et al., 2023). Another important extension in the area of SED building is the slim disk AGN SED models (Abramowicz et al., 1988; Wang et al., 2014; Panda and Marziani, 2023b) applicable to those sources accreting at or above the Eddington limit, that show signatures of strong outflows even in the low-ionization emitting regions (e.g., Rodríguez-Ardila et al., 2024).

3 QMS and AGN variability

Another equally important finding was the discovery of the variation in the intensities of emission lines over timescales of weeks to months, suggesting very small emitting regions of the order of a few thousand Schwarzschild radii (Greenstein and Schmidt, 1964). This region is now well-known as the broad-line region (BLR). This crucial discovery opened up a new sub-field called reverberation mapping (RM), which has led to the estimation of black hole masses in hundreds of low-to high-luminosity Seyferts and quasars (Blandford and McKee, 1982; Peterson, 1988; 1993; Peterson et al., 2004), supplemented by single/multi-epoch spectroscopy (Kaspi et al., 2000; Bentz et al., 2013; Du et al., 2016). The BLR's location (R_{BLR}) is closely related to the continuum properties of the underlying accretion disk, with luminosity being the primary observable quantity (Kaspi et al., 2005, and references therein). Subsequent studies, such as Bentz et al. (2013), refined the Hβ-based R_{BLR} - L_{5100} (or R-L) relation by including more sources and removing the host galaxy's contribution from the total luminosity. Increased monitoring of archival and newer sources has revealed a significant scatter from the empirical R-L relation (Du et al., 2015; Grier et al., 2017; Martínez-Aldama et al., 2019; Du and Wang, 2019; Panda et al., 2019b). This scatter indicates a subset of sources with relatively high luminosities (log L_{5100} = 43.0, in erg s^{-1}) that exhibit shorter time lags and thus shorter R_{BLR} than expected. Recent studies suggest that this scatter may be linked to the accretion rate, providing corrections to the empirical relation based on observables that trace the accretion rate, such as the strength of the optical Fe II emission (Du and Wang, 2019; Panda, 2022; Panda and Marziani, 2023a).

On the other hand, the complexity in the modeling and extracting Fe II emission from the spectra has led many to search for viable alternatives. Most prominent among the proxy is the Ca II triplet (or CaT) in the NIR given the similarity of the physical conditions required to produce the two ionic species in the BLR (Panda et al., 2020a; Panda, 2021b). In an ongoing series of works (Martínez-Aldama et al., 2015; Marinello et al., 2016; Panda et al., 2020a; Martínez-Aldama et al., 2021b), we have compiled optical Fe II and NIR CaT emission strengths and weighed them against each other. We find a robust correlation between the two (Martínez-Aldama et al., 2015; Panda et al., 2020a) primarily driven by the Eddington ratio and in parts to the BH mass (Martínez-Aldama et al., 2021b). This led us to investigate whether CaT can be a viable replacement for the strength of the Fe II emission (or $R_{Fe\,II}$) in the R-L relation (Martínez-Aldama et al., 2021a). Although the current sample statistics are small in the NIR regime, the spurt of high-quality AGN spectra with the JWST and other ground-based facilities is promising.

3.1 Changing-look AGNs and our renewed interest in them

Changing-look AGNs have been known for almost as long as the main sequence existed (see recent review by Komossa et al., 2024; Ricci and Trakhtenbrot, 2023). The spectral changes over multiple epochs have now been detected in numerous AGNs - be it extreme variability with the changes in the continuum and emission lines so strong that can be associated with external interference such as obscuration or tidal disruption events (LaMassa et al., 2015; Dodd et al., 2023; Trakhtenbrot et al., 2019), but could very well be associated with intrinsic effects such as disk transition/disk instabilities (Noda and Done, 2018; Ross et al., 2018; Sniegowska et al., 2020) although, the timescales of such events can be widely different (Czerny, 2006).

With the growing interest in finding new changing-look AGNs, the focus has been also to look for AGNs showing variations in their Fe II emission (see, e.g., Gaskell et al., 2022; Petrushevska et al., 2023). The regular variable nature of AGNs has helped to gain insights into their emitting regions, with some sources where we have estimates of their Fe II-emitting locations (see, e.g., Hu et al., 2015; Barth et al., 2013) although there are now instances of exceptional changes in the Fe II intensities. Panda and Śniegowska (2024) made a compilation of such sources and tracked their transition along the Eigenvector 1 schema and categorized sources that either stay within the same population (A or B, see right panel of Figure 1) or make an inter-population movement as a function of spectral epoch.

3.2 New avenues in reverberation mapping: BLR saturation and Fe II-based R-L relations

In addition to Changing-look AGNs, dedicated spectro-photometric monitoring campaigns on individual sources (e.g., Mrk 6, NGC 5548, NGC 4151, NGC 4051), have allowed us to re-affirm the Pronik-Chuvaev effect, i.e., the increase, albeit with a gradual saturation, in the Hβ emitting luminosity with increasing AGN continuum (Pronik and Chuvaev, 1972; Wang et al., 2005; Shapovalova et al., 2008; Gaskell et al., 2021) and more recently in Panda et al. (2022); 2023a. This assists in building the R-L relation for individual epochs and gaining insights into the temporal behavior of the line-emitting BLR relative to the continuum (Zu et al., 2011; Lu et al., 2022; Feng et al., 2024) although studies to reveal the temporal behavior specifically in Fe II are needed to complement the Hβ behavior in these AGNs.

Another interesting revelation has been the construction of the first Fe II UV R-L relation in Zajaček et al. (2024b). Here, in addition to improving the existing Mg II-based R-L with 194 sources [more recent compilation in Shen et al. (2024)], we have been able to constrain the R-L behavior in UV-emitting Fe II for 5 AGNs. The results are motivating as the slope of the R-L is in close agreement with one expected from the standard photoionization theory (i.e., = 0.5). Although it is interesting to note that this relation appears steeper than the Mg II R-L relations such that for low-luminosity regimes, the Fe II emitting region is closer than the Mg II-emitting region, whereas, at higher luminosities, both relations converge and intersect. This intriguing behaviour needs more explanation which the upcoming RM campaigns may have an answer to. We note that the optical Fe II-based R-L relation has been around for some time (see Gaskell et al., 2022, for a recent review). A recent compilation of 17 AGNs (including multiple epoch Fe II time lag measurements) from Prince et al. (2023) reveals an R-L for the optical Fe II with a slope close to 0.5, and the comparison with the aforementioned UV-based R-L reveals an offset by a factor of 1.8, i.e., the optical Fe II emitting regions are located 1.8 times further out relative to the UV Fe II regions.

3.3 Quasars for cosmology: role of the main sequence

Quasars, with their extragalactic origin and persistent bright nature, have long been proposed as "standardizable candles". With the knowledge of their luminosities (with the aid of the RM and R-L relation) and independently of their fluxes from spectroscopic monitoring, we can determine the luminosity distances of these sources. With a growing number of AGNs (now ≳200, Zajaček et al., 2024b; Shen et al., 2024) where we have such estimates, then allows us to prepare a Hubble diagram - stretching the redshift regime to higher ranges as compared to what we can achieve with other indicators, e.g., Cepheids, Tip of the Red Giant Branch (TRGB), and Type-1a Supernovae (SNIa). We can then scrutinize the various, existing cosmological models, in addition to gauging the performance of quasars to existing indicators, allowing us to link the cosmological measurements from the early Universe (e.g., Planck Collaboration et al., 2020) to the measurements from the late Universe (e.g., Cepheids, SNIa, and TRGBs; Riess et al., 1998; Riess et al., 2019; Freedman et al., 2019).

However, the recent detection of shorter lags in R-L linked to high-accreting sources (Du et al., 2015; Grier et al., 2017; Du et al., 2016) has put the use of R-L relation into uncertainty. In Martínez-Aldama et al. (2019), we looked into the dispersion in the R-L and upon further investigation found the extent of offset of the source's time-lag is proportional to the Eddington ratio (or more specifically its mass accretion rate). While this helped "standardize" the R-L relation, there remained a circularity problem - the mass accretion rate needs the knowledge of luminosity *apriori*, and the latter can be estimated assuming a cosmological model. This defeats the purpose of using quasars for cosmology and thus, requires us to find a direct observable parameter that can replace the mass accretion rate. What can be that? In Du and Wang (2019), the authors found that the Fe II strength (or $R_{Fe\,II}$) is a viable alternative to the mass accretion rate (as has been noted in earlier works of Marziani et al., 2018; Panda et al., 2019c) and can correct the dispersion in the R-L. This $R_{Fe\,II}$-dependent R-L relation has hence been tested and confirmed in other works (Panda, 2022; Panda and Marziani, 2023a). Other empirical relations notably the L_X - L_{UV} relation, are proposed as a viable alternative to the R-L relation (Risaliti and Lusso, 2015; 2019) although there are subtle differences between the two relations and their inferences. Yet another methodology has been proposed, i.e., with the aid of the existing correlation between the luminosity and the velocity distribution of the BELR (Dultzin et al., 2020; Marziani et al., 2021b), equivalent to the original formulation of the Faber-Jackson law (Faber and Jackson, 1976). We refer the readers to Panda and Marziani (2023a) for more details.

In a parallel direction, efforts to reconcile the use of quasars along with other distance indicators, e.g., SNIa, Gamma-ray bursts, Baryon Acoustic Oscillations, and temperature anisotropy across the microwave background, have been made including the $R_{Fe\,II}$ parameter for the quasar-based R-L relations (Cao et al., 2022; Khadka et al., 2023; Dainotti et al., 2023). Other systematics, such as dust extinction can contribute to and reconcile the observed difference between the R-L and L_X - L_{UV} relation (Zajaček et al., 2024a). As we enter into the discussions around Hubble-Lemaître law and the H_0 tension, a key to resolving this is better measurements of cosmological distances. VLT/GRAVITY has opened up avenues to probe the angular sizes of the BLR in nearby AGNs using high-resolution spectroastrometry (Gravity Collaboration et al., 2018; Gravity Collaboration et al., 2020; Gravity Collaboration et al., 2021; Gravity Collaboration et al., 2024). These angular sizes can be combined with the BLR linear sizes (the latter estimated using the RM technique) to give the parallax distance to these AGNs. The technique was originally conceived in Elvis and Karovska (2002) although thanks to the recent interferometric measurements by GRAVITY coupled with their long-term RM monitoring campaign, Wang et al. (2020) have been able to estimate, for the first time, a H_0 value using this joint analysis with AGNs. Ongoing improvements with GRAVITY (see, e.g., Nowak et al., 2024) will allow the compilation of a sizable sample of AGNs extending to z ~ two where the spectroastrometric-RM (or, SARM) technique can be applied to build the Hubble diagram for quasars. This however requires the knowledge of the BLR properties that are neatly tied to the quasar main sequence which positively affect the accuracy of the estimation of the cosmological distances to these cosmic objects.

4 Closing remarks and future perspective

Fe II emission has been long perceived as a contaminant in the AGN spectra and ways to remove this contamination were sought to enable study and reliable extraction of other emission line properties. The emission turned out to be so useful that a niche of studies linking to the Fe II emission was proposed and expanded. To date, the studies stemming from the Fe II analysis have crucial contributions in developing our understanding of the line-emitting regions in the BLR leading up to the standardization of quasar-based scaling relations. This mini-review cannot do justice to the enormous literature about the study of Fe II emission and its link to the quasar main sequence. Yet, we have tried to touch upon some key aspects in this short overview. We are already in the data-driven astronomy era with multiple facilities working in cohesion, to reveal more connections to the quasar main sequence.

Finally, we glance upon some recent avenues that will have a direct impact on the ongoing studies:

- Ongoing and upcoming spectroscopic surveys such as JWST (Rigby et al., 2023), MSE (Marshall et al., 2019), WST (Mainieri et al., 2024), 4MOST (de Jong et al., 2019) are going to help reveal intriguing Fe II signatures in low-luminosity regimes and distant quasars, e.g., JWST ASPIRE (and references therein Yang et al., 2023) showing high Fe II emitting AGNs beyond the cosmic noon; putting into question the prevalence of heavy metals in such early epochs. Additionally, Additionally, the first couple of years of observations with JWST has revealed the numerous faint, broad-line AGN at z > 5 (Onoue et al., 2023; Kocevski et al., 2023; Harikane et al., 2023; Matthee et al., 2024; Maiolino et al., 2023; Larson et al., 2023; Greene et al., 2024). A significant fraction of them (~20%) show a steep red continuum in the rest-frame optical region, in addition to being relatively bluer in the UV (Kocevski et al., 2023; Harikane et al., 2023; Matthee et al., 2024; Greene et al., 2024; Killi et al., 2023) giving the appearance of a "V-shape" in the SEDs for these intriguing objects. These sources, also known as "little red dots" (LRDs, Matthee et al., 2024; Kocevski et al., 2024), and while the prominent broad emission lines (i.e., Balmer lines) are relatively easier to deblend. Their profiles can be fitted even under moderate spectral quality, while complex emissions like the Fe II would require future deeper observations to check their location on the main sequence of quasars to reveal their nature and chemical history at such redshifts.
- On the other hand, the large-scale photometric surveys (e.g., ZTF: Bellm et al., 2019, LSST; Ivezić et al., 2019, Euclid; Euclid Collaboration et al., 2022) will identify newer AGNs, and combined with the wide-area spectroscopic surveys will allow constraining the Fe II contribution and improve our understanding of the various mechanisms involved in Fe II production across UV-optical-NIR regime, especially dealing with time-lag recovery and extracting broad-band SED for tens of hundreds of AGNs across a wide range of redshifts (see Panda et al., 2023b, for a recent review).
- With the LSST about to begin its decade-long survey, the use of meter-class ground-based facilities in cohesion with such massive surveys will be pertinent (Chelouche et al., 2019; Panda et al., 2024b); narrow-band filters will allow optimizing the lag-recovery by mitigating spectral windows with contamination. While, the use of traditional and machine-learning techniques are going to be integral for target selection from erstwhile surveys (Baron, 2019; Sánchez-Sáez et al., 2021; López-Navas et al., 2022; Śniegowska et al., 2023).

Author contributions

SP: Conceptualization, Data curation, Formal Analysis, Funding acquisition, Investigation, Methodology, Project administration, Resources, Software, Supervision, Validation, Visualization, Writing–original draft, Writing–review and editing.

Funding

The author(s) declare financial support was received for the research, authorship, and/or publication of this article. SP acknowledges the financial support of the Conselho Nacional de Desenvolvimento Científico e Tecnológico (CNPq) Fellowships

300936/2023-0 and 301628/2024-6. SP is supported by the international Gemini Observatory, a program of NSF NOIRLab, which is managed by the Association of Universities for Research in Astronomy (AURA) under a cooperative agreement with the U.S. National Science Foundation, on behalf of the Gemini partnership of Argentina, Brazil, Canada, Chile, the Republic of Korea, and the United States of America.

Acknowledgments

This mini-review has been made possible thanks to many past and ongoing collaborations; I would like to thank Bożena Czerny, Paola Marziani, Alberto Rodríguez Ardila, Mary Loli Martínez-Aldama, Murilo Marinello, Marzena Śniegowska, Francisco Pozo-Nuñez, Michal Zajaček, Edi and Nataša Bon, Szymon Kozłowski and many others for their invaluable support, constant motivation and fruitful discussions. I am grateful to the organizers of the "Frontiers in Astronomy and Space Sciences: A Decade of Discovery and Advancement - 10th Anniversary Conference" for the invitation to write this mini-review.

Conflict of interest

The author declares that the research was conducted in the absence of any commercial or financial relationships that could be construed as a potential conflict of interest.

Publisher's note

All claims expressed in this article are solely those of the authors and do not necessarily represent those of their affiliated organizations, or those of the publisher, the editors and the reviewers. Any product that may be evaluated in this article, or claim that may be made by its manufacturer, is not guaranteed or endorsed by the publisher.

References

Abramowicz, M. A., Czerny, B., Lasota, J. P., and Szuszkiewicz, E. (1988). Slim accretion disks. *ApJ* 332, 646. doi:10.1086/166683

Baldwin, J. A., Ferland, G. J., Korista, K. T., Hamann, F., and LaCluyzé, A. (2004). The origin of Fe II emission in active galactic nuclei. *ApJ* 615, 610–624. doi:10.1086/424683

Baron, D. (2019). Machine learning in astronomy: a practical overview. *arXiv e-prints, arXiv:1904.07248doi*. doi:10.48550/arXiv.1904.07248

Barth, A. J., Pancoast, A., Bennert, V. N., Brewer, B. J., Canalizo, G., Filippenko, A. V., et al. (2013). The lick AGN monitoring project 2011: Fe II reverberation from the outer broad-line region. *ApJ* 769, 128. doi:10.1088/0004-637X/769/2/128

Bellm, E. C., Kulkarni, S. R., Graham, M. J., Dekany, R., Smith, R. M., Riddle, R., et al. (2019). The zwicky transient facility: system overview, performance, and first results. *PASP* 131, 018002. doi:10.1088/1538-3873/aaecbe

Bentz, M. C., Denney, K. D., Grier, C. J., Barth, A. J., Peterson, B. M., Vestergaard, M., et al. (2013). The low-luminosity end of the radius-luminosity relationship for active galactic nuclei. *ApJ* 767, 149. doi:10.1088/0004-637X/767/2/149

Blandford, R. D., and McKee, C. F. (1982). Reverberation mapping of the emission line regions of Seyfert galaxies and quasars. *ApJ* 255, 419–439. doi:10.1086/159843

Boroson, T. A., and Green, R. F. (1992). The emission-line properties of low-redshift quasi-stellar objects. *ApJS* 80, 109. doi:10.1086/191661

Bruhweiler, F., and Verner, E. (2008). Modeling Fe II emission and revised Fe II (UV) empirical templates for the Seyfert 1 galaxy I Zw 1. *ApJ* 675, 83–95. doi:10.1086/525557

Cao, S., Zajaček, M., Panda, S., Martínez-Aldama, M. L., Czerny, B., and Ratra, B. (2022). Standardizing reverberation-measured C IV time-lag quasars, and using them with standardized Mg II quasars to constrain cosmological parameters. *MNRAS* 516, 1721–1740. doi:10.1093/mnras/stac2325

Chatzikos, M., Bianchi, S., Camilloni, F., Chakraborty, P., Gunasekera, C. M., Guzmán, F., et al. (2023). The 2023 release of cloudy. *RevMexA&A* 59, 327–343. doi:10.22201/ia.01851101p.2023.59.02.12

Chelouche, D., Pozo Nuñez, F., and Kaspi, S. (2019). Direct evidence of non-disk optical continuum emission around an active black hole. *Nat. Astron.* 3, 251–257. doi:10.1038/s41550-018-0659-x

Chen, S., Berton, M., La Mura, G., Congiu, E., Cracco, V., Foschini, L., et al. (2018). Probing narrow-line Seyfert 1 galaxies in the southern hemisphere. *A&A* 615, A167. doi:10.1051/0004-6361/201832678

Collin-Souffrin, S., Dyson, J. E., McDowell, J. C., and Perry, J. J. (1988). The environment of active galactic nuclei - I. A two-component broad emission line model. *MNRAS* 232, 539–550. doi:10.1093/mnras/232.3.539

Czerny, B. (2006). "The role of the accretion disk in AGN variability In *AGN Variability from X-Rays to radio waves*," in *360 of astronomical Society of the pacific conference series* Editors C. M. Gaskell, I. M. McHardy, B. M. Peterson, and S. G. Sergeev, 265

Dainotti, M. G., Bargiacchi, G., Bogdan, M., Lenart, A. L., Iwasaki, K., Capozziello, S., et al. (2023). Reducing the uncertainty on the Hubble constant up to 35% with an improved statistical analysis: different best-fit likelihoods for type ia Supernovae, Baryon acoustic Oscillations, quasars, and gamma-ray bursts. *ApJ* 951, 63. doi:10.3847/1538-4357/acd63f

de Jong, R. S., Agertz, O., Berbel, A. A., Aird, J., Alexander, D. A., Amarsi, A., et al. (2019). 4MOST: project overview and information for the first call for proposals. *Messenger* 175, 3–11. doi:10.18727/0722-6691/5117

Dias dos Santos, D., Panda, S., Rodriguez-Ardila, A., and Marinello, M. (2023). Modelling the strong Fe II emission: simultaneous photoionization modelling in optical and NIR. *Bol. Soc. Astron. Bras.* 34, 295–299.

Dias dos Santos, D., Panda, S., Rodríguez-Ardila, A., and Marinello, M. (2024). Joint analysis of the iron emission in the optical and near-infrared spectrum of I Zw 1. *Physics* 6, 177–193. doi:10.3390/physics6010013

Dietrich, M., Hamann, F., Appenzeller, I., and Vestergaard, M. (2003). Fe II/Mg II emission-line ratio in high-redshift quasars. *ApJ* 596, 817–829. doi:10.1086/378045

Dodd, S. A., Nukala, A., Connor, I., Auchettl, K., French, K. D., Law-Smith, J. A. P., et al. (2023). Mid-infrared outbursts in nearby galaxies: nuclear obscuration and connections to hidden tidal disruption events and changing-look active galactic nuclei. *ApJl* 959, L19. doi:10.3847/2041-8213/ad1112

Done, C., Davis, S. W., Jin, C., Blaes, O., and Ward, M. (2012). Intrinsic disc emission and the soft X-ray excess in active galactic nuclei. *MNRAS* 420, 1848–1860. doi:10.1111/j.1365-2966.2011.19779.x

D'Onofrio, M., Marziani, P., and Sulentic, J. W. (2012). *Fifty years of quasars: from early observations and ideas to future research* (Heidelberg, Germany: of Astrophysics and Space Science Library), 386. doi:10.1007/978-3-642-27564-7

Du, P., Hu, C., Lu, K.-X., Huang, Y.-K., Cheng, C., Qiu, J., et al. (2015). Supermassive black holes with high accretion rates in active galactic nuclei. IV. Hβ Time lags and implications for super-eddington accretion. *ApJ* 806, 22. doi:10.1088/0004-637X/806/1/22

Du, P., Lu, K.-X., Zhang, Z.-X., Huang, Y.-K., Wang, K., Hu, C., et al. (2016). Supermassive black holes with high accretion rates in active galactic nuclei. V. A new size-luminosity scaling relation for the broad-line region. *ApJ* 825, 126. doi:10.3847/0004-637X/825/2/126

Du, P., and Wang, J.-M. (2019). The radius-luminosity relationship depends on optical spectra in active galactic nuclei. *ApJ* 886, 42. doi:10.3847/1538-4357/ab4908

Dultzin, D., Marziani, P., de Diego, J. A., Negrete, C. A., Del Olmo, A., Martínez-Aldama, M. L., et al. (2020). Extreme quasars as distance indicators in cosmology. *Front. Astronomy Space Sci.* 6, 80. doi:10.3389/fspas.2019.00080

Dultzin-Hacyan, D., Taniguchi, Y., and Uranga, L. (1999). "Where is the Ca II triplet emitting region in AGN? In *Structure and Kinematics of quasar broad line regions*,". *Astronomical society of the pacific conference series*. Editors C. M. Gaskell, W. N. Brandt, M. Dietrich, D. Dultzin-Hacyan, and M. Eracleous, 175, 303.

Elvis, M., and Karovska, M. (2002). Quasar parallax: a method for determining direct geometrical distances to quasars. *ApJl* 581, L67–L70. doi:10.1086/346015

Euclid Collaboration, Scaramella, R., Amiaux, J., Mellier, Y., Burigana, C., Carvalho, C. S., and Cuillandre, J.-C. (2022). Euclid preparation. I. The Euclid wide survey. *A&A* 662, A112. doi:10.1051/0004-6361/202141938

Faber, S. M., and Jackson, R. E. (1976). Velocity dispersions and mass-to-light ratios for elliptical galaxies. *ApJ* 204, 668–683. doi:10.1086/154215

Feng, H.-C., Li, S.-S., Bai, J. M., Liu, H. T., Lu, K.-X., Pang, Y.-X., et al. (2024). *Velocity-resolved reverberation mapping of changing-look active galactic nucleus NGC 4151 during outburst stage. II. Four season observation results*. arXiv e-prints. arXiv:2409.01637.

Ferland, G. J., Chatzikos, M., Guzmán, F., Lykins, M. L., van Hoof, P. A. M., Williams, R. J. R., et al. (2017). The 2017 release cloudy. *RevMexA&Ap* 53, 385–438. doi:10.48550/arXiv.1705.10877

Ferland, G. J., Done, C., Jin, C., Landt, H., and Ward, M. J. (2020). State-of-the-art AGN SEDs for photoionization models: BLR predictions confront the observations. *MNRAS* 494, 5917–5922. doi:10.1093/mnras/staa1207

Ferland, G. J., Hu, C., Wang, J.-M., Baldwin, J. A., Porter, R. L., van Hoof, P. A. M., et al. (2009). Implications of infalling Fe II-emitting clouds in active galactic nuclei: anisotropic properties. *ApJl* 707, L82–L86. doi:10.1088/0004-637X/707/1/L82

Floris, A., Marziani, P., Panda, S., Sniegowska, M., D'Onofrio, M., Deconto-Machado, A., et al. (2024). Chemical abundances along the quasar main sequence. *arXiv e-prints, arXiv:2405.04456doi*. doi:10.1051/0004-6361/202450458

Francis, P. J., and Wills, B. J. (1999). "Introduction to principal components analysis," in *Quasars and cosmology. 162 of astronomical Society of the pacific conference series*. Editors G. Ferland, and J. Baldwin, 363. doi:10.48550/arXiv.astro-ph/9905079

Freedman, W. L., Madore, B. F., Hatt, D., Hoyt, T. J., Jang, I. S., Beaton, R. L., et al. (2019). The carnegie-chicago Hubble program VIII An independent determination of the Hubble constant based on the Tip of the red giant Branch. *ApJ* 882, 34. doi:10.3847/1538-4357/ab2f73

Garnica, K., Negrete, C. A., Marziani, P., Dultzin, D., Śniegowska, M., and Panda, S. (2022). High metal content of highly accreting quasars: analysis of an extended sample. *A&A* 667, A105. doi:10.1051/0004-6361/202142837

Gaskell, C. M., Bartel, K., Deffner, J. N., and Xia, I. (2021). Anomalous broad-line region responses to continuum variability in active galactic nuclei – I. Hβ variability. *MNRAS* 508, 6077–6091. doi:10.1093/mnras/stab2443

Gaskell, M., Thakur, N., Tian, B., and Saravanan, A. (2022). Fe II emission in active galactic nuclei. *Astron. Nachrichten* 343, e210112. doi:10.1002/asna.20210112

Gravity Collaboration, Sturm, E., Dexter, J., Pfuhl, O., Stock, M. R., Davies, R. I., and Lutz, D. (2018). Spatially resolved rotation of the broad-line region of a quasar at sub-parsec scale. *Nat* 563, 657–660. doi:10.1038/s41586-018-0731-9

GRAVITY Collaboration, Amorim, A., Bauböck, M., Brandner, W., Clénet, Y., Davies, R., and de Zeeuw, P. T. (2020). The spatially resolved broad line region of IRAS 09149-6206. *A&A* 643, A154. doi:10.1051/0004-6361/202039067

GRAVITY Collaboration, Amorim, A., Bauböck, M., Brandner, W., Bolzer, M., Clénet, Y., and Davies, R. (2021). The central parsec of NGC 3783: a rotating broad emission line region, asymmetric hot dust structure, and compact coronal line region. *A&A* 648, A117. doi:10.1051/0004-6361/202040061

GRAVITY Collaboration, Amorim, A., Bourdarot, G., Brandner, W., Cao, Y., Clénet, Y., and Davies, R. (2024). The size-luminosity relation of local active galactic nuclei from interferometric observations of the broad-line region. *A&A* 684, A167. doi:10.1051/0004-6361/202348167

Greene, J. E., Labbe, I., Goulding, A. D., Furtak, L. J., Chemerynska, I., Kokorev, V., et al. (2024). UNCOVER spectroscopy confirms the surprising ubiquity of active galactic nuclei in red sources at z > 5. *ApJ* 964, 39. doi:10.3847/1538-4357/ad1e5f

Greenhill, L. J., Kondratko, P. T., Lovell, J. E. J., Kuiper, T. B. H., Moran, J. M., Jauncey, D. L., et al. (2003). The discovery of H_2O maser emission in seven active galactic nuclei and at high velocities in the circinus galaxy. *ApJl* 582, L11–L14. doi:10.1086/367602

Greenstein, J. L., and Schmidt, M. (1964). The quasi-stellar radio sources 3C 48 and 3C 273. *ApJ* 140, 1. doi:10.1086/147889

Grier, C. J., Trump, J. R., Shen, Y., Horne, K., Kinemuchi, K., McGreer, I. D., et al. (2017). The sloan digital Sky survey reverberation mapping project: hα and Hβ reverberation measurements from first-year spectroscopy and Photometry. *ApJ* 851, 21. doi:10.3847/1538-4357/aa98dc

Guo, W.-J., Zou, H., Greenwell, C. L., Alexander, D. M., Fawcett, V. A., Pan, Z., et al. (2024) Changing-look active galactic nuclei from the dark energy spectroscopic instrument. II. Statistical properties from the first data release. *arXiv:2408*. doi:10.48550/arXiv.2408.00402

Hagen, S., and Done, C. (2023). Estimating black hole spin from AGN SED fitting: the impact of general-relativistic ray tracing. *MNRAS* 525, 3455–3467. doi:10.1093/mnras/stad2499

Hamann, F., and Ferland, G. (1993). The chemical evolution of QSOs and the implications for cosmology and galaxy formation. *ApJ* 418, 11. doi:10.1086/173366

Hamann, F., and Ferland, G. (1999). Elemental abundances in quasistellar objects: star formation and galactic nuclear evolution at high redshifts. *ARA* 37, 487–531. doi:10.1146/annurev.astro.37.1.487

Harikane, Y., Zhang, Y., Nakajima, K., Ouchi, M., Isobe, Y., Ono, Y., et al. (2023). A JWST/NIRSpec first census of broad-line AGNs at z = 4-7: detection of 10 faint AGNs with M_{BH} 10^6 -10^8 $M_\odot$ and their host galaxy properties. *ApJ* 959, 39. doi:10.3847/1538-4357/ad029e

Hertzsprung, E. (1911). Ueber die Verwendung photographischer effektiver Wellenlaengen zur Bestimmung von Farbenaequivalenten. *Publ. Astrophys. Obs. Potsdam* 63.

Hu, C., Du, P., Lu, K.-X., Li, Y.-R., Wang, F., Qiu, J., et al. (2015). Supermassive black holes with high accretion rates in active galactic nuclei. III. Detection of Fe II reverberation in nine narrow-line Seyfert 1 galaxies. *ApJ* 804, 138. doi:10.1088/0004-637X/804/2/138

Hu, C., Wang, J.-M., Ho, L. C., Chen, Y.-M., Zhang, H.-T., Bian, W.-H., et al. (2008). A systematic analysis of Fe II emission in quasars: evidence for inflow to the central black hole. *ApJ* 687, 78–96. doi:10.1086/591838

Ivezić, Ž., Kahn, S. M., Tyson, J. A., Abel, B., Acosta, E., Allsman, R., et al. (2019). LSST: from science drivers to reference design and anticipated data products. *ApJ* 873, 111. doi:10.3847/1538-4357/ab042c

Jiang, B.-W., Marziani, P., Savić, D., Shablovinskaya, E., Popović, L. Č., Afanasiev, V. L., et al. (2021). Linear spectropolarimetric analysis of Fairall 9 with VLT/FORS2. *MNRAS* 508, 79–99. doi:10.1093/mnras/stab2273

Jin, C., Done, C., Ward, M., and Gardner, E. (2017). Super-Eddington QSO RX J0439.6-5311 - II. Multiwavelength constraints on the global structure of the accretion flow. *MNRAS* 471, 706–721. doi:10.1093/mnras/stx1634

Jin, C., Done, C., Ward, M., Panessa, F., Liu, B., and Liu, H.-Y. (2023). The extreme super-eddington NLS1 RX J0134.2-4258 - II. A weak-line Seyfert linking to the weak-line quasar. *MNRAS* 518, 6065–6082. doi:10.1093/mnras/stac3513

Jin, C., Ward, M., and Done, C. (2012). A combined optical and X-ray study of unobscured type 1 active galactic nuclei - III. Broad-band SED properties. *MNRAS* 425, 907–929. doi:10.1111/j.1365-2966.2012.21272.x

Joly, M., Véron-Cetty, M., and Véron, P. (2008). "Fe II emission in AGN," in *Revista Mexicana de Astronomia y Astrofisica Conference Series. vol. 32 of Revista Mexicana de Astronomia y Astrofisica Conference Series*, 59–61.

Jose, J., Rakshit, S., Panda, S., Woo, J.-H., Stalin, C. S., Neha, S., et al. (2024). Spectropolarimetric view of the gamma-ray emitting NLS1 1H0323 + 342. *MNRAS* 532, 3187–3197. doi:10.1093/mnras/stae1691

Kaspi, S., Maoz, D., Netzer, H., Peterson, B. M., Vestergaard, M., and Jannuzi, B. T. (2005). The relationship between luminosity and broad-line region size in active galactic nuclei. *ApJ* 629, 61–71. doi:10.1086/431275

Kaspi, S., Smith, P. S., Netzer, H., Maoz, D., Jannuzi, B. T., and Giveon, U. (2000). Reverberation measurements for 17 quasars and the size-mass-luminosity relations in active galactic nuclei. *ApJ* 533, 631–649. doi:10.1086/308704

Kellermann, K. I., Sramek, R., Schmidt, M., Shaffer, D. B., and Green, R. (1989). VLA observations of objects in the palomar bright quasar survey. *AJ* 98, 1195. doi:10.1086/115207

Khadka, N., Zajaček, M., Prince, R., Panda, S., Czerny, B., Martínez-Aldama, M. L., et al. (2023). Quasar UV/X-ray relation luminosity distances are shorter than reverberation-measured radius-luminosity relation luminosity distances. *MNRAS* 522, 1247–1264. doi:10.1093/mnras/stad1040

Killi, M., Watson, D., Brammer, G., McPartland, C., Antwi-Danso, J., Newshore, R., et al. (2023). Deciphering the JWST spectrum of a 'little red dot' at z ~ 4.53: an obscured AGN and its star-forming host. *arXiv e-prints*. arXiv:2312.03065doi. doi:10.48550/arXiv.2312.03065

Kocevski, D. D., Finkelstein, S. L., Barro, G., Taylor, A. J., Calabrò, A., Laloux, B., et al. (2024). The rise of faint, red AGN at z > 4: a sample of little red dots in the JWST extragalactic legacy fields. *arXiv e-prints*. arXiv:2404.03576doi. doi:10.48550/arXiv.2404.03576

Kocevski, D. D., Onoue, M., Inayoshi, K., Trump, J. R., Arrabal Haro, P., Grazian, A., et al. (2023). Hidden little monsters: spectroscopic identification of low-mass, broad-line AGNs at z > 5 with CEERS. *ApJl* 954, L4. doi:10.3847/2041-8213/ace5a0

Komossa, S., Grupe, D., Marziani, P., Popovic, L. C., Marceta-Mandic, S., Bon, E., et al. (2024). The extremes of AGN variability: outbursts, deep fades, changing looks, exceptional spectral states, and semi-periodicities. *arXiv e-prints*, 00089. doi:10.48550/arXiv.2408.00089

Korista, K., Baldwin, J., Ferland, G., and Verner, D. (1997). An atlas of computed equivalent widths of quasar broad emission lines. *ApJS* 108, 401–415. doi:10.1086/312966

Kovačević, J., Popović, L. Č., and Dimitrijević, M. S. (2010). Analysis of optical Fe II emission in a sample of active galactic nucleus spectra. *ApJS* 189, 15–36. doi:10.1088/0067-0049/189/1/15

Kovačević-Dojčinović, J., and Popović, L. Č. (2015). The connections between the UV and optical Fe ii emission lines in type 1 AGNs. *ApJS* 221, 35. doi:10.1088/0067-0049/221/2/35

Kubota, A., and Done, C. (2018). A physical model of the broad-band continuum of AGN and its implications for the UV/X relation and optical variability. *MNRAS* 480, 1247–1262. doi:10.1093/mnras/sty1890

Kubota, A., and Done, C. (2019). Modelling the spectral energy distribution of super-Eddington quasars. *MNRAS* 489, 524–533. doi:10.1093/mnras/stz2140

LaMassa, S. M., Cales, S., Moran, E. C., Myers, A. D., Richards, G. T., Eracleous, M., et al. (2015). The discovery of the first "Changing look" Quasar: new insights into the physics and phenomenology of active galactic nuclei. *ApJ* 800, 144. doi:10.1088/0004-637X/800/2/144

Laor, A., Fiore, F., Elvis, M., Wilkes, B. J., and McDowell, J. C. (1997). The soft X-ray properties of a complete sample of optically selected quasars. II. Final results. *ApJ* 477, 93–113. doi:10.1086/303696

Larson, R. L., Finkelstein, S. L., Kocevski, D. D., Hutchison, T. A., Trump, J. R., Arrabal Haro, P., et al. (2023). A CEERS discovery of an accreting supermassive black hole 570 Myr after the big bang: identifying a progenitor of massive z > 6 quasars. *ApJl* 953, L29. doi:10.3847/2041-8213/ace619

Li, Y.-R., Hu, C., Yao, Z.-H., Chen, Y.-J., Bai, H.-R., Yang, S., et al. (2024). Spectroastrometry and reverberation mapping (SARM) of active galactic nuclei. I. The Hβ broad-line region structure and black hole mass of five quasars. arXiv:2407.08120. doi:10.48550/arXiv.2407.08120

Li, Y.-R., Wang, J.-M., Ho, L. C., Du, P., and Bai, J.-M. (2013). A bayesian approach to estimate the size and structure of the broad-line region in active galactic nuclei using reverberation mapping data. *ApJ* 779, 110. doi:10.1088/0004-637X/779/2/110

López-Navas, E., Martínez-Aldama, M. L., Bernal, S., Sánchez-Sáez, P., Arévalo, P., Graham, M. J., et al. (2022). Confirming new changing-look AGNs discovered through optical variability using a random forest-based light-curve classifier. *MNRAS* 513, L57–L62. doi:10.1093/mnrasl/slac033

Lu, K.-X., Bai, J.-M., Wang, J.-M., Hu, C., Li, Y.-R., Du, P., et al. (2022). Supermassive black hole and broad-line region in NGC 5548: results from five-season reverberation mapping. *ApJS* 263, 10. doi:10.3847/1538-4365/ac94d3

Mainieri, V., Anderson, R. I., Brinchmann, J., Cimatti, A., Ellis, R. S., Hill, V., et al. (2024). The wide-field spectroscopic telescope (WST) science white paper. *arXiv e-prints*, 05398doi. doi:10.48550/arXiv.2403.05398

Maiolino, R., Scholtz, J., Curtis-Lake, E., Carniani, S., Baker, W., de Graaff, A., et al. (2023). JADES. The diverse population of infant Black Holes at 4<z<11: merging, tiny, poor, but mighty. *arXiv e-prints*. doi:10.48550/arXiv.2308.01230

Marinello, M., Rodríguez-Ardila, A., Garcia-Rissmann, A., Sigut, T. A. A., and Pradhan, A. K. (2016). The Fe II emission in active galactic nuclei: excitation mechanisms and location of the emitting region. *ApJ* 820, 116. doi:10.3847/0004-637X/820/2/116

Marinello, M., Rodríguez-Ardila, A., Marziani, P., Sigut, A., and Pradhan, A. (2020). Panchromatic properties of the extreme Fe II emitter PHL 1092. *MNRAS* 494, 4187–4202. doi:10.1093/mnras/staa934

Marshall, J., Bolton, A., Bullock, J., Burgasser, A., Chambers, K., DePoy, D., et al. (2019). The maunakea spectroscopic explorer. *Bull. Am. Astronomical Soc.* 51, 126. doi:10.48550/arXiv.1907.07192

Martínez-Aldama, M. L., Czerny, B., Kawka, D., Karas, V., Panda, S., Zajaček, M., et al. (2019). Can reverberation-measured quasars Be used for cosmology? *ApJ* 883, 170. doi:10.3847/1538-4357/ab3728

Martínez-Aldama, M. L., Dultzin, D., Marziani, P., Sulentic, J. W., Bressan, A., Chen, Y., et al. (2015). O I and Ca II observations in intermediate redshift quasars. *ApJS* 217, 3. doi:10.1088/0067-0049/217/1/3

Martínez-Aldama, M. L., Panda, S., and Czerny, B. (2021a). A new radius-luminosity relation: using the near-infrared CaII triplet. *XIX Serbian Astron. Conf.* 100, 287–293.

Martínez-Aldama, M. L., Panda, S., Czerny, B., Marinello, M., Marziani, P., and Dultzin, D. (2021b). The CaFe project: optical Fe II and near-infrared Ca II triplet emission in active galaxies. II. The driver(s) of the Ca II and Fe II and its potential use as a chemical clock. *ApJ* 918, 29. doi:10.3847/1538-4357/ac03b6

Martínez-Ramírez, L. N., Calistro Rivera, G., Lusso, E., Bauer, F. E., Nardini, E., Buchner, J., et al. (2024). AGNfitter-rx: modelling the radio-to-X-ray SEDs of AGNs. *arXiv e-prints*. arXiv:2405.12111doi. doi:10.48550/arXiv.2405.12111

Marziani, P., Berton, M., Panda, S., and Bon, E. (2021a). Optical singly-ionized iron emission in radio-quiet and relativistically jetted active galactic nuclei. *Universe* 7, 484. doi:10.3390/universe7120484

Marziani, P., Dultzin, D., del Olmo, A., D'Onofrio, M., de Diego, J. A., Stirpe, G. M., et al. (2021b). "The quasar main sequence and its potential for cosmology," in *Nuclear activity in galaxies across cosmic time. 356 of IAU symposium*. Editors M. Pović, P. Marziani, J. Masegosa, H. Netzer, S. H. Negu, and S. B. Tessema, 66–71. doi:10.1017/S1743921320002598

Marziani, P., Dultzin, D., Sulentic, J. W., Del Olmo, A., Negrete, C. A., Martínez-Aldama, M. L., et al. (2018). A main sequence for quasars. *Front. Astronomy Space Sci.* 5, 6. doi:10.3389/fspas.2018.00006

Marziani, P., Floris, A., Deconto-Machado, A., Panda, S., Sniegowska, M., Garnica, K., et al. (2024). From sub-solar to super-solar chemical abundances along the quasar main sequence. *Physics* 6, 216–236. doi:10.3390/physics6010016

Marziani, P., and Sulentic, J. W. (2014). Highly accreting quasars: sample definition and possible cosmological implications. *MNRAS* 442, 1211–1229. doi:10.1093/mnras/stu951

Marziani, P., Sulentic, J. W., Zwitter, T., Dultzin-Hacyan, D., and Calvani, M. (2001). Searching for the physical drivers of the eigenvector 1 correlation space. *ApJ* 558, 553–560. doi:10.1086/322286

Mathews, W. G., and Ferland, G. J. (1987). What heats the hot phase in active nuclei? *ApJ* 323, 456. doi:10.1086/165843

Matthee, J., Naidu, R. P., Brammer, G., Chisholm, J., Eilers, A.-C., Goulding, A., et al. (2024). Little red dots: an abundant population of faint active galactic nuclei at z ~ 5 revealed by the EIGER and FRESCO JWST surveys. *ApJ* 963, 129. doi:10.3847/1538-4357/ad2345

Mineshige, S., Kawaguchi, T., Takeuchi, M., and Hayashida, K. (2000). Slim-disk model for soft X-ray excess and variability of narrow-line Seyfert 1 galaxies. *PASJ* 52, 499–508. doi:10.1093/pasj/52.3.499

Negrete, C. A., Dultzin, D., Marziani, P., Sulentic, J. W., Esparza-Arredondo, D., Martínez-Aldama, M. L., et al. (2017). Quasars as cosmological standard candles. *Front. Astronomy Space Sci.* 4, 59. doi:10.3389/fspas.2017.00059

Neufeld, D. A., Maloney, P. R., and Conger, S. (1994). Water maser emission from X-ray-heated circumnuclear gas in active galaxies. *ApJl* 436, L127–L130. doi:10.1086/187649

Noda, H., and Done, C. (2018). Explaining changing-look AGN with state transition triggered by rapid mass accretion rate drop. *MNRAS* 480, 3898–3906. doi:10.1093/mnras/sty2032

Nowak, M., Lacour, S., Abuter, R., Woillez, J., Dembet, R., Bordoni, M. S., et al. (2024). Upgrading the GRAVITY fringe tracker for GRAVITY+. Tracking the white-light fringe in the non-observable optical path length state-space. *A&A* 684, A184. doi:10.1051/0004-6361/202348771

Onoue, M., Inayoshi, K., Ding, X., Li, W., Li, Z., Molina, J., et al. (2023). A candidate for the least-massive black hole in the first 1.1 billion years of the Universe. *ApJl* 942, L17. doi:10.3847/2041-8213/aca9d3

Padovani, P., Alexander, D. M., Assef, R. J., De Marco, B., Giommi, P., Hickox, R. C., et al. (2017). Active galactic nuclei: what's in a name? *Astronomy and Astrophysics Rev.* 25, 2. doi:10.1007/s00159-017-0102-9

Paliya, V. S., Stalin, C. S., Domínguez, A., and Saikia, D. J. (2024). Narrow-line Seyfert 1 galaxies in sloan digital Sky survey: a new optical spectroscopic catalogue. *MNRAS* 527, 7055–7069. doi:10.1093/mnras/stad3650

Pancoast, A., Brewer, B. J., and Treu, T. (2011). Geometric and dynamical models of reverberation mapping data. *ApJ* 730, 139. doi:10.1088/0004-637X/730/2/139

Panda, S. (2021a). *Physical conditions in the broad-line regions of active galaxies*. Warsaw, Poland: Polish Academy of Sciences, Institute of Physics. Ph.D. thesis.

Panda, S. (2021b). The CaFe project: optical Fe II and near-infrared Ca II triplet emission in active galaxies: simulated EWs and the co-dependence of cloud size and metal content. *A&A* 650, A154. doi:10.1051/0004-6361/202140393

Panda, S. (2022). Parameterizing the AGN radius–luminosity relation from the eigenvector 1 viewpoint. *Front. Astronomy Space Sci.* 9, 850409. doi:10.3389/fspas.2022.850409

Panda, S., Bon, E., Marziani, P., and Bon, N. (2022). Taming the derivative: diagnostics of the continuum and Hβ emission in a prototypical Population B active galaxy. *Astron. Nachrichten* 343, e210091. doi:10.1002/asna.20210091

Panda, S., Bon, E., Marziani, P., and Bon, N. (2023a). Saturation of the curve: diagnostics of the continuum and Hβ emission in Population B active galaxy NGC 5548. *Bol. Soc. Astron. Bras.* 34, 246–250. doi:10.48550/arXiv.2308.05831

Panda, S., Czerny, B., Adhikari, T. P., Hryniewicz, K., Wildy, C., Kuraszkiewicz, J., et al. (2018). Modeling of the quasar main sequence in the optical plane. *ApJ* 866, 115. doi:10.3847/1538-4357/aae209

Panda, S., Czerny, B., Done, C., and Kubota, A. (2019a). CLOUDY view of the warm corona. *ApJ* 875, 133. doi:10.3847/1538-4357/ab11cb

Panda, S., Kozłowski, S., Gromadzki, M., Wrona, M., Iwanek, P., Udalski, A., et al. (2024a). Virial black hole masses for active galactic nuclei behind the magellanic clouds. *ApJS* 272, 11. doi:10.3847/1538-4365/ad3549

Panda, S., Martínez-Aldama, M. L., Marinello, M., Czerny, B., Marziani, P., and Dultzin, D. (2020a). The CaFe project: optical Fe II and near-infrared Ca II triplet emission in active galaxies. I. Photoionization modeling. *ApJ* 902, 76. doi:10.3847/1538-4357/abb5b8

Panda, S., Martínez-Aldama, M. L., and Zajaček, M. (2019b). Current and future applications of Reverberation-mapped quasars in Cosmology. *Front. Astronomy Space Sci.* 6, 75. doi:10.3389/fspas.2019.00075

Panda, S., and Marziani, P. (2023a). High Eddington quasars as discovery tools: current state and challenges. *Front. Astronomy Space Sci.* 10, 1130103. doi:10.3389/fspas.2023.1130103

Panda, S., and Marziani, P. (2023b). Modeling the quasar spectra for super-Eddington sources. *Bol. Soc. Astron. Bras.* 34, 241–245. doi:10.48550/arXiv.2308.05830

Panda, S., Marziani, P., and Czerny, B. (2019c). The quasar main sequence explained by the combination of eddington ratio, metallicity, and orientation. *ApJ* 882, 79. doi:10.3847/1538-4357/ab3292

Panda, S., Marziani, P., and Czerny, B. (2020b). Main trends of the quasar main sequence - effect of viewing angle. *Contributions Astronomical Observatory Skalnate Pleso* 50, 293–308. doi:10.31577/caosp.2020.50.1.293

Panda, S., Marziani, P., Czerny, B., Rodríguez-Ardila, A., and Pozo Nuñez, F. (2023b). Spectral variability studies in active galactic nuclei: exploring continuum and emission line regions in the age of LSST and JWST. *Universe* 9, 492. doi:10.3390/universe9120492

Panda, S., Pozo Nuñez, F., Bañados, E., and Heidt, J. (2024b). Probing the C IV continuum size–luminosity relation in active galactic nuclei with photometric reverberation mapping. *ApJl* 968, L16. doi:10.3847/2041-8213/ad5014

Panda, S., and Śniegowska, M. (2024). Changing-look active galactic nuclei. I. Tracking the transition on the main sequence of quasars. *ApJS* 272, 13. doi:10.3847/1538-4365/ad344f

Pandey, A., Czerny, B., Panda, S., Prince, R., Jaiswal, V. K., Martinez-Aldama, M. L., et al. (2023). Broad-line region in active galactic nuclei: dusty or dustless? *A&A* 680, A102. doi:10.1051/0004-6361/202347819

Pandey, A., Martínez-Aldama, M. L., Czerny, B., Panda, S., and Zajaček, M. (2024). New theoretical Fe II templates for bright quasars. *arXiv e-prints , arXiv:2401.18052*. doi:10.48550/arXiv.2401.18052

Park, D., Barth, A. J., Ho, L. C., and Laor, A. (2022). A new iron emission template for active galactic nuclei. *I. Opt. Template Hβ Region. ApJS* 258, 38. doi:10.3847/1538-4365/ac3f3e

Peterson, B. M. (1988). Emission-line variability in Seyfert galaxies. *PASP* 100, 18. doi:10.1086/132130

Peterson, B. M. (1993). Reverberation mapping of active galactic nuclei. *PASP* 105, 247. doi:10.1086/133140

Peterson, B. M., Ferrarese, L., Gilbert, K. M., Kaspi, S., Malkan, M. A., Maoz, D., et al. (2004). Central masses and broad-line region sizes of active galactic nuclei. II. A homogeneous analysis of a large reverberation-mapping database. *ApJ* 613, 682–699. doi:10.1086/423269

Petrushevska, T., Leloudas, G., Ilić, D., Bronikowski, M., Charalampopoulos, P., Jaisawal, G. K., et al. (2023). The rise and fall of the iron-strong nuclear transient PS16dtm. *A&A* 669, A140. doi:10.1051/0004-6361/202244623

Phillips, M. M. (1978a). Permitted fe II emission in Seyfert 1 galaxies and QSOs I. Observations. *ApJS* 38, 187. doi:10.1086/190553

Phillips, M. M. (1978b). Permitted Fe II emission in Seyfert 1 galaxies and QSOs. II. The excitation mechanism. *ApJ* 226, 736–752. doi:10.1086/156656

Planck Collaboration, Aghanim, N., Akrami, Y., Ashdown, M., Aumont, J., Baccigalupi, C., and Ballardini, M. (2020). Planck 2018 results. VI. Cosmological parameters. *A&A* 641, A6. doi:10.1051/0004-6361/201833910

Prince, R., Zajaček, M., Panda, S., Hryniewicz, K., Kumar Jaiswal, V., Czerny, B., et al. (2023). Wavelength-resolved reverberation mapping of intermediate-redshift quasars HE 0413-4031 and HE 0435-4312: dissecting Mg II, optical Fe II, and UV Fe II emission regions. *A&A* 678, A189. doi:10.1051/0004-6361/202346738

Pronik, V. I., and Chuvaev, K. K. (1972). Hydrogen lines in the spectrum of the galaxy Markaryan 6 during its activity. *Astrophysics* 8, 112–116. doi:10.1007/BF01002159

Rakshit, S., Stalin, C. S., and Kotilainen, J. (2020). Spectral properties of quasars from sloan digital Sky survey data release 14: the catalog. *ApJS* 249, 17. doi:10.3847/1538-4365/ab99c5

Ricci, C., and Trakhtenbrot, B. (2023). Changing-look active galactic nuclei. *Nat. Astron.* 7, 1282–1294. doi:10.1038/s41550-023-02108-4

Richards, G. T., Lacy, M., Storrie-Lombardi, L. J., Hall, P. B., Gallagher, S. C., Hines, D. C., et al. (2006). Spectral energy distributions and multiwavelength selection of type 1 quasars. *ApJS* 166, 470–497. doi:10.1086/506525

Riess, A. G., Casertano, S., Yuan, W., Macri, L. M., and Scolnic, D. (2019). Large magellanic cloud cepheid standards provide a 1% foundation for the determination of the Hubble constant and stronger evidence for physics beyond ΛCDM. *ApJ* 876, 85. doi:10.3847/1538-4357/ab1422

Riess, A. G., Filippenko, A. V., Challis, P., Clocchiatti, A., Diercks, A., Garnavich, P. M., et al. (1998). Observational evidence from Supernovae for an accelerating Universe and a cosmological constant. *AJ* 116, 1009–1038. doi:10.1086/300499

Rigby, J., Perrin, M., McElwain, M., Kimble, R., Friedman, S., Lallo, M., et al. (2023). The science performance of JWST as characterized in commissioning. *PASP* 135, 048001. doi:10.1088/1538-3873/acb293

Risaliti, G., and Lusso, E. (2015). A Hubble diagram for quasars. *ApJ* 815, 33. doi:10.1088/0004-637X/815/1/33

Risaliti, G., and Lusso, E. (2019). Cosmological constraints from the Hubble diagram of quasars at high redshifts. *Nat. Astron.* 3, 272–277. doi:10.1038/s41550-018-0657-z

Rodríguez-Ardila, A., Fonseca-Faria, M. A., Dias dos Santos, D., Panda, S., and Marinello, M. (2024). First detection of outflowing gas in the outskirts of the broad-line region in 1H 0707-495. *AJ* 167, 244. doi:10.3847/1538-3881/ad36bf

Ross, N. P., Ford, K. E. S., Graham, M., McKernan, B., Stern, D., Meisner, A. M., et al. (2018). A new physical interpretation of optical and infrared variability in quasars. *MNRAS* 480, 4468–4479. doi:10.1093/mnras/sty2002

Russell, H. N. (1914). Relations between the spectra and other characteristics of the stars. *Pop. Astron.* 22, 275–294.

Sánchez-Sáez, P., Lira, H., Martí, L., Sánchez-Pi, N., Arredondo, J., Bauer, F. E., et al. (2021). Searching for changing-state AGNs in massive data sets. I. Applying deep learning and anomaly-detection techniques to find AGNs with anomalous variability behaviors. *AJ* 162, 206. doi:10.3847/1538-3881/ac1426

Sarkar, A., Ferland, G. J., Chatzikos, M., Guzmán, F., van Hoof, P. A. M., Smyth, R. T., et al. (2021). Improved Fe II emission-line models for AGNs using new atomic data sets. *ApJ* 907, 12. doi:10.3847/1538-4357/abcaa6

Savić, D., Goosmann, R., Popović, L. Č., Marin, F., and Afanasiev, V. L. (2018). AGN black hole mass estimates using polarization in broad emission lines. *A&A* 614, A120. doi:10.1051/0004-6361/201732220

Schmidt, M., and Green, R. F. (1983). Quasar evolution derived from the Palomar bright quasar survey and other complete quasar surveys. *ApJ* 269, 352–374. doi:10.1086/161048

Shapovalova, A. I., Popović, L. Č., Collin, S., Burenkov, A. N., Chavushyan, V. H., Bochkarev, N. G., et al. (2008). Long-term variability of the optical spectra of NGC 4151. I. Light curves and flux correlations. *A&A* 486, 99–111. doi:10.1051/0004-6361:20079111

Shen, Y., Grier, C. J., Horne, K., Stone, Z., Li, J. I., Yang, Q., et al. (2024). The sloan digital Sky survey reverberation mapping project: key results. *ApJS* 272, 26. doi:10.3847/1538-4365/ad3936

Shen, Y., and Ho, L. C. (2014). The diversity of quasars unified by accretion and orientation. *Nat* 513, 210–213. doi:10.1038/nature13712

Shen, Y., Richards, G. T., Strauss, M. A., Hall, P. B., Schneider, D. P., Snedden, S., et al. (2011). A catalog of quasar properties from sloan digital Sky survey data release 7. *ApJS* 194, 45. doi:10.1088/0067-0049/194/2/45

Sniegowska, M., Czerny, B., Bon, E., and Bon, N. (2020). Possible mechanism for multiple changing-look phenomena in active galactic nuclei. *A&A* 641, A167. doi:10.1051/0004-6361/202038575

Śniegowska, M., Marziani, P., Czerny, B., Panda, S., Martínez-Aldama, M. L., del Olmo, A., et al. (2021). High metal content of highly accreting quasars. *ApJ* 910, 115. doi:10.3847/1538-4357/abe1c8

Śniegowska, M., Panda, S., Czerny, B., Savić, D., Martínez-Aldama, M. L., Marziani, P., et al. (2023). Spectropolarimetry and spectral decomposition of high-accreting narrow-line Seyfert 1 galaxies. *A&* 678, A63. doi:10.1051/0004-6361/202243434

Sulentic, J., and Marziani, P. (2015). Quasars in the 4D Eigenvector 1 Context: a stroll down memory lane. *Front. Astronomy Space Sci.* 2, 6. doi:10.3389/fspas.2015.00006

Sulentic, J. W., Zwitter, T., Marziani, P., and Dultzin-Hacyan, D. (2000). Eigenvector 1: an optimal correlation space for active galactic nuclei. *ApJl* 536, L5–L9. doi:10.1086/312717

Sun, J., and Shen, Y. (2015). Dissecting the quasar main sequence: insight from host galaxy properties. *ApJl* 804, L15. doi:10.1088/2041-8205/804/1/L15

Tananbaum, H., Avni, Y., Green, R. F., Schmidt, M., and Zamorani, G. (1986). X-ray observations of the bright quasar survey. *ApJ* 305, 57. doi:10.1086/164228

Trakhtenbrot, B., Arcavi, I., Ricci, C., Tacchella, S., Stern, D., Netzer, H., et al. (2019). A new class of flares from accreting supermassive black holes. *Nat. Astron.* 3, 242–250. doi:10.1038/s41550-018-0661-3

Tsuzuki, Y., Kawara, K., Yoshii, Y., Oyabu, S., Tanabé, T., and Matsuoka, Y. (2006). Fe II emission in 14 low-redshift quasars. I. Observations. *ApJ* 650, 57–79. doi:10.1086/506376

Vanden Berk, D. E., Richards, G. T., Bauer, A., Strauss, M. A., Schneider, D. P., Heckman, T. M., et al. (2001). Composite quasar spectra from the sloan digital Sky survey. *AJ* 122, 549–564. doi:10.1086/321167

Verner, E. M., Verner, D. A., Korista, K. T., Ferguson, J. W., Hamann, F., and Ferland, G. J. (1999). Numerical simulations of Fe II emission spectra. *ApJS* 120, 101–112. doi:10.1086/313171

Véron-Cetty, M. P., Joly, M., and Véron, P. (2004). The unusual emission line spectrum of I Zw 1. *A&A* 417, 515–525. doi:10.1051/0004-6361:20035714

Vestergaard, M., and Wilkes, B. J. (2001). An empirical ultraviolet template for iron emission in quasars as derived from I zwicky 1. *ApJS* 134, 1–33. doi:10.1086/320357

Wang, J., Wei, J. Y., and He, X. T. (2005). Variability of optical Fe II complex in narrow-line Seyfert 1 galaxy NGC 4051. *A&A* 436, 417–426. doi:10.1051/0004-6361:20042014

Wang, J.-M., Qiu, J., Du, P., and Ho, L. C. (2014). Self-shadowing effects of slim accretion disks in active galactic nuclei: the diverse appearance of the broad-line region. *ApJ* 797, 65. doi:10.1088/0004-637X/797/1/65

Wang, J.-M., Songsheng, Y.-Y., Li, Y.-R., Du, P., and Zhang, Z.-X. (2020). A parallax distance to 3C 273 through spectroastrometry and reverberation mapping. *Nat. Astron.* 4, 517–525. doi:10.1038/s41550-019-0979-5

Williams, P. R., Pancoast, A., Treu, T., Brewer, B. J., Barth, A. J., Bennert, V. N., et al. (2018). The lick AGN monitoring project 2011: dynamical modeling of the broad-line region. *ApJ* 866, 75. doi:10.3847/1538-4357/aae086

Wu, Q., and Shen, Y. (2022). A catalog of quasar properties from sloan digital Sky survey data release 16. *ApJS* 263, 42. doi:10.3847/1538-4365/ac9ead

Yang, G., Boquien, M., Buat, V., Burgarella, D., Ciesla, L., Duras, F., et al. (2020). X-CIGALE: fitting AGN/galaxy SEDs from X-ray to infrared. *MNRAS* 491, 740–757. doi:10.1093/mnras/stz3001

Yang, J., Wang, F., Fan, X., Hennawi, J. F., Barth, A. J., Bañados, E., et al. (2023). A SPectroscopic survey of biased halos in the reionization era (ASPIRE): a first look at the rest-frame optical spectra of z > 6.5 quasars using JWST. *ApJl* 951, L5. doi:10.3847/2041-8213/acc9c8

York, D. G., Adelman, J., Anderson, J., John, E., Anderson, S. F., Annis, J., et al. (2000). The sloan digital Sky survey: technical summary. *AJ* 120, 1579–1587. doi:10.1086/301513

Zajaček, M., Czerny, B., Khadka, N., Martínez-Aldama, M. L., Prince, R., Panda, S., et al. (2024a). Effect of extinction on quasar luminosity distances determined from UV and X-ray flux measurements. *ApJ* 961, 229. doi:10.3847/1538-4357/ad11dc

Zajaček, M., Panda, S., Pandey, A., Prince, R., Rodríguez-Ardila, A., Jaiswal, V., et al. (2024b). UV FeII emission model of HE 0413–4031 and its relation to broad-line time delays. *A&A* 683, A140. doi:10.1051/0004-6361/202348172

Zamfir, S., Sulentic, J. W., Marziani, P., and Dultzin, D. (2010). Detailed characterization of Hβ emission line profile in low-zSDSS quasars. *MNRAS* 403, 1759–1786. doi:10.1111/j.1365-2966.2009.16236.x

Zeltyn, G., Trakhtenbrot, B., Eracleous, M., Yang, Q., Green, P., Anderson, S. F., et al. (2024). Exploring changing-look active galactic nuclei with the sloan digital Sky survey V: first year results. *ApJ* 966, 85. doi:10.3847/1538-4357/ad2f30

Zu, Y., Kochanek, C. S., and Peterson, B. M. (2011). An alternative approach to measuring reverberation lags in active galactic nuclei. *ApJ* 735, 80. doi:10.1088/0004-637X/735/2/80

frontiers | Frontiers in Astronomy and Space Sciences

TYPE Mini Review
PUBLISHED 24 October 2024
DOI 10.3389/fspas.2024.1493917

Check for updates

OPEN ACCESS

EDITED BY
Joseph E. Borovsky,
Space Science Institute (SSI), United States

REVIEWED BY
Subhamoy Chatterjee,
Southwest Research Institute Boulder,
United States

*CORRESPONDENCE
Olga Khabarova,
olgakhabar@tauex.tau.ac.il

RECEIVED 10 September 2024
ACCEPTED 10 October 2024
PUBLISHED 24 October 2024

CITATION
Khabarova O and Price C (2024) Importance and challenges of geomagnetic storm forecasting.
Front. Astron. Space Sci. 11:1493917.
doi: 10.3389/fspas.2024.1493917

COPYRIGHT
© 2024 Khabarova and Price. This is an open-access article distributed under the terms of the Creative Commons Attribution License (CC BY). The use, distribution or reproduction in other forums is permitted, provided the original author(s) and the copyright owner(s) are credited and that the original publication in this journal is cited, in accordance with accepted academic practice. No use, distribution or reproduction is permitted which does not comply with these terms.

Importance and challenges of geomagnetic storm forecasting

Olga Khabarova* and Colin Price

Geophysical Department, Porter School of the Environment and Earth Sciences, Tel Aviv University, Tel Aviv, Israel

Space weather prediction is a central focus of solar-terrestrial studies, with forecasts of geomagnetic storms deemed critical due to their significant practical implications. We have gathered facts that highlight the effects of geomagnetic storms on electric power systems and satellites. Recent studies indicate that geomagnetic storms of moderate intensity are statistically associated with larger spike amplitudes of telluric currents potentially leading to power outages compared to those caused by major storms. This underscores the importance of building reliable forecasts for all geomagnetic storms, especially given that solar cycles 20–24 saw less than 1% of storms classified as severe or extreme. A major challenge in current prediction models, even those utilizing advanced machine learning techniques, is the decline in accuracy for forecast lead times beyond 3 h, limiting the ability to mitigate infrastructure damage effectively. In this work, we provide a concise overview of geomagnetic storm statistics, describe key forecasting methods, recent advancements, and discuss the challenges in achieving accurate and timely storm predictions.

KEYWORDS

space weather, geomagnetic storm, solar wind, forecasting, blackouts, solar-terrestrial couplings

1 Introduction

A prediction of geomagnetic storms has significant implications for modern society, especially as our reliance on space and terrestrial technology grows. These intense geomagnetic field disturbances are associated with severe space weather events, solar cosmic rays and energetic particles damaging sensitive satellite equipment, creating disruptions of radiowave propagation and connection to satellites, inducing telluric currents that lead to power system transformer saturation and excessive heating in all elongated wired systems, and causing negative biological effects (e.g., Pulkkinen et al., 2005; Khabarova and Dimitrova, 2009; Lakhina and Tsurutani, 2016; Malandraki and Crosby, 2018; Daglis et al., 2021; Buzulukova and Tsurutani, 2022; Khabarova et al., 2024).

Prediction of geomagnetic storms involves understanding a complex interplay of solar phenomena and their interaction with the Earth's magnetosphere. The challenge lies in estimating initial properties of potentially geoeffective streams, such as fast Interplanetary Coronal Mass Ejections (ICMEs) and Stream Interaction Regions (SIRs) or longer-lived Corotating Interaction regions (CIRs) surrounding high-speed flows from coronal holes, tracing their evolution during propagation, and finding dependencies that allow giving an alert in a reasonable time (Joselyn, 1995; Vennerstroem, 2001; Siscoe and Schwenn, 2006; Tsurutani et al., 2006; Zhang et al., 2007; Kay et al., 2017; Luhmann et al., 2022; Mursula et al., 2022). A scheme of the key solar-terrestrial couplings linking the solar activity, flows and streams in the heliosphere and their effects on the Earth is given by Daglis et al. (2021).

Besides the purely academic significance of understanding solar-terrestrial couplings, it is crucial to comprehend the mechanisms of how the solar wind impacts Earth's magnetosphere to predict the risks geomagnetic storms pose to power grid systems and space technology. This understanding aims to forecast all geomagnetic storms, not just the severe ones, with lead times ranging from hours to days, allowing society to prepare and mitigate potential damage, which is a complex challenge that remains unresolved (see Srivastava et al., 2021 and references therein). This mini-review highlights the practical importance of geomagnetic storm forecasting, consolidates findings from various studies to identify current challenges in improving predictions, and proposes potential solutions to advance the field.

2 Practical importance of predicting geomagnetic storms

The potential harms of geomagnetic storms are frequently highlighted in space physics literature as a justification for in-depth research on solar and space plasma processes. However, there are relatively few practical studies addressing the direct consequences of space weather impacts on terrestrial infrastructure or proposing mitigation measures. While solar activity does not directly affect the Earth or humans, several key indirect impacts of space weather must be considered (see Lakhina and Tsurutani, 2016; Buzulukova and Tsurutani, 2022, and references therein). Solar flares emit X-rays and cosmic rays that disrupt radio waves and GPS signals, making the dayside ionosphere particularly vulnerable (e.g., Daglis et al., 2021; Buzás et al., 2023). High-speed solar wind streams with a strong southward-directed IMF trigger geomagnetic storms, inducing electric fields that disrupt power grids (Molinski, 2002; Sorokin et al., 2023). These streams also accelerate charged particles locally and re-accelerate solar energetic particles, which collectively bombard Earth's magnetosphere, causing auroras, particle precipitation, and thermosphere heating (Zank et al., 2015; Malandraki and Crosby, 2018; Daglis et al., 2019; Daglis et al., 2021; Reames, 2021; Khabarova et al., 2021). Particle enhancements can occur even without geomagnetic storms. Additionally, varying geomagnetic fields and cosmic rays affect biological systems, especially in high-latitude regions and the South Atlantic Anomaly area, though the exact mechanisms remain unclear (Tchijevsky, 1938; Khabarova and Dimitrova, 2009; Dimitrova and Babayev, 2018; Khabarova et al., 2024). See details in Supplementary Material S1.

Among risks listed above, Geomagnetically Induced Currents (GICs) represent the biggest space-weather relater problem pushing the governments over the world seeking for the scientific community's help since telluric GICs can severely impact power grids during geomagnetic storms (e.g., Daglis et al., 2021; Boutsi et al., 2023; Calabia et al., 2023; Evans et al., 2024; Souza et al., 2024). An analysis of related risks have been carried out in several developed countries (e.g., Hines et al., 2008; Persons and Rusco, 2018; Lucas et al., 2020; Ryu et al., 2020; Gritsutenko et al., 2023). It shows that some of measures preventing blackouts, such as a targeted disconnection of high-voltage transmission lines, can only be achieved if they are based on correct and timely predictions of geomagnetic storms. Recently, (Mac Manus et al., 2022; Mac Manus et al., 2023) simulated GIC levels across New Zealand's network transformers under various extreme storm scenarios, finding up to 35% of transformers at risk. More details can be found in the Supplementary Material S1.

Figure 1 illustrates potential connections between power outages and space weather by comparing the annual number of major blackouts in the United States with sunspot numbers and the Kp index over two solar cycles. Hines et al., 2008 suggest that smaller-scale events, under 400 MW, occur irregularly but increase in frequency over time. In contrast, the most common larger events, in the 400–999 MW range (derived from Figure 3 of Hines et al., 2008), smoothly wave, showing two peaks between 1984 and 2006, as depicted in Figure 1A.

The fluctuation in large blackout numbers follows variations of the sunspot numbers and the Kp index recorded in the OMNI2 database for the same period. Geomagnetic activity, indicated by the Kp index in Figure 1B, does not perfectly align with the solar cycle reflected in the sunspot number because it is influenced by both geoeffective ICMEs and SIRs/CIRs (e.g., Boroyev et al., 2020). The latter peak from the declining phase of solar activity through the solar minimum, as shown by Mursula et al. (2022). Consequently, the Kp profile is smoother and slightly shifted to the right compared to the solar cycle peak marked by sunspot numbers. Blackouts may be linked to the solar cycle both directly, via the damaging effects of GICs, and indirectly, through changes in the atmosphere and weather events or even human factors.

It is important to note that the highest GIC amplitudes do not always match the strongest geomagnetic activity (Ngwira et al., 2015; Dimmock et al., 2020; Gritsutenko et al., 2023). The sudden GIC spikes resulting in dramatic changes in the power grid are related to the time derivative of the ground horizontal magnetic field. Significant GIC jump excitations, potentially leading to power system failures, occur not only during the main storm phase but are also related to magnetospheric-ionospheric sudden impulses or sudden storm commencements prior geomagnetic storms caused by sharp changes in the solar wind dynamic pressure, VLF-ULF pulsations in the geomagnetic field, and even intensification of substorms. Gritsutenko et al. (2023) show that the peak of the excitement of GIC spikes is statistically associated with Kp ranging from 4 to 6, not with the maximal Kp values. This finding aligns with the results of the recent analysis of the most intense storms with Dst < −150 nT observed during solar cycle 24 in the Mediterranean region (Boutsi et al., 2023).

A similar effect can be observed in the analysis of satellite losses and malfunctions (Baker, 2001; Cilden-Guler et al., 2021). While severe geomagnetic storms are known to damage satellites, such as disrupting their trajectories, as recently noted during the extreme Gannon geomagnetic storm in May 2024 (Parker and Linares, 2024) — moderate storms also pose significant risks. The primary threat comes from energetic "killer" electrons with energies ranging from 0.5 to 5 MeV at geostationary orbit. These electrons are linked to the arrival of geoeffective ICMEs and SIRs, which are nonlinearly associated with the geomagnetic activity level and may peak before or after the geomagnetic storm maximum (see

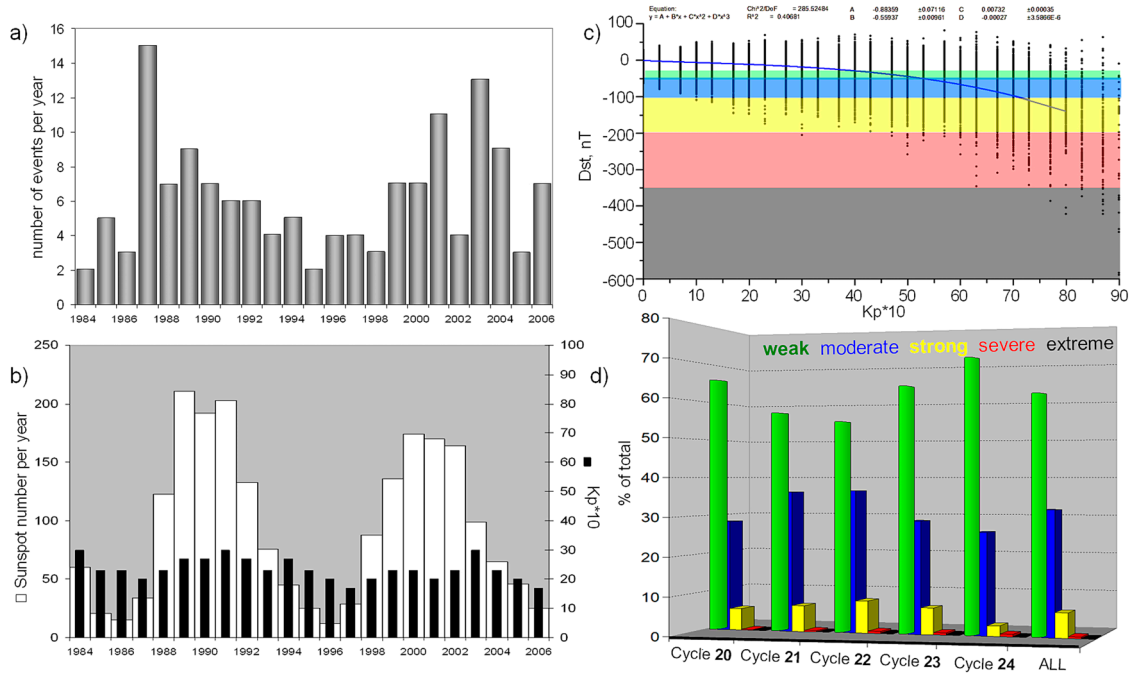

FIGURE 1
Electric power system failures modulated by solar activity and statistical properties of geomagnetic storms. **(A)** Number of large blackouts per year in the United States with the event size (amount of electricity taken off) of 400–999 MW. Data are provided by Hines et al. (2008). **(B)** Sunspot number per year (white) and Kp·10 (black), OMNI2 database data. **(C)** Dst index vs. Kp·10. OMNI2 hourly data for 1964–2023. **(D)** Percentage of storms of the certain intensity for cycles 20–24 and for all cycles in total (ALL). Data are taken from Abe et al. (2023). The Kp and Dst datasets can be found in the NASA's Space Physics Data Facility – OMNI web data repository: https://omniweb.gsfc.nasa.gov/ow.html, and WDC Kyoto: https://wdc.kugi.kyoto-u.ac.jp/dst_provisional/. Storm intensity categories are based on Dst values and indicated by colors in **(C, D)**. Weak intensity is marked by green, moderate—by blue, strong is yellow, severe is red, and extreme is black. Although there is significant variation in Dst values relative to Kp, an approximate correspondence between the level of geomagnetic field disturbances characterized by Dst can be found for Kp values greater than 4 (see https://www.swpc.noaa.gov/noaa-scales-explanation). Kp = 4 is typically considered to indicate a disturbed geomagnetic field or a weak geomagnetic storm. Kp = 5 corresponds to a weak or minor storm, Kp = 6 indicates a moderate storm, Kp = 7 signifies a strong storm, Kp = 8 represents a severe storm, and Kp = 9 denotes an extreme storm.

Baker, 2001; Wrenn, 2009; Daglis et al., 2019; Miteva et al., 2023, and references therein).

Information about satellite malfunctions or losses is often proprietary and not publicly available, complicating research into the physical factors affecting sensitive satellite equipment. However, some general data is accessible in the literature. For instance, NASA reported that an ICME caused the loss of 38 commercial satellites in February 2022 (https://svs.gsfc.nasa.gov/5193/). A moderate geomagnetic storm with a Dst minimum of −66 nT on 3 February 2022 coincided with the launch of Starlink satellites, leading to such significant losses (Miteva et al., 2023; Baruah et al., 2024).

As Solar Cycle 25 peaks, the risk to Earth-orbiting satellites and spacecraft operating in the solar wind increases. For instance, the ACE and DSCOVR L1 spacecraft malfunctioned after the severe geomagnetic storm of 24 March 2004, failing to provide critical solar wind density data for 2 weeks, which halted related forecasts. This highlights the urgent need for the scientific community to prioritize methods for predicting all geomagnetic storms, from weak to extreme, rather than focusing only on intense events, which remains a challenge despite the growing number of prediction models.

3 Geomagnetic storm prediction: geomagnetic storm intensity classifications, general approaches, solutions and problems

3.1 Classifications

Space weather prediction models commonly rely on two key geomagnetic activity indices: Kp and Dst (Wintoft and Wik, 2018; Chakraborty and Morley, 2020; Matzka et al., 2021; Xu et al., 2020; Park et al., 2021; Wang J. et al., 2023; Zhang et al., 2023; Sierra-Porta et al., 2024). See https://kp.gfz-potsdam.de/en/and https://wdc.kugi.kyoto-u.ac.jp/index.html and Supplementary Material S1 for details.

Kp and Dst indices, which characterize geomagnetic activity at different geomagnetic latitudes and are calculated differently, do not have a direct correspondence which complicates a comparison of the results of prognostic techniques using different indices (Borovsky and Shprits, 2017). Figure 1C displays the relationship between Dst and Kp·10, fitted with a cubic polynomial (with coefficient values provided above the panel). The categorization of Dst, from weak to extreme storm intensity, is represented in different colors.

Figure 1D shows that the occurrence rate of geomagnetic storms of varying intensities is inversely related to the color proportions representing storm intensity in Figure 1C. Based on statistics from Abe et al. (2023), which we used to calculate the percentage of storms by intensity, weak storms constitute 61% of all storms observed during solar cycles 20–24 (labeled as "ALL" in Figure 1D). Moderate storms account for 32%, strong storms – 6.4%, severe storms – 0.45%, and extreme storms — just 0.12%. Over these five solar cycles, the occurrence of moderate and strong storms shows an anticorrelation with the rate of weak storms, with a correlation coefficient of −0.9. Although the number of cycles is too small to draw definitive conclusions, if this trend continues in solar cycle 25, it could offer insights for predicting the probability of moderate and strong storms in future cycles. Figure 1D illustrates the importance of forecasting all geomagnetic storms because the majority of storms are weak and moderate.

3.2 General approaches

Geomagnetic storm forecasting relies on understanding solar wind-magnetosphere interactions. The Earth's magnetosphere reacts to any solar wind variations (Borovsky, 2023), but storms occur when magnetic reconnection is triggered by specific solar wind conditions, particularly when the IMF is southward and the solar wind speed is high, known as the "VB_z paradigm" (Lakhina and Tsurutani, 2016). These conditions typically arise from high-speed ICMEs or SIRs surrounding fast solar wind flows from coronal holes (Vennerstroem, 2001; Siscoe and Schwenn, 2006; Tsurutani et al., 2006; Zhang et al., 2007; Cid et al., 2014; Kim et al., 2014; Kay et al., 2017; Daglis et al., 2021; Echer and Gonzalez, 2022; Luhmann et al., 2022; Mursula et al., 2022).

The accuracy of predictions depends on the timescale considered, as well as the quality of the input data and models used. In terms of the alert time, the geomagnetic storm prognoses are divided into three categories: long-term, mid-term, and short-term. *Long-term predictions* from 3 days to a week based on estimations of the development of active processes and coronal hole dynamics at the Sun are rarely used since they are accurate for predicting the likelihood of a geomagnetically active period but cannot correctly forecast the exact timing or intensity of individual storms.

Mid-term forecasts aim to predict storms up to several days in advance. Some of them are based on the expert estimation of the direction of CMEs or the occurrence of low-latitude coronal holes, and some of them use modeling. They can be given in the simple verbal alert ways sometimes complemented with the Kp level forecast or in the probabilistic form, when a certain probability is given next to the certain intensity of the geomagnetic storm (e.g., https://spaceweather.com/ and https://www.swpc.noaa.gov/products/3-day-forecast).

Some empirical techniques use MHD or semi-empirical models to estimate V and B_z at the Earth's orbit. The models rely on the solar magnetic field data and recalculate the corresponding IMF and plasma parameters from the source surface to the Earth (see Pizzo et al., 2011; Reiss et al., 2016; https://www.swpc.noaa.gov/products/wsa-enlil-solar-wind-prediction) or use interplanetary scintillation data (Jackson et al., 1998; https://ips.ucsd.edu). More details can be found in Supplementary Material S1.

There are also models employing the L1 spacecraft data. These are usually the same models as used for *short-term predictions* but with larger leading times. Mid-term predictions based on the empirical models aim to extend the forecasting horizon from 1 h to 3 h and beyond, yet challenges arise due to the diminishing relevance of data as the time frame increases (Shprits et al., 2019; Nair et al., 2023; Xu et al., 2023; Wang C et al., 2023). Achieving reliable forecasts beyond 3 h has proven to be complex and, as of now, is thought to reach a practical limit (Pulkkinen et al., 2022).

Short-term predictions focus on forecasting geomagnetic storms minutes or hours before they occur, primarily using data from L1 spacecraft and geomagnetic indices (see Shprits et al., 2019; Nair et al., 2023; Wang C et al., 2023; Wang J et al., 2023 and references therein). They are reliable for determining if a storm will happen within a specific timeframe based on the propagation time of the geoeffective stream or flow from L1 to the magnetosphere. Such forecasts not only provide probabilistic predictions but also compare predicted Dst and Kp indices with real-time geomagnetic activity indices (e.g., https://lasp.colorado.edu/space_weather/dsttemerin/dsttemerin.html, https://swx-trec.com/dst/, https://spaceweather.ru/content/extended-geomagnetic-storm-forecast; http://eng.sepc.ac.cn/dstModel.php).

3.3 Solutions

Methodologies of the geomagnetic storm prediction based on the knowledge of solar-terrestrial couplings have traditionally ranged from MHD-based models, like ENLIL, to empirical models, using primarily V and the IMF B_z (see Joselyn, 1995; Luo et al., 2017 and references therein). Predictions are sometimes based on other known physical principles, such as pre-storm variations in the X-ray, cosmic ray and energetic particle fluxes associated with the arrival of geoeffective streams (e.g., Chakraborty and Morley, 2020; Wang C et al., 2023; Belov et al., 2024). Another approach involves the similarity technique, where models assess the resemblance between the current situation and past geomagnetic storms (e.g., Xu et al., 2023). There are also hybrid models and models that differentiate between ICMEs and SIRs as drivers of geomagnetic storms (e.g., Kim et al., 2014; Park et al., 2021). In recent years, many models have incorporated machine learning (ML) techniques.

ML methods for predicting geomagnetic storms represent a significant shift towards data-driven approaches in geomagnetic storm prediction, which increasingly leverage advanced ML algorithms to improve forecast accuracy and adaptability (e.g., Gruet et al., 2018; Pulkkinen et al., 2022; Conde et al., 2023; Hu et al., 2023; Wang J et al., 2023; Zhang et al., 2023; Xu et al., 2023). These algorithms utilize vast datasets related to solar activity and geomagnetic indicators to anticipate storm events, adapting various techniques to enhance predictive accuracy.

A recent competition, the "MagNet: Model the Geomagnetic Field" challenge, organized by the National Oceanic and Atmospheric Administration and the University of Colorado, attracted 1,197 models competing to predict real-time Dst values using a shared dataset (Nair et al., 2023). The winning model, a

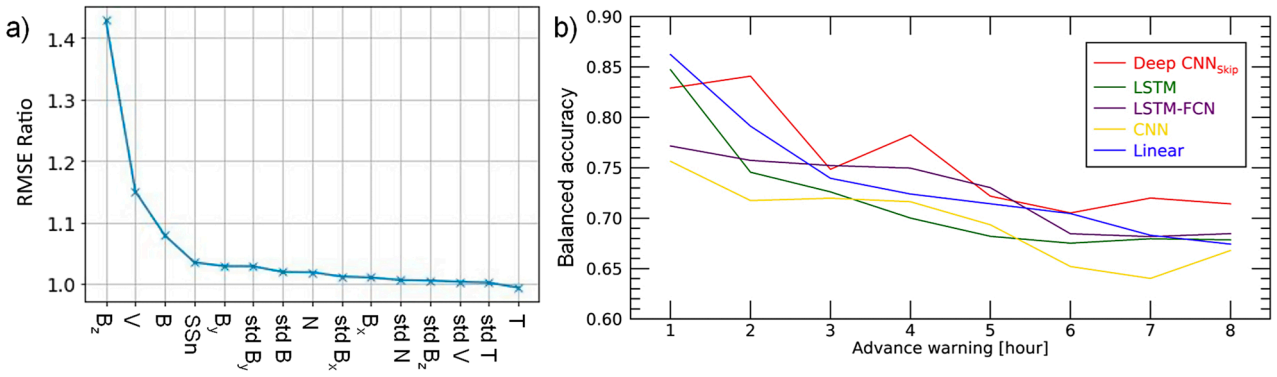

FIGURE 2
Examples of characteristics of machine learning models predicting geomagnetic storms. **(A)** Ratio of the root-mean-square for each feature (parameter) to IMF B_z, the main predictive feature. Blue curve characterizes the importance of parameters on which the model is based. B_x, B_y, and B_z are three IMF components (GSM). V, N, and T are the solar wind speed, density and temperature, respectively. "Std" means standard deviation. Adapted from Nair et al. (2023) under the terms of the Creative Commons CC BY license. **(B)** Balanced accuracy for the five most effective neural network architectures (represented by different colored lines as indicated in the legend) shown for multi-hour advance warnings of geomagnetic storms with SYM-H< −50 nT. Adapted from Telloni et al. (2023) under Copyright 2024 IOP Publishing, CC: Daniele Telloni and authors.

bidirectional Long Short-Term Memory (LSTM)-Gated Recurrent Unit (GRU) with three Flattening Layers and three Dense Layers, utilized the parameters shown in Figure 2A. The data were grouped into 1-h intervals, with the mean and standard deviation calculated for each feature. The model used normalized data from the 128 h preceding the prediction time.

Figure 2A shows the permutation feature importance for the winning model, where RMSE (root-mean-square error) represents the error between observed and predicted Dst values. The x-axis lists the model's input parameters, and the y-axis shows the ratio of the RMSE for each feature compared to the most important one (see more information in Supplementary Material S1). This technique assesses the impact of each input feature. Upon forecasting of indices such as Dst or SYM-H, the model inputs (e.g., V, B_z, and B, and other parameters) are tested for their importance. The method starts by measuring the model's baseline performance using RMSE. At the next step, each feature is shuffled (permuted) one by one, breaking its link to the target variable, and the model's performance is recalculated. The larger the performance drop occurs after a feature is shuffled, the more important that feature is. Balanced accuracy representing the average of recall values is another useful metric, particularly valuable when dealing with imbalanced datasets (e.g., Cristoforetti et al., 2022), which is a common issue in geomagnetic storm forecasting since severe storms are much rarer than quiet periods (see Supplementary Material S1).

As one can see in Figure 2A, the model easily finds the VB_z dominance in the ability to predict Dst, to which it adds the parameters known as secondary-important features in empirical modeling, namely, total IMF (B), the smoothed sunspot numbers (SSn), and IMF B_y component, with the tail of less-important parameters that still improve the quality of predictions: standard deviations of the most important parameters that can characterize the level of turbulence of the solar wind as well as the solar wind density (N), the radial IMF component B_x, the temperature (T), and their standard deviations.

3.4 Problems

The main challenge in space weather forecasting is that even well-known hazards associated with geomagnetic storms are poorly predicted, with most techniques providing reliable alerts only 60 min in advance, leaving insufficient time for implementing space weather countermeasures. The five models compared in Figure 2B, adapted from Telloni et al. (2023), utilize V, B_z, B, T, N, and the SYM-H index — an analogue of hourly Dst with one-minute resolution. The correlation matrix between the parameters and SYM-H and performance metrics values are given, respectively, in Figure 1 and Tables 3, 4 of Telloni et al. (2023). As illustrated in Figure 2B, the prediction accuracy tends to decline as the forecast lead time increases. This issue is corroborated by numerous studies using various models and input parameters (e.g., Shprits et al., 2019; Xu et al., 2020; Nair et al., 2023; Wang C et al., 2023; Xu et al., 2023), which similarly find that extending the forecast lead time compromises prediction accuracy. The solar wind conditions measured at L1 have both linear and near-linear links with the state of the magnetosphere and, subsequently, with geomagnetic indices at different timescales. For lower advance warning hours, linear models outperform deep CNNs because the relationship between solar wind parameters and geomagnetic storms is near-linear in the short term. As a result, linear models capture the direct connection effectively with fewer parameters. On the other hand, the magnetospheric response to changes in solar wind conditions at longer timescales involves more complex interactions and delayed effects, which require sophisticated models capable of capturing complex patterns and temporal dependencies. As a result, deep CNNs perform better for longer advance warning periods, which is important for mid-term forecasts (e.g., see Siciliano et al., 2021 and references therein). The performance difference reflects the models' differing abilities to handle simpler vs. more complex relationships, though data quality and training can still impact the exact magnitude of improvement.

One can also find the geomagnetic storm forecast accuracy of NOAA mid-term prognoses (24 h in advance) www.swpc.noaa.gov/sites/default/files/images/u30/SWPC%20GPRA%20Metric%20Description.pdf and https://www.swpc.noaa.gov/content/geomagnetic-activity-forecast-verification, which remains at the probabilistic ~50% level. Note that G1 storm in the NOAA classification corresponds to Kp = 5. Alternative techniques, such as remote sensing of the solar wind or MHD large-scale modeling are useful to understand the propagation of streams in the interplanetary medium in general, but they are often wrong or give a 12-h-delay in predictions of the increase in the speed or density of the solar wind (e.g., Jian et al., 2011).

Another major issue in geomagnetic storm prediction is the lack of open-access platforms for real-time data and difficulty in comparing different models, as many do not provide historical data or rely on different indices. Additionally, significant storms are rare, making up less than 1% of the data, which creates challenges for ML models that struggle with imbalanced datasets, often overlooking rare events. Incomplete datasets, such as the OMNI dataset with 20% missing data, further complicate training, leading to variable predictions. Traditional model-based methods, often paired with ML, assume Gaussian noise, but real spacecraft data deviate from this, reducing reliability. These challenges show that we are still in the early stages of achieving reliable geomagnetic storm forecasts.

4 Discussion

The ultimate goal of predicting geomagnetic storms is to provide a sufficient warning time for these events, which is critical for mitigating potential damages to satellites, power grids, and communication infrastructures. To address these challenges, various methodologies are explored, including the use of ensemble models that combine multiple predictive algorithms to enhance the accuracy of predictions. Meanwhile, the biggest problem of the current geomagnetic storm forecasts is the low accuracy of mid-term predictions with the advance time from 3 h to 3 days.

Short-term geomagnetic storm forecasts are highly accurate, primarily due to the time lag between detecting an approaching geoeffective stream by spacecraft at L1 and its actual impact on the Earth's magnetosphere. This allows us to take advantage of the fact that solar wind conditions signaling the onset of a storm are observable about an hour in advance. There is the assumption that the magnetosphere responds almost instantly to changes in solar wind, with the influx of energy mainly depending on VB_z. Consequently, most mid-term forecasts rely on the same approach as short-term ones, monitoring the solar wind speed and the IMF strength and direction measured at L1 as primary model inputs. Efforts to enhance these predictions, including models combining solar source data with L1 observations, continue to follow this paradigm, focusing on the same solar wind parameters.

The core problem with current storm prediction methods is that they are very effective for short-term forecasts but almost useless for mid-term ones. This is because predicting what is going to happen requires analyzing events leading up to the phenomenon under study, i.e., to the geomagnetic storm in our case — not just studying solar wind conditions once the storm has already started but looking for precursors. Another major flaw in the dominant approach is the assumption that all geomagnetic storms, regardless of their cause or intensity, are driven by the same key solar wind parameters.

In these terms, future studies of pre-storm conditions applied to the geomagnetic storm prognosis seem to be the way to solve the problems discussed above. The pre-storm variations in the X-ray (Chakraborty and Morley, 2020), energetic particle flux (Ameri and Valtonen, 2019; http://tromos.space.noa.gr/aspecs/#home), the cosmic ray intensity (Wang C et al., 2023), ULF variations, and enhancements in the solar wind plasma parameters (Khabarova, 2007; Khabarova and Yermolaev, 2008; Balasis et al., 2024; Santoso et al., 2024) may increase the accuracy of mid-term predictions, especially being combined with those distinguishing between different storm sources (e.g., Park et al., 2021).

Given that around 90% of storms during solar cycles 20–24 were weak to moderate, focusing on predicting all storms — not just extreme events — is critical, as these moderate storms statistically cause greater power grid disruptions. The fact that recent satellite issues occurred during a moderate storm further emphasizes the need for reliable forecasts as solar cycle 25 peaks. AI advancements, combined with real-time models like SWX-TREC (https://swx-trec.com/geoelectric/), may improve mitigating storm impacts, while creation of regional space weather centers like the recently opened Chinese Meridian Project (https://www.meridianproject.ac.cn/en/) and Tel Aviv University Space Weather Center (https://www.spaceweather.sites.tau.ac.il/) can help integrate scientific research into operational forecasting, improving preparedness for space weather. Future directions should include both studies of pre-storm conditions in the solar wind and exploring more sophisticated ML algorithms to automate feature selection processes, thereby improving prediction accuracy for geomagnetic storm events.

Author contributions

OK: Conceptualization, Formal Analysis, Investigation, Methodology, Visualization, Writing–original draft, Writing–review and editing. CP: Conceptualization, Project administration, Supervision, Writing–review and editing.

Funding

The author(s) declare financial support was received for the research, authorship, and/or publication of this article. The authors thank the International Office at Tel Aviv University for partial funding.

Acknowledgments

This study was carried out as a part of the activity of the Space Weather Center of the Tel Aviv University

(https://www.spaceweather.sites.tau.ac.il/). Olga Khabarova thanks the Center for Absorption in Science, Ministry of Immigration and Absorption, State of Israel for the support.

Conflict of interest

The authors declare that the research was conducted in the absence of any commercial or financial relationships that could be construed as a potential conflict of interest.

The author(s) declared that they were an editorial board member of Frontiers, at the time of submission. This had no impact on the peer review process and the final decision.

Publisher's note

All claims expressed in this article are solely those of the authors and do not necessarily represent those of their affiliated organizations, or those of the publisher, the editors and the reviewers. Any product that may be evaluated in this article, or claim that may be made by its manufacturer, is not guaranteed or endorsed by the publisher.

Supplementary material

The Supplementary Material for this article can be found online at: https://www.frontiersin.org/articles/10.3389/fspas.2024.1493917/full#supplementary-material

References

Abe, O. E., Fakomiti, M. O., Igboama, W. N., Akinola, O. O., Ogunmodimu, O., and Migoya-Orué, Y. O. (2023). Statistical analysis of the occurrence rate of geomagnetic storms during solar cycles 20–24. *Adv. Space Res.* 71 (5), 2240–2251. doi:10.1016/j.asr.2022.10.033

Ameri, Dh., and Valtonen, E. (2019). Potential role of energetic particle observations in geomagnetic storm forecasting. *Adv. Space Res.* 64 (3), 801–813. doi:10.1016/j.asr.2019.05.012

Baker, D. N. (2001). "Satellite anomalies due to space storms," in *Space storms and space weather hazards. NATO science series*. Editor I. A. Daglis (Dordrecht: Springer), 38, 285–311. doi:10.1007/978-94-010-0983-6_11

Balasis, G., De Santis, A., Papadimitriou, C., Boutsi, A. Z., Cianchini, G., Giannakis, O., et al. (2024). Swarm investigation of ultra-low-frequency (ULF) pulsation and plasma irregularity signatures potentially associated with geophysical activity. *Remote Sens.* 16, 3506. doi:10.3390/rs16183506

Baruah, Y., Roy, S., Sinha, S., Palmerio, E., Pal, S., Oliveira, D. M., et al. (2024). The loss of Starlink satellites in February 2022: how moderate geomagnetic storms can adversely affect assets in low-earth orbit. *Space weather* 22, e2023SW003716. doi:10.1029/2023SW003716

Belov, A. V., Belova, E. A., Shlyk, N. S., Abunina, M. A., Abunin, A. A., and Belov, S. M. (2024). Forbush effects and geomagnetic storms. *Geomagn. Aeron.* 64, 289–301. doi:10.1134/S0016793224600097

Borovsky, J. E. (2023). Further investigation of the effect of upstream solar-wind fluctuations on solar-wind/magnetosphere coupling: is the effect real? *Front. Astron. Space Sci.* 9 (id), 433. doi:10.3389/fspas.2022.975135

Borovsky, J. E., and Shprits, Y. Y. (2017). Is the Dst index sufficient to define all geospace storms? *J. Geoph. Res.* 122 (11), 11543–11547. doi:10.1002/2017ja024679

Boroyev, R. N., Vasiliev, M. S., and Baishev, D. G. (2020). The relationship between geomagnetic indices and the interplanetary medium parameters in magnetic storm main phases during CIR and ICME events. *J. Atmosph. Sol-Terr. Phys.* 204, 105290. doi:10.1016/j.jastp.2020.105290

Boutsi, A. Z., Balasis, G., Dimitrakoudis, S., Daglis, I. A., Tsinganos, K., Papadimitriou, C., et al. (2023). Investigation of the geomagnetically induced current index levels in the Mediterranean region during the strongest magnetic storms of solar cycle 24. *Space weather* 21, e2022SW003122. doi:10.1029/2022SW003122

Buzás, A., Kouba, D., Mielich, J., Burešová, D., Mošna, Z., Koucká Knížová, P., et al. (2023). Investigating the effect of large solar flares on the ionosphere based on novel Digisonde data comparing three different methods. *Front. Astron. Space Sci.* 10, 1201625. doi:10.3389/fspas.2023.1201625

Buzulukova, N., and Tsurutani, B. (2022). Space weather: from solar origins to risks and hazards evolving in time. *Front. Astron. Space Sci.* 9, 1017103. doi:10.3389/fspas.2022.1017103

Calabia, A., Lu, G., and Bolaji, O. S. (2023). Editorial: advances on upper atmosphere characterization for geodetic space weather research and applications. *Front. Astron. Space Sci.* 10, 1211582. doi:10.3389/fspas.2023.1211582

Chakraborty, S., and Morley, S. K. (2020). Probabilistic prediction of geomagnetic storms and thepindex. *J. Space Weather Space Clim.* 10, 36. doi:10.1051/swsc/2020037

Cid, C., Palacios, J., Saiz, E., Guerrero, A., and Cerrato, Y. (2014). On extreme geomagnetic storms. *J. Space Weather Space Clim.* 4, A28. doi:10.1051/swsc/2014026

Cilden-Guler, D., Kaymaz, Z., and Hajiyev, Ch. (2021). Geomagnetic disturbance effects on satellite attitude estimation. *Acta Astronaut.* 180, 701–712. doi:10.1016/j.actaastro.2020.12.044

Conde, D., Castillo, F. L., Escobar, C., García, C., García, J. E., Sanz, V., et al. (2023). Forecasting geomagnetic storm disturbances and their uncertainties using deep learning. *Space weather* 21, e2023SW003474. doi:10.1029/2023SW003474

Cristoforetti, M., Battiston, R., Gobbi, A., Iuppa, R., and Piersanti, M. (2022). Prominence of the training data preparation in geomagnetic storm prediction using deep neural networks. *Sci. Rep.* 12, 7631. doi:10.1038/s41598-022-11721-8

Daglis, I. A., Chang, L. C., Dasso, S., Gopalswamy, N., Khabarova, O. V., Kilpua, E., et al. (2021). Predictability of variable solar–terrestrial coupling. *Ann. Geophys.* 39, 1013–1035. doi:10.5194/angeo-39-1013-2021

Daglis, I. A., Katsavrias, C., and Georgiou, M. (2019). From solar sneezing to killer electrons: outer radiation belt response to solar eruptions. *Philosophical Trans. Ser. A, Math. Phys. Eng. sci* 377 (2148), 20180097. doi:10.1098/rsta.2018.0097

Dimitrova, S., and Babayev, E. (2018). "Space weather effects on human health," in *Variability of the Sun and sun-like stars: from asteroseismology to space weather*. Editors J. P. Rozelot, and E. S. Babayev (Les Ulis, France: EDP Sciences), 177–186. doi:10.1051/978-2-7598-2196-9.c012

Dimmock, A. P., Rosenqvist, L., Welling, D. T., Viljanen, A., Honkonen, I., Boynton, R. J., et al. (2020). On the regional variability of dB/dt and its significance to GIC. *Space weather* 18, e2020SW002497. doi:10.1029/2020SW002497

Echer, E., and Gonzalez, W. D. (2022). Relation between Dst ∗ and interplanetary parameters during single-step geomagnetic storms. *Adv. Space Res.* 70 (10), 2830–2841. doi:10.1016/j.asr.2022.07.031

Evans, J. S., Correira, J., Lumpe, J. D., Eastes, R. W., Gan, Q., Laskar, F. I., et al. (2024). GOLD observations of the thermospheric response to the 10–12 May 2024 Gannon superstorm. *Geophys. Res. Lett.* 51, e2024GL110506. doi:10.1029/2024GL110506

Gritsutenko, S., Korovkin, N., Sakharov, Y., and Sokolova, O. (2023). Assessment of geomagnetically induced currents impact on power grid modelling. *Magnetism* 3, 135–147. doi:10.3390/magnetism3020011

Gruet, M. A., Chandorkar, M., Sicard, A., and Camporeale, E. (2018). Multiple-hour-ahead forecast of the Dst index using a combination of long short-term memory neural network and Gaussian process. *Space weather* 16, 1882–1896. doi:10.1029/2018SW001898

Hines, P., Apt, J., and Talukdar, S. (2008). "Trends in the history of large blackouts in the United States," in *2008 IEEE power and energy society general meeting - conversion and delivery of electrical energy in the 21st century* (Pittsburgh, PA, USA), 1–8. doi:10.1109/PES.2008.4596715

Hu, A., Camporeale, E., and Swiger, B. (2023). Multi-hour-ahead Dst index prediction using multi-fidelity boosted neural networks. *Space weather* 21, e2022SW003286. doi:10.1029/2022SW003286

Jackson, B. V., Hick, P. L., Kojima, M., and Yokobe, A. (1998). Heliospheric tomography using interplanetary scintillation observations: 1. Combined Nagoya and Cambridge data. *J. Geophys. Res.* 103 (A6), 12049–12067. doi:10.1029/97JA02528

Jian, L. K., Russell, C. T., Luhmann, J. G., MacNeice, P. J., Odstrcil, D., Riley, P., et al. (2011). Comparison of observations at ACE and Ulysses with Enlil model results: stream interaction regions during Carrington rotations 2016–2018. *Sol. Phys.* 273 (1), 179–203. doi:10.1007/s11207-011-9858-7

Joselyn, J. A. (1995). Geomagnetic activity forecasting: the state of the art. *Rev. Geophys.* 33 (3), 383–401. doi:10.1029/95RG01304

Kay, C., Gopalswamy, N., Reinard, A., and Opher, M. (2017). Predicting the magnetic field of earth-impacting CMEs. *Astrophys. J.* 835, 117. doi:10.3847/1538-4357/835/2/117

Khabarova, O., and Dimitrova, S. (2009). On the nature of people's reaction to space weather and meteorological weather changes. *Sun Geosph.* 4 (2), 60–71. Available at: http://www.shao.az/SG/v4n2/SG_v4_No2_2009-p-60-71.pdf.

Khabarova, O., Malandraki, O., Malova, H., Kislov, R., Greco, A., Bruno, R., et al. (2021). Current sheets, plasmoids and flux ropes in the heliosphere. Part I. 2-D or not 2-D? General and observational aspects. *Space Sci. Rev.* 217, 38. doi:10.1007/s11214-021-00814-x

Khabarova, O., Pinaev, S. K., Chakov, V. V., Chizhov, A. Y., and Pinaeva, O. G. (2024). Trends in childhood leukemia incidence in urban countries and their relation to environmental factors, including space weather. *Front. Public Health* 12, 1295643. doi:10.3389/fpubh.2024.1295643

Khabarova, O. V. (2007). Current problems of magnetic storm prediction and possible ways of their solving. *Sun Geosph.* 2 (1), 33–38. Available at: http://sg.shao.az/v2n1/SG_v2_No1_2007-pp-33-38.pdf.

Khabarova, O. V., and Yermolaev, Yu.I. (2008). Solar wind parameters' behavior before and after magnetic storms. *J. Atm Sol. Terr. Phys.* 70 (2-4), 384–390. doi:10.1016/j.jastp.2007.08.024

Kim, R.-S., Moon, Y.-J., Gopalswamy, N., Park, Y.-D., and Kim, Y.-H. (2014). Two-step forecast of geomagnetic storm using coronal mass ejection and solar wind condition. *Space weather* 12 (4), 246–256. doi:10.1002/2014SW001033

Lakhina, G. S., and Tsurutani, B. T. (2016). Geomagnetic storms: historical perspective to modern view. *Geosci. Lett.* 3, 5. doi:10.1186/s40562-016-0037-4

Lucas, G., Love, J. J., Kelbert, A., Bedrosian, P. A., and Rigler, E. J. (2020). A 100-year geoelectric hazard analysis for the U.S. high-voltage power grid. *Space weather* 18, e2019SW002329. doi:10.1029/2019SW002329

Luhmann, J. G., Li, Y., Lee, C. O., Jian, L. K., Arge, C. N., and Riley, P. (2022). Solar cycle variability in coronal holes and their effects on solar wind sources. *Space weather* 20, e2022SW003110. doi:10.1029/2022SW003110

Luo, B., Liu, S., and Gong, J. (2017). Two empirical models for short-term forecast of Kp. *Space weather* 15 (3), 503–516. doi:10.1002/2016SW001585

Mac Manus, D. H., Rodger, C. J., Dalzell, M., Renton, A., Richardson, G. S., Petersen, T., et al. (2022). Geomagnetically induced current Modeling in New Zealand: extreme Storm analysis using multiple disturbance scenarios and industry provided hazard magnitudes. *Space weather* 20, 12. doi:10.1029/2022SW003320

Mac Manus, D. H., Rodger, C. J., Renton, A., Ronald, J., Harper, D., Taylor, C., et al. (2023). Geomagnetically induced current mitigation in New Zealand: operational mitigation method development with industry input. *Space weather* 21, e2023SW003533. doi:10.1029/2023SW003533

Malandraki, O. E., and Crosby, N. B. (2018). "Solar energetic particles and space weather: science and applications," in *Solar particle radiation storms forecasting and analysis*. *Astrophysics and space science library*. Editors O. Malandraki, and N. Crosby (Cham: Springer), 444, 1–26. doi:10.1007/978-3-319-60051-2_1

Matzka, J., Stolle, C., Yamazaki, Y., Bronkalla, O., and Morschhauser, A. (2021). The geomagnetic Kp index and derived indices of geomagnetic activity. *Space weather* 19, e2020SW002641. doi:10.1029/2020SW002641

Miteva, R., Samwel, S. W., and Tkatchova, S. (2023). Space weather effects on satellites. *Astronomy* 2, 165–179. doi:10.3390/astronomy2030012

Molinski, T. S. (2002). Why utilities respect geomagnetically induced currents. *J. Atmosph. Sol-Ter. Phys.* 64, 1765–1778. doi:10.1016/S1364-6826(02)00126-8

Mursula, K., Qvick, T., Holappa, L., and Asikainen, T. (2022). Magnetic storms during the space age: occurrence and relation to varying solar activity. *J. Geophys. Res.* 27, e2022JA030830. doi:10.1029/2022JA030830

Nair, M., Redmon, R., Young, L.-Y., Chulliat, A., Trotta, B., Chung, C., et al. (2023). MagNet—a data-science competition to predict disturbance storm-time index (Dst) from solar wind data. *Space weather* 21, e2023SW003514. doi:10.1029/2023SW003514

Ngwira, C. M., Pulkkinen, A. A., Bernabeu, E., Viljanen, A., and Crowley, G. (2015). Characteristics of extreme geoelectric fields and their possible causes: localized peak enhancements. *Geophys. Res. Lett.* 42, 6916–6921. doi:10.1002/2015GL065061

Park, W., Lee, J., Kim, K. C., Lee, J., Park, K., Miyashita, Y., et al. (2021). Operational Dst index prediction model based on combination of artificial neural network and empirical model. *J. Space Weather Space Clim.* 11, 38. doi:10.1051/swsc/2021021

Parker, W. E., and Linares, R. (2024). Satellite drag analysis during the may 2024 Gannon geomagnetic storm. *J. Spacecr. Rockets* 61, 1412–1416. doi:10.2514/1.A36164

Persons, T. M., and Rusco, F. (2018). "Technology assessment. Critical infrastructure protection," in *Protecting the electric grid from geomagnetic disturbances* (United States Senate: United States Government Accountability Office Report to the Committee on Homeland Security and Governmental Affairs). Available at: https://www.gao.gov/products/gao-19-98.

Pizzo, V., Millward, G., Parsons, A., Biesecker, D., Hill, S., and Odstrcil, D. (2011). Wang-sheeley-arge–enlil cone model transitions to operations. *Space weather* 9, S03004. doi:10.1029/2011SW000663

Pulkkinen, A., Lindahl, S., Viljanen, A., and Pirjola, R. (2005). Geomagnetic storm of 29-31 October 2003: geomagnetically induced currents and their relation to problems in the Swedish high-voltage power transmission system. *Space weather* 3 (8). doi:10.1029/2004SW000123

Pulkkinen, T. I., Brenner, A., Al Shidi, Q., and Toth, G. (2022). Statistics of geomagnetic storms: global simulations perspective. *Front. Astron. Space Sci.* 9, 972150. doi:10.3389/fspas.2022.972150

Reames, D. V. (2021). *Solar energetic particles, 2nd ed.; open access*. Cham, Switzerland: Springer Nature. doi:10.1007/978-3-030-66402-2

Reiss, M. A., Temmer, M., Veronig, A. M., Nikolic, L., Vennerstrom, S., Schöngassner, F., et al. (2016). Verification of high-speed solar wind stream forecasts using operational solar wind models. *Space weather* 14 (7), 495–510. doi:10.1002/2016SW001390

Ryu, M., Nagarajan, H., and Bent, R. (2020). Algorithms for mitigating the effect of uncertain geomagnetic disturbances in electric grids. *Electr. Power Syst. Res.* 189, 106790–107796. doi:10.1016/j.epsr.2020.106790

Santoso, A., Sismanto, S., Priyatikanto, Rh., Hartantyo, E., and Martiningrum, D. R. (2024). The intensity of the geomagnetic storms associated with imf and solar wind parameters during solar cycle 24. *Earth Planet. Phys.* doi:10.26464/epp2024069

Shprits, Y. Y., Vasile, R., and Zhelavskaya, I. S. (2019). Nowcasting and predicting the Kp index using historical values and real-time observations. *Space weather* 17, 1219–1229. doi:10.1029/2018SW002141

Siciliano, F., Consolini, G., Tozzi, R., Gentili, M., Giannattasio, F., and De Michelis, P. (2021). Forecasting SYM-H index: a comparison between long short-term memory and convolutional neural networks. *Space weather* 19, e2020SW002589. doi:10.1029/2020SW002589

Sierra-Porta, D., Petro-Ramos, J. D., Ruiz-Morales, D. J., Herrera-Acevedo, D. D., García-Teheran, A. F., and Tarazona Alvarado, M. (2024). Machine learning models for predicting geomagnetic storms across five solar cycles using Dst index and heliospheric variables. *Adv. Space Res.* 74 (8), 3483–3495. doi:10.1016/j.asr.2024.08.031

Siscoe, G., and Schwenn, R. (2006). CME disturbance forecasting. *Space Sci. Rev.* 123, 453–470. doi:10.1007/s11214-006-9024-y

Sorokin, V., Yaschenko, A., Mushkarev, G., and Novikov, V. (2023). Telluric currents generated by solar flare radiation: physical model and numerical estimations. *Atmosphere* 14 (3), 458. doi:10.3390/atmos14030458

Souza, J. R., Dandenault, P., Santos, A. M., Riccobono, J., Migliozzi, M. A., Kapali, S., et al. (2024). Impacts of storm electric fields and traveling atmospheric disturbances over the Americas during 23–24 April 2023 geomagnetic storm: experimental analysis. *J. Geophys. Res.* 129, e2024JA032698. doi:10.1029/2024JA032698

Srivastava, N., Mierla, M., and Zhang, J. (2021). Editorial: space weather prediction: challenges and prospects. *Front. Astron. Space Sci.* 8, 818878. doi:10.3389/fspas.2021.818878

Tchijevsky, A. L. (1938). *Les epidémies et les perturbations electromagnétiques du milieu extérieur*. Paris, France: Hippocrate. Available at: https://search.worldcat.org/formats-editions/14724886.

Telloni, D., Lo Schiavo, M., Magli, E., Fineschi, S., Guastavino, S., Nicolini, G., et al. (2023). Prediction capability of geomagnetic events from solar wind data using neural networks. *Astrophys. J.* 952, 111. doi:10.3847/1538-4357/acdeea

Tsurutani, B. T., Gonzalez, W. D., Gonzalez, A. L. C., Guarnieri, F. L., Gopalswamy, N., Grande, M., et al. (2006). Corotating solar wind streams and recurrent geomagnetic activity: a review. *J. Geophys. Res.* 111, A7. doi:10.1029/2005JA011273

Vennerstroem, S. (2001). Interplanetary sources of magnetic storms: a statistical study. *J. Geophys. Res.* 106 (A12), 29175–29184. doi:10.1029/2001JA000004

Wang, C., Ye, Q., He, F., Chen, B., and Zhang, X. (2023). A new method for predicting non-recurrent geomagnetic storms. *Space weather* 21, e2023SW003522. doi:10.1029/2023SW003522

Wang, J., Luo, B., Liu, S., and Shi, L. (2023). A machine learning-based model for the next 3-day geomagnetic index (Kp) forecast. *Front. Astron. Space Sci.* 10, 1082737. doi:10.3389/fspas.2023.1082737

Wintoft, P., and Wik, M. (2018). Evaluation of Kp and Dst predictions using ACE and DSCOVR solar wind data. *Space weather* 16, 1972–1983. doi:10.1029/2018SW001994

Wrenn, G. L. (2009). Chronology of 'killer' electrons: solar cycles 22 and 23. *J. Atmosph. Sol.-Terr. Phys.* 71 (10–11), 1210–1218. doi:10.1016/j.jastp.2008.08.002

Xu, S., Huang, S., Yuan, Z., Deng, X., and Jiang, K. (2020). Prediction of the Dst index with bagging ensemble-learning algorithm. *Astrophys. J. Suppl. Ser.* 248, 14. doi:10.3847/1538-4365/ab880e

Xu, W., Zhu, Y. M., Zhu, L., Lu, J., Wei, G., Wang, M., et al. (2023). A class of Bayesian machine learning model for forecasting Dst during intense geomagnetic storms. *Adv. Space Res.* 72 (9), 3882–3889. doi:10.1016/j.asr.2023.07.009

Zank, G. P., Hunana, P., Mostafavi, P., Roux, J. A. L., Li, G., Webb, G. M., et al. (2015). Diffusive shock acceleration and reconnection acceleration processes. *Astrophys. J.* 814 (1), 137. doi:10.1088/0004-637X/814/2/137

Zhang, J., Feng, Y., Zhang, J., and Li, Y. (2023). The short time prediction of the Dst index based on the long-short time memory and empirical mode decomposition–long-short time memory models. *Appl. Sci.* 13, 11824. doi:10.3390/app132111824

Zhang, J., Richardson, I. G., Webb, D. F., Gopalswamy, N., Huttunen, E., Kasper, J. C., et al. (2007). Solar and interplanetary sources of major geomagnetic storms (Dst < -100 nT) during 1996–2005. *J. Geophys. Res.* 112, A10102. doi:10.1029/2007JA012321

frontiers | Frontiers in Astronomy and Space Sciences

TYPE Mini Review
PUBLISHED 25 October 2024
DOI 10.3389/fspas.2024.1479301

Check for updates

OPEN ACCESS

EDITED BY
Paola Marziani,
Osservatorio Astronomico di Padova (INAF), Italy

REVIEWED BY
Anna Lia Longinotti,
Universidad Nacional Autonoma de Mexico, Mexico

*CORRESPONDENCE
A. Danehkar,
danehkar@eurekasci.com

RECEIVED 12 August 2024
ACCEPTED 01 October 2024
PUBLISHED 25 October 2024

CITATION
Danehkar A (2024) Relativistic reflection modeling in AGN and related variability from PCA: a brief review.
Front. Astron. Space Sci. 11:1479301.
doi: 10.3389/fspas.2024.1479301

COPYRIGHT
© 2024 Danehkar. This is an open-access article distributed under the terms of the Creative Commons Attribution License (CC BY). The use, distribution or reproduction in other forums is permitted, provided the original author(s) and the copyright owner(s) are credited and that the original publication in this journal is cited, in accordance with accepted academic practice. No use, distribution or reproduction is permitted which does not comply with these terms.

Relativistic reflection modeling in AGN and related variability from PCA: a brief review

A. Danehkar*

Eureka Scientific, Oakland, CA, United States

X-ray observations of active galactic nuclei (AGNs) reveal relativistic reflections from the innermost regions of accretion disks, which contain general-relativistic footprints caused by spinning supermassive black holes (SMBH). We anticipate the spin of a SMBH to be stable over the human timeframe, so brightness changes in the high-energy corona above the SMBH should slightly alter relativistic reflection. In this brief review, we discuss the latest developments in modeling relativistic reflection, as well as the rapid small variation in relativistic emission disclosed by the principal component analysis (PCA) of X-ray variability in AGN. PCA studies of X-ray spectra from AGNs have shown that relativistically blurred reflection has negligible fluctuations over the course of observations, which could originate from rapid (intrahour) intrinsic variations in near-horizon accretion flows and photon rings. The PCA technique is an effective way to disclose relativistic reflection from X-ray observations of AGNs, simplifying the complexity of largely variable X-ray data for automated spectral analysis with machine learning algorithms.

KEYWORDS

active galactic nuclei, relativistic disks, black hole spin, reflection, X-ray sources, principal component analysis

1 Introduction

The center of of the Milky Way is characterized by a supermassive black hole (SMBH), which is supported by indirect but compelling observational evidence such as stellar orbits in the vicinity of Sagittarius A* (Sgr A*; Ghez et al., 1998; Ghez et al., 2005) and the near-infrared luminosity of Sgr A* being consistent with the presence of an event horizon (Broderick and Narayan, 2006; Broderick et al., 2009). Similarly, we expect that active galactic nuclei (AGNs) in other galaxies host SMBHs at their centers (Kormendy, 1988; Kormendy and Richstone, 1992; Kormendy et al., 1997; Cretton and van den Bosch, 1999), which are essential to explaining the X-ray features of quasars and AGNs (see review by Mushotzky et al., 1993). Several techniques, such as the reverberation mapping (Blandford and McKee, 1982), spectral energy distribution (SED) fitting (Shields, 1978; Malkan, 1983), and broad-line region size–luminosity correlation (Vestergaard, 2002), have been developed to validate the presence of SMBHs and estimate their masses (e.g., Kormendy and Richstone, 1995; Miyoshi et al., 1995; Wandel et al., 1999; Peterson et al., 2004; Calderone et al., 2013; Capellupo et al., 2015; Bentz and Katz, 2015; Mejía-Restrepo et al., 2016). Our constraints on SMBH masses have allowed us to establish the connections between SMBHs and the evolution of their host galaxies (e.g.,

Magorrian et al., 1998; Ferrarese and Merritt, 2000; Häring and Rix, 2004; Heckman and Best, 2014).

Some solutions of standard general relativity simply characterize black holes using two parameters, mass and spin (Kerr, 1963), which can fully describe the properties of SMBHs. In this regard, spins of SMBHs, along with masses, could produce some of the fundamental mechanisms for powering relativistic jets (e.g., Garofalo et al., 2010; Tchekhovskoy and McKinney, 2012), as well as describing the discrepancy between radio-loud and radio-quiet AGNs (Wilson and Colbert, 1995; Moderski et al., 1998), galaxy evolution (Di Matteo et al., 2005; Volonteri et al., 2013; Sesana et al., 2014), and galaxy mergers (Hughes and Blandford, 2003; Volonteri et al., 2005; Berti and Volonteri, 2008). In particular, ultra-fast outflows (UFOs) have been detected in X-ray observations of several radio-quiet AGNs (e.g., Tombesi et al., 2010; 2011; 2012; Danehkar et al., 2018; Boissay-Malaquin et al., 2019), while extended relativistic jets have been seen in radio observations of radio-loud AGNs (see review by Blandford et al., 2019). The spins of SMBHs could have a potential role in the formation of UFOs and jets seen in AGNs and quasars (MacDonald et al., 1986; Thorne et al., 1986). These phenomena can be explained by spinning SMBHs according to the Blandford–Znajek (Blandford and Znajek, 1977) and Penrose mechanism (Penrose, 1969; 2002; Penrose and Floyd, 1971), as well as frame-dragging vortexes (e.g., Owen et al., 2011; Nichols et al., 2011; Danehkar, 2020). Alternatively, they could originate magnetically from the innermost accretion disk in the vicinity of a spinning SMBH according to the Blandford–Payne mechanism (Blandford and Payne, 1982).

In the Boyer–Lindquist coordinates, the Kerr metric (Kerr, 1963) of a spinning black hole is expressed using the set of oblate spheroidal coordinates (r, θ, ϕ) as follows (Boyer and Lindquist, 1967):

$$ds^2 = -\left(1 - \frac{r_s r}{\Sigma}\right) c^2 dt^2 - \frac{2\bar{a} r_s r \sin^2\theta}{\Sigma} c\,dt\,d\phi + \frac{\Sigma}{\Delta} dr^2 + \Sigma\, d\theta^2 + \left(r^2 + \bar{a}^2 + \frac{\bar{a}^2 r_s r \sin^2\theta}{\Sigma}\right) \sin^2\theta\, d\phi^2, \quad (1)$$

where $\Sigma = r^2 + \bar{a}^2 \cos^2\theta$, $\Delta = r^2 - r_s r + \bar{a}^2$, $r_s = 2GM/c^2$ is the Schwarzschild radius, $\bar{a} = J/Mc$ is called the Kerr spin parameter describing angular momentum per unit mass having the length dimension, J the black hole angular momentum, M the black hole mass, G the Newtonian constant of gravitation, and c the speed of light. The *dimensionless spin parameter*, which is frequently used in the astrophysical community, is defined as $a \equiv 2\bar{a}/r_s = Jc/(GM^2)$, while $-1 \le a \le 1$; negative values describe retrograde rotation, in which the black hole rotates in the opposite direction of the accretion disk, whereas positive values are associated with prograde rotation, and zero implies non-rotating black holes. The outer and inner event horizons are determined by the roots of $\Delta = 0$, which are $r_\pm = r_s(1 \pm \sqrt{1 - a^2})/2$. In the case of $a = 0$, Equation 1 reduces to the Schwarzschild metric (Schwarzschild, 1916) with the event horizon at $r = r_s$. Unlike the Schwarzschild metric, which has a singularity at $r = 0$, the Kerr metric has one at $\Sigma = 0$. The innermost stable circular orbit (ISCO) of the accretion disk is located at a radius of marginal stability, r_{ms}, which is given by (Bardeen et al., 1972):

$$r_{ms}(a) = \frac{GM}{c^2}\left(3 + Z_2 - \mathrm{sgn}(a)\sqrt{(3 - Z_1)(3 + Z_1 + 2Z_2)}\right), \quad (2)$$

where $\mathrm{sgn}(a)$ is the signum function having the value −1, 1 or 0 according to the sign of a, while Z_1 and Z_2 are defined as,

$$Z_1 = 1 + (1 - a^2)^{1/3}\left[(1 + a)^{1/3} + (1 - a)^{1/3}\right],$$

$$Z_2 = \sqrt{3a^2 + Z_1^2}.$$

This implies that the accretion disk has a limited extent at the marginal stability radius (r_{ms}), also called the ISCO radius. The value of this radius depends upon the dimensionless spin parameter, e.g.,

$$r_{ms} = \begin{cases} 0.5 r_s & \text{for } a = 1 \\ 3 r_s & \text{for } a = 0 \\ 4.5 r_s & \text{for } a = -1 \end{cases}.$$

In prograde rotation, the ISCO radius shrinks to nearly half of the Schwarzschild radius as it approaches a near-maximal spin ($a \approx 1$), while it expands in retrograde rotation ($-1 < a < 0$). For a non-spinning black hole, the ISCO radius is precisely three times the Schwarzschild radius.

There are different methods available to measure the spin of a single SMBH (see review by Brenneman, 2013). All of them are based on general relativity solutions of the Kerr spacetime in the vicinity of the black hole. They use the aforementioned fact that the ISCO radius (r_{ms}) of the accretion disk depends on the spin, as seen in Equation 2, and assume a geometrically thin disk that is capable of irradiating the corona radiation with light-bending in the innermost regions (see Figure 1 bottom-left). Below are the techniques that have been used to constrain the spins of SMBHs:

1.1 X-ray reflection spectroscopy

High-energy radiation from a corona or the base of a jet illuminates the accretion disk, reflecting scattered photons, which forms the basis of this method. Multiple Compton scatterings (Comptonization) of soft thermal photons lead to the cooling of the hot electrons in the corona (Haardt and Maraschi, 1991; 1993). A portion of the comptonized radiation undergoes scattering outside of the ionizing source, resulting in the formation of a power-law-shaped continuum that is typically observed in X-rays from AGN (Haardt and Maraschi, 1991). However, a fraction of the scattered photons will undergo reflection on the surface of the disk (Haardt and Maraschi, 1993), as seen in Figure 1 (top). If the disk is not fully ionized, the continuum includes the emission of various fluorescent emission lines at energies below 7 keV, in addition to the Compton hump with a peak at around 20–30 keV caused by downscattering, as seen in Figure 1 (top panel). The most notable line is Fe Kα, with a rest-frame energy of 6.4 keV, which is produced due to the significant iron abundance and fluorescence process. This line is the most important tool for describing the relativistic reflection from the innermost disk, as it becomes broadened and skewed due to Doppler and general-relativistic effects (see reviews by Reynolds and Nowak, 2003; Miller, 2007; Reynolds, 2013; 2014; 2019; Bambi -et al., 2021). The truncation of its low-energy tail directly corresponds to the ISCO radius, i.e., the spin. This feature, independent of mass or distance from the black hole, enables the measurement of black

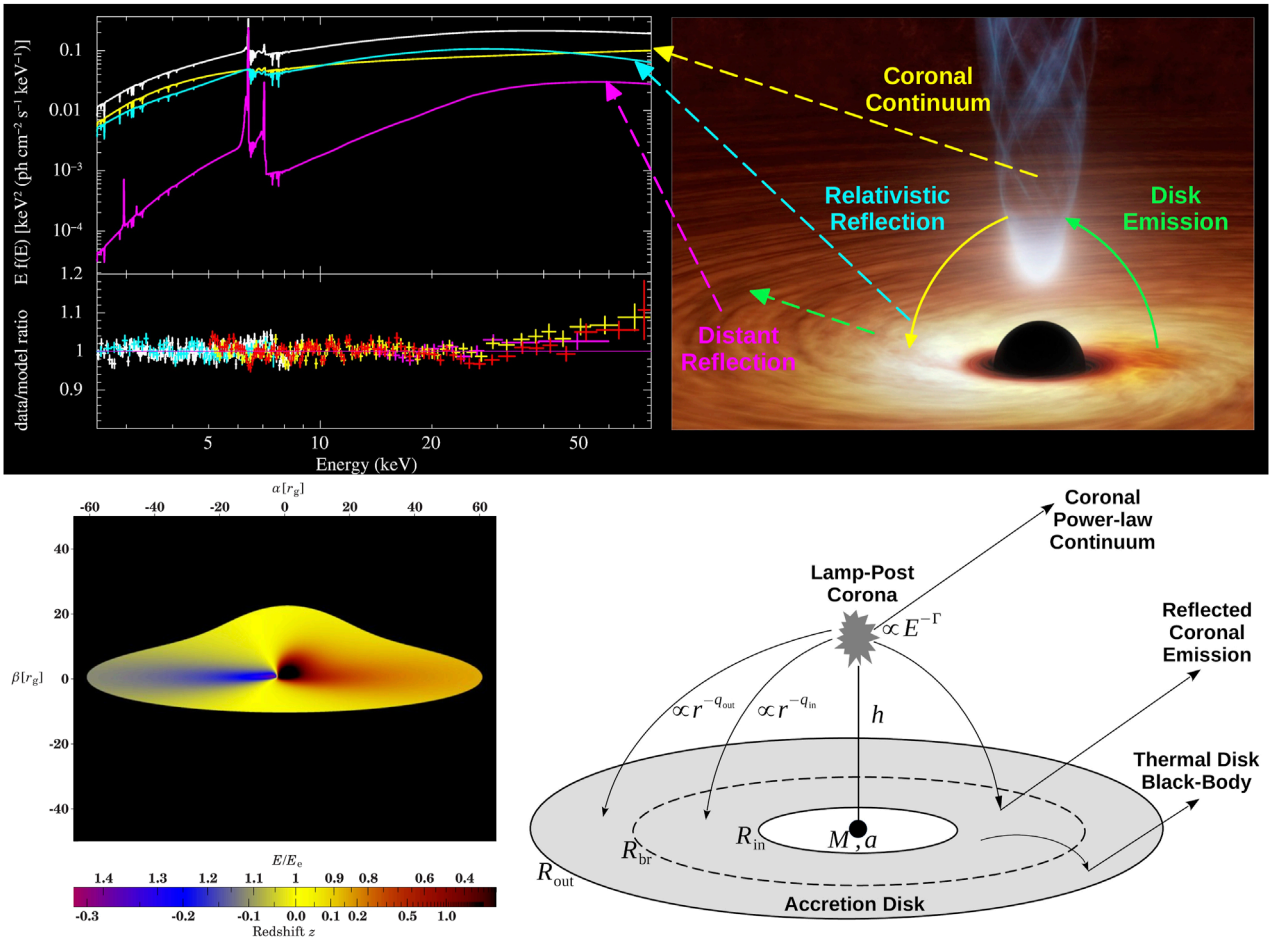

FIGURE 1
Top: A schematic view of X-ray relativistic reflection. Spectral model (left panel) of the Seyfert 1.5 galaxy NGC 4151, consisting of a coronal continuum (highecut × zpowerlw; yellow), relativistic reflection (relconv × xillver; light blue), and distant reflection (xillver; purple), fitted to *NuSTAR* and *Suzaku* observations, from Keck et al. (2015). An artist's illustration (right) of the radiation reflection from the accretion disk around a black hole (courtesy of NASA/JPL-Caltech/R. Hurt at IPAC/R. Connors at Caltech). Bottom: A simulated image (left panel) of an accretion disk, inclined with $i = 80°$ (relative to the line of sight), gravitationally distorted by general-relativistic light-bending effects of a black hole at the center, from García et al. (2014). A diagram (right) illustrating the lamp-post corona with a power-law-shaped continuum ($\propto E^{-\Gamma}$) situated at a height (h) above a black hole simply described by its mass (M) and spin (a), and the innermost accretion disk characterized by the boundary radii (R_{in} and R_{out}) and the break radius (R_{br}) to describe the coronal emissivity laws $\propto r^{-q_{in}}$ ($R_{in} < r < R_{br}$) and $\propto r^{-q_{out}}$ ($R_{br} < r < R_{out}$), as well as corresponding thermal disk black-body and reflected coronal emission, adopted from Dauser (2014) and Hoormann et al. (2016).

hole spins. One of the drawbacks of this method for AGN is the complex absorption from line-of-sight material, typically found at lower energies in the red tail. Moreover, exceptionally high counts are required to properly constrain the spin; 2×10^5 (Guainazzi et al., 2006) or 1.5×10^5 counts (de La Calle Pérez et al., 2010) in the energy range of 2–10 keV. Furthermore, this approach is actually model-dependent, as demonstrated by a list of reflection models in Table 1. However, the advancements in X-ray spectroscopy above 10 keV with the *Nuclear Spectroscopic Telescope Array* (*NuSTAR*; Harrison et al., 2013), which has no pile-up effects, have significantly improved the reliability of this approach by including the Compton hump reflection at high energies (> 10 keV, peaking within 20–30 keV; see, e.g., Parker et al., 2014c; Keck et al., 2015; Victoria-Ceballos et al., 2023). Most of the spectral models developed for X-ray relativistic reflection are briefly reviewed in Section 2.

1.2 Broad-band SED fitting

This method was initially began to be deployed for X-ray binaries by Zhang et al. (1997) and Gierliński et al. (2001). This approach depends on the distance, mass, and disk inclination angle of the accretion disk (see review by Remillard and McClintock, 2006), so it has mostly been used for the spin measurement of stellar-mass black holes (e.g., Shafee et al., 2006; McClintock et al., 2006). This method was first exploited by Done et al. (2013) to put constraints on the spins of SMBHs with the optxconv model (based on optxagnf; Done et al., 2012), which contains the SED spectrum made by a (color-temperature-corrected) blackbody, an optically thick warm Comptonisation (soft excess; < 2 keV) component, and an optically thin, hot Comptonisation (power-law; > 2 keV) component. Later, the same technique was employed to measure the spins of AGNs at $z \sim 1.5$ that evolved just after cosmic noon (Capellupo et al.,

TABLE 1 A list of spectral models developed for relativistically broadened emission of the accretion disk.

Relativistic broad line			
Model	Parameters[a]	Convolution	References
diskline	$a = 0$, i, Γ, R_{in}, R_{out}	rdblur	Fabian et al. (1989)
laor	$a = 0.998$, i, q, R_{in}, R_{out}	kdblur	Laor (1991)
kerrspec	$a = 0.001, 0.9981$, i, Γ, R_{in}, R_{out}, h	—	Martocchia et al. (2000)
kyrline/ky	a ($\geq$0), i, R_{in}, R_{out}, R_{br}, q_{in}, q_{out}, limb	kyconv	Dovčiak et al. (2004, 2022)
kerrdisk	a ($\geq$0), i, R_{in}, R_{out}, R_{br}, q_{in}, q_{out}	kerrconv	Brenneman and Reynolds (2006)
relline	a, i, R_{in}, R_{out}, R_{br}, q_{in}, q_{out}, limb	relconv	Dauser et al. (2010)
relline_lp	a, i, Γ, R_{in}, R_{out}, R_{br}, h, limb	relconv_lp	Dauser et al. (2013)
relxill[b]	a, i, Γ, R_{in}, R_{out}, R_{br}, q_{in}, q_{out}, $\log \xi$, A_{Fe}, $f_{refl,rel}$, E_{cut}	—	García et al. (2014), Dauser et al. (2014, 2016)
relxilllp[b]	a, i, Γ, R_{in}, R_{out}, h, β, $\log \xi$, A_{Fe}, $f_{refl,rel}$, E_{cut}	—	García et al. (2014), Dauser et al. (2014, 2016)
relxillCp[c]	a, i, Γ, R_{in}, R_{out}, R_{br}, q_{in}, q_{out}, $\log \xi$, A_{Fe}, $f_{refl,rel}$, kT_e, $\log n$	—	García et al. (2014), Dauser et al. (2014, 2016)
relxilllpCp[c]	a, i, Γ, R_{in}, R_{out}, h, β, $\log \xi$, A_{Fe}, $f_{refl,rel}$, kT_e, $\log n$	—	García et al. (2014), Dauser et al. (2014, 2016)
relline_nk[d]	a, i, R_{in}, R_{out}, R_{br1}, R_{br2}, q_1, q_2, q_3, limb, $\dot{m}$, $\alpha_{13}/\alpha_{22}/\epsilon_3$	relconv_nk	Bambi et al. (2017), Abdikamalov et al. (2019, 2020)
rellinelp_nk[d]	a, i, Γ, R_{in}, R_{out}, R_{br}, h, limb, $\dot{m}$, $\alpha_{13}/\alpha_{22}/\epsilon_3$	relconvlp_nk	Bambi et al. (2017), Abdikamalov et al. (2019, 2020)
relxill_nk[d]	a, i, Γ, R_{in}, R_{out}, R_{br}, R_{br}, q_1, q_2, q_3, $\log \xi$, A_{Fe}, $f_{refl,rel}$, E_{cut}, $\dot{m}$, $\alpha_{13}/\alpha_{22}/\epsilon_3$	—	Bambi et al. (2017), Abdikamalov et al. (2019, 2020)
relxilllp_nk[d]	a, i, Γ, R_{in}, R_{out}, h, $\log \xi$, A_{Fe}, $f_{refl,rel}$, E_{cut}, $\dot{m}$, $\alpha_{13}/\alpha_{22}/\epsilon_3$	—	Bambi et al. (2017), Abdikamalov et al. (2019, 2020)
relxillCp_nk[d]	a, i, Γ, R_{in}, R_{out}, R_{br1}, R_{br2}, q_1, q_2, q_3, $\log \xi$, A_{Fe}, $f_{refl,rel}$, kT_e, $\dot{m}$, $\alpha_{13}/\alpha_{22}/\epsilon_3$	—	Bambi et al. (2017), Abdikamalov et al. (2019, 2020)
relxilllpCp_nk[d]	a, i, Γ, R_{in}, R_{out}, h, $\log \xi$, A_{Fe}, $f_{refl,rel}$, kT_e, $\dot{m}$, $\alpha_{13}/\alpha_{22}/\epsilon_3$	—	Bambi et al. (2017), Abdikamalov et al. (2019, 2020)
reflkerr	a, i, τ/Γ, R_{in}, R_{out}, R_{br}, q_{in}, q_{out}, $\log \xi$, A_{Fe}, $f_{refl,rel}$, kT_e, kT_{bb}, geom	—	Niedźwiecki and Życki (2008), Niedźwiecki et al. (2016, 2019)
reflkerr_lp	a, i, τ/Γ, R_{in}, R_{out}, h, δ, $\log \xi$, A_{Fe}, $f_{refl,rel}$, kT_e, kT_{bb}, geom	—	Niedźwiecki and Życki (2008), Niedźwiecki et al. (2016, 2019)
reltrans	a, i, Γ, R_{in}, R_{out}, h, $\log \xi$, A_{Fe}, E_{cut}, N_H, $1/\mathcal{B}$, M_{BH}, ν_{min}, ν_{max}, ϕ_A, ReIm	—	Ingram et al. (2019), Mastroserio et al. (2021)

(Continued on the following page)

TABLE 1 (*Continued*) A list of spectral models developed for relativistically broadened emission of the accretion disk.

Relativistic broad line			
Model	Parameters[a]	Convolution	References
reltransCp	a, i, Γ, R_{in}, R_{out}, h, log ξ, A_{Fe}, kT_e, N_H, $1/\mathcal{B}$, M_{BH}, v_{min}, v_{max}, ϕ_A, ReIm	—	Ingram et al. (2019), Mastroserio et al. (2021)

[a]Parameters of relativistic broad line models are as follows: dimensionless black-hole spin parameter (a), disk inclination angle relative to the line of sight (i), power-law index (Γ), inner radius (R_{in}), outer radius (R_{out}), break radius (R_{br}), coronal emissivity law indexes (q as r^{-q} between R_{in} and R_{out}; q_{in} as $r^{-q_{in}}$ between R_{in} and R_{br}; and q_{out} as $r^{-q_{out}}$ between R_{br} and R_{out}), height of the primary source above the black hole (h), velocity of the primary source relative to the speed of light (β), limb describes limb-darkening/-brightening law (0: isotropic emission, 1: Laor's limb-darkening $1 + 2.06\mu$, and 2: Haardt's limb-brightening $\ln[1 + 1/\mu]$), ionization parameter of the accretion disk (log ξ), iron abundance relative to solar (A_{Fe}), reflection fraction parameter ($f_{refl,rel}$), high energy cutoff (E_{cut}) of the primary source described by cutoffpl, the electron temperature (kT_e) in the corona described by nthcomp, logarithmic number density of the innermost accretion disk (log n), break radii (R_{br1} and R_{br2}) for non-Kerr spacetimes, coronal emissivity law indexes in non-Kerr spacetimes (q_1 between R_{in} and R_{br1}; q_2 between R_{br1} and R_{br2}; and q_2 between R_{br2} and R_{out}), hydrogen column density of the line-of-sight material (N_H), boosting factor of the reflection spectrum ($1/\mathcal{B}$), black hole mass (M_{BH}), frequency range of the transfer function (v_{min} and v_{max}), phase normalization (ϕ_A), cross-spectrum modes (ReIm = 1, 2, 3, 4, 5, or 6), blackbody soft-excess temperature (kT_{bb}), Thomson optical depth $\tau(\Gamma, kT_e)$ yielding Γ, bottom-lamp attenuation ($0 < \delta < 1$), and geometry (geom = −5, −4, 0, 4, or 5) defined similar to the same parameter in compPS (Poutanen and Svensson, 1996).

[b]The model relxill is a combination of relconv, xillver, and cutoffpl. The model relxilllp is a mixture of relconv_lp, xillver, and cutoffpl. The number density is fixed (log $n = 15$) in the models relxill and relxilllp.

[c]The models relxillCp and relxilllpCp are, respectively, similar to relxill and relxilllp, but they use nthcomp instead of cutoffattenuation of the pl, as well as a free parameter for the number density (log $n = 15$–20).

[d]"nk" at the end of the spectral models stands for non-Kerr spacetimes, which are describe by the deformation parameters α_{13}, α_{22}, or ϵ_3 in the Johannsen metric (Johannsen, 2013), as well as the thickness of the accretion disk described by $\dot{m}$ (0: infinitesimally-thin, 1: 5%, 2: 10%, 3: 20%, 4: 30% of the Eddington accretion rate).

2015; Capellupo et al., 2016), and was benchmarked against X-ray reflection measurements for NGC 3783, an AGN known for its relativistically broadened Fe Kα line (Capellupo et al., 2017). This method was employed to constrain the masses and spins of SMBSH in four blazars at high redshifts (Campitiello et al., 2018), which was implemented using the kerrbb model (Li et al., 2005) of multi-temperature blackbody spectrum of a thin accretion disk around a spinning black hole. The optxconv SED model (Done et al., 2012; Done et al., 2013) was also used by Porquet et al. (2019) to derive a well-measured spin rate of the SMBH in Ark 120, a well-known bare AGN with no intrinsic absorption along the line-of-sight. Subsequently, new SED models of the broad-band continuum of AGN, called agnsed and qsosed (Kubota and Done, 2018; Petrucci et al., 2018), have been developed, followed by a super-Eddington accretion model of the slim disk (agnslim; Kubota and Done, 2019), which provide better constraints on the masses and spins of SMBHs. More recently, Hagen and Done (2023) made a fully general-relativistic implementation of agnsed, referred to as the relagn model that includes general-relativistic ray tracing and the relativistic Novikov–Thorne disk model (Novikov and Thorne, 1973), leading to a complex disk spectrum in the soft excess instead of a simple blackbody, and was utilized to determine the SMBH spin in Fairall 9 from the broad-band spectrum, extending from Optical/UV to the X-ray.

1.3 Radio event horizon imaging

This method employs sub-mm data collected by several very long baseline interferometry (VLBI) stations over different locations (e.g., JCMT, SMT, SPT, IRAM, APEX, and ALMA) to achieve micro-arcsecond spatial resolution images of an SMBH event horizon (Event Horizon Telescope Collaboration et al., 2019a; Event Horizon Telescope Collaboration et al., 2022a). This has enabled the first-ever images of the accretion flow in the vicinity of nearby SMBHs to be produced, namely M87 and Sgr A* (Event Horizon Telescope Collaboration et al., 2019b; Event Horizon Telescope Collaboration et al., 2022b). We can determine the SMBH spin by accurately modeling the appearance of accretion flows in VLBI images, accounting for general-relativistic light bending (see Figure 1 bottom-left) based on various characteristics such as the ISCO radius (r_{ms}). The VLBI imaging techniques have recently been used to deduce the spin values according to high-spatial-resolution images in Sgr A* and M87 (Event Horizon Telescope Collaboration et al., 2019c; Event Horizon Telescope Collaboration et al., 2021b; Event Horizon Telescope Collaboration et al., 2022c; Event Horizon Telescope Collaboration et al., 2022d). This method has the disadvantage of only being suitable for nearby SMBHs.

2 Relativistic reflection modeling

Various spectral models have been constructed to reproduce the general-relativistic effects of the Kerr metric on the iron Kα line profile. Table 1 summarizes most of the well-known spectral models made for X-ray data analysis of relativistically blurred emission, along with their key parameters. The basic parameters in these models are the dimensionless spin parameter ($a = Jc/GM^2$), the line-of-sight inclination angle (i) of the accretion disk, the spectral photon index (Γ) of the primary source – the corona or the base of a jet above the black hole –, as well as the boundary radii (R_{in} and R_{out}) of the innermost accretion disk. Most of these models can be loaded into tools for X-ray spectral analysis, particularly the X-ray spectral fitting package XSPEC[1] (Arnaud, 1996; Arnaud et al., 1999) of HEASoft's data analysis package for X-ray astronomy XANADU (NASA HEASARC, 2014), MIT's Interactive Spectral Interpretation System[2] (ISIS; Houck and

1 https://heasarc.gsfc.nasa.gov/xanadu/xspec/

2 https://space.mit.edu/cxc/isis/

Denicola, 2000), CXC[3]'s Modeling and Fitting Package Sherpa[4] (Freeman et al., 2001; Doe et al., 2007) of the Chandra Interactive Analysis of Observation (CIAO; Fruscione et al., 2006), and SRON[5]'s X-ray high-resolution spectral modeling and fitting package SPEX[6] (Kaastra et al., 1996; de Plaa et al., 2020). These models are often applied to integrated spectra of AGNs without accounting for the variability of the X-ray sources.

The early models, developed to analyze relativistic reflection, featured fiducial values for the spin parameter. Black hole spin measurement began with the diskline (Fabian et al., 1989) and laor (Laor, 1991) fixed-spin models, which were run with fiducial spin values of $a = 0$ and 0.998, respectively. The diskline model was based on analytic, time-consuming calculations, whereas the laor model relied on extensive pre-calculated tabulated Flexible Image Transport System (FITS) data created for different combinations of the model parameters: inclination angle, spectral photon index (Γ), inner radius ($R_{\rm in}$), and outer radius ($R_{\rm out}$). The laor model recreates the relativistic line shape by interpolating data from the extensive FITS table. Later, Martocchia and Matt (1996) examined how the "lamp post" geometry affected the broad iron Kα lines, in which the ionizing source is located on the polar axis at a height (h) above the black hole, as illustrated in Figure 1 (bottom-right). This investigation was followed by a comprehensive analysis for a = 0.001 and 0.9981 leading to the kerrspec model (Martocchia et al., 2000; Martocchia et al., 2002). We should note that the reflection continuum was not included in these models and needed to be handled by a separate model such as reflionx (Ross et al., 1999; Ross and Fabian, 2005; Ross and Fabian, 2007), which should be convolved with the corresponding convolution models to make a smoothed spectrum of relativistic smearing in an accretion disk. The convolution models rdblur and kdblur were prepared using diskline and laor, respectively, which can be used with a reflection model (e.g., reflionx). Nandra et al. (2007) used a modified version of the kdblur model to characterize the broad iron Kα line in *XMM-Newton* observations of a sample of Seyfert galaxies. However, the spectral models with fixed spin rates obviously prevented us from straightforwardly measuring the black hole spin.

The next-generation of relativistic reflection models has a free parameter for the positive spin rates, which allows for the determination of the black hole spin in prograde rotation ($0 \leqslant a < 1$). The kyrline (or ky) model (Dovčiak, 2004; Dovčiak et al., 2004; Dovčiak et al., 2022) was developed to incorporate extensive tables calculated for transfer functions. This model rapidly computes the shape of relativistically broadened line emission using transfer function tables without relying heavily on interpolation, yielding a significantly greater level of spectral resolution compared to the laor model. Furthermore, the black hole spin was a free parameter, ranging from $a = 0$ to 1. The model can therefore reproduce the relativistic blurred emission more accurately than the laor model for all positive spin rates and inclination degrees. In addition, the kyrline model features coronal emissivity law indexes ($q_{\rm in}$ as $r^{-q_{\rm in}}$ between $R_{\rm in}$ and $R_{\rm br}$; and $q_{\rm out}$ as $r^{-q_{\rm out}}$ between $R_{\rm br}$ and $R_{\rm out}$) for precisely creating the emitted radiation (see Figure 1 bottom-right), describing the emissivity characteristics on both sides of the break radius ($R_{\rm br}$), as well as including the limb prescriptions for limb-darkening/-brightening laws (Chandrasekhar, 1960), namely isotropic emission ($I \propto 1$), Laor's limb-darkening ($I \propto 1 + 2.06\mu$; Laor, 1991), and Haardt's limb-brightening ($I \propto \ln(1 + 1/\mu)$; Haardt, 1993), where $\mu = \cos(\theta_{\rm e})$ and $\theta_{\rm e}$ is the inclination angle of the emitted radiation with respect to the disk. These features were accomplished by computing them for inclusion in the comprehensive FITS table. In order to address the problems with the excessive table size and lack of smoothness in the kyrline model, Brenneman and Reynolds (2006) created an alternative model for relativistic reflection known as kerrdisk (Brenneman, 2007). Their model has a relatively smaller FITS table and a robust interpolation approach. Using a high level of smoothness in the transfer function allows for effective interpolation in kerrdisk. Furthermore, this model employs a distinct methodology, approximating the narrow line of the distant reflection from the accretion disk using a δ-function instead of a Gaussian function. Their model computes a larger portion of the integration using analytic approaches, thereby excluding the emissivity law from the calculated table. However, fitting methods can handle the modeling of the emissivity law. This model effectively reduces the table size to a fraction of the kyrline FITS table. Nevertheless, the relativistic emission produced by kerrdisk appears less smooth than those made by kyrline, with some noticeable spikes in the red wing of the relativistic line. However, data accumulated with the spectral resolutions of detectors aboard the *XMM-Newton* and *Suzaku* telescopes could not distinguish these spikes. The kyrline model has been used to conduct an *XMM-Newton* survey on a sample of radio-quiet Type 1 AGNs (de La Calle Pérez et al., 2010). Unlike the fixed-spin models (laor and diskline), kyrline and kerrdisk, which can relativistically be convolved with a reflection model (e.g., reflionx) using the kyconv and kerrconv models, respectively, are more accurate in producing the shape of relativistic emission for any positive spin rates. However, a black hole spinning in retrograde relative to the accretion disk ($-1 < a < 0$) could not have its spin constrained by the kyrline and kerrdisk models.

Since 2010, several spectral models have been developed for relativistic blurred emission (see Table 1) that incorporate both positive and negative spin values, enabling the measurement of the black hole's spin in both the prograde and retrograde directions with respect to the accretion disk. To accommodate the full spin range ($-0.998 \leqslant a \leqslant +0.998$), Dauser et al. (2010) has created the relline model, together with relline_lp, featuring the "lamp post" geometry (for detail see Dauser, 2010), using FITS tables for Cunningham's photon transfer function (Cunningham, 1975) pre-calculated with a customized version of the F77 program photon_transferfct[7] (also called spx; Speith, 1993; Speith et al., 1995) (a gravitationally-distorted appearance of an accretion disk made with a modified version of this program is shown in the bottom-left panel of Figure 1). The relline model employs Green's functions to calculate the radiated radiation for arbitrary angular and radial

3 The Chandra X-Ray Center (CXC) is operated for NASA by the Smithsonian Astrophysical Observatory (SAO).

4 https://cxc.cfa.harvard.edu/sherpa/

5 Netherlands Institute for Space Research (Stichting Ruimteonderzoek Nederland; SRON) is a Dutch institute for astrophysical research.

6 https://www.sron.nl/astrophysics-spex/

7 https://pisrv1.am14.uni-tuebingen.de/~speith/misc.html

variations, as well as robust interpolation techniques that lead to a decrease in pre-calculated tabulated data. Moreover, relativistic line profiles calculated for a hard X-ray source located on the rotational axis at a height (h) above the black hole, i.e., the "lamp post" geometry, are provided in the relline_lp model (Dauser et al., 2013). Both the models includes prescriptions for the limb-darkening/-brightening laws. Their corresponding convolution models, relconv and relconv_lp, are able to convolve the reflection continuum created by a reflection model such as reflionx (Ross et al., 1999; Ross and Fabian, 2005; Ross and Fabian, 2007) and xillver (García, 2010; García and Kallman, 2010; García et al., 2011; García et al., 2013). As this simple combination of the relativistic convolution model (relconv) and the reflection model (xillver) can lead to inconsistent results, García et al. (2014) made a self-consistent implementation of the spectrum reflected from the disk irradiated by an ionizing source and relativistically blurred emission in a new model called relxill, as well as an additional new model called relxill_lp for a lamp-post geometry.[8] These models incorporated angle-dependent reflection tables of xillver[9] into the relativistic blurring calculations, which exhibits like behavior to a convolution of xillver and relconv (or relconv_lp), albeit with self-consistently calculated X-ray reflection (Dauser, 2014). Subsequently, Dauser et al. (2014) and Dauser et al. (2016), further extended them to include the reflection fraction parameter ($f_{\rm refl,rel}$), a flux ratio between the direct and reflected radiation that depends on the geometry and location of the radiation source. In the updated model relxillCp (Dauser et al., 2016), the primary source is made by a thermally Comptonized continuum model (nthcomp; Zdziarski et al., 1996; Życki et al., 1999) and offers a free parameter for the disk density ranging from 10^{15} to 10^{20} cm^{-3}, whereas the previous model relxill uses a power law with a high-energy exponential cutoff (zcutoffpl) and assumes a disk density of 10^{15} cm^{-3}. Recently, the inclusion of returning radiation is implemented in the latest model of relxilllpCp by Dauser et al. (2022), featuring the "lamp post" geometry with a thermally comptonized continuum as the primary source and an unrestricted density parameter (10^{15}–10^{20} cm^{-3}). Additionally, García et al. (2022) also present the model relxillNS featuring a black body spectrum, specifically tailored to accommodate the reflection from the disk around an accreting neutron star. The relativistic X-ray reflection models provided by the relxill package were also extended to describe the reflection spectrum in the Johannsen metric (Johannsen, 2013), referred to as relline_nk (Bambi et al., 2017; Abdikamalov et al., 2019; Abdikamalov et al., 2020; Abdikamalov et al., 2021b; Abdikamalov et al., 2021a),[10, 11] whose model names contain "nk" at the end (e.g., relxill_nk and relxillCp_nk stand for non-Kerr spacetimes) to distinguish them from those in the Kerr metric (see Table 1). These models allow to validate the Kerr metric through the deformation parameters α_{13}, α_{22}, or ϵ_3 in the Johannsen metric, where $\alpha_{13} = \alpha_{22} = \epsilon_3 = 0$ restores the Kerr metric (for non-Kerr metrics, see review by Bambi, 2017).

X-ray time-resolved observations of AGNs have shown *variability* in the relativistically blurred reflection (e.g., MCG–6-30-15; Fabian and Vaughan, 2003; Vaughan and Fabian, 2004; Larsson et al., 2007; Miller et al., 2008) that could be caused by general relativistic effects, particularly light bending near the black hole event horizon. Niedźwiecki and Życki (2008) and Niedźwiecki and Miyakawa (2010) investigated variability patterns of the red wing in X-ray reflection of the AGN in the Seyfert 1 galaxy MCG–6-30-15 using a detailed light-bending model (Miniutti and Fabian, 2004), which led to the development of the spectral model reflkerr and its corresponding lamp-post model reflkerr_lp (Niedźwiecki et al., 2016; Niedźwiecki et al., 2019).[12] In particular, Niedźwiecki et al. (2016) identified some inconsistencies between reflkerr and relxilllp owing to the neglect of the general-relativistic redshift of the direct coronal radiation in relxilllp, though they found that the relxilllp model still produces acceptable results in weak-gravity in the energies below 80 keV. Moreover, the lamp-post model reflkerr_lp developed by Niedźwiecki et al. (2019) demonstrated a departure from relxilllp in the energies above 30 keV. Another model-family for spectral and timing variability in accreting black holes has been developed (Ingram et al., 2019; Mastroserio et al., 2021; 2022), named reltrans and reltransCp,[13] which calculated the emergent reflection spectrum using xillver (or xillverCp in the case of reltransCp). The reltrans model considers all the general-relativistic effects to calculate the time delays and energy changes that occur when X-ray photons from the corona reflect from the accretion disk and scatter towards the observer. The calculations of reltrans incorporate both continuum lags and reverberation lags in a self-consistent manner to produce most of the practical X-ray variability time scales.

3 Variability in relativistic reflection from PCA

Principal component analysis (PCA; Hotelling, 1933),[14] also referred to as the "Hotelling transform," is a well-known method in multivariate statistics relying on eigenvalues and eigenvectors (see review by Jolliffe and Cadima, 2016) that has been extensively discussed in detail in the literature (e.g., Mardia et al., 1979; Jolliffe, 2002; Izenman, 2008; Rencher and Christensen, 2012). It bears a close relation to the "Kosambi–Karhunen–Loève transform" (Kosambi, 1943; Karhunen, 1947; Loève, 1948) in probability theory, and is among three classical techniques in multivariate analysis to determine the principal dimensions of large data, along with independent component analysis (ICA; Hérault and Ans, 1984; Hérault et al., 1985; Hérault and Jutten, 1986) and non-negative matrix factorization (NMF; Lee and Seung, 1999; Lee and Seung, 2000). PCA can be employed to separate various characteristics

8 https://www.sternwarte.uni-erlangen.de/~dauser/research/relxill/

9 https://sites.srl.caltech.edu/~javier/xillver/

10 https://www.tat.physik.uni-tuebingen.de/~nampalliwar/relxill_nk/

11 https://github.com/ABHModels/relxill_nk, doi:10.5281/zenodo.13906295

12 https://users.camk.edu.pl/mitsza/reflkerr/

13 https://adingram.bitbucket.io/reltrans.html

14 It was first innovated by Pearson (1901) in the context of principal axes of ellipsoids in geometry, but it was independently developed and called *the method of principal components* by Hotelling (1933) for statistical analysis.

that are mostly responsible for complex variations in large data in astronomy (e.g., Wall and Jenkins, 2012; Ivezić et al., 2020) as well as to simplify complex data for machine learning approaches (e.g., Bishop, 2006; Müller and Guido, 2016; Witten et al., 2017; Géron, 2019). This is implemented by reducing the number of available data into a group of independent PCA components, which then provide information about the different levels of their contributions to the complexity of the entire data. Astronomers have extensively employed it as a practical multivariate method. The early application of this technique in astronomy (see review by Francis and Wills, 1999) can be traced back to some studies on spectral analyses of stars (Deeming, 1964; Whitney, 1983), galaxies (Faber, 1973; Bujarrabal et al., 1981; Efstathiou and Fall, 1984), and quasars (Mittaz et al., 1990; Francis et al., 1992; Boroson and Green, 1992). This approach was also employed for imaging analysis of the interstellar medium (Heyer and Schloerb, 1997; Brunt et al., 2009). It was later used for X-ray binaries (e.g., Malzac et al., 2006; Koljonen et al., 2013; Koljonen, 2015) and blazars (Gallant et al., 2018), and more recently for X-ray variability in symbiotic stars (Danehkar et al., 2024a) and starburst regions (Danehkar et al., 2024b). Especially, it has extensively been leveraged for X-ray data analysis of AGNs in Seyfert 1 galaxies (e.g., Vaughan and Fabian, 2004; Miller et al., 2008; Parker et al., 2014b; Gallo et al., 2015).

PCA can decompose time-resolved spectroscopic data into groups of PCA components and eigenvectors, yielding eigenvalues in the process. Normalized eigenvalues can yield the contribution of each eigenvector to the temporal evolution of the whole data over time. Each decomposed PCA component and eigenvector can be referred to as a principal spectrum with its corresponding light curve. The process of conducting PCA requires performing the decomposition of a matrix into its eigenvectors and eigenvalues. To analyze variability of a source in astronomy, this data matrix for PCA contains a set of spectroscopic data collected at n time intervals, each binned into m spectral channels. Let consider a rectangular $(m \times n)$ matrix $\mathbf{X}$ consisting of n rows by m columns, one can determine the principal components of $\mathbf{X}$ through the following three methods:

3.1 Singular value decomposition

The most common approach to obtaining the PCA components is the singular value decomposition (SVD; Beltrami, 1873; Jordan, 1874a; Jordan, 1874b; Sylvester, 1889a; Sylvester, 1889b; Sylvester, 1889c). The SVD of $\mathbf{X}$ is performed as follows:

$$\mathbf{X} = \mathbf{U}\mathbf{\Sigma}\mathbf{V}^{\intercal}, \tag{3}$$

where $\mathbf{U}$ is a square matrix of order m containing *principal components* (spectra in time-resolved spectroscopic data), $\mathbf{\Sigma}$ is a rectangular diagonal matrix $(m \times n)$ containing square roots of *eigenvalues* in its diagonal, i.e., $\mathbf{\Lambda} = \mathbf{\Sigma}^{\intercal}\mathbf{\Sigma} = \mathrm{diag}(\lambda_1, \ldots, \lambda_n)$ (contribution fractions in spectral variability), $\mathbf{V}$ is a square matrix of order n containing *eigenvectors* (light curves in astronomical data).

3.2 Eigendecomposition

A classical way to determine the PCA components is through the eigenvalue decomposition (EVD; Cauchy, 1829a; Cauchy, 1829b)[15] of the covariance matrix expressed as $\mathbf{C}_{XX} = \mathbf{X}^{\intercal}\mathbf{X}$, which is a square matrix of order m. The eigendecomposition of $\mathbf{C}_{XX}$ is as follows:

$$\mathbf{C}_{XX} = \mathbf{V}\mathbf{\Lambda}\mathbf{V}^{\intercal},$$

which yields eigenvectors ($\mathbf{V}$) and eigenvalues ($\mathbf{\Lambda}$). The principal components ($\mathbf{U}$) are obtained from the decomposed eigenvectors and eigenvalues by considering Equation 6, which leads to the following solution:[16]

$$\mathbf{X}\mathbf{V} = \mathbf{U}\mathbf{\Sigma}\mathbf{V}^{\intercal}\mathbf{V} = \mathbf{U}\mathbf{\Sigma}.$$

Constructing the diagonal matrix $\mathbf{\Sigma} = \mathbf{\Lambda}^{\frac{1}{2}}$ from the eigenvalues ($\mathbf{\Lambda}$) and obtaining the least-squares solution to $\mathbf{X}\mathbf{V} = \mathbf{U}\mathbf{\Sigma}$ lead to the principal components ($\mathbf{U}$) of $\mathbf{X}$.

3.3 QR decomposition

Another faster method suitable for high-performance computing, which was proposed by Sharma et al. (2013) to conduct PCA, is performed using QR decomposition (Golub, 1965), also known as QR factorization (Golub and van Loan, 1996; Trefethen and Bau, 1997). In this approach, $\mathbf{X}$ is first factorized into an orthogonal matrix $\mathbf{R}$ of $n \times m$ dimensions and an upper triangular square matrix $\mathbf{R}$ of order m:

$$\mathbf{X} = \mathbf{Q}\mathbf{R}.$$

Then, the SVD of $\mathbf{R}^{\intercal}$ is obtained:

$$\mathbf{R}^{\intercal} = \bar{\mathbf{U}}\bar{\mathbf{\Sigma}}\bar{\mathbf{V}}^{\intercal}.$$

As demonstrated by Sharma et al. (2013), this leads to the same diagonal matrix and eigenvectors of Equation 3, $\mathbf{\Sigma} = \bar{\mathbf{\Sigma}}$ and $\mathbf{V} = \bar{\mathbf{U}}$, while the equivalent principal components are obtained via $\mathbf{U} = \mathbf{Q}\bar{\mathbf{V}}$.

For a set of timing spectroscopic data stored in a data matrix, the PCA components ($\mathbf{U}$), the eigenvectors ($\mathbf{V}$), and the eigenvalues ($\mathbf{\Lambda} = \mathbf{\Sigma}^2$) decomposed from the data matrix via either SVD, EVD, or QR are the principal spectra, the corresponding light curves, and their contribution fractions, respectively. As shown in Supplementary Material, these PCA methods can simply implemented with the linear algebra functions of NumPy in Python, albeit with neither CPU parallelization nor GPU acceleration. Currently, there are two publicly available packages made for PCA in the astronomical community: (1) the SVD-based Python package PCA[17] (Parker et al., 2015) based on the SVD function (Press et al., 1997) from NumPy (Harris et al., 2020), and (2) the QR-based

15 For a historical review, see Hawkins (1975).

16 Based on the fast that $\mathbf{V}^{\intercal}\mathbf{V} = \mathbf{I}$, where $\mathbf{I} = \mathrm{diag}(1, \ldots, 1)$ is the identity matrix of order n, so $\mathbf{\Sigma}\mathbf{I} = \mathbf{\Sigma}$ and $\mathbf{\Lambda}\mathbf{I} = \mathbf{\Sigma}$.

17 https://www.michaelparker.space/pca-code

library qrpca in Python[18] and R[19] (de Souza et al., 2022a; de Souza et al., 2022b) implemented with pyTorch (Paszke et al., 2019) and Scikit-learn (Pedregosa et al., 2011) in Python, and with torch (Falbel and Luraschi, 2022) and the built-in prcomp function in R, allowing for seamless GPU acceleration. In particular, the package PCA distributed by Parker et al. (2015) is capable of conducting PCA on X-ray *XMM-Newton* EPIC-pn observations. To perform PCA with this package, it is necessary to generate a set of X-ray spectra sliced at fixed time intervals (e.g., 10 ks) from event data via custom reduction methods (for details, see Danehkar et al., 2024a).

Vaughan and Fabian (2004) made initial attempts to conduct PCA on X-ray variability in AGN using low-spectral resolution data, suggesting that the X-ray variations in MCG–6-30-15 reported by Fabian and Vaughan (2003) are primarily due to a variable power-law component, with a small partial fraction likely originating from a reflection-dominated component. Later, Miller et al. (2007) employed SVD for PCA, resulting in the generation of exhaustive principal spectra of Mrk 766, which Turner et al. (2007) confirmed these spectral variations through time-resolved spectroscopy. Moreover, Miller et al. (2008) investigated the X-ray variability of MCG–6-30-15 using PCA, resulting in similar spectral components (absorbed, varying power-law) in MCG–6-30-15 and Mrk 766, with a less variable, heavily absorbed component characterizing the relativistically broadened red wing. PCA conducted by Parker et al. (2014a) and Parker et al. (2014b) demonstrated that SVD can successfully separate different spectral components responsible for the X-ray variability in AGNs by exploiting large archival data. In particular, Parker et al. (2014a) discovered that the X-ray variations in MCG–6-30-15 are mostly caused by only three spectral components (see Figure 2): the normalization factor of the power-law continuum (variability fraction of ~96%), the power-law spectral index (~2.1%), and the normalization factor of a relativistically broadened reflection emission (~0.5%). Similarly, PCA by Parker et al. (2015) provided evidence for the slight variability ($\lesssim 0.5\%$) of relativistic reflection in other AGNs hosted by other Seyfert 1 galaxies (NGC 4051, NGC 3516, Mrk 766, and 1H 0707-495), as seen in Figure 2. Various spectral analysis approaches, including PCA, performed by Gallo et al. (2015) also indicated that the variability in the narrow-line Seyfert 1 galaxy, Mrk 335, is mostly caused by changes in the power-law flux and photon index, although small variations in the ionization state of the reflection were found to be necessary. The PCA study of the extreme narrow-line Seyfert 1 galaxy IRAS 13224–3,809 by Parker et al. (2017a) also showed three principal spectra: a varying power-law continuum, a slightly variable soft excess, and a less variable broad soft excess being linked to strong reflection (see Figure 2 bottom). In addition, the PCA component associated with a variable power-law continuum contain absorption footprints caused by the relativistic UFO detected by Parker et al. (2017b).

As seen in Figure 2, the third or/and fourth PCA components obtained by Parker et al. from X-ray observations of five AGNs (MCG –6-30–15, NGC 4051, NGC 3516, Mrk 766, and 1H 0707-495) resemble the relativistically broadened iron emission features shown in Figure 1 (top). Their normalized eigenvalues of $\lesssim 0.5\%$ imply that they have negligible variations compared to the X-ray variability in the power-low source continuum. This insignificant variability in the relativistic emission is consistent with the fact that the SMBH spin remains constant over the course of the human timescale. Magnetohydrodynamic (MHD) simulations of an black hole accretion disk by Schnittman et al. (2006) revealed that the light curves indeed contain very low levels of variability (see animations by Schnittman, 2019). Further MHD simulations

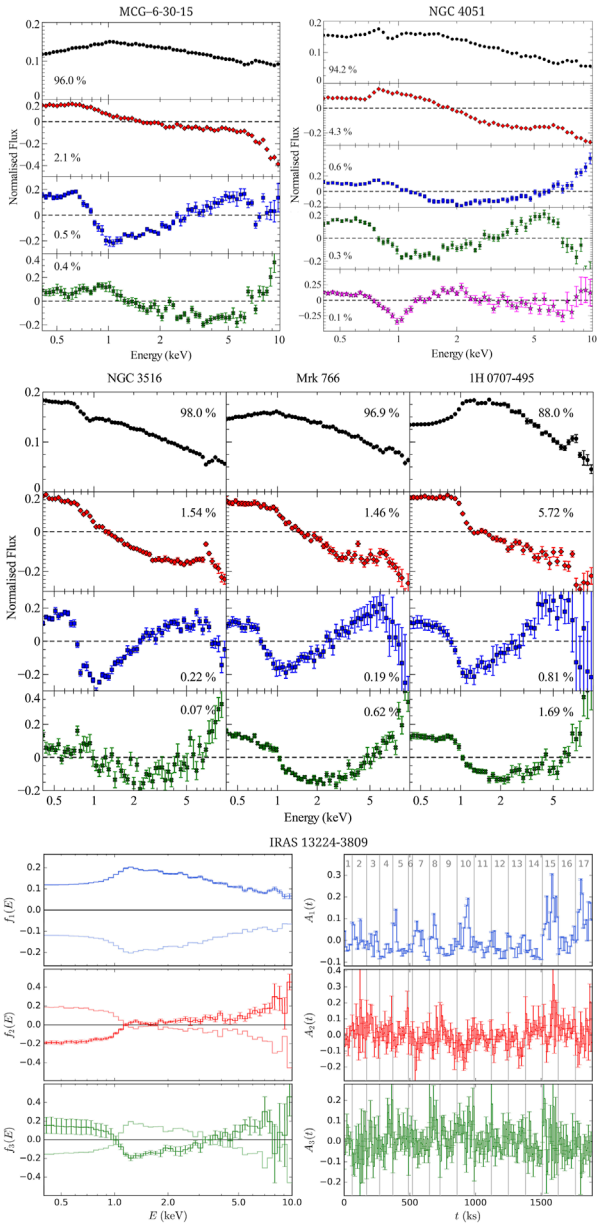

FIGURE 2
PCA spectra found in different AGNs hosted by nearby Seyfert 1 galaxies: MCG –6-30–15 (Parker et al., 2014a), NGC 4051, NGC 3516, Mrk 766, and 1H 0707-495 (Parker et al., 2015), with percentages of variability fractions, as well as PCA spectra $f_{1-3}(E)$ and related light curves $A_{1-3}(t)$ found in IRAS 13224-3,809 (Parker et al., 2017a). The PCA components from the first to the third or/and fourth order, respectively, correspond to variations in the power-law normalization, the power-law spectral index, and the relativistic reflection.

18 https://github.com/xuquanfeng/qrpca

19 https://github.com/RafaelSdeSouza/qrpca

by Schnittman et al. (2013) suggested that the noticeable X-ray variability mostly originates from the corona and not the disk. This is in agreement with the results found by Parker et al., which show $\gtrsim 90\%$ of X-ray variations are due to changes in the power-law continuum, i.e., the corona. General-relativistic magnetohydrodynamic (GRMHD) simulations by Shiokawa et al. (2017) also indicated the presence of some flux fluctuations in the emission from the innermost accretion disk due to the fast-moving turbulent formations, as well as some variations in the photon ring with spin-dependent frequencies (see animations by Shiokawa, 2017). Interestingly, the polarimetric light-curve observations of Sgr A* have also shown intraday variability in circular polarization (Bower et al., 2002) and linear polarization (Marrone et al., 2006), as well as Faraday rotation variability on timescales from hours to months (Marrone et al., 2007; Bower et al., 2018). Similarly, the near-infrared GRAVITY-Very Large Telescope Interferometer (VLTI) observations exhibited that the polarization loop in Sgr A* is regularly changing clockwise over ~30 min, indicating a closed, loop motion with the speed of $0.3c$ (GRAVITY Collaboration et al., 2018). The observed polarization variations in Sgr A* were in line with predictions from general-relativistic ray-tracing models of slightly tilted accretion flows in the presence of powerful magnetic fields (GRAVITY Collaboration et al., 2020). More recently, the polarimetric Event Horizon Telescope (EHT) imaging observations of the SMBHs in M87 and SgrA* confirmed rapid (intrahour) intrinsic variations in near-horizon accretion flows and polarized rings, which were attributed to spiraling polarization structures based on the results from GRMHD simulations (Event Horizon Telescope Collaboration et al., 2021a; Event Horizon Telescope Collaboration et al., 2021b; Event Horizon Telescope Collaboration et al., 2023; Event Horizon Telescope Collaboration et al., 2024a; Event Horizon Telescope Collaboration et al., 2024b). Therefore, the recent polarization GRAVITY-VLTI and EHT imaging observations of two nearby SMBHs (Sgr A ∗ and M87), together with numerical simulations, imply that small variations in the relativistically broadened iron emission revealed by PCA could be associated with intrahour intrinsic variations and varying spiraling polarization features in near-horizon accretion flows and photon rings.

4 Future perspective: machine learning

SVD and PCA decomposition closely relate to the optimal solution for neural networks in auto-association mode (Bourlard and Kamp, 1988; Baldi and Hornik, 1989). As discussed by Hertz et al. (1991) in the context of unsupervised Hebbian learning, PCA can be used for dimensionality reduction of large data before proceeding with machine learning algorithms, such as artificial neural networks (ANNs). PCA can indeed alleviate the "curse of dimensionality" (coined by Bellman, 1957; Bellman, 1961), also known as the "Hughes phenomenon" (Hughes, 1968) or "peaking phenomenon" (Trunk, 1979), which often arises when searching for patterns in unknown large data. It has been extensively demonstrated in the literature that PCA can be utilized as a pre-processing step to simplify complex data prior to machine learning (e.g., Bishop, 2006), data mining (Witten et al., 2017), and deep learning (Goodfellow et al., 2017). Recently, Ivezić et al. (2020) also discussed in detail the applications of PCA, ICA, and NMF in dimensionality reduction for data mining and machine learning in astronomy.

Using PCA for the pre-processing of astronomical data enables a significant reduction in dimensionality and complexity of data, leading to an improvement in machine learning performance. The use of PCA to reduce the dimensionality of the data for training ANNs can be traced back to earlier efforts on the classification of galaxy spectra (Folkes et al., 1996; Lahav et al., 1996) and stellar spectra (Bailer-Jones et al., 1998; Singh et al., 1998). Later, Zhang and Zhao (2003) applied PCA to the multiwavelength data of AGNs, stars, and normal galaxies in order to reduce the dimensionality of the parameter space for support vector machines (SVM) and learning vector quantization (LVQ), two supervised classification algorithms in machine learning, resulting in the classification of stars, AGNs, and normal galaxies. PCA also reduced the complexity of image data for the morphological classification of galaxies with an ANN (de la Calleja and Fuentes, 2004). Moreover, Bu and Pan (2015) deployed PCA to pre-assemble stellar atmospheric parameters from spectra for Gaussian process regression (GPR) and then compared the results of GPR with those from ANNs, kernel regression (KR), and support-vector regression (SVR). Kuntzer et al. (2016) also conducted stellar classification from single-band images using pre-processed data from PCA to train ANNs to determine the spectral type. More recently, we see the application of PCA to construct input data for ANNs in stellar population synthesis modeling (Alsing et al., 2020), finding thermal components in X-ray spectra of the Perseus cluster (Rhea et al., 2020), and finally X-ray spectral analysis of AGN (Parker et al., 2022).

The avenue of automated spectral analysis with machine learning algorithms has not yet been fully explored for constraining the relativistically broadened iron emission in AGN, mostly because of the complicated variability seen in the X-rays over the course of observations. X-ray observations of AGNs have shown some X-ray changes in power-law continua, which were ascribed to so-called transient obscuration events caused by eclipsing material near the primary source, such as NGC 3783 (Mehdipour et al., 2017), NGC 3227 (Turner et al., 2018), and Mrk 335 (Longinotti et al., 2019; Parker et al., 2019), or flaring variations in the corona in the innermost central regions, e.g., PDS 456 (Matzeu et al., 2017; Reeves et al., 2021) and NGC 3516 (Mehdipour et al., 2022). This kind of change in X-rays over time, along with a relatively large number of parameters in relativistic reflection models (see Table 1), makes it much more complicated for machine learning algorithms to automatically determine the spins of SMBHs from the archival X-ray data. Nevertheless, as seen in Figure 2, the dimensionality reduction offered by PCA can avoid the curse of dimensionality in the X-ray data of AGNs. In the future, we will be able to use machine learning to automatically conduct the spin analysis of SMBHs in AGNs thanks to the principal spectra of relativistic reflection disentangled by PCA from X-ray observations.

Author contributions

AD: Writing–original draft, Writing–review and editing.

Funding

The author(s) declare that financial support was received for the research, authorship, and/or publication of this article. The author acknowledges financial support from the National Aeronautics and Space Administration (NASA) for an Astrophysics Data Analysis Program grant under no. 80NSSC22K0626.

Acknowledgments

The author would like to express his gratitude for the invitation to speak at the 'Frontiers in Astronomy and Space Sciences: A Decade of Discovery and Advancement, 10th Anniversary Conference,' as well as to the editor who requested a concise review of that presentation. The author thanks Michael Parker for permission to use figures from his publications and useful discussions; Javier García, Thomas Dauser, and Laura Brenneman for permission to use figures from their publications; and the reviewer for careful reading of the manuscript and constructive comments.

Conflict of interest

The author declares that the research was conducted in the absence of any commercial or financial relationships that could be construed as a potential conflict of interest.

Publisher's note

All claims expressed in this article are solely those of the authors and do not necessarily represent those of their affiliated organizations, or those of the publisher, the editors and the reviewers. Any product that may be evaluated in this article, or claim that may be made by its manufacturer, is not guaranteed or endorsed by the publisher.

Supplementary material

The Supplementary Material for this article can be found online at: https://www.frontiersin.org/articles/10.3389/fspas.2024.1479301/full#supplementary-material

References

Abdikamalov, A. B., Ayzenberg, D., Bambi, C., Dauser, T., García, J. A., and Nampalliwar, S. (2019). Public release of relxill_NK: a relativistic reflection model for testing einstein's gravity. *Astrophys. J.* 878, 91. doi:10.3847/1538-4357/ab1f89

Abdikamalov, A. B., Ayzenberg, D., Bambi, C., Dauser, T., García, J. A., Nampalliwar, S., et al. (2020). Testing the Kerr black hole hypothesis using X-ray reflection spectroscopy and a thin disk model with finite thickness. *Astrophys. J.* 899, 80. doi:10.3847/1538-4357/aba625

Abdikamalov, A. B., Ayzenberg, D., Bambi, C., Liu, H., and Tripathi, A. (2021a). A reflection model with a radial disk density profile. *Astrophys. J.* 923, 175. doi:10.3847/1538-4357/ac3237

Abdikamalov, A. B., Ayzenberg, D., Bambi, C., Liu, H., and Zhang, Y. (2021b). Implementation of a radial disk ionization profile in the relxill_nk model. *Phys. Rev. D.* 103, 103023. doi:10.1103/PhysRevD.103.103023

Alsing, J., Peiris, H., Leja, J., Hahn, C., Tojeiro, R., Mortlock, D., et al. (2020). SPECULATOR: emulating stellar population synthesis for fast and accurate galaxy spectra and photometry. *Astrophys. J. Suppl.* 249, 5. doi:10.3847/1538-4365/ab917f

Arnaud, K., Dorman, B., and Gordon, C. (1999). XSPEC: an X-ray spectral fitting package. *Astrophys. Source Code Libr. Rec. ascl:9910.005*.

Arnaud, K. A. (1996). "XSPEC: the first ten years. In *astronomical data analysis Software and systems V*,". *ASP, vol. 101 of astronomical Society of the pacific conf. Ser.* Editors G. H. Jacoby, and J. Barnes (San Francisco, CA), 17.

Bailer-Jones, C. A. L., Irwin, M., and von Hippel, T. (1998). Automated classification of stellar spectra - II. Two-dimensional classification with neural networks and principal components analysis. *Mon. Not. R. Astron. Soc.* 298, 361–377. doi:10.1046/j.1365-8711.1998.01596.x

Baldi, P., and Hornik, K. (1989). Neural networks and principal component analysis: learning from examples without local minima. *Neural Netw.* 2, 53–58. doi:10.1016/0893-6080(89)90014-2

Bambi, C. (2017). Testing black hole candidates with electromagnetic radiation. *Rev. Mod. Phys.* 89, 025001. doi:10.1103/RevModPhys.89.025001

Bambi, C., Brenneman, L. W., Dauser, T., García, J. A., Grinberg, V., Ingram, A., et al. (2021). Towards precision measurements of accreting black holes using X-ray reflection spectroscopy. *Space Sci. Rev.* 217, 65. doi:10.1007/s11214-021-00841-8

Bambi, C., Cárdenas-Avendaño, A., Dauser, T., García, J. A., and Nampalliwar, S. (2017). Testing the Kerr black hole hypothesis using X-ray reflection spectroscopy. *Astrophys. J.* 842, 76. doi:10.3847/1538-4357/aa74c0

Bardeen, J. M., Press, W. H., and Teukolsky, S. A. (1972). Rotating black holes: locally nonrotating frames, energy extraction, and scalar synchrotron radiation. *Astrophys. J.* 178, 347–370. doi:10.1086/151796

Bellman, R. E. (1957). *Dynamic programming*. Princeton: Princeton Univ. Press.

Bellman, R. E. (1961). *Adaptive control processes: a guided tour*. Princeton: Princeton Univ. Press.

Beltrami, E. (1873). Sulle funzioni bilineari (English: on bilinear functions). *G. Mat.* XI, 98–106.

Bentz, M. C., and Katz, S. (2015). The AGN black hole mass database. *Publ. Astron. Soc. Pac.* 127, 67–73. doi:10.1086/679601

Berti, E., and Volonteri, M. (2008). Cosmological black hole spin evolution by mergers and accretion. *Astrophys. J.* 684, 822–828. doi:10.1086/590379

Bishop, C. M. (2006). *Pattern recognition and machine learning*. New York: Springer.

Blandford, R., Meier, D., and Readhead, A. (2019). Relativistic jets from active galactic nuclei. *Ann. Rev. Astron. Astrophys.* 57, 467–509. doi:10.1146/annurev-astro-081817-051948

Blandford, R. D., and McKee, C. F. (1982). Reverberation mapping of the emission line regions of Seyfert galaxies and quasars. *Astrophys. J.* 255, 419–439. doi:10.1086/159843

Blandford, R. D., and Payne, D. G. (1982). Hydromagnetic flows from accretion discs and the production of radio jets. *Mon. Not. R. Astron. Soc.* 199, 883–903. doi:10.1093/mnras/199.4.883

Blandford, R. D., and Znajek, R. L. (1977). Electromagnetic extraction of energy from Kerr black holes. *Mon. Not. R. Astron. Soc.* 179, 433–456. doi:10.1093/mnras/179.3.433

Boissay-Malaquin, R., Danehkar, A., Marshall, H. L., and Nowak, M. A. (2019). Relativistic components of the ultra-fast outflow in the quasar PDS 456 from Chandra/HETGS, NuSTAR, and XMM-Newton observations. *Astrophys. J.* 873, 29. doi:10.3847/1538-4357/ab0082

Boroson, T. A., and Green, R. F. (1992). The emission-line properties of low-redshift quasi-stellar objects. *Astrophys. J. Suppl.* 80, 109. doi:10.1086/191661

Bourlard, H., and Kamp, Y. (1988). Auto-association by multilayer perceptrons and singular value decomposition. *Biol. Cybern.* 59, 291–294. doi:10.1007/BF00332918

Bower, G. C., Broderick, A., Dexter, J., Doeleman, S., Falcke, H., Fish, V., et al. (2018). ALMA polarimetry of Sgr A ∗ : probing the accretion flow from the event horizon to the bondi radius. *Astrophys. J.* 868, 101. doi:10.3847/1538-4357/aae983

Bower, G. C., Falcke, H., Sault, R. J., and Backer, D. C. (2002). The spectrum and variability of circular polarization in Sagittarius A ∗ from 1.4 to 15 GHz. *Astrophys. J.* 571, 843–855. doi:10.1086/340064

Boyer, R. H., and Lindquist, R. W. (1967). Maximal analytic extension of the Kerr metric. *J. Math. Phys.* 8, 265–281. doi:10.1063/1.1705193

Brenneman, L. (2013). *Measuring the angular momentum of supermassive black holes*. New York: Springer. doi:10.1007/978-1-4614-7771-6

Brenneman, L. W. (2007). *A spectral survey of black hole spin in active galactic nuclei*. College Park: University of Maryland Ph.D. thesis.

Brenneman, L. W., and Reynolds, C. S. (2006). Constraining black hole spin via X-ray spectroscopy. *Astrophys. J.* 652, 1028–1043. doi:10.1086/508146

Broderick, A. E., Loeb, A., and Narayan, R. (2009). The event horizon of Sagittarius A. *Astrophys. J.* 701, 1357–1366. doi:10.1088/0004-637X/701/2/1357

Broderick, A. E., and Narayan, R. (2006). On the nature of the compact dark mass at the galactic center. *Astrophys. J. Lett.* 638, L21–L24. doi:10.1086/500930

Brunt, C. M., Heyer, M. H., and Mac Low, M. M. (2009). Turbulent driving scales in molecular clouds. *Astron. Astrophys.* 504, 883–890. doi:10.1051/0004-6361/200911797

Bu, Y., and Pan, J. (2015). Stellar atmospheric parameter estimation using Gaussian process regression. *Mon. Not. R. Astron. Soc.* 447, 256–265. doi:10.1093/mnras/stu2063

Bujarrabal, V., Guibert, J., and Balkowski, C. (1981). Multidimensional statistical analysis of normal galaxies. *Astron. Astrophys.* 104, 1–9.

Calderone, G., Ghisellini, G., Colpi, M., and Dotti, M. (2013). Black hole mass estimate for a sample of radio-loud narrow-line Seyfert 1 galaxies. *Mon. Not. R. Astron. Soc.* 431, 210–239. doi:10.1093/mnras/stt157

Campitiello, S., Ghisellini, G., Sbarrato, T., and Calderone, G. (2018). How to constrain mass and spin of supermassive black holes through their disk emission. *Astron. Astrophys.* 612, A59. doi:10.1051/0004-6361/201731897

Capellupo, D. M., Netzer, H., Lira, P., Trakhtenbrot, B., and Mejía-Restrepo, J. (2015). Active galactic nuclei at z 1.5 - I. Spectral energy distribution and accretion discs. *Mon. Not. R. Astron. Soc.* 446, 3427–3446. doi:10.1093/mnras/stu2266

Capellupo, D. M., Netzer, H., Lira, P., Trakhtenbrot, B., and Mejía-Restrepo, J. (2016). Active galactic nuclei at z 1.5 - III. Accretion discs and black hole spin. *Mon. Not. R. Astron. Soc.* 460, 212–226. doi:10.1093/mnras/stw937

Capellupo, D. M., Wafflard-Fernandez, G., and Haggard, D. (2017). A comparison of two methods for estimating black hole spin in active galactic nuclei. *Astrophys. J. Lett.* 836, L8. doi:10.3847/2041-8213/aa5cac

Cauchy, A.-L. (1829a). Sur l'équation à l'aide de laquelle on détermine les inégalités séculaires des mouvements des planètes. *Exer. math.* 4, 174–195.

Cauchy, A.-L. (1829b). Sur l'équation à l'aide de laquelle on détermine les inégalités séculaires des mouvements des planètes. *Oeuvres Complètes (IIème Série)* 9, 174–195. doi:10.1017/CBO9780511702686.009

Chandrasekhar, S. (1960). *Radiative transfer*. New York: Dover.

Cretton, N., and van den Bosch, F. C. (1999). Evidence for a massive black hole in the S0 galaxy NGC 4342. *Astrophys. J.* 514, 704–724. doi:10.1086/306971

Cunningham, C. T. (1975). The effects of redshifts and focusing on the spectrum of an accretion disk around a Kerr black hole. *Astrophys. J.* 202, 788–802. doi:10.1086/154033

Danehkar, A. (2020). Gravitational fields of the magnetic-type. *Int. J. Mod. Phys. D.* 29, 2043001. doi:10.1142/S0218271820430014

Danehkar, A., Drake, J. J., and Luna, G. J. M. (2024a). X-ray variability in the symbiotic binary RT Cru: principal component analysis. *Astrophys. J.* 972, 109. doi:10.3847/1538-4357/ad5cf6

Danehkar, A., Nowak, M. A., Lee, J. C., Kriss, G. A., Young, A. J., Hardcastle, M. J., et al. (2018). The ultra-fast outflow of the quasar PG 1211+143 as viewed by time-averaged Chandra grating spectroscopy. *Astrophys. J.* 853, 165. doi:10.3847/1538-4357/aaa427

Danehkar, A., Silich, S., Herenz, E. C., and Östlin, G. (2024b). Disentangling the X-ray variability in the Lyman continuum emitter Haro 11. *Astron. Astrophys.* 689, A333. doi:10.1051/0004-6361/202449388

Dauser, T. (2010). *Theoretical modeling of broad emission lines*. Germany: Friedrich Alexander University of Erlangen-Nuremberg. Master's thesis.

Dauser, T. (2014). *Relativistic reflection around black holes: theory and observation*. Germany: Friedrich Alexander University of Erlangen-Nuremberg. Ph.D. thesis.

Dauser, T., Garcia, J., Parker, M. L., Fabian, A. C., and Wilms, J. (2014). The role of the reflection fraction in constraining black hole spin. *Mon. Not. R. Astron. Soc.* 444, L100–L104. doi:10.1093/mnrasl/slu125

Dauser, T., García, J., Walton, D. J., Eikmann, W., Kallman, T., McClintock, J., et al. (2016). Normalizing a relativistic model of X-ray reflection. Definition of the reflection fraction and its implementation in relxill. *Astron. Astrophys.* 590, A76. doi:10.1051/0004-6361/201628135

Dauser, T., Garcia, J., Wilms, J., Böck, M., Brenneman, L. W., Falanga, M., et al. (2013). Irradiation of an accretion disc by a jet: general properties and implications for spin measurements of black holes. *Mon. Not. R. Astron. Soc.* 430, 1694–1708. doi:10.1093/mnras/sts710

Dauser, T., García, J. A., Joyce, A., Licklederer, S., Connors, R. M. T., Ingram, A., et al. (2022). The effect of returning radiation on relativistic reflection. *Mon. Not. R. Astron. Soc.* 514, 3965–3983. doi:10.1093/mnras/stac1593

Dauser, T., Wilms, J., Reynolds, C. S., and Brenneman, L. W. (2010). Broad emission lines for a negatively spinning black hole. *Mon. Not. R. Astron. Soc.* 409, 1534–1540. doi:10.1111/j.1365-2966.2010.17393.x

Deeming, T. J. (1964). Stellar spectral classification. I. Application of component analysis. *Mon. Not. R. Astron. Soc.* 127, 493–516. doi:10.1093/mnras/127.6.493

de la Calleja, J., and Fuentes, O. (2004). Machine learning and image analysis for morphological galaxy classification. *Mon. Not. R. Astron. Soc.* 349, 87–93. doi:10.1111/j.1365-2966.2004.07442.x

de La Calle Pérez, I., Longinotti, A. L., Guainazzi, M., Bianchi, S., Dovčiak, M., Cappi, M., et al. (2010). FERO: finding extreme relativistic objects: I. Statistics of relativistic Fe K_α lines in radio-quiet Type 1 AGN⋆. *Astron. Astrophys.* 524, A50. doi:10.1051/0004-6361/200913798

de Plaa, J., Kaastra, J. S., Gu, L., Mao, J., and Raassen, T. (2020). *SPEX: high-resolution spectral modeling and fitting for X-ray astronomy. In astronomical data analysis software and systems XXIX*, 527. Editors R. Pizzo, E. R. Deul, J. D. Mol, J. de Plaa, and H. Verkouter (San Francisco, CA: ASP), Astronomical Society of the Pacific Conf. Ser. 725. doi:10.48550/arXiv.1912.07897

de Souza, R. S., Quanfeng, X., Shen, S., Peng, C., and Mu, Z. (2022a). qrpca: a package for fast principal component analysis with GPU acceleration. *Astron. Comput.* 41, 100633. doi:10.1016/j.ascom.2022.100633

de Souza, R. S., Quanfeng, X., Shen, S., Peng, C., and Mu, Z.(2022b). qrpca: QR-based Principal Components Analysis. *Astrophys. Source Code Libr. Rec.* ascl:2208.002.

Di Matteo, T., Springel, V., and Hernquist, L. (2005). Energy input from quasars regulates the growth and activity of black holes and their host galaxies. *Nature* 433, 604–607. doi:10.1038/nature03335

Doe, S., Nguyen, D., Stawarz, C., Refsdal, B., Siemiginowska, A., Burke, D., et al. (2007). *Developing Sherpa with Python. In astronomical data analysis software and systems XVI*. Editors R. A. Shaw, F. Hill, and D. J. Bell (San Francisco, CA: ASP), 376. Astronomical Society of the Pacific Conf. Ser., 543.

Done, C., Davis, S. W., Jin, C., Blaes, O., and Ward, M. (2012). Intrinsic disc emission and the soft X-ray excess in active galactic nuclei. *Mon. Not. R. Astron. Soc.* 420, 1848–1860. doi:10.1111/j.1365-2966.2011.19779.x

Done, C., Jin, C., Middleton, M., and Ward, M. (2013). A new way to measure supermassive black hole spin in accretion disc-dominated active galaxies. *Mon. Not. R. Astron. Soc.* 434, 1955–1963. doi:10.1093/mnras/stt1138

Dovčiak, M. (2004). *Radiation of accretion discs in strong gravity*. Prague: Charles University. Ph.D. thesis.

Dovčiak, M., Karas, V., and Yaqoob, T. (2004). An extended scheme for fitting X-ray data with accretion disk spectra in the strong gravity regime. *Astrophys. J. Suppl.* 153, 205–221. doi:10.1086/421115

Dovčiak, M., Papadakis, I. E., Kammoun, E. S., and Zhang, W. (2022). Physical model for the broadband energy spectrum of X-ray illuminated accretion discs: fitting the spectral energy distribution of NGC 5548. *Astron. Astrophys.* 661, A135. doi:10.1051/0004-6361/202142358

Efstathiou, G., and Fall, S. M. (1984). Multivariate analysis of elliptical galaxies. *Mon. Not. R. Astron. Soc.* 206, 453–464. doi:10.1093/mnras/206.3.453

Event Horizon Telescope Collaboration, Akiyama, K., Alberdi, A., Alef, W., Asada, K., Azulay, R., et al. (2019a). First M87 event horizon telescope results. I. The shadow of the supermassive black hole. *Astrophys. J. Lett.* 875, L1. doi:10.3847/2041-8213/ab0ec7

Event Horizon Telescope Collaboration, Akiyama, K., Alberdi, A., Alef, W., Asada, K., Azulay, R., et al. (2019b). First M87 event horizon telescope results. IV. Imaging the central supermassive black hole. *Astrophys. J. Lett.* 875, L4. doi:10.3847/2041-8213/ab0e85

Event Horizon Telescope Collaboration, Akiyama, K., Alberdi, A., Alef, W., Asada, K., Azulay, R., et al. (2019c). First M87 event horizon telescope results. V. Physical origin of the asymmetric ring. *Astrophys. J. Lett.* 875, L5. doi:10.3847/2041-8213/ab0f43

Event Horizon Telescope Collaboration, Akiyama, K., Algaba, J. C., Alberdi, A., Alef, W., Anantua, R., et al. (2021a). First M87 event horizon telescope results. VII. Polarization of the ring. *Astrophys. J. Lett.* 910, L12. doi:10.3847/2041-8213/abe71d

Event Horizon Telescope Collaboration, Akiyama, K., Algaba, J. C., Alberdi, A., Alef, W., Anantua, R., et al. (2021b). First M87 event horizon telescope results. VIII. Magnetic field structure near the event horizon. *Astrophys. J. Lett.* 910, L13. doi:10.3847/2041-8213/abe4de

Event Horizon Telescope Collaboration, Akiyama, K., Alberdi, A., Alef, W., Algaba, J. C., Anantua, R., et al. (2022a). First Sagittarius A ∗ event horizon telescope results. I. The shadow of the supermassive black hole in the center of the Milky way. *Astrophys. J. Lett.* 930, L12. doi:10.3847/2041-8213/ac6674

Event Horizon Telescope Collaboration, Akiyama, K., Alberdi, A., Alef, W., Algaba, J. C., Anantua, R., et al. (2022b). First Sagittarius A ∗ event horizon telescope results. III. Imaging of the galactic center supermassive black hole. *Astrophys. J. Lett.* 930, L14. doi:10.3847/2041-8213/ac6429

Event Horizon Telescope Collaboration, Akiyama, K., Alberdi, A., Alef, W., Algaba, J. C., Anantua, R., et al. (2022c). First Sagittarius A ∗ event horizon telescope results. V. Testing astrophysical models of the galactic center black hole. *Astrophys. J. Lett.* 930, L16. doi:10.3847/2041-8213/ac6672

Event Horizon Telescope Collaboration, Akiyama, K., Alberdi, A., Alef, W., Algaba, J. C., Anantua, R., et al. (2022d). First Sagittarius A ∗ event horizon telescope results. VI. Testing the black hole metric. *Astrophys. J. Lett.* 930, L17. doi:10.3847/2041-8213/ac6756

Event Horizon Telescope Collaboration, Akiyama, K., Alberdi, A., Alef, W., Algaba, J. C., Anantua, R., et al. (2023). First M87 event horizon telescope results. IX. Detection

of near-horizon circular polarization. *Astrophys. J. Lett.* 957, L20. doi:10.3847/2041-8213/acff70

Event Horizon Telescope Collaboration, Akiyama, K., Alberdi, A., Alef, W., Algaba, J. C., Anantua, R., et al. (2024a). First Sagittarius A ∗ event horizon telescope results. VII. Polarization of the ring. *Astrophys. J. Lett.* 964, L25. doi:10.3847/2041-8213/ad2df0

Event Horizon Telescope Collaboration, Akiyama, K., Alberdi, A., Alef, W., Algaba, J. C., Anantua, R., et al. (2024b). First Sagittarius A ∗ event horizon telescope results. VIII. Physical interpretation of the polarized ring. *Astrophys. J. Lett.* 964, L26. doi:10.3847/2041-8213/ad2df1

Faber, S. M. (1973). Variations in spectral-energy distributions and absorption-line strengths among elliptical galaxies. *Astrophys. J.* 179, 731–754. doi:10.1086/151912

Fabian, A. C., Rees, M. J., Stella, L., and White, N. E. (1989). X-ray fluorescence from the inner disc in Cygnus X-1. *Mon. Not. R. Astron. Soc.* 238, 729–736. doi:10.1093/mnras/238.3.729

Fabian, A. C., and Vaughan, S. (2003). The iron line in MCG-6-30-15 from XMM-Newton: evidence for gravitational light bending? *Mon. Not. R. Astron. Soc.* 340, L28–L32. doi:10.1046/j.1365-8711.2003.06465.x

Falbel, D., and Luraschi, J. (2022). Torch: tensors and neural networks with 'GPU' acceleration. Available at: https://torch.mlverse.org/docs https://github.com/mlverse/torch

Ferrarese, L., and Merritt, D. (2000). A fundamental relation between supermassive black holes and their host galaxies. *Astrophys. J. Lett.* 539, L9–L12. doi:10.1086/312838

Folkes, S. R., Lahav, O., and Maddox, S. J. (1996). An artificial neural network approach to the classification of galaxy spectra. *Mon. Not. R. Astron. Soc.* 283, 651–665. doi:10.1093/mnras/283.2.651

Francis, P. J., Hewett, P. C., Foltz, C. B., and Chaffee, F. H. (1992). An objective classification scheme for QSO spectra. *Astrophys. J.* 398, 476. doi:10.1086/171870

Francis, P. J., and Wills, B. J. (1999). "Introduction to principal components analysis," in *Quasars and cosmology*. Editors G. Ferland, and J. Baldwin, 363. doi:10.48550/arXiv.astro-ph/9905079

Freeman, P., Doe, S., and Siemiginowska, A. (2001). "Sherpa: a mission-independent data analysis application," in *Astronomical Data Analysis* (Bellingham: SPIE), 4477 proc. SPIE conf. Ser. Editors J.-L. Starck, and F. D. Murtagh, 76–87. doi:10.1117/12.447161

Fruscione, A., McDowell, J. C., Allen, G. E., Brickhouse, N. S., Burke, D. J., Davis, J. E., et al. (2006). . "CIAO: Chandra's data analysis system," in *Observatory Operations: Strategies, Processes, and Systems*, Editors D. R. Silva, and R. E. Doxsey (Bellingham: SPIE), vol. 6270 of Proc. SPIE Conf. Ser., 62701V. doi:10.1117/12.671760

Gallant, D., Gallo, L. C., and Parker, M. L. (2018). X-ray spectral variability of blazars using principal component analysis. *Mon. Not. R. Astron. Soc.* 480, 1999–2010. doi:10.1093/mnras/sty1987

Gallo, L. C., Wilkins, D. R., Bonson, K., Chiang, C. Y., Grupe, D., Parker, M. L., et al. (2015). Suzaku observations of Mrk 335: confronting partial covering and relativistic reflection. *Mon. Not. R. Astron. Soc.* 446, 633–650. doi:10.1093/mnras/stu2108

García, J., Dauser, T., Lohfink, A., Kallman, T. R., Steiner, J. F., McClintock, J. E., et al. (2014). Improved reflection models of black hole accretion disks: treating the angular distribution of X-rays. *Astrophys. J.* 782, 76. doi:10.1088/0004-637X/782/2/76

García, J., Dauser, T., Reynolds, C. S., Kallman, T. R., McClintock, J. E., Wilms, J., et al. (2013). X-ray reflected spectra from accretion disk models. III. A complete grid of ionized reflection calculations. *Astrophys. J.* 768, 146. doi:10.1088/0004-637X/768/2/146

García, J., and Kallman, T. R. (2010). X-Ray reflected spectra from accretion disk models. I. Constant density atmospheres. *Astrophys. J.* 718, 695–706. doi:10.1088/0004-637X/718/2/695

García, J., Kallman, T. R., and Mushotzky, R. F. (2011). X-Ray reflected spectra from accretion disk models. II. Diagnostic tools for X-ray observations. *Astrophys. J.* 731, 131. doi:10.1088/0004-637X/731/2/131

García, J. A. (2010). *Modeling high-resolution spectra from x-ray illuminated accretion disks*. Washington DC: Catholic University. Ph.D. thesis.

García, J. A., Dauser, T., Ludlam, R., Parker, M., Fabian, A., Harrison, F. A., et al. (2022). Relativistic X-ray reflection models for accreting neutron stars. *Astrophys. J.* 926, 13. doi:10.3847/1538-4357/ac3cb7

Garofalo, D., Evans, D. A., and Sambruna, R. M. (2010). The evolution of radio-loud active galactic nuclei as a function of black hole spin. *Mon. Not. R. Astron. Soc.* 406, 975–986. doi:10.1111/j.1365-2966.2010.16797.x

Géron, A. (2019). Hands-on machine learning with scikit-learn, keras, and TensorFlow: concepts, tools, and techniques to build intelligent systems. (Sebastopol, CA: O'Reilly).

Ghez, A. M., Klein, B. L., Morris, M., and Becklin, E. E. (1998). High proper-motion stars in the vicinity of Sagittarius A ∗ : evidence for a supermassive black hole at the center of our galaxy. *Astrophys. J.* 509, 678–686. doi:10.1086/306528

Ghez, A. M., Salim, S., Hornstein, S. D., Tanner, A., Lu, J. R., Morris, M., et al. (2005). Stellar orbits around the galactic center black hole. *Astrophys. J.* 620, 744–757. doi:10.1086/427175

Gierliński, M., Maciołek-Niedźwiecki, A., and Ebisawa, K. (2001). Application of a relativistic accretion disc model to X-ray spectra of LMC X-1 and GRO J1655-40. *Mon. Not. R. Astron. Soc.* 325, 1253–1265. doi:10.1046/j.1365-8711.2001.04540.x

Golub, G. (1965). Numerical methods for solving linear least squares problems. *Numer. Math.* 7, 206–216. doi:10.1007/BF01436075

Golub, G. H., and van Loan, C. F. (1996). *Matrix computations*. 3rd edn. Baltimore: Johns Hopkins Univ. Press.

Goodfellow, I., Bengio, Y., and Courville, A. (2017). *Deep learning*. Cambridge, MA: MIT Press.

GRAVITY Collaboration, Abuter, R., Amorim, A., Bauböck, M., Berger, J. P., Bonnet, H., et al. (2018). Detection of orbital motions near the last stable circular orbit of the massive black hole SgrA. *Astron. Astrophys.* 618, L10. doi:10.1051/0004-6361/201834294

GRAVITY Collaboration, Jiménez-Rosales, A., Dexter, J., Widmann, F., Bauböck, M., Abuter, R., et al. (2020). Dynamically important magnetic fields near the event horizon of Sgr A. *Astron. Astrophys.* 643, A56. doi:10.1051/0004-6361/202038283

Guainazzi, M., Bianchi, S., and Dovčiak, M. (2006). Statistics of relativistically broadened Fe Kα lines in AGN. *Astron. Nachr.* 327, 1032–1038. doi:10.1002/asna.200610687

Haardt, F. (1993). Anisotropic comptonization in thermal plasmas: spectral distribution in plane-parallel geometry. *Astrophys. J.* 413, 680. doi:10.1086/173036

Haardt, F., and Maraschi, L. (1991). A two-phase model for the X-ray emission from Seyfert galaxies. *Astrophys. J. Lett.* 380, L51. doi:10.1086/186171

Haardt, F., and Maraschi, L. (1993). X-ray spectra from two-phase accretion disks. *Astrophys. J.* 413, 507. doi:10.1086/173020

Hagen, S., and Done, C. (2023). Estimating black hole spin from AGN SED fitting: the impact of general-relativistic ray tracing. *Mon. Not. R. Astron. Soc.* 525, 3455–3467. doi:10.1093/mnras/stad2499

Häring, N., and Rix, H.-W. (2004). On the black hole mass-bulge mass relation. *Astrophys. J. Lett.* 604, L89–L92. doi:10.1086/383567

Harris, C. R., Millman, K. J., van der Walt, S. J., Gommers, R., Virtanen, P., Cournapeau, D., et al. (2020). Array programming with NumPy. *Nature* 585, 357–362. doi:10.1038/s41586-020-2649-2

Harrison, F. A., Craig, W. W., Christensen, F. E., Hailey, C. J., Zhang, W. W., Boggs, S. E., et al. (2013). The nuclear spectroscopic telescope Array (NuSTAR) high-energy X-ray mission. *Astrophys. J.* 770, 103. doi:10.1088/0004-637X/770/2/103

Hawkins, T. (1975). Cauchy and the spectral theory of matrices. *Hist. Math.* 2, 1–29. doi:10.1016/0315-0860(75)90032-4

Heckman, T. M., and Best, P. N. (2014). The coevolution of galaxies and supermassive black holes: insights from surveys of the contemporary universe. *Ann. Rev. Astron. Astrophys.* 52, 589–660. doi:10.1146/annurev-astro-081913-035722

Hérault, J., and Ans, B. (1984). Neuronal network with modifiable synapses: decoding of composite sensory messages under unsupervised and permanent learning. *C.R. Acad. Sci. Paris* 299, 525–528.

Hérault, J., and Jutten, C. (1986). Space or time adaptive signal processing by neural network models. *AIP Conf. Proc.* 151, 206–211. doi:10.1063/1.36258

Hérault, J., Jutten, C., and Ans, B. (1985). Détection de grandeurs primitives dans un message composite par une architecture de calcul neuromimétique en apprentissage non supervisé. *Actes Du. Xème Colloq*. (Nice, France: GRETSI) 2, 1017–1020.

Hertz, J., Krogh, A., and Palmer, R. G. (1991). *Introduction to the theory of neural computation*. Redwood City, CA: Addison-Wesley.

Heyer, M. H., and Schloerb, F. P. (1997). Application of principal component analysis to large-scale spectral line imaging studies of the interstellar medium. *Astrophys. J.* 475, 173–187. doi:10.1086/303514

Hoormann, J. K., Beheshtipour, B., and Krawczynski, H. (2016). Testing general relativity's no-hair theorem with x-ray observations of black holes. *Phys. Rev. D.* 93, 044020. doi:10.1103/PhysRevD.93.044020

Hotelling, H. (1933). Analysis of a complex of statistical variables into principal components. *J. Educ. Psychol.* 24, 417–441. doi:10.1037/h0071325

Houck, J. C., and Denicola, L. A. (2000). "ISIS: an interactive spectral interpretation System for high resolution X-ray spectroscopy," In *Astronomical Data Analysis Software and Systems IX* (San Francisco, CA: ASP) vol. 216 of *astronomical Society of the pacific conf. Ser.* Editors N. Manset, C. Veillet, and D. Crabtree, 591.

Hughes, G. (1968). On the mean accuracy of statistical pattern recognizers. *IEEE Trans. Inf. Theory* 14, 55–63. doi:10.1109/TIT.1968.1054102

Hughes, S. A., and Blandford, R. D. (2003). Black hole mass and spin coevolution by mergers. *Astrophys. J. Lett.* 585, L101–L104. doi:10.1086/375495

Ingram, A., Mastroserio, G., Dauser, T., Hovenkamp, P., van der Klis, M., and García, J. A. (2019). A public relativistic transfer function model for X-ray

reverberation mapping of accreting black holes. *Mon. Not. R. Astron. Soc.* 488, 324–347. doi:10.1093/mnras/stz1720

Ivezić, Ž., Connolly, A. J., VanderPlas, J. T., and Gray, A. (2020). *Statistics, data mining, and machine learning in astronomy: a practical Python guide for the analysis of survey data*. Princeton: Princeton Univ. Press. doi:10.1515/9780691197050

Izenman, A. J. (2008). *Modern multivariate statistical techniques: regression, classification, and manifold learning*. Berlin: Springer. doi:10.1007/978-0-387-78189-1

Johannsen, T. (2013). Regular black hole metric with three constants of motion. *Phys. Rev. D.* 88, 044002. doi:10.1103/PhysRevD.88.044002

Jolliffe, I. T. (2002). *Principal component analysis*. Berlin: Springer. doi:10.1007/b98835

Jolliffe, I. T., and Cadima, J. (2016). Principal component analysis: a review and recent developments. *Philos. Trans. R. Soc. A* 374, 20150202. doi:10.1098/rsta.2015.0202

Jordan, C. (1874a). Mémoire sur les formes bilinéaires (English: Memory on bilinear forms). *J. Math. Pures Appl. Paris* 19, 35–54.

Jordan, C. (1874b). Sur la réduction des formes bilinéaires (English: On the reduction of bilinear forms). *C. R. Acad. Sci. Paris* 78, 614–617.

Kaastra, J. S., Mewe, R., and Nieuwenhuijzen, H. (1996). "SPEX: a new code for spectral analysis of X and UV spectra," in *UV and X-ray spectroscopy of astrophysical and laboratory plasmas*, 411–414.

Karhunen, K. (1947). "Über lineare methoden in der wahrscheinlich-keitsrechnung. *Ann. Acad. Sci. Fennicea, Ser. A1* 37. Trans. by I. Selin (1960)" "*On Linear Methods in Probability Theory*" T-131. Santa Monica, CA: RAND Corp.

Keck, M. L., Brenneman, L. W., Ballantyne, D. R., Bauer, F., Boggs, S. E., Christensen, F. E., et al. (2015). NuSTAR and Suzaku X-ray spectroscopy of NGC 4151: evidence for reflection from the inner accretion disk. *Astrophys. J.* 806, 149. doi:10.1088/0004-637X/806/2/149

Kerr, R. P. (1963). Gravitational field of a spinning mass as an example of algebraically special metrics. *Phys. Rev. Lett.* 11, 237–238. doi:10.1103/PhysRevLett.11.237

Koljonen, K. I. I. (2015). Unsupervised spectral decomposition of X-ray binaries with application to GX 339-4. *Mon. Not. R. Astron. Soc.* 447, 2981–2991. doi:10.1093/mnras/stu2663

Koljonen, K. I. I., McCollough, M. L., Hannikainen, D. C., and Droulans, R. (2013). 2006 May-July major radio flare episodes in Cygnus X-3: spectrotiming analysis of the X-ray data. *Mon. Not. R. Astron. Soc.* 429, 1173–1188. doi:10.1093/mnras/sts404

Kormendy, J. (1988). Evidence for a supermassive black hole in the nucleus of M31. *Astrophys. J.* 325, 128–141. doi:10.1086/165988

Kormendy, J., Bender, R., Magorrian, J., Tremaine, S., Gebhardt, K., Richstone, D., et al. (1997). Spectroscopic evidence for a supermassive black hole in NGC 4486B. *Astrophys. J. Lett.* 482, L139–L142. doi:10.1086/310720

Kormendy, J., and Richstone, D. (1992). Evidence for a supermassive black hole in NGC 3115. *Astrophys. J.* 393, 559–578. doi:10.1086/171528

Kormendy, J., and Richstone, D. (1995). Inward bound—the search for supermassive black holes in galactic nuclei. *Ann. Rev. Astron. Astrophys.* 33, 581–624. doi:10.1146/annurev.aa.33.090195.003053

Kosambi, D. D. (1943). Statistics in function space. *J. Indian Math. Soc.* 7, 115–123. doi:10.1007/978-81-322-3676-4_15

Kubota, A., and Done, C. (2018). A physical model of the broad-band continuum of AGN and its implications for the UV/X relation and optical variability. *Mon. Not. R. Astron. Soc.* 480, 1247–1262. doi:10.1093/mnras/sty1890

Kubota, A., and Done, C. (2019). Modelling the spectral energy distribution of super-Eddington quasars. *Mon. Not. R. Astron. Soc.* 489, 524–533. doi:10.1093/mnras/stz2140

Kuntzer, T., Tewes, M., and Courbin, F. (2016). Stellar classification from single-band imaging using machine learning. *Astron. Astrophys.* 591, A54. doi:10.1051/0004-6361/201628660

Lahav, O., Naim, A., Sodré, J. L., and Storrie-Lombardi, M. C. (1996). Neural computation as a tool for galaxy classification: methods and examples. *Mon. Not. R. Astron. Soc.* 283, 207–221. doi:10.1093/mnras/283.1.207

Laor, A. (1991). Line profiles from a disk around a rotating black hole. *Astrophys. J.* 376, 90. doi:10.1086/170257

Larsson, J., Fabian, A. C., Miniutti, G., and Ross, R. R. (2007). Exploring the X-ray spectral variability of MCG-6-30-15 with XMM-Newton. *Mon. Not. R. Astron. Soc.* 376, 348–352. doi:10.1111/j.1365-2966.2007.11436.x

Lee, D. D., and Seung, H. S. (1999). Learning the parts of objects by non-negative matrix factorization. *Nature* 401, 788–791. doi:10.1038/44565

Lee, D. D., and Seung, H. S. (2000). "Algorithms for non-negative matrix factorization," *Advances in neural information processing systems*. Editors T. Leen, T. Dietterich, and V. Tresp (Cambridge, MA: MIT Press), 13, 556–562.

Li, L.-X., Zimmerman, E. R., Narayan, R., and McClintock, J. E. (2005). Multitemperature blackbody spectrum of a thin accretion disk around a Kerr black hole: model computations and comparison with observations. *Astrophys. J. Suppl.* 157, 335–370. doi:10.1086/428089

Loève, M. (1948). "Fonctions Aléatoires de second order," in *Processus Stochastiques et Movement Brownien*. Editor P. Lévy (Paris, France: Gauthier-Villars).

Longinotti, A. L., Kriss, G., Krongold, Y., Arellano-Cordova, K. Z., Komossa, S., Gallo, L., et al. (2019). The XMM-Newton/HST view of the obscuring outflow in the Seyfert galaxy Mrk 335 observed at extremely low X-ray flux. *Astrophys. J.* 875, 150. doi:10.3847/1538-4357/ab125a

MacDonald, D. A., Thorne, K. S., Price, R. H., and Zhang, X. H. (1986). "Astrophysical applications of black-hole electrodynamics," in *Black holes: the membrane paradigm*. Editors K. S. Thorne, R. H. Price, and D. A. MacDonald (New Haven, CT: Yale Univ. Press), 121–145.

Magorrian, J., Tremaine, S., Richstone, D., Bender, R., Bower, G., Dressler, A., et al. (1998). The demography of massive dark objects in galaxy centers. *Astron. J.* 115, 2285–2305. doi:10.1086/300353

Malkan, M. A. (1983). The ultraviolet excess of luminous quasars. II. Evidence for massive accretion disks. *Astrophys. J.* 268, 582–590. doi:10.1086/160981

Malzac, J., Petrucci, P. O., Jourdain, E., Cadolle Bel, M., Sizun, P., Pooley, G., et al. (2006). Bimodal spectral variability of Cygnus X-1 in an intermediate state. *Astron. Astrophys.* 448, 1125–1137. doi:10.1051/0004-6361:20053614

Mardia, K. V., Kent, J. T., and Bibby, J. M. (1979). *Multivariate analysis*. London: Academic Press.

Marrone, D. P., Moran, J. M., Zhao, J.-H., and Rao, R. (2006). Interferometric measurements of variable 340 GHz linear polarization in Sagittarius A $*$. *Astrophys. J.* 640, 308–318. doi:10.1086/500106

Marrone, D. P., Moran, J. M., Zhao, J.-H., and Rao, R. (2007). An unambiguous detection of Faraday rotation in Sagittarius A $*$. *Astrophys. J. Lett.* 654, L57–L60. doi:10.1086/510850

Martocchia, A., Karas, V., and Matt, G. (2000). Effects of Kerr space-time on spectral features from X-ray illuminated accretion discs. *Mon. Not. R. Astron. Soc.* 312, 817–826. doi:10.1046/j.1365-8711.2000.03205.x

Martocchia, A., and Matt, G. (1996). Iron Kα line intensity from accretion discs around rotating black holes. *Mon. Not. R. Astron. Soc.* 282, L53–L57. doi:10.1093/mnras/282.4.L53

Martocchia, A., Matt, G., Karas, V., Belloni, T., and Feroci, M. (2002). Evidence for a relativistic iron line in GRS 1915+105. *Astron. Astrophys.* 387, 215–221. doi:10.1051/0004-6361:20020359

Mastroserio, G., Ingram, A., Wang, J., García, J. A., van der Klis, M., Cavecchi, Y., et al. (2021). Modelling correlated variability in accreting black holes: the effect of high density and variable ionization on reverberation lags. *Mon. Not. R. Astron. Soc.* 507, 55–73. doi:10.1093/mnras/stab2056

Mastroserio, G., Ingram, A., Wang, J., Lucchini, M., Nathan, E., and Garcia, J. (2022). RELTRANS: a public spectral-timing model to fit X-ray reverberation in accreting black holes. *44th COSPAR Sci. Assem.* 44, 2345. *Held 16-24 July*.

Matzeu, G. A., Reeves, J. N., Nardini, E., Braito, V., Turner, T. J., and Costa, M. T. (2017). X-ray flaring in PDS 456 observed in a high-flux state. *Mon. Not. R. Astron. Soc.* 465, 2804–2819. doi:10.1093/mnras/stw2673

McClintock, J. E., Shafee, R., Narayan, R., Remillard, R. A., Davis, S. W., and Li, L.-X. (2006). The spin of the near-extreme Kerr black hole GRS 1915+105. *Astrophys. J.* 652, 518–539. doi:10.1086/508457

Mehdipour, M., Kaastra, J. S., Kriss, G. A., Arav, N., Behar, E., Bianchi, S., et al. (2017). Chasing obscuration in type-I AGN: discovery of an eclipsing clumpy wind at the outer broad-line region of NGC 3783. *Astron. Astrophys.* 607, A28. doi:10.1051/0004-6361/201731175

Mehdipour, M., Kriss, G. A., Brenneman, L. W., Costantini, E., Kaastra, J. S., Branduardi-Raymont, G., et al. (2022). Changing-look event in NGC 3516: continuum or obscuration variability? *Astrophys. J.* 925, 84. doi:10.3847/1538-4357/ac42ca

Mejía-Restrepo, J. E., Trakhtenbrot, B., Lira, P., Netzer, H., and Capellupo, D. M. (2016). Active galactic nuclei at z ~ 1.5 - II. Black hole mass estimation by means of broad emission lines. *Mon. Not. R. Astron. Soc.* 460, 187–211. doi:10.1093/mnras/stw568

Miller, J. M. (2007). Relativistic X-ray lines from the inner accretion disks around black holes. *Ann. Rev. Astron. Astrophys.* 45, 441–479. doi:10.1146/annurev.astro.45.051806.110555

Miller, L., Turner, T. J., and Reeves, J. N. (2008). An absorption origin for the X-ray spectral variability of MCG-6-30-15. *Astron. Astrophys.* 483, 437–452. doi:10.1051/0004-6361:200809590

Miller, L., Turner, T. J., Reeves, J. N., George, I. M., Kraemer, S. B., and Wingert, B. (2007). The variable X-ray spectrum of Markarian 766. I. Principal components analysis. *Astron. Astrophys.* 463, 131–143. doi:10.1051/0004-6361:20066548

Miniutti, G., and Fabian, A. C. (2004). A light bending model for the X-ray temporal and spectral properties of accreting black holes. *Mon. Not. R. Astron. Soc.* 349, 1435–1448. doi:10.1111/j.1365-2966.2004.07611.x

Mittaz, J. P. D., Penston, M. V., and Snijders, M. A. J. (1990). Ultraviolet variability of NGC 4151: a study using principal component analysis. *Mon. Not. R. Astron. Soc.* 242, 370–378. doi:10.1093/mnras/242.3.370

Miyoshi, M., Moran, J., Herrnstein, J., Greenhill, L., Nakai, N., Diamond, P., et al. (1995). Evidence for a black hole from high rotation velocities in a sub-parsec region of NGC4258. *Nature* 373, 127–129. doi:10.1038/373127a0

Moderski, R., Sikora, M., and Lasota, J. P. (1998). On the spin paradigm and the radio dichotomy of quasars. *Mon. Not. R. Astron. Soc.* 301, 142–148. doi:10.1046/j.1365-8711.1998.02009.x

Müller, A. C., and Guido, S. (2016). Introduction to machine learning with Python (Sebastopol, CA: O'Reilly)

Mushotzky, R. F., Done, C., and Pounds, K. A. (1993). X-ray spectra and time variability of active galactic nuclei. *Ann. Rev. Astron. Astrophys.* 31, 717–761. doi:10.1146/annurev.aa.31.090193.003441

Nandra, K., O'Neill, P. M., George, I. M., and Reeves, J. N. (2007). An XMM-Newton survey of broad iron lines in Seyfert galaxies. *Mon. Not. R. Astron. Soc.* 382, 194–228. doi:10.1111/j.1365-2966.2007.12331.x

NASA HEASARC(2014). HEAsoft: unified release of FTOOLS and XANADU. *Astrophys. Source Code Libr. Rec. ascl:1408.004*.

Nichols, D. A., Owen, R., Zhang, F., Zimmerman, A., Brink, J., Chen, Y., et al. (2011). Visualizing spacetime curvature via frame-drag vortexes and tidal tendexes: general theory and weak-gravity applications. *Phys. Rev. D.* 84, 124014. doi:10.1103/PhysRevD.84.124014

Niedźwiecki, A., and Miyakawa, T. (2010). General relativistic models of the X-ray spectral variability of MCG-6-30-15. *Astron. Astrophys.* 509, A22. doi:10.1051/0004-6361/200911919

Niedźwiecki, A., Szanecki, M., and Zdziarski, A. A. (2019). Improved spectral models for relativistic reflection. *Mon. Not. R. Astron. Soc.* 485, 2942–2955. doi:10.1093/mnras/stz487

Niedźwiecki, A., Zdziarski, A. A., and Szanecki, M. (2016). On the lamppost model of accreting black holes. *Astrophys. J. Lett.* 821, L1. doi:10.3847/2041-8205/821/1/L1

Niedźwiecki, A., and Życki, P. T. (2008). On the variability and spectral distortion of fluorescent iron lines from black hole accretion discs. *Mon. Not. R. Astron. Soc.* 386, 759–780. doi:10.1111/j.1365-2966.2008.12735.x

Novikov, I. D., and Thorne, K. S. (1973). "Astrophysics of black holes," in *Black holes (les astres occlus)*. Editors C. Dewitt, and B. S. Dewitt (New York: Gordon & Breach), 343–450.

Owen, R., Brink, J., Chen, Y., Kaplan, J. D., Lovelace, G., Matthews, K. D., et al. (2011). Frame-dragging vortexes and tidal tendexes attached to colliding black holes: visualizing the curvature of spacetime. *Phys. Rev. Lett.* 106, 151101. doi:10.1103/PhysRevLett.106.151101

Parker, M. L., Alston, W. N., Buisson, D. J. K., Fabian, A. C., Jiang, J., Kara, E., et al. (2017a). Revealing the ultrafast outflow in IRAS 13224-3809 through spectral variability. *Mon. Not. R. Astron. Soc.* 469, 1553–1558. doi:10.1093/mnras/stx945

Parker, M. L., Fabian, A. C., Matt, G., Koljonen, K. I. I., Kara, E., Alston, W., et al. (2015). Revealing the X-ray variability of AGN with principal component analysis. *Mon. Not. R. Astron. Soc.* 447, 72–96. doi:10.1093/mnras/stu2424

Parker, M. L., Lieu, M., and Matzeu, G. A. (2022). AGN X-ray spectroscopy with neural networks. *Mon. Not. R. Astron. Soc.* 514, 4061–4068. doi:10.1093/mnras/stac1639

Parker, M. L., Longinotti, A. L., Schartel, N., Grupe, D., Komossa, S., Kriss, G., et al. (2019). The nuclear environment of the NLS1 Mrk 335: obscuration of the X-ray line emission by a variable outflow. *Mon. Not. R. Astron. Soc.* 490, 683–697. doi:10.1093/mnras/stz2566

Parker, M. L., Marinucci, A., Brenneman, L., Fabian, A. C., Kara, E., Matt, G., et al. (2014a). Principal component analysis of MCG-06-30-15 with XMM-Newton. *Mon. Not. R. Astron. Soc.* 437, 721–729. doi:10.1093/mnras/stt1925

Parker, M. L., Pinto, C., Fabian, A. C., Lohfink, A., Buisson, D. J. K., Alston, W. N., et al. (2017b). The response of relativistic outflowing gas to the inner accretion disk of a black hole. *Nature* 543, 83–86. doi:10.1038/nature21385

Parker, M. L., Walton, D. J., Fabian, A. C., and Risaliti, G. (2014b). PCA of PCA: principal component analysis of partial covering absorption in NGC 1365. *Mon. Not. R. Astron. Soc.* 441, 1817–1824. doi:10.1093/mnras/stu712

Parker, M. L., Wilkins, D. R., Fabian, A. C., Grupe, D., Dauser, T., Matt, G., et al. (2014c). The NuSTAR spectrum of Mrk 335: extreme relativistic effects within two gravitational radii of the event horizon? *Mon. Not. R. Astron. Soc.* 443, 1723–1732. doi:10.1093/mnras/stu1246

Paszke, A., Gross, S., Massa, F., Lerer, A., Bradbury, J., Chanan, G., et al. (2019). PyTorch: an imperative style, high-performance deep learning library. In *Advances in neural information processing systems*, Editors H. Wallach, H. Larochelle, A. Beygelzimer, F. d'Alché-Buc, E. Fox, and R. Garnett (Vancouver, Canada: Curran Associates, Inc.), vol. 32

Pearson, K. (1901). LIII. On lines and planes of closest fit to systems of points in space. *Philos. Mag.* 2, 559–572. doi:10.1080/14786440109462720

Pedregosa, F., Varoquaux, G., Gramfort, A., Michel, V., Thirion, B., Grisel, O., et al. (2011). Scikit-learn: machine learning in Python. *J. Mach. Learn. Res.* 12, 2825–2830. doi:10.48550/arXiv.1201.0490

Penrose, R. (1969). Gravitational collapse: the role of general relativity. *Nuovo Cimento Riv. Ser.* 1, 252.

Penrose, R. (2002). "Golden oldie": gravitational collapse: the role of general relativity. *Gen. Relativ. Gravit.* 7, 1141–1165. doi:10.1023/A:1016578408204

Penrose, R., and Floyd, R. M. (1971). Extraction of rotational energy from a black hole. *Nat. Phys. Sci.* 229, 177–179. doi:10.1038/physci229177a0

Peterson, B. M., Ferrarese, L., Gilbert, K. M., Kaspi, S., Malkan, M. A., Maoz, D., et al. (2004). Central masses and broad-line region sizes of active galactic nuclei. II. A homogeneous analysis of a large reverberation-mapping database. *Astrophys. J.* 613, 682–699. doi:10.1086/423269

Petrucci, P. O., Ursini, F., De Rosa, A., Bianchi, S., Cappi, M., Matt, G., et al. (2018). Testing warm Comptonization models for the origin of the soft X-ray excess in AGNs. *Astron. Astrophys.* 611, A59. doi:10.1051/0004-6361/201731580

Porquet, D., Done, C., Reeves, J. N., Grosso, N., Marinucci, A., Matt, G., et al. (2019). A deep X-ray view of the bare AGN Ark 120. V. Spin determination from disc-Comptonisation efficiency method. *Astron. Astrophys.* 623, A11. doi:10.1051/0004-6361/201834448

Poutanen, J., and Svensson, R. (1996). The two-phase pair corona model for active galactic nuclei and X-ray binaries: how to obtain exact solutions. *Astrophys. J.* 470, 249. doi:10.1086/177865

Press, W. H., Teukolsky, S. A., Vetterling, W. T., and Flannery, B. P. (1997). *Numerical recipes in fortran 77. The art of scientific computing* vol. 1. 2nd Edn. Cambridge, UK: Cambridge University Press.

Reeves, J. N., Braito, V., Porquet, D., Lobban, A. P., Matzeu, G. A., and Nardini, E. (2021). The flaring X-ray corona in the quasar PDS 456. *Mon. Not. R. Astron. Soc.* 500, 1974–1991. doi:10.1093/mnras/staa3377

Remillard, R. A., and McClintock, J. E. (2006). X-ray properties of black-hole binaries. *Ann. Rev. Astron. Astrophys.* 44, 49–92. doi:10.1146/annurev.astro.44.051905.092532

Rencher, A. C., and Christensen, W. F. (2012). *Methods of multivariate analysis*. 3rd edn. Hoboken: Wiley. doi:10.1002/9781118391686

Reynolds, C. S. (2013). The spin of supermassive black holes. *Class. Quantum Gravity* 30, 244004. doi:10.1088/0264-9381/30/24/244004

Reynolds, C. S. (2014). Measuring black hole spin using X-ray reflection spectroscopy. *Space Sci. Rev.* 183, 277–294. doi:10.1007/s11214-013-0006-6

Reynolds, C. S. (2019). Observing black holes spin. *Nat. Astron.* 3, 41–47. doi:10.1038/s41550-018-0665-z

Reynolds, C. S., and Nowak, M. A. (2003). Fluorescent iron lines as a probe of astrophysical black hole systems. *Phys. Rep.* 377, 389–466. doi:10.1016/S0370-1573(02)00584-7

Rhea, C., Hlavacek-Larrondo, J., Perreault-Levasseur, L., Gendron-Marsolais, M.-L., and Kraft, R. (2020). A novel machine learning approach to disentangle multitemperature regions in galaxy clusters. *Astron. J.* 160, 202. doi:10.3847/1538-3881/abb468

Ross, R. R., and Fabian, A. C. (2005). A comprehensive range of X-ray ionized-reflection models. *Mon. Not. R. Astron. Soc.* 358, 211–216. doi:10.1111/j.1365-2966.2005.08797.x

Ross, R. R., and Fabian, A. C. (2007). X-ray reflection in accreting stellar-mass black hole systems. *Mon. Not. R. Astron. Soc.* 381, 1697–1701. doi:10.1111/j.1365-2966.2007.12339.x

Ross, R. R., Fabian, A. C., and Young, A. J. (1999). X-ray reflection spectra from ionized slabs. *Mon. Not. R. Astron. Soc.* 306, 461–466. doi:10.1046/j.1365-8711.1999.02528.x

Schnittman, J. D. (2019). *Black hole accretion disk visualization. NASA scientific visualization studio*. Goddard Space Flight Center. (Greenbelt, MD: NASA). Available at: https://svs.gsfc.nasa.gov/13326.

Schnittman, J. D., Krolik, J. H., and Hawley, J. F. (2006). Light curves from an MHD simulation of a black hole accretion disk. *Astrophys. J.* 651, 1031–1048. doi:10.1086/507421

Schnittman, J. D., Krolik, J. H., and Noble, S. C. (2013). X-ray spectra from magnetohydrodynamic simulations of accreting black holes. *Astrophys. J.* 769, 156. doi:10.1088/0004-637X/769/2/156

Schwarzschild, K. (1916). On the gravitational field of a mass point according to einstein's theory. *Sitzber. Dtsch. Akad. Wiss. Berl. Kl. Math. Phys.*, 189–196.

Sesana, A., Barausse, E., Dotti, M., and Rossi, E. M. (2014). Linking the spin evolution of massive black holes to galaxy kinematics. *Astrophys. J.* 794, 104. doi:10.1088/0004-637X/794/2/104

Shafee, R., McClintock, J. E., Narayan, R., Davis, S. W., Li, L.-X., and Remillard, R. A. (2006). Estimating the spin of stellar-mass black holes by spectral fitting of the X-ray continuum. *Astrophys. J. Lett.* 636, L113–L116. doi:10.1086/498938

Sharma, A., Paliwal, K. K., Imoto, S., and Miyano, S. (2013). Principal component analysis using QR decomposition. *Int. J. Mach. Learn. and Cyber.* 4, 679–683. doi:10.1007/s13042-012-0131-7

Shields, G. A. (1978). Thermal continuum from accretion disks in quasars. *Nature* 272, 706–708. doi:10.1038/272706a0

Shiokawa, H. (2017). Simulations of accretion disk. Event horizon telescope collaboration. Available at: https://eventhorizontelescope.org/simulations-gallery.

Shiokawa, H., Gammie, C. F., and Doeleman, S. S. (2017). Time domain filtering of resolved images of Sgr A*. *Astrophys. J.* 846, 29. doi:10.3847/1538-4357/aa82b7

Singh, H. P., Gulati, R. K., and Gupta, R. (1998). Stellar spectral classification using principal component analysis and artificial neural networks. *Mon. Not. R. Astron. Soc.* 295, 312–318. doi:10.1046/j.1365-8711.1998.01255.x

Speith, R. (1993). Rotverschiebung längs Photonenbahnen in der Nähe Aktiver Galaktischer Kerne English: Redshift along Photon Trajectories near Active Galactic Nuclei. Germany: Eberhard Karls University of Tubingen. Master's thesis.

Speith, R., Riffert, H., and Ruder, H. (1995). The photon transfer function for accretion disks around a Kerr black hole. *Comput. Phys. Commun.* 88, 109–120. doi:10.1016/0010-4655(95)00067-P

Sylvester, J. J. (1889a). A new proof that a general quadric may be reduced to its canonical form (that is, a linear function of squares) by means of a real orthogonal substitution. *Messenger Math.* 19, 1–5.

Sylvester, J. J. (1889b). On the reduction of a bilinear quantic of the nth order to the form of a sum of n products by a double orthogonal substitution. *Messenger Math.* 19, 42–46.

Sylvester, J. J. (1889c). Sur la réduction biorthogonale d'une forme linéo-linéaire à sa forme canonique. *C. R. Acad. Sci. Paris* 108, 651–653.

Tchekhovskoy, A., and McKinney, J. C. (2012). Prograde and retrograde black holes: whose jet is more powerful? *Mon. Not. R. Astron. Soc.* 423, L55–L59. doi:10.1111/j.1745-3933.2012.01256.x

Thorne, K. S., Price, R. H., and MacDonald, D. A. (1986). *Black holes: the membrane paradigm*. New Haven, CT: Yale Univ. Press.

Tombesi, F., Cappi, M., Reeves, J. N., and Braito, V. (2012). Evidence for ultrafast outflows in radio-quiet AGNs - III. Location and energetics. *Mon. Not. R. Astron. Soc.* 422, 1–5. doi:10.1111/j.1745-3933.2012.01221.x

Tombesi, F., Cappi, M., Reeves, J. N., Palumbo, G. G. C., Braito, V., and Dadina, M. (2011). Evidence for ultra-fast outflows in radio-quiet active galactic nuclei. II. Detailed photoionization modeling of Fe K-shell absorption lines. *Astrophys. J.* 742, 44. doi:10.1088/0004-637X/742/1/44

Tombesi, F., Cappi, M., Reeves, J. N., Palumbo, G. G. C., Yaqoob, T., Braito, V., et al. (2010). Evidence for ultra-fast outflows in radio-quiet AGNs: I. Detection and statistical incidence of Fe K-shell absorption lines. *Astron. Astrophys.* 521, A57. doi:10.1051/0004-6361/200913440

Trefethen, L. N., and Bau, D. I. (1997). *Numerical linear algebra*. Philadelphia, PA: Society for Industrial and Applied Mathematics.

Trunk, G. V. (1979). A problem of dimensionality: a simple example. *IEEE Trans. Pattern Anal. Mach. Intell.* PAMI-1, 306–307. doi:10.1109/TPAMI.1979.4766926

Turner, T. J., Miller, L., Reeves, J. N., and Kraemer, S. B. (2007). The variable X-ray spectrum of Markarian 766. II. Time-resolved spectroscopy. *Astron. Astrophys.* 475, 121–131. doi:10.1051/0004-6361:20077947

Turner, T. J., Reeves, J. N., Braito, V., Lobban, A., Kraemer, S., and Miller, L. (2018). A rapid occultation event in NGC 3227. *Mon. Not. R. Astron. Soc.* 481, 2470–2478. doi:10.1093/mnras/sty2447

Vaughan, S., and Fabian, A. C. (2004). A long hard look at MCG-6-30-15 with XMM-Newton- II. Detailed EPIC analysis and modelling. *Mon. Not. R. Astron. Soc.* 348, 1415–1438. doi:10.1111/j.1365-2966.2004.07456.x

Vestergaard, M. (2002). Determining central black hole masses in distant active galaxies. *Astrophys. J.* 571, 733–752. doi:10.1086/340045

Victoria-Ceballos, C. I., González-Martín, O., Masegosa, J., Longinotti, A. L., Esparza-Arredondo, D., and Osorio-Clavijo, N. (2023). Testing physical scenarios for the reflection features of type-1 AGNs using XMM-Newton and NuSTAR simultaneous observations. *Astrophys. J.* 954, 96. doi:10.3847/1538-4357/ace785

Volonteri, M., Madau, P., Quataert, E., and Rees, M. J. (2005). The distribution and cosmic evolution of massive black hole spins. *Astrophys. J.* 620, 69–77. doi:10.1086/426858

Volonteri, M., Sikora, M., Lasota, J.-P., and Merloni, A. (2013). The evolution of active galactic nuclei and their spins. *Astrophys. J.* 775, 94. doi:10.1088/0004-637X/775/2/94

Wall, J. V., and Jenkins, C. R. (2012). *Practical statistics for astronomers*. 2nd edn. Cambridge, UK: Cambridge Univ. Press.

Wandel, A., Peterson, B. M., and Malkan, M. A. (1999). Central masses and broad-line region sizes of active galactic nuclei. I. Comparing the photoionization and reverberation techniques. *Astrophys. J.* 526, 579–591. doi:10.1086/308017

Whitney, C. A. (1983). Principal components analysis of spectral data. I. Methodology for spectral classification. *Astron. Astrophys. Suppl. Ser.* 51, 443–461.

Wilson, A. S., and Colbert, E. J. M. (1995). The difference between radio-loud and radio-quiet active galaxies. *Astrophys. J.* 438, 62. doi:10.1086/175054

Witten, I. H., Frank, E., Hall, M. A., and Pal, C. J. (2017). *Data mining: practical machine learning tools and techniques*. Cambridge, MA: Elsevier. doi:10.1016/C2009-0-19715-5

Zdziarski, A. A., Johnson, W. N., and Magdziarz, P. (1996). Broad-band -ray and X-ray spectra of NGC 4151 and their implications for physical processes and geometry. *Mon. Not. R. Astron. Soc.* 283, 193–206. doi:10.1093/mnras/283.1.193

Zhang, S. N., Cui, W., and Chen, W. (1997). Black hole spin in X-ray binaries: observational consequences. *Astrophys. J. Lett.* 482, L155–L158. doi:10.1086/310705

Zhang, Y., and Zhao, Y. (2003). Classification in multidimensional parameter space: methods and examples. *Publ. Astron. Soc. Pac.* 115, 1006–1018. doi:10.1086/376847

Życki, P. T., Done, C., and Smith, D. A. (1999). The 1989 May outburst of the soft X-ray transient GS 2023+338 (V404 Cyg). *Mon. Not. R. Astron. Soc.* 309, 561–575. doi:10.1046/j.1365-8711.1999.02885.x

frontiers | Frontiers in Astronomy and Space Sciences

TYPE Mini Review
PUBLISHED 06 December 2024
DOI 10.3389/fspas.2024.1479907

Check for updates

OPEN ACCESS

EDITED BY
Michel Blanc,
UMR5277 Institut de recherche en astrophysique et planétologie (IRAP), France

REVIEWED BY
RS Pandey,
Amity University, India
Marie Devinat,
UMR5277 Institut de recherche en astrophysique et planétologie (IRAP), France

*CORRESPONDENCE
Simon Wing,
simon.wing@jhuapl.edu

RECEIVED 13 August 2024
ACCEPTED 18 November 2024
PUBLISHED 06 December 2024

CITATION
Wing S, Johnson JR, Thomsen MF and Ma X (2024) Evolution of the flux tube instability parameters in plasma injections at saturnian magnetosphere.
Front. Astron. Space Sci. 11:1479907.
doi: 10.3389/fspas.2024.1479907

COPYRIGHT
© 2024 Wing, Johnson, Thomsen and Ma. This is an open-access article distributed under the terms of the Creative Commons Attribution License (CC BY). The use, distribution or reproduction in other forums is permitted, provided the original author(s) and the copyright owner(s) are credited and that the original publication in this journal is cited, in accordance with accepted academic practice. No use, distribution or reproduction is permitted which does not comply with these terms.

Evolution of the flux tube instability parameters in plasma injections at saturnian magnetosphere

Simon Wing[1]*, Jay R. Johnson[2], Michelle F. Thomsen[3] and Xuanye Ma[4]

[1]Applied Physics Laboratory, The Johns Hopkins University, Laurel, MD, United States, [2]School of Engineering, Andrews University, Berrien Springs, MI, United States, [3]Planetary Science Institute, Tucson, AZ, United States, [4]Physical Sciences Department, Embry-Riddle Aeronautical University, Florida, United States

The evolution of the flux tube stability parameters in plasma injections at the Saturnian magnetosphere is reviewed. Plasma injections result from an imbalance in the centrifugal, total pressure gradient, and magnetic tension forces acting on plasma in the magnetosphere. Plasma originating from Enceladus tends to move outward due to centrifugal forces while reconnected flux tubes that are depleted of plasma collapse because of the magnetic tension leading to plasma injections. As the flux tube moves inward and contracts, the ambient density and pressure increase sufficiently to resist further collapse and the injected flux tube brakes. During this process the flux tube may also lose its integrity due to particle drifts, which allow exchange of plasma with adjacent flux tubes so as to bring the flux tube closer to equilibrium and stability so that it is indistinguishable from adjacent plasma. Stability parameters using this energy approach are defined and examined. The results show that the net forces push the plasma moves inward for $L > 11$ and outward for $L < 8.5$, while equilibrium is generally reached for $8.5 < L < 11$, where L is the equatorial magnetic field crossing measured in Saturnian radii. The evolution of the stability parameters can also apply to Jovian and other fast rotating planetary magnetospheres.

KEYWORDS

flux tube interchange, plasma injection, plasma transport, saturn magnetosphere, flux tube entropy instability, braking of plasma injection, Rayleigh-Taylor instability

1 Introduction

In the study of the Saturnian magnetosphere, the radially inward plasma transport or plasma injection has long been a fascinating and confounding topic. The plasma injection in the inner magnetosphere is often characterized by a sudden incursion of plasma having higher temperature and lower density than the ambient plasma (Burch et al., 2005; Azari et al., 2018; Thomsen, 2013). The injected plasma or flux tube has been observed to be nearly in pressure balance with the ambient plasma and hence there is often an accompanying sudden increase or decrease in the magnetic field strength and pressure (André et al., 2005; 2007; Azari et al., 2018; Wing et al., 2022). As the injected hot plasma moves radially inward, the ions and electrons execute an energy

dependent curvature and gradient azimuthal drift, leading to an energy dispersion signature from which the age and location of the injection can be estimated (Burch et al., 2005; Chen and Hill, 2008; Yin et al., 2023; Thomsen, 2013). Hill et al. (2005) reported that injections have typical ages <11 h and azimuthal widths <1 Rs in a sample of 48 events. Azari et al. (2018), Azari et al. (2019) found that plasma injections rarely reach r < 6 Rs in observations gathered by Cassini spacecraft. Paranicas et al. (2020) found that the inflow speeds of the energetic particle injections range from 0 to 50 km s^{-1} in 20 events. The flux-tube interchange injections have been associated with electron cyclotron harmonic (ECH), whistler mode, and upper-hybrid waves (Kennelly et al., 2013; Long et al., 2023; Menietti et al., 2008) and periodic 5 kHz narrowband radio wave emissions (Mitchell et al., 2009; Mitchell et al., 2015; Menietti et al., 2016; Wing et al., 2020). A comprehensive review of the plasma injections at the Saturnian magnetosphere can be found in Thomsen (2013) and Achilleos et al. (2015).

Two key factors contribute to the complexity of the plasma injections: (1) Saturn rotates on its axis rapidly with a periodicity of about 10–11 h (Azari et al., 2019) and (2) Enceladus, a moon located at r ~ 4 Rs where Rs = Saturn radius ~60,268 km, continuously sources cold plasma at the rate of 12–250 kg s^{-1} in the magnetosphere (Bagenal and Delamere, 2011). Thus, many or most studies considered the effective gravity or Rayleigh-Taylor like instability as the mechanism for plasma injections where hot tenuous flux tube moves in and replaces the cold dense flux tube that moves out (e.g., Hill, 1976; Chen and Hill, 2008; Sittler et al., 2008; Bagenal and Delamere, 2011; Liu and Hill, 2012; Thomsen et al., 2013; Azari et al., 2019; Ma et al., 2016; Stauffer et al., 2019; Thomsen and Coates, 2019). Liu et al. (2010) simulated this process using Rice Convection Model (RCM) showing narrow radial fingers of hot tenuous inflowing plasma adjacent to fingers of cold dense outflowing plasma.

At Earth where the planet rotates more slowly and its moon does not source plasma, observations and simulations have shown that flux tube entropy instability where injected flux tube having depleted flux tube entropy (S) resulting from magnetotail reconnection can move inward until its S reaches the same value as that of the ambient plasma (e.g., Birn et al., 2006; 2009; Pontius and Wolf, 1990; Wing and Johnson, 2009; Johnson and Wing, 2009; Dubyagin et al., 2010). Ma et al. (2019) investigated the role of the flux tube entropy instability in the plasma injections at Saturnian magnetosphere, but they did not consider the effective gravity. Nonadiabatic plasma heating such as turbulent heating can increase flux tube entropy and hence can affect the plasma injection (Saur, 2004; Neupane et al., 2021; Wing et al., 2014).

Plasma in the rotating magnetosphere is affected by the centrifugal force that tends to push plasma outward, magnetic tension that resists stretching of field lines, and total pressure, which tends to push plasma outward. Dense plasma originating at Enceladus in the inner magnetosphere is pushed outward by the centrifugal force, while flux tubes that are depleted by reconnection in the magnetotail collapse under the magnetic tension leading to plasma injections. Southwood and Kivelson (1987) developed an energy-based formalism for the stability requirement of an inward moving flux tube that includes both the effective gravity (centrifugal force + gravity) and the flux tube entropy instabilities in fast rotating magnetosphere (*cf.*, Ferrière et al., 2001). Based on the Southwood and Kivelson (1987) formalism, Wing et al. (2022) examined the roles of the effective gravity and flux tube entropy in seven plasma injection events observed by Cassini spacecraft in the Saturnian magnetosphere.

The present paper reviews the above studies of the plasma injections at the Saturnian magnetosphere, but narrowly focuses on the following two questions: (1) What roles do the effective gravity and flux tube entropy play in the Saturnian plasma injections? Which term is dominant? and (2) Why do injections rarely reach r < 6 Rs as reported in Azari et al. (2018), Azari et al. (2019)?

2 Flux tube instability parameters

The stability requirement for the inward moving flux tube interchange for a fast rotating magnetosphere is given in Equation 1 (Southwood and Kivelson, 1987):

$$\left[\frac{K\left(\frac{\partial S}{\partial X_p}\right)}{V^{\gamma}}-\left(\frac{mg_e h}{V}\right)\left(\frac{\partial N}{\partial X_p}\right)\right]<0 \tag{1}$$

where $K=\left[2\left(B^2/\mu_o\right)(hc)+nmhg\right]/P_{\gamma}$, n = plasma density, N = flux-tube content, $P_{\gamma}=\left(\gamma p+B^2/\mu_o\right)$, p = flux-tube averaged plasma pressure, γ = polytropic index = 5/3, B = magnitude of the magnetic field, X_p = the displacement of the interchange motion, h = Lamé coefficient along X_p, m = average ion mass, μ_o = magnetic field permeability constant, c = component of the magnetic field curvature in the X_p direction, S = flux-tube or total entropy = pV^{γ}, V = flux-tube volume, and g_e = effective gravity given by Equation 2,

$$g_e=r\Omega^2-g \tag{2}$$

where g = gravity, Ω = planet angular velocity and r = radial distance.

The first term of Equation 1 tends toward instability when the entropy gradient is negative radially outward given that the curvature is negative. In this case, an outward perturbation of plasma governed by an adiabatic pressure law would have a higher entropy than the flux tube it displaced and therefore a higher pressure. The increased pressure would push the perturbed plasma further outward leading to instability. On the other hand, if the entropy gradient were positive, the displaced flux tube would have a lower pressure than the flux tube it displaced. In this case, the JxB force would push the low pressure flux tube back toward its original position and the configuration is stable. The second term of Equation 1 tends toward instability when the gradient of the flux tube content is negative outwards. In this case an outward displacement of a flux tube increases the outward force it exerts relative to that of the displaced plasma leading to instability. On the other hand, a positive outward gradient of the flux tube content is stable because the total outward force exerted by the flux tube decreases relative to the displaced flux tube and therefore the surrounding flux tubes will push it back toward the original position. At the Saturnian magnetosphere, Enceladus provides a steady plasma source and therefore the overall profile of the flux tube content is generally decreasing in the radial direction at r > 5–6 Rs, and such a configuration is unstable to centrifugal interchange.

Based on Equation 1, Wing et al. (2022) considered the stability of the inner and outer edges of the injected flux tube and derived

a Total Stability (TS) parameter, which quantifies the conditions for which flux tubes are unstable to inward and outward displacement. Additionally, in order to study the roles of the flux tube entropy and the effective gravity separately, they separated the TS parameter into its two components as shown in Equation 3:

$$TS = E_t + G_t \tag{3}$$

where the first term is the entropy term (Equation 4),

$$E_t = V^{-\gamma}\Delta S \tag{4}$$

and the second term is the effective gravity term (Equation 5),

$$G_t = (-1)K^{-1}\left(\frac{mg_e h}{V}\right)(\Delta N). \tag{5}$$

If TS = 0, the condition predicts that the flux-tube is in equilibrium, but if TS < 0 or TS > 0, it would describe the flux tube instability condition for inward and outward moving flux tube, respectively. If TS > 0, the net force would push the flux tube outward and conversely, if TS < 0, the net force would push the flux tube inward. If the effective gravity is negligible, i.e., $G_t = 0$, then TS = E_t, which is similar to the formalism for the flux tube interchange developed for Earth (e.g., Erickson and Wolf, 1980; Pontius and Wolf, 1990; Birn et al., 2006; Birn et al., 2009).

3 Evolution of the stability parameters TS, E_t, and G_t in the plasma injection

The Cassini spacecraft orbited Saturn 2004 to 2017 and carried Cassini Magnetospheric Imaging Instrument (MIMI), Cassini Plasma Spectrometer (CAPS), and Dual Technique Magnetometer (MAG) instruments. The CAPS instrument observed ions with energy range 1 eV/q–50 keV/q and electrons with energy range 1 eV–30 keV (Young et al., 2004). CAPS ion moments (density, temperature, flow velocity) have been calculated by numerical integration over the observed distribution (Thomsen et al., 2010) while the CAPS electron moments are computed as described by Lewis et al. (2008). The CHarge Energy Mass Spectrometer (CHEMS) is part of the MIMI instrument suite and observed ions with energy range 3–220 keV/q (Krimigis et al., 2004). The MAG instrument detected magnetic fields up to 44,000 nT (Dougherty et al., 2004).

Wing et al. (2022) used CAPS, CHEMS, and MAG data, which are publicly available at the NASA Planetary Data System (PDS) Planetary Plasma Interaction (PPI) node (https://pds-ppi.igpp.ucla.edu/index.jsp). The Wing et al. (2022) study selected 7 plasma injections from previously published injection events in Thomsen et al. (2014); (events 1, 2, 3), Mitchell et al. (2015); (events 4, 5, 6), and Rymer et al. (2009); (event 7). These events were selected because they have clear injection signatures and CAPS, CHEMS, and MAG have good data. The 7 events, which range from L ~ 14 to 7, are given in Table 1 in Wing et al. (2022). The L-value gives the distance in planetary radii where the magnetic field intersects the equatorial plane (McIlwain, C. E., 1961) and is computed using Achilleos et al. (2010) magnetic field model. For completeness, these 7 events are listed here in quintuplets.

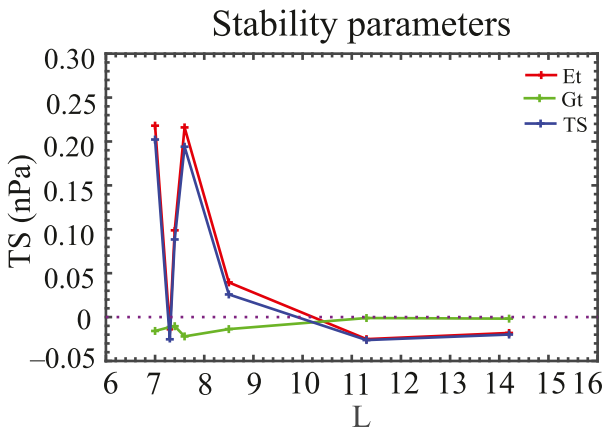

FIGURE 1
The evolution of the stability parameters TS, E_t, and G_t. The red, green, and blue curves correspond to E_t, G_t, and TS, respectively (from Wing et al., 2022).

(event number, time (UT), location SZS (X, Y, Z) Rs, L, Latitude (degree)):

{(1, 2010–06–02 12:20:00, (−8.9, 7.6, 2.4), 14.2, 11.6),
(2, 2007–05–27 14:38:00, (9.2, −0.46, −2.2), 11.3, −13.4),
(3, 2007–10–24 19:27:30, (5.7, −6.1, 0.5), 8.5, 3.4),
(4, 2006–03–21 05:15:53, (−2.5, 7.2, 4.0e-2), 7.6, 0.3),
(5, 2006–03–21 04:44:25, (−2.2, 7.1, 3.0e-2), 7.4, 0.2),
(6, 2006–03–21 04:23:05, (−1.9, 7.0, 3.0e-2), 7.3, 0.2),
(7, 2005–10–30 07:34:48, (−6.9, 1.4, 5.0e-2), 7.0, 0.4)}.

Flux tube entropy, S, and content, N, were calculated from the Cassini (CAPS, CHEMS, MAG) observations, the pressure and density scale height parameters obtained from a method developed in Thomsen et al. (2010), and Achilleos magnetic field model (Achilleos et al., 2010). S and N were calculated inside and outside (ambient) the injected flux tubes with the assumption that the injected flux tube plasma is isotropic and outside is anisotropic. This assumption is perhaps more similar to old injections (Mitchell et al., 2015) and to the selected events.

Figure 1 shows TS, E_t, and G_t for the 7 injected events. At large L (L > 11), $E_t < 0$, $G_t < 0$, and hence TS < 0. Apparently, the entropy and effective gravity terms work in tandem to destabilize flux tube to move inward. As the plasma moves inward, the ambient flux tube entropy (S_a) becomes smaller, which allows G_t to become more positive. At some point, at 8.5 < L < 11, $E_t > 0$, $G_t < 0$, $|E_t| = |G_t|$, and hence TS = 0, and equilibrium is reached. At L < 8.5, with the exception of one event (Event 6), $E_t > 0$ and $|E_t| > |G_t|$, which causes TS > 0. A possible interpretation is that the injection may overshoot the equilibrium and oscillate around equilibrium as observed at Earth (Wolf et al., 2012; Panov et al., 2013; Merkin et al., 2019; Yang et al., 2019). Thus, at L < 8.5, if the flux tube is not moving outward, its inward motion is decelerating.

It is worth noting that in all cases but one, $|E_t|$ dominates $|G_t|$. G_t is negative in all cases. If the plasma injection stops, it is because of the E_t term. In other words, the entropy term, E_t, acts to brake the injections at L < 11.

Wing et al. (2022) repeated the stability calculations using dipole and Khurana et al. (2006) magnetic field models. They

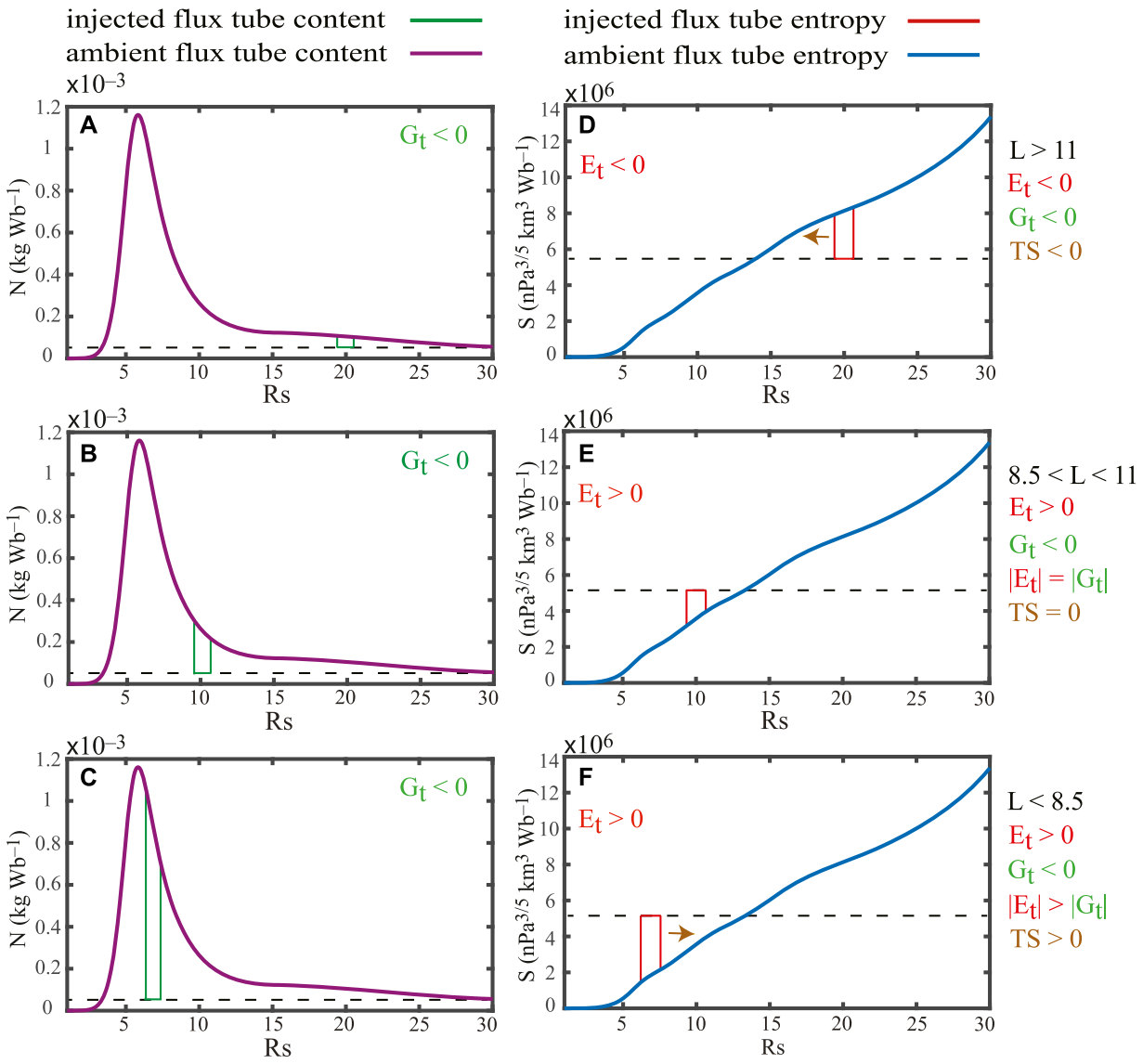

FIGURE 2
Schematic diagram illustrating the evolutions of TS, E_t, and G_t as the plasma injection moves inward based on Wing et al. (2022). The magenta curve on the left panels (panels **A–C**) show the ambient flux tube content (N_a) whereas the blue curve on the right panels (panels **D–F**) show the ambient flux tube entropy (S_a). In panels **(A–C)**, the green tube is an injected flux tube content, which has lower N than N_a. The red tube is an injected flux tube entropy, which has lower S than S_a in panel **(D)**, but higher S than S_a in panels **(E, F)**. N_a and S_a are based on the Cassini measurements [CAPS (Thomsen et al., 2010) and CHEMS (Wing et al., 2022) moment data products] and a steady-state magnetic field model [i.e., the Saturn version of Caudal model (Caudal, 1986), see details in Ma et al. (2019)].

found that qualitatively the results are similar to those obtained using Achileos et al. (2010) magnetic field model (plotted in Figure 1). However, the results obtained from using Khurana et al. (2006) and Achileos et al. (2010) models are closer to each other than those obtained using dipole magnetic field.

Ma et al. (2019) found that based on the flux tube entropy alone, plasma injections resulting from magnetodisk reconnections at r = 22.5–27.5 Rs, should reach equilibrium at r = 8.8–10.5 Rs. As shown in Figure 1, $E_t < 0$ at L ~ 11.3 and $E_t > 0$ at L = 8.5 (the red curve in Figure 1), suggesting that based on the consideration of the flux tube entropy alone, equilibrium should be reached somewhere between 8.5 and 11.3. This result is similar to the equilibrium positions obtained in Ma et al. (2019).

4 Conclusion and summary

Wing et al. (2022) examined the stability parameters (TS, E_t, G_t) in 7 injection events ranging from L ~ 14 to 7. Figure 1 plots these parameters.

Figure 2 shows a schematic diagram that can help illustrate the evolution of TS, E_t, G_t as plasma injection moves inward. In the left panels (panels A, B, and C), the magenta curve shows the ambient flux tube content N_a while in the right panels (panels D, E, and F), the blue curve shows the ambient flux tube entropy S_a. N_a has an outward negative gradient whereas S_a has a positive gradient. These opposite gradients have an impact on the evolution of the plasma injection as it moves inward, as discussed next.

The evolution of G_t is illustrated in Figure 2 panels A, B, and C. The injected flux tube is characterized as having lower density (Chen and Hill, 2008; Liu et al., 2010; Thomsen et al., 2014; Thomsen et al., 2016; Azari et al., 2018) and flux tube content (Thomsen and Coates, 2019) relative to those of ambient plasma (depicted with a green tube in Figure 2). As a result, at $L > 11$, $G_t < 0$ and based on N alone, the flux tube should move inward (panel A). The centrifugal force pushes the flux tube with higher content outward while the flux tube with lower content moves inward. The flux tube that has $G_t < 0$ would continue having $G_t < 0$ as the injection moves inward because the ambient flux tube content N_a has negative gradient (panels B and C). As the injection moves inward, the difference between N_a and N_i (injected flux tube content) becomes larger and as a result, G_t becomes more negative as shown by the green tube in Figure 1 panels A–C.

However, E_t evolves differently. At large L, $L > 11$, the injected flux tube (depicted by the red tube in Figure 2) has lower flux tube entropy S_i relative to that of the ambient plasma S_a (panel D) and hence $E_t < 0$. Thus, at large L, $TS < 0$ because $E_t < 0$ and $G_t < 0$ (panel A) and hence, plasma moves inward. The reconnected flux tube with lower plasma density and content collapses and moves inward due to the magnetic tension force. Here, the centrifugal and the magnetic tension forces work in tandem to push the flux tube inward. As the injection moves inward, the ambient flux tube entropy S_a gets smaller, but the pressure increases, which would tend to resist further collapse of the injected flux tube. As a result, E_t becomes more positive. At some point at $8.5 < L < 11$, the injected flux tube entropy S_i is slightly larger than that of the ambient plasma S_a, E_t is slightly positive, G_t remains negative (panel B), $|E_t| = |G_t|$, $TS = 0$, the net force is zero, and equilibrium is reached (panel E). However, the injection may overshoot and oscillate around the equilibrium as seen in observations and simulations at Earth (e.g., Wolf et al., 2012; Panov et al., 2013; Merkin et al., 2019; Yang et al., 2019). So, at $L < 8.5$, the injected flux tube entropy S_i is much larger than that of the ambient plasma S_a, $E_t > 0$ (panel F), $G_t < 0$ (panel C), but because E_t dominates G_t, $TS > 0$ (panel f). The ambient pressure force, which dominates other forces, pushes the injected flux tube outward. If the flux tube is not actually moving outward, its inward motion should be decelerating at this point. While the injected flux tube moves inward, it can lose integrity as plasma from the injected flux tube drifts out while the ambient plasma drifts in, which can also help stabilize the injection. After a while, the injected flux tube would be indistinguishable from the background or ambient plasma.

The schematic diagram depicted in Figure 2 is constructed using only the 7 events in the Wing et al. (2022) study. Even with the small number events, the equilibrium locations obtained from the consideration of flux tube entropy alone (E_t) are remarkably similar to those obtained statistically in Ma et al. (2019). Nonetheless, the exact L or region where the equilibrium is reached ($TS = 0$) can be expected to vary slightly from one event to another, depending on magnetospheric activity and other conditions. With more data points, one can perhaps determine statistically the region where the transitions from $TS < 0$ to $TS = 0$ and to $TS > 0$ occur, which may differ from those shown in Figure 2. However, the basic description of the evolution of TS, E_t, and G_t parameters as the plasma moves inward should still apply.

It is interesting to compare the roles of E_t and G_t in plasma injections at the terrestrial and Saturnian magnetospheres. At Earth, E_t plays a significant role in moving plasma injection inward and braking the injection (Birn et al., 2006; 2009; Pontius and Wolf, 1990; Wing and Johnson, 2009; Wing and Johnson, 2010; Wing et al., 2014; Johnson and Wing, 2009; Dubyagin et al., 2010). The G_t term is negligible. The injection reaches equilibrium when $E_t = 0$. At Saturn, the picture is more complicated. E_t and G_t work in tandem to move the injection inward at $L > 11$. The G_t term is always negative because of the negative gradient of the ambient flux tube content. As the injection gets closer to the planet ($L < 11$), the E_t term becomes positive and acts to oppose that of G_t. Because E_t dominates G_t, E_t acts to brake the injection.

Azari et al. (2018), Azari et al. (2019) found that statistically, plasma injections rarely reach $r < 6$ Rs. The stability analysis presented in Wing et al. (2022) and reviewed herein can be seen as consistent with the observations.

Author contributions

SW: Conceptualization, Data curation, Formal Analysis, Funding acquisition, Investigation, Methodology, Project administration, Resources, Software, Supervision, Validation, Visualization, Writing–original draft, Writing–review and editing. JRJ: Formal Analysis, Investigation, Methodology, Writing–review and editing, Conceptualization. MFT: Formal Analysis, Investigation, Methodology, Writing–review and editing, Data curation. XM: Data curation, Writing–review and editing.

Funding

The author(s) declare that financial support was received for the research, authorship, and/or publication of this article. We acknowledge the support of NASA grants 80NSSC22K0310, 80NSSC20K0704, 80NSSC22K0515, 80NSSC19K0899, 80NSSC23K0904, 80NSSC20K1279 and NSF grant 2131013.

Conflict of interest

The authors declare that the research was conducted in the absence of any commercial or financial relationships that could be construed as a potential conflict of interest.

The author(s) declared that they were an editorial board member of Frontiers, at the time of submission. This had no impact on the peer review process and the final decision.

Publisher's note

All claims expressed in this article are solely those of the authors and do not necessarily represent those of their affiliated organizations, or those of the publisher, the editors and the reviewers. Any product that may be evaluated in this article, or claim that may be made by its manufacturer, is not guaranteed or endorsed by the publisher.

References

Achilleos, N., André, N., Blanco-Cano, X., Brandt, P. C., Delamere, P. A., and Winglee, R. (2015). 1. Transport of mass, momentum and energy in planetary magnetodisc regions. *Space Sci. Rev.* 187 (1–4), 229–299. doi:10.1007/s11214-014-0086-y

Achilleos, N., Guio, P., and Arridge, C. S. (2010). A model of force balance in Saturn's magnetodisc. *Mon. Notices R. Astronomical Soc.* 401 (4), 2349–2371. doi:10.1111/j.1365-2966.2009.15865.x

André, N., Dougherty, M. K., Russell, C. T., Leisner, J. S., and Khurana, K. K. (2005). Dynamics of the Saturnian inner magnetosphere: first inferences from the Cassini magnetometers about small-scale plasma transport in the magnetosphere. *Geophys. Res. Lett.* 32, L14S06. doi:10.1029/2005GL022643

André, N., Persoon, A. M., Goldstein, J., Burch, J. L., Louarn, P., Lewis, G. R., et al. (2007). Magnetic signatures of plasma-depleted flux tubes in the Saturnian inner magnetosphere. *Geophys. Res. Lett.* 34, L14108. doi:10.1029/2007GL030374

Azari, A. R., Jia, X., Liemohn, M. W., Hospodarsky, G. B., Provan, G., Ye, S.-Y., et al. (2019). Are Saturn's interchange injections organized by rotational longitude? *J. Geophys. Res. Space Phys.* 124, 1806–1822. doi:10.1029/2018JA026196

Azari, A. R., Liemohn, M. W., Jia, X., Thomsen, M. F., Mitchell, D. G., Sergis, N., et al. (2018). Interchange injections at Saturn: statistical survey of energetic H^+ sudden flux intensifications. *J. Geophys. Res. Space Phys.* 123, 4692–4711. doi:10.1029/2018JA025391

Bagenal, F., and Delamere, P. A. (2011). Flow of mass and energy in the magnetospheres of Jupiter and Saturn. *J. Geophys. Res.* 116, A05209. doi:10.1029/2010JA016294

Birn, J., Hesse, M., and Schindler, K. (2006). Entropy conservation in simulations of magnetic reconnection. *Phys. Plasmas* 13, 092117. doi:10.1063/1.2349440

Birn, J., Hesse, M., Schindler, K., and Zaharia, S. (2009). Role of entropy in magnetotail dynamics. *J. Geophys. Res.* 114, A00D03. doi:10.1029/2008JA014015

Burch, J. L., Goldstein, J., Hill, T. W., Young, D. T., Crary, F. J., Coates, A. J., et al. (2005). Properties of local plasma injections in Saturn's magnetosphere. *Geophys. Res. Lett.* 32, L14S02. doi:10.1029/2005GL022611

Caudal, G. (1986). A self-consistent model of Jupiter's magnetodisc including the effects of centrifugal force and pressure. *J. Geophys. Res.* 91 (A4), 4201–4221. doi:10.1029/JA091iA04p04201

Chen, Y., and Hill, T. W. (2008). Statistical analysis of injection/dispersion events in Saturn's inner magnetosphere. *J. Geophys. Res.* 113, A07215. doi:10.1029/2008JA013166

Dougherty, M. K., Kellock, S., Southwood, D. J., Balogh, A., Smith, E. J., Tsurutani, B. T., et al. (2004). The Cassini magnetic field investigation. *Space Sci. Rev.* 114, 331–383. doi:10.1007/978-1-4020-2774-1_4

Dubyagin, S., Sergeev, V., Apatenkov, S., Angelopoulos, V., Nakamura, R., McFadden, J., et al. (2010). Pressure and entropy changes in the flow-braking region during magnetic field dipolarization. *J. Geophys. Res.* 115, A10225. doi:10.1029/2010JA015625

Erickson, G. M., and Wolf, R. A. (1980). Is steady convection possible in the Earth's magnetotail? *Geophys. Res. Lett.* 7, 897–900. doi:10.1029/GL007i011p00897

Ferrière, K. M., Zimmer, C., and Blanc, M. (2001). Quasi-interchange modes and interchange instability in rotating magnetospheres. *J. Geophys. Res.* 106 (A1), 327–343. doi:10.1029/2000JA000133

Hill, T. W. (1976). Interchange stability of a rapidly rotating magnetosphere. *Planet. Space Sci.* 24, 1151–1154. doi:10.1016/0032-0633(76)90152-5

Hill, T. W., Rymer, A. M., Burch, J. L., Crary, F. J., Young, D. T., Thomsen, M. F., et al. (2005). Evidence for rotationally driven plasma transport in Saturn's magnetosphere. *Geophys. Res. Lett.* 32, L14S10. doi:10.1029/2005GL022620

Johnson, J. R., and Wing, S. (2009). Northward interplanetary magnetic field plasma sheet entropies. *J. Geophys. Res.* 114, A00D08. doi:10.1029/2008JA014017

Kennelly, T. J., Leisner, J. S., Hospodarsky, G. B., and Gurnett, D. A. (2013). Ordering of injection events within Saturnian SLS longitude and local time. *J. Geophys. Res. Space Phys.* 118, 832–838. doi:10.1002/jgra.50152

Khurana, K. K., Arridge, C. S., Schwarzl, H., and Dougherty, M. K. (2006). A model of Saturn's magnetospheric field based on latest Cassini observations. *Eos Trans. AGU* 87 (36).

Krimigis, T., Mitchell, D. G., Hamilton, D. C., Livi, S., Dandouras, J., Jaskulek, S., et al. (2004). Magnetosphere imaging instrument (MIMI) on the Cassini mission to saturn/titan. *Space Sci. Rev.* 114, 233–329. doi:10.1007/s11214-004-1410-8

Lewis, G. R., Andre, N., Arridge, C. S., Coates, A. J., Gilbert, L. K., Linder, D. R., et al. (2008). Derivation of density and temperature from the Cassini-Huygens CAPS electron spectrometer. *Planet. Space Sci.* 56, 901–912. doi:10.1016/j.pss.2007.12.017

Liu, X., and Hill, T. W. (2012). Effects of finite plasma pressure on centrifugally driven convection in Saturn's inner magnetosphere. *J. Geophys. Res.* 117, A07216. doi:10.1029/2012JA017827

Liu, X., Hill, T. W., Wolf, R. A., Sazykin, S., Spiro, R. W., and Wu, H. (2010). Numerical simulation of plasma transport in Saturn's inner mag-netosphere using the Rice Convection Model. *J. Geophys. Res.* 115, A12254. doi:10.1029/2010JA015859

Long, M., Cao, X., Gu, X., Ni, B., Qu, S., Lou, Y., et al. (2023). Excitation of Saturnian ECH waves within remote plasma injections: Cassini observations. *Geophys. Res. Lett.* 50, e2022GL101969. doi:10.1029/2022GL101969

Ma, X., Delamere, P. A., and Otto, A. (2016). Plasma transport driven by the Rayleigh-Taylor instability. *J. Geophys. Res. Space Phys.* 121, 5260–5271. doi:10.1002/2015JA022122

Ma, X., Delamere, P. A., Thomsen, M. F., Otto, A., Neupane, B., Burkholder, B. L., et al. (2019). Flux tube entropy and specific entropy in Saturn's magnetosphere. *J. Geophys. Res. Space Phys.* 124, 1593–1611. doi:10.1029/2018JA026150

McIlwain, C. E. (1961). Coordinates for mapping the distribution of magnetically trapped particles. *J. Geophys. Res.* 66 (11), 3681–3691. doi:10.1029/JZ066i011p03681

Menietti, J. D., Santolik, O., Rymer, A. M., Hospodarsky, G. B., Persoon, A. M., Gurnett, D. A., et al. (2008). Analysis of plasma waves observed within local plasma injections seen in Saturn's magnetosphere. *J. Geophys. Res.* 113, A05213. doi:10.1029/2007JA012856

Menietti, J. D., Yoon, P. H., Písa, D., Ye, S.-Y., Santolík, O., Arridge, C. S., et al. (2016). Source region and growth analysis of narrowband *Z*-mode emission at Saturn. *J. Geophys. Res. Space Phys.* 121 (11), 929–1011. doi:10.1002/2016JA022913

Merkin, V. G., Panov, E. V., Sorathia, K., and Ukhorskiy, A. Y. (2019). Contribution of bursty bulk flows to the global dipolarization of the magnetotail during an isolated substorm. *J. Geophys. Res. Space Phys.* 124, 8647–8668. doi:10.1029/2019JA026872

Mitchell, D. G., Brandt, P. C., Carbary, J. F., Kurth, W. S., Krimigis, S. M., Paranicas, C., et al. (2015). "Injection, interchange, and reconnection," in *Magnetotails in the solar System*. Editors A. Keiling, C. M. Jackman, and P. A. Delamere (Hoboken, NJ: John Wiley and Sons, Inc). doi:10.1002/9781118842324.ch19

Mitchell, D. G., Krimigis, S., Paranicas, C., Brandt, P., Carbary, J., Roelof, E., et al. (2009). Recurrent energization of plasma in the midnight-to-dawn quadrant of Saturn's magnetosphere, and its relationship to auroral UV and radio emissions. *Planet. Space Sci.* 57, 1732–1742. doi:10.1016/j.pss.2009.04.002

Neupane, B. R., Delamere, P. A., Ma, X., Ng, C.-S., Burkholder, B., and Damiano, P. (2021). On the nature of turbulent heating and radial transport in Saturn's magnetosphere. *J. Geophys. Res. Space Phys.* 126, e2020JA027986. doi:10.1029/2020JA027986

Panov, E. V., Kubyshkina, M. V., Nakamura, R., Baumjohann, W., Angelopoulos, V., Sergeev, V. A., et al. (2013). Oscillatory flow braking in the magnetotail: THEMIS statistics. *Geophys. Res. Lett.* 40, 2505–2510. doi:10.1002/grl.50407

Paranicas, C., Thomsen, M. F., Kollmann, P., Azari, A. R., Bader, A., Badman, S. V., et al. (2020). Inflow speed analysis of interchange injections in Saturn's magnetosphere. *J. Geophys. Res. Space Phys.* 125, e2020JA028299. doi:10.1029/2020JA028299

Pontius, D. H., and Wolf, R. A. (1990). Transient flux tubes in the terrestrial magnetosphere. *Geophys. Res. Lett.* 17 (1), 49–52. doi:10.1029/gl017i001p00049

Rymer, A. M., Mauk, B., Hill, T., André, N., Mitchell, D., Paranicas, C., et al. (2009). Cassini evidence for rapid interchange transport at Saturn. *Planet. Space Sci.* 57, 1779–1784. doi:10.1016/j.pss.2009.04.010

Saur, J. (2004). Turbulent heating of Jupiter's middle magnetosphere. *Astrophysical J. Lett.* 602, L137–L140. doi:10.1086/382588

Sittler, E. C., André, N., Blanc, M., Burger, M., Johnson, R. E., Coates, A., et al. (2008). Ion neutral sources and sinks within Saturn's inner magnetosphere: Cassini results. *Planet. Space Sci.* 54 (1). doi:10.1016/j.pss.2007.06.006

Southwood, D. J., and Kivelson, M. G. (1987). Magnetospheric interchange instability. *J. Geophys. Res.* 92 (A1), 109–116. doi:10.1029/JA092iA01p00109

Stauffer, B. H., Delamere, P. A., Ma, X., Neupane, B. R., and Burkholder, B. L. (2019). Hybrid simulations of magnetodisc transport driven by the Rayleigh-taylor instability. *J. Geophys. Res. Space Phys.* 124 (7), 5107–5120. doi:10.1029/2018JA026420

Thomsen, M. F. (2013). Saturn's magnetospheric dynamics. *Geophys. Res. Lett.* 40, 5337–5344. doi:10.1002/2013GL057967

Thomsen, M. F., and Coates, A. J. (2019). Saturn's plasmapause: signature of magnetospheric dynamics. *J. Geophys. Res. Space Phys.* 124, 8804–8813. doi:10.1029/2019JA027075

Thomsen, M. F., Reisenfeld, D. B., Delapp, D. M., Tokar, R. L., Young, D. T., Crary, F. J., et al. (2010). Survey of ion plasma parameters in Saturn's magnetosphere. *J. Geophys. Res.* 115, A10220. doi:10.1029/2010JA015267

Thomsen, M. F., Coates, A. J., Roussos, E., Wilson, R. J., Hansen, K. C., Lewis, G. R., et al. (2016). Suprathermal electron penetration into the inner magnetosphere of Saturn. *J. Geophys. Res. Space Phy.* 121, 5436–5448. doi:10.1002/2016JA022692

Thomsen, M. F., Reisenfeld, D. B., Wilson, R. J., Andriopoulou, M., Crary, F. J., Hospodarsky, G. B., et al. (2014). Ion composition in interchange injection events in Saturn's magnetosphere. *J. Geophys. Res. Space Phys.* 119, 9761–9772. doi:10.1002/2014JA020489

Thomsen, M. F., Wilson, R. J., Tokar, R. L., Reisenfeld, D. B., and Jackman, C. M. (2013). Cassini/CAPS observations of duskside tail dynamics at Saturn. *J. Geophys. Res. Space Phys.* 118, 5767–5781. doi:10.1002/jgra.50552

Wing, S., Brandt, P. C., Mitchell, D. G., Johnson, J. R., Kurth, W. S., and Menietti, J. D. (2020). Periodic narrowband radio wave emissions and inward plasma transport at saturn's magnetosphere. *Ap J.* 159, 249. doi:10.3847/1538-3881/ab818d

Wing, S., and Johnson, J. R. (2009). Substorm entropies. *J. Geophys. Res.* 114, A00D07. doi:10.1029/2008JA013989

Wing, S., and Johnson, J. R. (2010). Introduction to special section on entropy properties and constraints related to space plasma transport. *J. Geophys. Res.* 115, A00D00. doi:10.1029/2009JA014911

Wing, S., Johnson, J. R., Chaston, C. C., Echim, M., Escoubet, C. P., Lavraud, B., et al. (2014). Review of solar wind entry into and transport within the plasma sheet. *Space Sci. Rev.* 184, 33–86. doi:10.1007/s11214-014-0108-9

Wing, S., Thomsen, M. F., Johnson, J. R., Mitchell, D. G., Allen, R. C., Ma, X., et al. (2022). The roles of flux tube entropy and effective gravity in the inward plasma transport at Saturn. *Astrophysical J.* 937 (1), 42. doi:10.3847/1538-4357/ac85b2

Wolf, R. A., Chen, C. X., and Toffoletto, F. R. (2012). Thin filament simulations for Earth's plasma sheet: interchange oscillations. *J. Geophys. Res.* 117, A02215. doi:10.1029/2011JA016971

Yang, J., Wolf, R., Toffoletto, F., Sazykin, S., Wang, W., and Cui, J. (2019). The inertialized rice convection model. *J. Geophys. Res. Space Phys.* 124, 10294–10317. doi:10.1029/2019JA026811

Yin, Z.-F., Sun, Y.-X., Zhou, X.-Z., Pan, D.-X., Yao, Z.-H., Yue, C., et al. (2023). Trapped and leaking energetic particles in injection flux tubes of Saturn's magnetosphere. *Geophys. Res. Lett.* 50, e2023GL105687. doi:10.1029/2023GL105687

Young, S., Berthelier, J. J., Blanc, M., Burch, J. L., Coates, A. J., Goldstein, R., et al. (2004). Cassini plasma spectrometer investigation. *Space Sci. Rev.* 114, 1–112. doi:10.1007/978-1-4020-2774-1_1

frontiers | Frontiers in Astronomy and Space Sciences

TYPE Mini Review
PUBLISHED 17 December 2024
DOI 10.3389/fspas.2024.1523977

Check for updates

OPEN ACCESS

EDITED BY
Cristina Puzzarini,
University of Bologna, Italy

REVIEWED BY
Stefano Pantaleone,
University of Turin, Italy
Yuki Kimura,
Hokkaido University, Japan

*CORRESPONDENCE
Stefan T. Bromley,
s.bromley@ub.edu

RECEIVED 06 November 2024
ACCEPTED 25 November 2024
PUBLISHED 17 December 2024

CITATION
Bromley ST (2024) Nanosilicates and molecular silicate dust species: properties and observational prospects .
Front. Astron. Space Sci. 11:1523977.
doi: 10.3389/fspas.2024.1523977

COPYRIGHT
© 2024 Bromley. This is an open-access article distributed under the terms of the Creative Commons Attribution License (CC BY). The use, distribution or reproduction in other forums is permitted, provided the original author(s) and the copyright owner(s) are credited and that the original publication in this journal is cited, in accordance with accepted academic practice. No use, distribution or reproduction is permitted which does not comply with these terms.

Nanosilicates and molecular silicate dust species: properties and observational prospects

Stefan T. Bromley[1,2]*

[1]Departament de Ciència de Materials i Química Física and Institut de Química Teòrica i Computacional (IQTCUB), Universitat de Barcelona, Barcelona, Spain, [2]Institució Catalana de Recerca i Estudis Avançats (ICREA), Barcelona, Spain

Silicate dust is found in a wide range of astrophysical environments. Nucleation and growth of silicate dust grains in circumstellar environments likely involves species with diameters ranging from <1 nm (molecular silicates) to a few nanometers (nanosilicates). When fully formed silicate grains with sizes ~0.1 μm enter the interstellar medium, supernovae shockwaves cause collision-induced shattering which is predicted to redistribute a significant proportion of the silicate dust mass into a huge number of nanosilicates. This presumed population has thus far not been unambiguously confirmed by observation but is one of the main candidates for causing the anomalous microwave emission. By virtue of their extreme small size, nanosilicates and molecular silicates could exhibit significantly different properties to larger silicate grains, which could be of astrochemical and astrophysical importance. Herein, we briefly review the properties of these ultrasmall silicate dust species with a focus on insights arising from bottom-up atomistic computational modelling. Finally, we highlight how such modelling also has the unique potential to predict observationally verifiable spectral features of nanosilicates that may be detectable using the James Webb Space Telescope.

KEYWORDS

cosmic nanosilicates, interstellar dust, ultrasmall grains, circumstellar nucleation, astrophysical dust processing, IR spectra, microwave emission

Introduction

Cosmic dust, consisting mainly of sub-micron sized grains, permeates the interstellar medium (ISM) (Draine, 2003). Although contributing to only 1% of the mass of the ISM, dust has a disproportionately high impact, both astrophysically (e.g., shielding high energy radiation) and astrochemically (e.g., providing adsorption sites for chemicial reactions) (van Dishoeck, 2014). The majority of ISM dust grains are formed from silicates (Henning, 2010), which encompass a wide class of solids formed from the interactions between anions based on silicon and oxygen (e.g., SiO_3^{2-}, SiO_4^{4-}) and cations. In astronomical silicates, the cations are mainly magnesium (Mg^{2+}) with a much smaller proportion of iron (Fe^{2+}) (Min et al., 2007). It is usually assumed that most silicate dust has stoichiometric pyroxene or olivine chemical compositions, for which $MgSiO_3$ (enstatite) and Mg_2SiO_4 (forsterite) are the corresponding Mg-based examples. Silicates with intermediate compositions have also been proposed (Fogerty et al., 2016). Observations suggest that the number of dust grains (n_g) in the ISM with respect to their diameter (d) approximately follows an inverse power relationship ($n_g \propto d^{-3.5}$) (Mathis et al., 1977), which massively favours higher populations

of smaller grains. Such a distribution can be rationalised by models which redistribute mass from larger grains into smaller grains by collisional shattering, leading to predictions that ~5% of the silicate dust mass in the ISM should end up in small nanosilicate grains with approximate sizes $d \leq 6$ nm (Jones et al., 1996). Considering infrared (IR) emission observations of the ISM, it has been estimated that small nanosilicates ($d \leq 3$ nm) could account for up to 10% of all silicon in the dust population (Li and Draine, 2001). Even if accounting for only a relatively small fraction of the total silicate dust grain mass in the ISM, nanosilicates could thus potentially dominate dust populations by number. Speculatively extrapolating such predictions would lead to the possibility that nanosilicates could be the most common class of solid object in the Universe. Herein, we focus on the smallest silicate dust species, ranging from molecular silicates containing a few atoms to nanosilicates, with approximate diameters ranging between 1–10 nm. When the dimensions of oxide materials are reduced to the nanoscale new structures and properties can emerge (Bromley et al., 2009). Compared to larger dust grains, nanosilicates are thus likely to have novel and distinct astrophysical and astrochemical impacts. Herein, we provide an overview what is currently known about molecular silicates and nanosilicates from an atomistic level, and how such knowledge can inform us on the prospects for their observational detection.

Due the extreme small sizes of nanoscale grain species it is often extremely difficult to characterise them experimentally. Here, atomistic level computational modelling can play an essential role in providing realistic nanoscale structural models and atomic/electronic level insights, which would be otherwise unobtainable (Bromley et al., 2014). Atomistically detailed nano-models can subsequently be used to calculate properties (e.g., atomic and electronic structures, chemical reactivity, spectroscopy), which can be compared with, and used together with, any available experimental/observational data. Even when the latter is unavailable, such bottom-up computational modelling can provide detailed predictions and helpful insights which can help to guide future experimental/observational research. In Figure 1 we show a range of ultrasmall silicate species for which atomistic computational modelling has provided a wealth of astronomical relevant information. Below we summarise results from selected studies on molecular silicates (<1 nm diameter) and nanosilicates with respect to: i) nucleation, ii) energetic processing, iii) chemical interactions and iv) spectroscopic signatures.

Nucleation and molecular silicates

Most silicate dust is thought to originate in the circumstellar envelopes of oxygen-rich M-type asymptotic giant branch (AGB) stars. Here, the excess oxygen strongly binds with abundant silicon atoms, leading to the formation of silicon monoxide (SiO) molecules (González Delgado et al., 2003). The formation of silicates should involve several chemical processes which enable the incorporation of Mg (and Fe) and the increase of a 1:1 silicon-to-oxygen stoichiometry in SiO monomers to that found in silicates (e.g., $MgSiO_3$, Mg_2SiO_4). These required chemical transitions suggest that silicate nucleation pathways likely involve complex homogeneous molecular processes in the gas phase and heterogeneous processes on existing grains. Based on typical elemental abundances and physical conditions in a circumstellar silicate dust condensation zone (1,000–1,200 K, 0.1–0.001 Pa), the available chemical pathways for silicates are likely dictated by the abundance of stable oxygen-containing molecules (H_2O, OH and SiO), while Mg is stable in atomic form (Gail and Sedlmayr, 1986; Gail and Sedlmayr, 1998). Systematic searches using accurate computer modelling can reveal molecular silicate species resulting from the chemical reactions of these components which are stable under such conditions (Goumans and Bromley, 2012). Using this data, a general alternating oxidation/metal-incorporation silicate nucleation scheme has been proposed and validated in detailed kinetic nucleation theory models of dust formation in supernovae (Sarangi and Cherchneff, 2013) and AGB stars (Gobrecht et al., 2016), see Figure 2. At the high temperatures in circumstellar environments, the initial production of small silicon oxide molecules [e.g., $(SiO)_2$, Si_2O_3] is most difficult and is a bottleneck to subsequent nucleation (Bromley et al., 2016; Andersson et al., 2023). It is thus likely that the very first species that initiate circumstellar silicate nucleation are, as yet unidentified, extremely stable refractory seeds (e.g., Ti-based (Jeong et al., 2003; Goumans and Bromley, 2013; Plane, 2013) or Al-based (Gobrecht et al., 2022; Gobrecht et al., 2023) oxide species). We note that this does not rule out homogeneous SiO nucleation being involved in silicate dust formation in lower temperature environments [e.g., cold dense clouds (Krasnokutski et al., 2014), around Mira-type variable stars (Gail et al., 2016)].

At the end of their growth phase around evolved stars, silicate dust grains are thought to attain a typical radius of ~0.1 μm before they enter the ISM. The morphology of these grains is unknown but will depend on the efficiency of nucleation and growth, and the availability of monomeric species. For example, the highly inefficient monomeric-based growth of SiO_x grains can leads to a high number of nanosized particles, which can condense into larger fractal aggregates (Kimura et al., 2022). For silicates, laboratory studies show that dust formation often also proceeds via primary particles of a few nanometres in radius (i.e., nanosilicates), followed by rapid growth through agglomeration producing a smaller number of large fractal-like particles (Saunders and Plane, 2006). A similar nanosilicate aggregation process could potentially also play a role in dust (re)formation in the ISM (Rimola and Bromley, 2021). Relative to more spherical compact grains, such nanosilicate aggregates (see Figure 1) possess high surface areas and porosities which could have astrochemical implications (Potapov et al., 2024).

Energetic processing of silicate dust

Newly formed silicate dust from evolved AGB stars is thought to be Mg-rich, with an olivinic chemical composition (Dorschner et al., 1995) and with ~10% being crystalline (Molster et al., 2002). From analysis of IR spectra, the extent of crystallinity of silicates in the ISM is estimated to be between 0%–5% by mass (Kemper et al., 2004; Li et al., 2007), suggesting that the original crystalline fraction of the grain population is amorphized in the ISM. Laboratory experiments have shown that amorphisation of silicates could

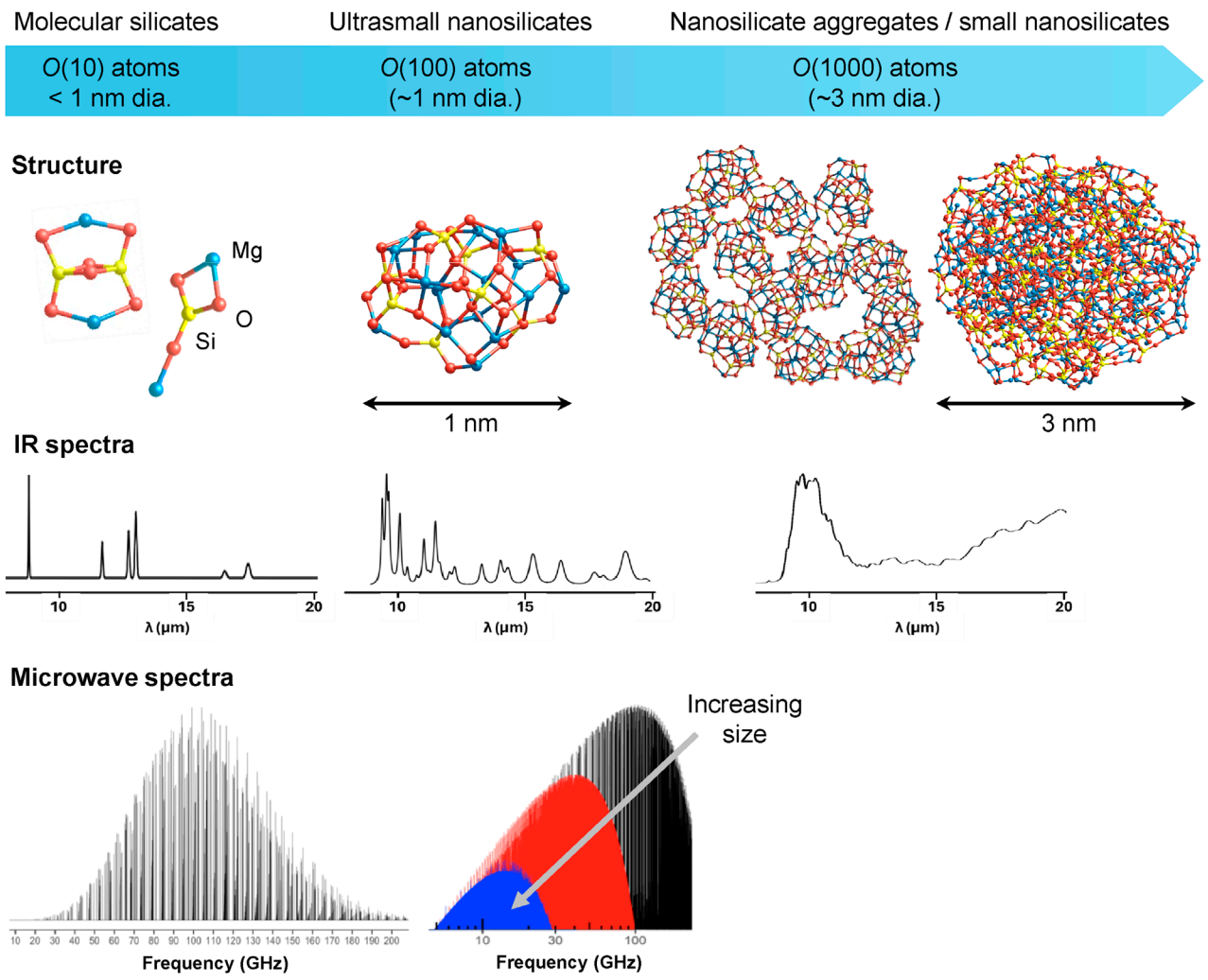

FIGURE 1
Examples of small silicate dust species studied with atomistic computational modelling ranging from molecular silicates containing of the order 10 atoms [i.e., *O* (10)] to small nanosilicates containing *O* (1,000) atoms. Representative structures for silicate species and their characteristic predicted IR spectra are approximately positioned with respect to the three corresponding silicate size classes (blue bar). Calculated microwave emission spectra are shown for a molecular silicate (left) and for three different silicate sizes (right): black (5 atoms), red (21 atoms), blue (50 atoms). All spectra are shown with intensity in arbitrary units.

result from impacts from high velocity ions in supernovae shocks and heavy ions in cosmic rays (Demyk et al., 2001; Jäger et al., 2003a; Bringa et al., 2007). However, it is often overlooked that, below a certain size, nanosilicate grains are inherently not able to maintain long range crystalline order, thus being effectively amorphous. Energetically stable ultrasmall nanosilicates (≤1 nm diameter) of pyroxene and olivine composition have been confirmed to be inherently non-crystalline by accurate quantum chemical calculations (Maciá Escatller et al., 2019). Computational modelling of larger nanosilicate grains up to approximately 5 nm diameter, still show that amorphous structures obtained by thermal annealing are more energetically stable than crystalline nanograins (Zamirri et al., 2019). Aggregates formed from nanosilicate building blocks will thus also tend to be amorphous. Indications of crystallinity have been inferred in laboratory produced silicate grains with diameters of a few 10 s of nm, indicating a possible lower grain size for maintaining crystalline order (Ishizuka et al., 2015). Generally, the fact that crystallinity is only possible in larger silicate grains should be considered when interpreting observed spectra.

In the diffuse ISM, dust grains are subject to energetic processing by supernovae shockwaves which lead to shattering in grain-grain collisions. Shattering leads to a redistribution of mass from a smaller number of larger grains into a larger number of smaller grains tending to lead to an abundance of nanosized grains (Jones et al., 1996). For porous nanosilicate aggregates, such processing would likely lead to disaggregation. Smaller grains are also more resilient than larger grains to shattering which could help them persist in the harsh conditions of the diffuse ISM (Jones et al., 1994). Shockwave-induced collisions and other processes can also lead to vaporization of grain mass into the gas phase (i.e., dust destruction). Models of grain processing typically predict that the estimated dust destruction rate in the ISM is significantly more than the stardust production rate (Slavin et al., 2015). This situation is clearly at odds with the observed

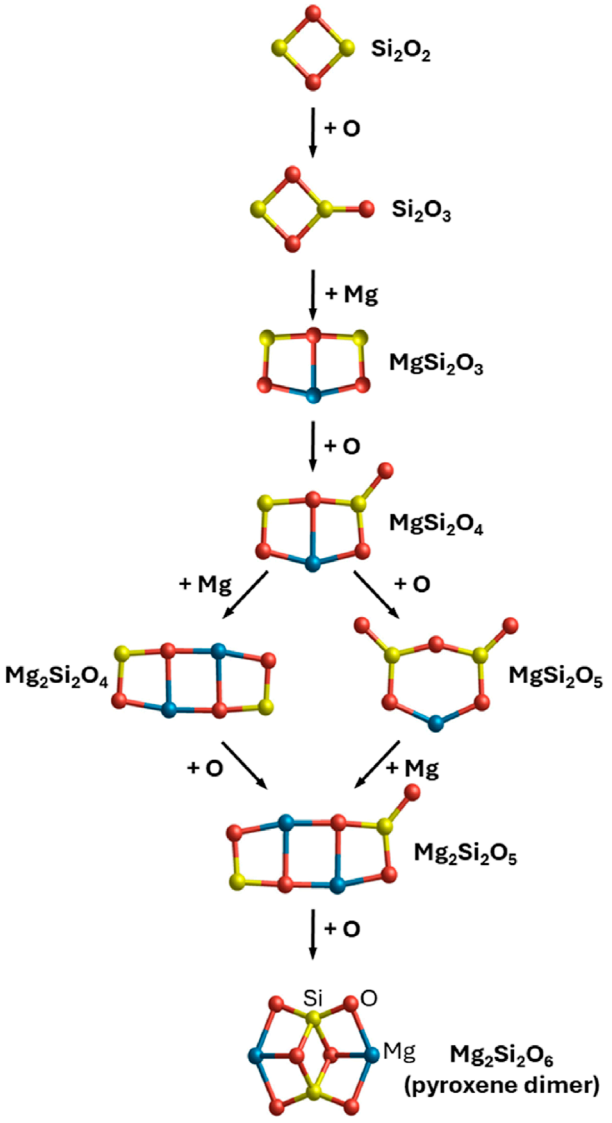

FIGURE 2
Possible thermodynamically viable initial steps in silicate dust nucleation starting from the SiO dimer (i.e., Si_2O_2) up to the pyroxene dimer (i.e., $Mg_2Si_2O_6$) molecular silicate. Steps show incorporation of Mg or O (via H_2O or OH) with respect to the previous step. The lowest energy structure is shown for all molecular species. See Goumans and Bromley (2012) for more details.

abundance of dust in the ISM. The discrepancy probably reflects the large uncertainties in our estimates of dust lifetimes, based on our current understanding of dust formation/destruction (Jones and Nuth, 2011).

Through their interaction with the strong ultraviolet (UV) radiation field in the ISM, dust grains with sizes of only a few nanometres are also susceptible to sporadic temperature spikes (Duley, 1973). Stochastically heated nanosilicate grains with 10 nm diameters are expected to exhibit temperature fluctuations up to 20–40 K, which is predicted to have a significant impact on their role in astrochemical processes (Cuppen et al., 2006; Chen et al., 2018). For ultrasmall nanosilicates possessing only a few tens of atoms (≤1 nm diameter) the fluctuations in temperature from stochastic heating has been estimated to be up to ~1000 K (Draine and Li, 2001), with, as yet, unknown consequences for astrochemistry. We note that molecular silicates and ultrasmall silicates are found to be surprisingly structurally stable in molecular dynamics simulations at such elevated temperatures where they exhibit only small conformational changes (Mariñoso Guiu et al., 2021a; Oueslati et al., 2015). The temperature and emissivity of stochastically heated nanograins depends on the rates of UV energy absorption and subsequent IR emission, which, in turn is intimately linked to their specific heat capacity. Typical estimates of stochastic heating employ empirical fits to bulk silicate heat capacities (Draine and Li, 2001; Camps et al., 2015). The heat capacity of a system depends on the range of available vibrational modes, which is dramatically affected by size constraints in nanosized solids. Accurate quantum chemical calculation of vibrational modes in ultrasmall nanosilcates have shown that empirically fitted models tend to underestimate the stochastic heating of small nanosilicates by tens of Kelvin (Mariñoso Guiu and Bromley, 2022). This could imply that ultrasmall nanosilicates could be easier to detect by their IR emission than previously expected.

The strong UV field in the ISM can also lead to ionisation of small dust grains. Due to the dominance of photoelectric electron ejection over recombination in very small grains in the ISM, small nanosilicates are also likely to be positively ionized by their interaction with high energy UV photons (Weingartner and Draine, 2001). UV-induced charging of small grains has been suggested as a way to enhancing their role as seed species for dust (re)nucleation in the ISM (Zhukovska et al., 2016). Cationic molecular silicates have also been produced in cluster beam experiments and their structures and properties elucidated by quantum chemical calculations (Mariñoso Guiu et al., 2022). These studies also suggest that ionised molecular silicates could act as sinks for oxygen depletion, potentially contributing to the unresolved problem of the "missing" oxygen in the ISM (Whittet, 2010).

Chemical processing of silicate dust

Processing from ion irradiation (e.g., protons, He^+) in supernovae shocks also induces chemical tranformations in silicate dust grains in the ISM. From early laboratory studies of the effect of the solar wind on lunar surface silicate material, two important intertwined chemical processes were established to be the result of proton-iradiation: (i) the formation of hydroxyls (Zeller et al., 1996), and (ii) the depletion of magnesium and oxygen through preferential sputtering (Keller and McKay, 1997). Confirmation of these results has come from more recent experiments (Demyk et al., 2001; Jäger et al., 2003b; Bringa et al., 2007) and from analysis of interplanetary dust (Bradley, 1994). Hydroxylated silicate grains formed by such processing could also be relevant as potential reservoirs of water during the formation of planetary systems (Djouadi et al., 2011).

Starting from Mg-rich olivine nanograins, sputtering of magnesium and oxygen would tend to lead to a transformation towards a pyroxene-like chemical composition. Elevated levels of pyroxene (relative to the initial dominance of olivine) is consistent with estimates of the amorphous pyroxene fraction of the grain

population in the ISM (Kemper et al., 2004), and with the pyroxene-rich environments of protostars (Demyk et al., 1999). Combining chemical processing with energetic processing (i.e., shockwave-induced shattering and ionisation), the extreme end result would be molecular pyroxene-based cations (e.g., $MgSiO_3^+$). Higher proton-induced sputtering could potentially lead to extreme reduction of Mg^{2+} and hydroxyl formation from H^+ implantation, leading to $(Si_xO_yH_z)^+$ species. By approximately mimicking silicate dust grain processing occurring in the diffuse ISM by ablation/cooling of a mixed Si/Mg source in the presence of O_2, clusters based on discrete ionized pyroxene monomers ($MgSiO_3^+$) were readily formed (Mariñoso Guiu et al., 2022). Similar experiments, using a pure Si source and a small amount of water vapour, led to the production of small $(Si_xO_yH_z)^+$ clusters with one or two -OH groups (de Donato et al., 2024). This indicates that such ionised molecular silicate species could also be a common result of energetic and chemical processing in the ISM. More speculatively, such experiments could also suggest that molecular silicate formation from hot gas phase atoms could directly compete with dust destruction during energetic processing.

Quantum chemical calculations have also shown that formation of Si-OH groups is highly energetically favourable on pyroxene nanosilicates (Goumans and Bromley, 2011) and $(SiO_2)_N$ nanoclusters (Jelfs et al., 2013; Maciá Escatller et al., 2017). Such hydroxylation is likely to be a precursor stage to the subsequent formation of water ice mantles. However, UV irradiation is known to reduce hydroxylation of silica surfaces (Imai et al., 1996) and lead to water photodesorption. As such, high degrees of nanosilicate hydroxylation and water ice mantle growth are only likely to occur in interstellar clouds that are opaque enough to shield the intense UV field of the ISM. Bare nanosilicates (i.e., without mantles) been predicted to be able to promote dissociation and/or formation of H_2 molecules (Kerkeni and Bromley, 2013). Other theoretical studies have shown that such chemical processes can be significantly affected by the low degree of hydroxylation likely to be possible in the diffuse/translucent ISM (Kerkeni et al., 2017; Kerkeni et al., 2019).

Spectroscopic signatures of nanosilicates

Microwave emission

The best current observational evidence for the presence of nanosilicates is from their proposed role as the source of the anomalous microwave emission (AME) (Hensley and Draine, 2017; Hoang et al., 2016). The AME is a broad foreground ISM feature centred at around 30 GHz which is most likely to originate from a population of fast spinning nanosized grains with a sufficiently large dipoles (Ali-Haïmoud et al., 2018). Quantum chemical modelling has shown that nanosilicates (unlike most carbonaceous species) have high inherent dipoles. As such, it would only require 1% of the available silicon dust mass to be in ultrasmall nanosilicates to make them a viable source of the AME (Maciá Escatller and Bromley, 2020). Similar studies have shown that this results still holds if we consider weak hydroxylation of the nanosilicates (Mariñoso Guiu et al., 2021b). The lack of distinct features in AME spectra means that a definite assignment to nanosilicates is difficult. However, for small molecular silicates with specific structures and high dipoles, the microwave emission spectrum would be more detailed and potentially assignable to specific species (e.g., pyroxene monomers) (Maciá Escatller and Bromley, 2020; Valencia et al., 2020). See Figure 1 for a comparison of microwave emission spectra expected for small molecular silicates and ultrasmall nanosilicates.

IR spectra

Interpretations of silicate dust IR observations typically employ laboratory-based measurements of bulk silicate samples. Such measurements confirm the typically-observed IR spectra of silicate dust characterised by two broad peaks at 9.8 μm (Si-O stretching mode) and 18–20 μm (O-Si-O bending mode) (Jäger et al., 2003b; Henning, 2010). Experimental IR spectra of laboratory produced silicate grains with diameters of a few 10 s of nm also show these characteristic modes (Ishizuka et al., 2015). For much smaller molecular silicates, IR spectra can also be obtained using cluster beam experiments. Here, the spectra exhibit sharp individual peaks which allow for accurate assignments of structure and composition via quantum chemical calculations. Clearly, between these two extremes there should be a size-dependent transition of the IR spectra of silicate dust.

Calculations suggest that the emergence of bulk-like double-peaked IR spectra should emerge for non-porous nanosilicate grains with diameters ≥5 nm (Zamirri et al., 2019), or upon aggregation of ultrasmall nanosilicates (Rimola and Bromley, 2021). This implies that the IR spectra of smaller nanosilicates should have specific non-bulk-like IR spectra, as explicitly confirmed by accurate quantum chemical modelling for ultrasmall nanosilicates. A summary of the size-dependency of IR spectra of small silicates is shown in Figure 1. As populations of ultrasmall silicates are expected to be extremely numerous, their cumulative IR spectra may be observationally discernible from the dominant IR signal of larger silicates. We note that the highly sensitive spectrometers of the Mid-IR instrument (MIRI) on the James Webb Space telescope (JWST) are well suited to probe the signature wavelength range for silicates (i.e., approximately between 8–20 μm). Using accurately calculated individual IR spectra of 10 s of ultrasmall nanosilicates, characteristic IR spectra of populations of ultrasmall nanosilicates with pyroxene and olivine compositions have been produced. Assuming that the silicate dust population has 3%–10% of its mass of Si in ultrasmall nanosilicates, several small but distinct influences on the bulk-like silicate IR spectra are predicted (e.g., increased intensity slightly above and below 9.8 μm) (Zeegers et al., 2023). In principle, such subtle effects should be detectable with JWST observations using MIRI, which should thus be able to confirm and/or place limits on the nanosilicate content of the diffuse ISM.

Summary

In summary, we highlight the importance of molecular silicates and nanosilicates in the formation and processing of larger silicate

dust grains. It is expected that these ultrasmall species should be prevalent in the ISM where their astrochemical influence could be highly significant. While currently lacking direct observational conformation of nanosilicates, we show the role that atomistic bottom-up computational modelling, often together with laboratory experiments, can play in providing detailed insights into these species. Looking to the future, we expect that the combination of computational modelling and detailed observations will be indispensable for confirming the presence and assessing the abundance of nanosilicates in the ISM and other astrophysical environments.

Author contributions

SB: Conceptualization, Funding acquisition, Writing–original draft, Writing–review and editing.

Funding

The author(s) declare that financial support was received for the research, authorship, and/or publication of this article. Financial support from the Spanish Ministerio de Ciencia e Innovación and Agencia Estatal de Investigación (AEI) MCIN/AEI/10.13039/501100011033 through projects PID2021-127957NB-I00 and TED2021-132550B-C21 and CEX2021-001202-M (Maria de Maeztu program for Spanish Structures of Excellence) and from the Generalitat de Catalunya through project grant 2021SGR00354 are all acknowledged.

Conflict of interest

The author declares that the research was conducted in the absence of any commercial or financial relationships that could be construed as a potential conflict of interest.

The author(s) declared that they were an editorial board member of Frontiers, at the time of submission. This had no impact on the peer review process and the final decision.

Publisher's note

All claims expressed in this article are solely those of the authors and do not necessarily represent those of their affiliated organizations, or those of the publisher, the editors and the reviewers. Any product that may be evaluated in this article, or claim that may be made by its manufacturer, is not guaranteed or endorsed by the publisher.

References

Ali-Haïmoud, Y., Barr, A., Battistelli, E. S., Bell, A., Bernstein, L., Casassus, S., et al. (2018). The state-of-play of anomalous microwave emission (AME) research, new astron. *New.Astron. Rev* 80, 1–28. doi:10.1016/j.newar.2018.02.001

Andersson, S., Gobrecht, D., and Valero, R. (2023). Mechanisms of SiO oxidation: implications for dust formation. *Front. Astron. Space Sci.* 10, 1135156. doi:10.3389/fspas.2023.1135156

Bradley, J. P. (1994). Chemically anomalous, preaccretionally irradiated grains in interplanetary dust from comets. *Science* 265, 925–929. doi:10.1126/science.265.5174.925

Bringa, E. M., Kucheyev, S. O., Loeffler, R. A., Baragiola, R. A., Tielens, A., Da, Z. R., et al. (2007). Energetic processing of interstellar silicate grains by cosmic rays. *Astrophys. J.* 662, 372–378. doi:10.1086/517865

Bromley, S. T., Gómez Martín, J. C., and Plane, J. C. (2016). Under what conditions does $(SiO)_N$ nucleation occur? A bottom-up kinetic modelling evaluation. *Phys. Chem. Chem. Phys.* 18, 26913–26922. doi:10.1039/c6cp03629e

Bromley, S. T., Goumans, T. P. M., Herbst, E., Jones, A. P., and Slater, B. (2014). Challenges in modelling the reaction chemistry of interstellar dust. *Phys. Chem. Chem. Phys.* 16, 18623. doi:10.1039/c4cp00774c

Bromley, S. T., Moreira, I., de, P. R., Neyman, K. M., and Illas, F. (2009). Approaching nanoscale oxides: models and theoretical methods. *Chem. Soc. Rev.* 38, 2657–2670. doi:10.1039/b806400h

Camps, P., Misselt, K., Bianchi, S., Lunttila, T., Pinte, C., Natale, G., et al. (2015). Benchmarking the calculation of stochastic heating and emissivity of dust grains in the context of radiative transfer simulations. *Astron. Astrophys.* 580, A87. doi:10.1051/0004-6361/201525998

Chen, L.-F., Chang, Q., and Xi, H.-W. (2018). Effect of stochastic grain heating on cold dense clouds chemistry. *Mon. Not. R. Astron. Soc.* 479, 2988–3001. doi:10.1093/mnras/sty1525

Cuppen, H. M., Morata, O., and Herbst, E. (2006). Monte Carlo simulations of H_2 formation on stochastically heated grains. *Mon. Not. R. Astron. Soc.* 367, 1757–1765. doi:10.1111/j.1365-2966.2006.10079.x

de Donato, A. A., Ghejan, B.-A., Bakker, J. M., Bernhardt, T. M., Bromley, S. T., and Lang, S. M. (2024). Gas-phase production of hydroxylated silicon oxide cluster cations: structure, infrared spectroscopy, and astronomical relevance. *ACS Earth Space Chem.* 8, 1154–1164. doi:10.1021/acsearthspacechem.3c00346

Demyk, K., Carrez, Ph., Leroux, H., Cordier, P., Jones, A. P., Borg, J., et al. (2001). Structural and chemical alteration of crystalline olivine under low energy He+ irradiation. *Astron. Astrophys.* 368, L38–L41. doi:10.1051/0004-6361:20010208

Demyk, K., Jones, A. P., Dartois, E., Cox, P., and d´Hendecourt, L. (1999). The chemical composition of the silicate dust around RAFGL7009S and IRAS 19110+1045 Astron. *Astrophys.* 349, 267–275.

Djouadi, Z., Robert, F., Le Sergeant d´Hendecourt, L., Mostefaoui, S., Leroux, H., Jones, A. P., et al. (2011). Hydroxyl radical production and storage in analogues of amorphous interstellar silicates: a possible "wet" accretion phase for inner telluric planets. *Astron. Astrophys.* 531, A96. doi:10.1051/0004-6361/201116722

Dorschner, J., Begemann, B., Henning, T., Jäger, C., and Mutschke, H. (1995). Steps toward interstellar silicate mineralogy. II. Study of Mg-Fe-silicate glasses of variable composition. *Astron. Astrophys.* 300, 503–520.

Draine, B. T. (2003). Interstellar dust grains. *Annu. Rev. Astron. Astrophys.* 41, 241–289. doi:10.1146/annurev.astro.41.011802.094840

Draine, B. T., and Li, A. (2001). Infrared emission from interstellar dust. I. Stochastic heating of small grains. *Astrophys. J.* 551, 807–824. doi:10.1086/320227

Duley, W. W. (1973). Fluctuations in interstellar grain temperatures. *Astrophys. Space Sci.* 23, 43–50. doi:10.1007/bf00647650

Fogerty, S., Forrest, W., Watson, D. M., Sargent, B. A., and Koch, I. (2016). Silicate composition of the interstellar medium. *Astrophys. J.* 830, 71. doi:10.3847/0004-637x/830/2/71

Gail, H.-P., Scholz, M., and Pucci, A. (2016). Silicate condensation in Mira variables. *Astron. Astrophys. J.* 591, A17. doi:10.1051/0004-6361/201628113

Gail, H. P., and Sedlmayr, E. (1986). The primary condensation process for dust around late M-type stars. *Astron. Astrophys.* 166, 225–236.

Gail, H. P., and Sedlmayr, E. (1998). Inorganic dust formation in astrophysical environments. *Faraday Discuss.* 109, 303–319. doi:10.1039/a709290c

Gobrecht, D., Cherchneff, I., Sarangi, A., Plane, J. M. C., and Bromley, S. T. (2016). Dust formation in the oxygen-rich AGB star Ik Tauri. *Astron. Astrophys.* 585, A6. doi:10.1051/0004-6361/201425363

Gobrecht, D., Hashemi, S. R., Plane, J. M. C., Bromley, S. T., Nyman, G., and Decin, L. (2023). Bottom-up dust nucleation theory in oxygen-rich evolved stars II. Magnesium and calcium aluminate clusters. *Astron. Astrophys.* 680, A18. doi:10.1051/0004-6361/202347546

Gobrecht, D., Plane, J. M. C., Bromley, S. T., Decin, L., Cristallo, S., and Sekaran, S. (2022). Bottom-up dust nucleation theory in oxygen-rich evolved stars I. Aluminium oxide clusters. *Astron. Astrophys.* 658, A167. doi:10.1051/0004-6361/202141976

González Delgado, D., Olofsson, H., Kerschbaum, F., Schöier, F. L., Lindqvist, M., and Groenewegen, M. A. T. (2003). "Thermal" SiO radio line emission towards M-type AGB stars: a probe of circumstellar dust formation and dynamics. *Astron. Astrophys.* 411, 123–147. doi:10.1051/0004-6361:20031068

Goumans, T. P. M., and Bromley, S. T. (2011). Hydrogen and oxygen adsorption on a nanosilicate – a quantum chemical study. *Mon. Not. R. Astron. Soc.* 141, 1285–1291. doi:10.1111/j.1365-2966.2011.18463.x

Goumans, T. P. M., and Bromley, S. T. (2012). Efficient nucleation of stardust silicates via heteromolecular homogeneous condensation. *Mon. Not. R. Astron. Soc.* 420, 3344–3349. doi:10.1111/j.1365-2966.2011.20255.x

Goumans, T. P. M., and Bromley, S. T. (2013). Stardust silicate nucleation kick-started by SiO+TiO_2. *Phil. Trans. R. Soc. A* 371, 20110580. doi:10.1098/rsta.2011.0580

Henning, T. (2010). Cosmic silicates. *Annu. Rev. Astron. Astrophys.* 48, 21–46. doi:10.1146/annurev-astro-081309-130815

Hensley, B. S., and Draine, B. T. (2017). Modeling the anomalous microwave emission with spinning nanoparticles: No PAHs required. *Astrophys. J.* 836, 179–192. doi:10.3847/1538-4357/aa5c37

Hoang, T., Vinh, N.-A., and Lan, N. Q. (2016). Spinning dust emission from ultra-small silicates: emissivity and polarization spectrum. *Astrophys. J.* 824, 18–28. doi:10.3847/0004-637x/824/1/18

Imai, H., Yasumori, M., Hirashima, H., Awazu, K., and Onuki, H. (1996). Significant densification of sol-gel derived amorphous silica films by vacuum ultraviolet irradiation. *J. Appl. Phys.* 79, 8304–8309. doi:10.1063/1.362541

Ishizuka, Y., Kimura, I., Sakon, (2015). *In-situ* infrared measurements of free-flying silicate during condensation in the laboratory. *Astrophysical J.* 803, 88. doi:10.1088/0004-637x/803/2/88

Jager, C., Dorschner, J., Mutschke, H., Posch, Th., and Henning, Th. (2003b). Steps toward interstellar silicate mineralogy: VII. Spectral properties and crystallization behaviour of magnesium silicates produced by the sol-gel method. *Astron. Astrophys.* 408, 193–204. doi:10.1051/0004-6361:20030916

Jäger, C., Fabian, D., Schrempel, F., Dorschner, J., Henning, Th., and Wesch, W. (2003a). Structural processing of enstatite by ion bombardment. *Astron. Astrophys.* 401, 57–65. doi:10.1051/0004-6361:20030002

Jelfs, K. E., Flikkema, E., and Bromley, S. T. (2013). Hydroxylation of silica nanoclusters $(SiO_2)_M(H_2O)_N$, M = 4, 8, 16, 24: stability and structural trends. *Phys. Chem. Chem. Phys.* 15, 20438. doi:10.1039/c3cp53347f

Jeong, K. S., Winters, J. M., Le Bertre, T., and Sedlmayr, E. (2003). Self-consistent modeling of the outflow from the O-rich Mira IRC –20197. *Astron. Astrophys.* 407, 191–206. doi:10.1051/0004-6361:20030693

Jones, A. P., and Nuth, J. A. (2011). Dust destruction in the ISM: a re-evaluation of dust lifetimes. *Astron. Astrophys.* 530, A44. doi:10.1051/0004-6361/201014440

Jones, A. P., Tielens, A. G. G. M., and Hollenbach, D. J. (1996). Grain shattering in shocks: the interstellar grain size distribution. *Astrophys. J.* 469, 740. doi:10.1086/177823

Jones, A. P., Tielens, A. G. G. M., Hollenbach, D. J., and McKee, C. F. (1994). Grain destruction in shocks in the interstellar medium. *Astrophys. J.* 433, 797. doi:10.1086/174689

Keller, L. P., and McKay, D. S. (1997). The nature and origin of rims on lunar soil grains. *Geochim. Cosmochim. Acta* 61, 2331–2341. doi:10.1016/s0016-7037(97)00085-9

Kemper, F., Vriend, W. J., and Tielens, A. (2004). The absence of crystalline silicates in the diffuse interstellar medium. *Astrophys. J.* 609, 826–837. doi:10.1086/421339

Kerkeni, B., Bacchus-Montabonel, M.-C., and Bromley, S. T. (2017). How hydroxylation affects hydrogen adsorption and formation on nanosilicates. *Mol. Astrophys.* 7, 1–8. doi:10.1016/j.molap.2017.04.001

Kerkeni, B., Bacchus-Montabonel, M. C., Shan, X., and Bromley, S. T. (2019). Understanding H_2 formation on hydroxylated pyroxene nanoclusters: *ab initio* study of reaction energetics and kinetics. *J. Phys. Chem. A* 123, 9282–9291. doi:10.1021/acs.jpca.9b06713

Kerkeni, B., and Bromley, S. T. (2013). Competing mechanisms of catalytic H_2 formation and dissociation on ultrasmall silicate nanocluster dust grains. *Mon. Not. R. Astron. Soc.* 435, 1486–1492. doi:10.1093/mnras/stt1389

Kimura, Y., Tanaka, K. K., Inatomi, Y., Ferguson, F. T., and Nuth, J. A. (2022). Inefficient growth of SiO_x grains: implications for circumstellar outflows. *Astrophys. J. Lett.* 934, L10. doi:10.3847/2041-8213/ac8002

Krasnokutski, S. A., Rouille, G., Jäger, C., Huisken, F., Zhukovska, S., and Henning, Th. (2014). Formation of silicon oxide grains at low temperature. *Astrophys. J.* 782, 15. doi:10.1088/0004-637x/782/1/15

Li, A., and Draine, B. T. (2001). On ultrasmall silicate grains in the diffuse interstellar medium. *Astrophys. J.* 550, L213–L217. doi:10.1086/319640

Li, M. P., Zhao, G., and Li, A. G. (2007). On the crystallinity of silicate dust in the interstellar medium. *Mon. Not. R. Astron. Soc.* 382, L26–L29. doi:10.1111/j.1745-3933.2007.00382.x

Macià Escatllar, A., and Bromley, S. T. (2020). Assessing the viability of silicate nanoclusters as carriers of the anomalous microwave emission: a quantum mechanical study. *Astron. Astrophys.* 634, A77. doi:10.1051/0004-6361/201936419

Macià Escatllar, A., Ugliengo, P., and Bromley, S. T. (2017). Modeling hydroxylated nanosilica: testing the performance of ReaxFF and FFSiOH force fields. *J. Chem. Phys.* 146, 224704. doi:10.1063/1.4985083

Macià Escatller, A., Lazaukas, T., Woodley, S. M., and Bromley, S. T. (2019). Structure and properties of nanosilicates with olivine $(Mg_2SiO_4)_N$ and pyroxene $(MgSiO_3)_N$ compositions. *ACS Earth Space Chem.* 3, 2390–2403. doi:10.1021/acsearthspacechem.9b00139

Mariñoso Guiu, J., and Bromley, S. T. (2022). Efficiency of interstellar nanodust heating: accurate bottom-up calculations of nanosilicate specific heat capacities. *J. Phys. Chem. A* 126, 3854–3862. doi:10.1021/acs.jpca.2c02199

Mariñoso Guiu, J., Ferrero, S., Macià Escatllar, A., Rimola, A., and Bromley, S. T. (2021b). Does processing or formation of water ice mantles affect the capacity of nanosilicates to be the source of anomalous microwave emission? *Front. Astron. Space Sci.* 8, 676548. doi:10.3389/fspas.2021.676548

Mariñoso Guiu, J., Ghejan, B.-A., Bernhardt, T. M., Bakker, J. M., Lang, S. M., and Bromley, S. T. (2022). Cluster beam study of $(MgSiO_3)^+$-based monomeric silicate species and their interaction with oxygen: implications for interstellar astrochemistry. *ACS Earth Space Chem.* 6 (10), 2465–2470. doi:10.1021/acsearthspacechem.2c00186

Mariñoso Guiu, J., Macià Escatllar, A., and Bromley, S. T. (2021a). How does temperature affect the infrared vibrational spectra of nanosized silicate dust? *ACS Earth Space Chem.* 5 (4), 812–823. doi:10.1021/acsearthspacechem.0c00341

Mathis, J. S., Rumple, W., and Nordsieck, K. H. (1977). The size distribution of interstellar grains. *Astrophys. J.* 217, 425. doi:10.1086/155591

Min, M., Waters, L. B. F. M., de Koter, A., Hovenier, J. W., Keller, L. P., and Markwick-Kemper, F. (2007). The shape and composition of interstellar silicate grains. *Astron. Astrophys.* 46, 667–676. doi:10.1051/0004-6361:20065436

Molster, F. J., Waters, L. B. F. M., Tielens, A. G. G. M., Koike, C., and Chihara, H. (2002). Crystalline silicate dust around evolved stars III. A correlations study of crystalline silicate features. *Astron. Astrophys.* 382, 241–255. doi:10.1051/0004-6361:20011552

Oueslati, I., Kerkeni, B., and Bromley, S. T. (2015). Trends in the adsorption and reactivity of hydrogen on magnesium silicate nanoclusters. *Phys. Chem. Chem. Phys.* 17, 8951–8963. doi:10.1039/c4cp05128a

Plane, J. M. C. (2013). On the nucleation of dust in oxygen-rich stellar outflows. *Phil. Trans. R. Soc. A* 371, 20120335. doi:10.1098/rsta.2012.0335

Potapov, A., Jäger, C., Mutschke, H., and Henning, T. (2024). Trapped water on silicates in the laboratory and in astrophysical environments. *Astrophys. J.* 965, 48. doi:10.3847/1538-4357/ad2c07

Rimola, A., and Bromley, S. T. (2021). Formation of interstellar silicate dust via nanocluster aggregation: insights from quantum chemistry simulations. *Front. Astron. Space Sci.* 8, 659494. doi:10.3389/fspas.2021.659494

Sarangi, A., and Cherchneff, I. (2013). The chemically controlled synthesis of dust in type II-P supernovae. *Astrophys. J.* 776, 107–126. doi:10.1088/0004-637x/776/2/107

Saunders, R. W., and Plane, J. M. C. (2006). A laboratory study of meteor smoke analogues: composition, optical properties and growth kinetics. *J. Atmos. Solar-Terr. Phys.* 68, 2182–2202. doi:10.1016/j.jastp.2006.09.006

Slavin, J. D., Dwek, E., and Jones, A. P. (2015). Destruction of interstellar dust in evolving supernova remnant shock waves. *Astrophys. J.* 803, 7. doi:10.1088/0004-637x/803/1/7

Valencia, E. M., Worth, C. J., and Fortenberry, R. C. (2020). Enstatite $(MgSiO_3)$ and forsterite (Mg_2SiO_4) monomers and dimers: highly detectable infrared and radioastronomical molecular building blocks. *Mon. Not. R. Astron. Soc.* 492, 276–282. doi:10.1093/mnras/stz3209

van Dishoeck, E. F. (2014). Astrochemistry of dust, ice and gas: introduction and overview. *Faraday Discuss.* 168, 9–47. doi:10.1039/c4fd00140k

Weingartner, J. C., and Draine, B. T. (2001). Photoelectric emission from interstellar dust: grain charging and gas heating. *Astrophys. J. Suppl. Ser.* 134, 263–281. doi:10.1086/320852

Whittet, D. C. B. (2010). Oxygen depletion in the interstellar medium: implications for grain models and the distribution of elemental oxygen. *Astrophys. J.* 710, 1009–1016. doi:10.1088/0004-637x/710/2/1009

Zamirri, L., Macià Escatllar, A., Mariñoso Guiu, J., Ugliengo, P., and Bromley, S. T. (2019). What can infrared spectra tell us about the crystallinity of nanosized interstellar silicate dust grains? *ACS Earth Space Sci.* 3, 2323–2338. doi:10.1021/acsearthspacechem.9b00157

Zeegers, S. T., Guiu, J. M., Kemper, F., Marshall, J. P., and Bromley, S. T. (2023). Predicting observable infrared signatures of nanosilicates in the diffuse interstellar medium. *Faraday Discuss.* 245, 609–619. doi:10.1039/d3fd00055a

Zeller, E. J., Ronca, L. B., and Levy, P. W. (1966). Proton-induced hydroxyl formation on the lunar surface. *J. Geophys. Res.* 71, 4855–4860. doi:10.1029/jz071i020p04855

Zhukovska, S., Dobbs, C., Jenkins, E. B., and Klessen, R. S. (2016). Modeling dust evolution in galaxies with a multiphase, inhomogeneous ISM. *Astrophys. J.* 831, 147. doi:10.3847/0004-637x/831/2/147

frontiers | Frontiers in Astronomy and Space Sciences

TYPE Brief Research Report
PUBLISHED 03 March 2025
DOI 10.3389/fspas.2025.1427387

Check for updates

OPEN ACCESS

EDITED BY
Alberto Fairén,
CSIC-INTA, Spain

REVIEWED BY
Josep M. Trigo-Rodríguez,
Spanish National Research Council (CSIC), Spain
Zuzana Kaňuchová,
Astronomical Institute of Slovak Academy of Sciences, Slovakia

*CORRESPONDENCE
A. Kereszturi,
kereszturi.akos@csfk.org

RECEIVED 03 May 2024
ACCEPTED 23 January 2025
PUBLISHED 03 March 2025

CITATION
Kereszturi A, Gyollai I, Biri S, Juhász Z, Király C, Pál BD, Rácz R, Rezes D, Sulik B, Szabó M, Szalai Z and Szávai P (2025) Evaluation of simulated space weathering-based meteorite alteration and potential influence on mechanical deformation of rubble pile asteroids.
Front. Astron. Space Sci. 12:1427387.
doi: 10.3389/fspas.2025.1427387

COPYRIGHT
© 2025 Kereszturi, Gyollai, Biri, Juhász, Király, Pál, Rácz, Rezes, Sulik, Szabó, Szalai and Szávai. This is an open-access article distributed under the terms of the Creative Commons Attribution License (CC BY). The use, distribution or reproduction in other forums is permitted, provided the original author(s) and the copyright owner(s) are credited and that the original publication in this journal is cited, in accordance with accepted academic practice. No use, distribution or reproduction is permitted which does not comply with these terms.

Evaluation of simulated space weathering-based meteorite alteration and potential influence on mechanical deformation of rubble pile asteroids

A. Kereszturi[1,2]*, I. Gyollai[2,3], S. Biri[4], Z. Juhász[4], Cs. Király[2,5], B. D. Pál[1,2], R. Rácz[4], D. Rezes[1,2], B. Sulik[4], M. Szabó[2,3], Z. Szalai[2,5,6] and P. Szávai[2,5]

[1]Konkoly Thege Astronomical Institute, Research Centre for Astronomy and Earth Sciences, Hungarian Research Network (HUN-REN), Budapest, Hungary, [2]CSFK, MTA Centre of Excellence, Budapest, Hungary, [3]Institute for Geological and Geochemical Research, Research Centre for Astronomy and Earth Sciences, Hungarian Research Network (HUN-REN), Budapest, Hungary, [4]Hungarian Research Network (HUN-REN), Institute for Nuclear Research (ATOMKI), Debrecen, Hungary, [5]Geographical institute, Research Centre for Astronomy and Earth Sciences, Hungarian Research Network (HUN-REN), Budapest, Hungary, [6]Department of Environmental and Landscape Geography, ELTE Eötvös Loránd University, Budapest, Hungary

Asteroids with the potential to impact Earth have become a significant focus of scientific research and applied space technology. These bodies are expected to be key targets for mitigation actions and space mining activities in the coming decades. Understanding their material characteristics is challenging due to the effects of space weathering, which alters the mineral composition and structure of their surfaces, resulting in featureless infrared spectra. This study details laboratory tests of artificial solar wind effects on meteorites, revealing key changes including decreasing magnesium content in olivine, water loss-induced mineral changes, and general amorphization of the crystalline lattice. Although these alterations affect only a thin surface layer (and not the bulk regolith volume) of grains exposed on asteroid surfaces, they can influence the mechanical properties of most small (100 m-class) asteroids through physical surface contacts as most small asteroids are rubble piles with rotation, shape-altering grain migration, and surface mixing. The mechanical properties of only a very thin surface layer of specific grains are influenced; however, the behavior of granular aggregates with such influenced surfaces could be mixed by the YORP effect. This study reviews established findings, explores potential implications for asteroid behavior, and identifies future research directions.

KEYWORDS

meteorites, asteroids, space weathering, mineral changes, laboratory analysis

1 Introduction

Space weathering significantly affects asteroid surfaces, but its influence on the internal properties and joint behavior of grain within rubble pile asteroids, particularly on the mixing processes under unique microgravity conditions, remains poorly understood

(Kereszturi A. 2014). Asteroids occasionally impact Earth, with large-scale collisions causing rare, catastrophic extinctions over geological timescales. Smaller, more frequent impacts, however, can still have devastating consequences for humanity (De and Rene, 2023; Lubin and Cohen, 2023). As a result, near-Earth asteroids (NEAs) have become a key focus of recent research, particularly regarding their orbital dynamics, physical characteristics, and mineralogical properties, to prepare effective mitigation strategies. Beyond optical camera-based detections, infrasound detectors (Ott et al., 2021) and space-based observations have confirmed the current rate of fireballs and bolide explosions (Peña-Asensio et al., 2022), highlighting the persistent danger these bodies represent. Understanding NEA composition and mechanical properties is crucial, with studies analyzing meteorites on Earth and meteorite analogs (Amiko et al., 2020) to investigate their mineralogy and the effects of space weathering on airless bodies (Chapman, 2004). Space weathering processes universally affect the surfaces of solar system bodies that lack atmospheres or magnetic fields, contributing to the spectral discrepancies between meteorites and asteroids. Meteorites typically represent the intact or less-weathered interiors of asteroids, while asteroid spectra reflect heavily weathered surfaces. Artificial space weathering tests were conducted to better understand the spectral differences between meteorites and their weathered surface host asteroids in order to properly correlate their spectra.

Space weathering processes are driven by various factors, including irradiation, implantation, sputtering from galactic and solar ions, UV irradiation, impacts, and daily temperature fluctuations. At the mineral scale, artificial space weathering experiments have revealed several key effects. Ion irradiation causes silica amorphization, as recorded via IR spectroscopy (Demyk et al., 2004), which is often accompanied by an increase in the Fe/Si ratio (Dukes et al., 2015), as observed in the Tagish Lake sample. Lantz et al. (2015) identified shifts in the infrared bands of phyllosilicate and olivine within 2.7–10 μm toward the Fe-rich range, indicating Mg loss and an increased Fe ratio. The process of sputtering is preferential because Mg is lost more easily than the heavier Fe (Hapke et al., 1975), resulting in amorphization and band broadening, as confirmed via Raman spectroscopy (Brucato et al., 2004; Demyk et al., 2004). Irradiation causes amorphization and chemical changes, attenuating absorption bands (Hapke, 2001; Clark et al., 2002; Chapman, 2004) in general, along with erosion, transport, and redeposition of elements through ion sputtering. These processes form chemically distinct, surface-deposited rims (Noguchi et al., 2014). Micrometeorite impacts can induce melting, vaporization, and recondensation, leading to the formation of reduced iron nanoparticles on the grain rims, which contribute to optical changes (Noble et al., 2007) by reddening and darkening the surfaces. Band position shifts of olivine toward longer wavelengths in the Murchison meteorite were observed after irradiation (Brunetto et al., 2014), as well as the formation of Fe nanoparticles (Thompson et al., 2019). Similarly, npFe0 and nanophase iron–nickel particles were also detected in irradiated CV and CO chondrites (Zhang et al., 2022).

This study investigates the primary effects of simulated space weathering on grain surfaces and the potential secondary consequences for grain–grain interactions within rubble pile asteroids. The findings may have implications for mitigation strategies targeting NEAs. Space weathering alters the thin surface layers of grains, potentially affecting mineral strength and grain–grain interactions at points of physical contact. These changes could theoretically influence the mechanical behavior of rubble pile asteroids, which are composed of loosely bound grains that are mixed and redistributed during shape-altering processes. Improved understanding of grain-scale behavior, as well as the previously mentioned specific effects, is essential for developing effective mitigation strategies against asteroids, such as artificial impact-induced consequences. This work aims to outline the background, raise key questions, and guide future research in this underexplored area. It is important to note that laboratory irradiation tests do not fully replicate regolith weathering as they exclude factors such as temperature cycling and impact effects.

An important milestone in the defense against NEAs was NASA's Double Asteroid Redirection Test (DART), which demonstrated the kinetic impact method by targeting Dimorphos, the secondary of the S-type binary NEA (65,803) Didymos (Daly et al., 2023). The action produced a well-observable impact plume and altered the orbital period of Dimorphos by approximately 33 s (Thomas et al., 2023), indicating that the ejecta (Li et al., 2023) of a diminishing tail feature (Kareta et al., 2023) significantly contributed to the momentum transfer. High-resolution images of the surface, down to approximately 5 cm in spatial resolution, were captured during the mission. Observations of moderately small NEAs, such as Dimorphos, suggest rubble pile structures based on their boulder field observations and porosity volumes. For instance, Dimorphos exhibits a porosity of approximately 30%, contrasting with the lower porosities of compositionally similar L and LL meteorite analogs (8.0% and 9.5%, respectively). This elevated porosity might indicate a rubble-pile interior, which may also be influenced by the shapes of granular materials.

Recent asteroid sample return missions have provided new insights into the role of space weathering on various asteroids. Evidence of space weathering has been observed on Bennu, where young craters are darker and redder than their surroundings (exhibiting a positive spectral slope) due to smaller particle sizes and/or fresh exposure of organics from impacts (Clark et al., 2023). The equator, the oldest surface on Bennu, has similar darker and redder characteristics, possibly due to the development of nano- and microphase opaques. Samples from the carbonaceous asteroid Bennu (Lauretta et a. 2024) revealed dark grains with hummocky and irregular shapes, which were composed of hydrated phyllosilicates, magnetite, organics, carbonates, sulfides, presolar grains, and phosphates, all indicating past aqueous alteration. The sampled mid-latitude location experienced moderate peak temperatures, suggesting that the regolith collected by OSIRIS-REx is not heavily space-weathered. However, the presence of particle surfaces with vesiculated melt droplets and weathered or etched magnetite grains is indicative of space weathering.

Samples from Ryugu, acquired by the Hayabusa2 mission, revealed grains with diverse silicate mineralogies, indicating heterogeneous and incomplete aqueous alteration enriched with many organics (Yesiltas et al., 2024). Near-infrared band changes observed on the surface of Ryugu suggest a global space weathering (Hiroi et al., 2023). Matsouka et al. (2023) demonstrated that micrometeoroid bombardment, which promotes dehydration, is a more effective weathering mechanism on Ryugu than solar wind implantation. This process has resulted in more homogeneous

space-weathered grain surfaces compared to those observed on Itokawa. Additionally, possible analogies have been identified between the scoriaceous fusion crust of the Tagish Lake meteorite and the space-weathered "frothy layer" on Ryugu's grain surfaces, particularly in terms of vesicularity (Shehaj et al., 2024). The origin of these vesicles remains uncertain, but recent analyses suggest that they may result from space weathering. This hypothesis is being further investigated through simulations using 400 keV Ar^+ ion bombardment, which aims to replicate space weathering processes and support the interpretation of features observed on Ryugu's grains (Palomba et al., 2024).

Samples from the S-type asteroid 25,143 Itokawa exhibited evidence of space weathering, with sulfur-bearing Fe-rich nanoparticles identified in a 5–15-nm surface layer of olivine, pyroxene, and plagioclase. These nanoparticles were likely formed by vapor deposition. Sulfur-free Fe-rich nanoparticles were also observed deeper within ferromagnesian silicates, potentially resulting from metamictization and reduction of Fe^{2+} (Noguchi et al., 2011). A black zone on Itokawa was found to be more space-weathered than a surrounding bright region, with spectra similar to those of LL5-6 chondrites. The dark region exhibited a shorter mean optical path length and a higher concentration of nanophase iron, suggesting that small asteroids like Itokawa could serve as parent bodies for LL chondrites (Hiroi et al., 2006).

2 Methods

This section outlines the general methodological framework relevant to simulated space weathering and its consequences, providing context for the mineral-scale effects of artificial particle irradiation. Specific examples are provided, presenting laboratory measurements and numerical data to illustrate observable changes.

Over the past decades, numerous artificial space weathering experiments have been conducted on various meteorites and reference minerals, using protons and heavier nuclei. Although interactions with protons represent the most common type of event, heavier nuclei, including those of galactic cosmic ray origin, may exert stronger but less frequent effects. The cumulative impact and relative roles of solar wind ions and cosmic ray-originated ions, however, remain poorly understood.

Changes induced by artificial irradiation have been analyzed primarily via Fourier transform infrared (FTIR) spectroscopy, typically on bulk samples (Lantz et al., 2017; Brunetto et al., 2014; 2020). Raman spectroscopy-based measurements have also been employed, for example, in studies of olivine (Lantz et al., 2015). Additionally, measurements in the near-ultraviolet (NUV) and visible-near-infrared (VNIR) ranges have been conducted on silicates and meteorites (Kanuchova et al., 2015), as well as on materials such as polystyrene (Kanuchova et al., 2010; Kanuchova et al., 2017).

Example numerical values from the authors' own work are provided below to illustrate the scale of changes caused by simulated space weathering. These results were obtained from the irradiation of the NWA 10,580 CO_3-type meteorite, a poorly altered primitive meteorite containing unweathered material. The meteorite was irradiated with 1 keV H^+ protons produced by an ECR ion source (for technical details, see Biri et al., 2021) at the ATOMKI institute under vacuum conditions. Three irradiation sessions were conducted as follows: 15 s (10^{11} ion/cm^2) for the first irradiation, 1 h (10^{14} ion/cm^2) for the second, and 1 day (10^{17} ion/cm^2) for the third. All ion fluences were cumulative. As each irradiation reinforced the effects of previous sessions, the cumulative consequences must be considered. The strongest effects were expected after the third irradiation.

The observed changes were analyzed via infrared spectroscopy using a VERTEX 70 FTIR spectrometer. Measurements were conducted with 32 scans over the 400–4,000 cm^{-1} range and performed for 30 s at a spectral resolution of 4 cm^{-1}. Spectral data were processed using Bruker Optics' Opus 5.5 software. The field of view using the IR × 15 objective was 200 μm in diameter, making this method suitable for moderately smooth rock sample surfaces, while the DRIFTS Praying Mantis accessory was also used and showed characteristics of bulk samples. Two key parameters were determined, namely, peak position and full width at half maximum (FWHM). FWHM values were calculated manually by measuring the width of spectral bands at their half height. The accuracy of peak position measurements was ±0.5 cm^{-1}, as determined by the OPUS software manual. Peak shifts were quantified by comparing band appearance and maximal positions before and after irradiation and correlated with databases like those by Lafuente et al. (2016).

3 Summary of mineral changes

The results of the authors' tests are presented below, along with related findings from other studies for review and context. According to the increasing impact, the following types of alterations are expected to occur as the crystalline lattice is progressively disrupted during irradiation:

1. Emergence of metastable phases: Metastable phases may form ephemerally under conditions differing from those of stability. Although these aspects have primarily been studied under Earth-related conditions, such as in sediments and thermal alterations (Milliken, 2014), previous research by Lindsley et al. (1972) evaluated the metastable properties of pyroxferroite related to smectites in cosmic materials. Radiation-induced metastable structures have also been observed in specific mineral-like alloys as well (Lilienfeld et al., 1987), where irradiation can modify grain boundaries and dislocations (Chesser et al., 2024). However, these effects have rarely been explored in irradiated meteorites.
2. Defect production in the crystalline lattice: The next stage involves the formation of defects, where the long-term behavior, such as vacancy migration, is influenced by temperature (Campbell et al., 2002, Closel et al., 1994). These defects might reduce the band strength and increase FWHM values in general.
3. Element migration, replacement, and ion integration: Irradiation can lead to changes in the crystalline lattice. For example, olivine composition changed from Fo-50–60 (Hamilton 2010) to Fo-30–35 after irradiation in Frontier Mountain 95,002 and Lancé meteorites (Brunetto et al., 2020). Similarly, an increase in the Fe/Si ratio was observed in the Tagish Lake sample after ion irradiation (Dukes et al., 2015).

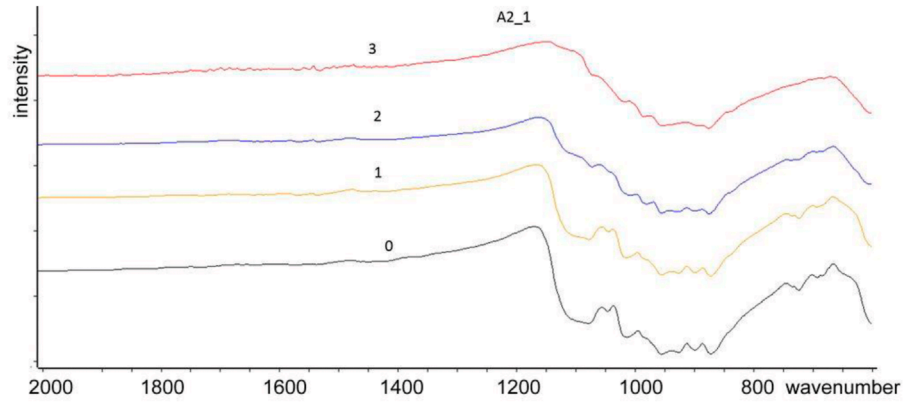

FIGURE 1
Example DRIFT detector-based infrared reflection spectral curves for the NWA 10580 sample before irradiation (0) and after gradually increasing irradiation actions by Gyollai et al., 2024. Please note the vertical offset of the curves for better visualization, the horizontal axis shows the cm^{-1} values.

4. Amorphization and mineral decomposition: At higher levels of irradiation, excessive defects and element loss or implantation result in amorphization and decomposition. For silicates, this occurs through the depolymerization of SiO_4 tetrahedra and the decomposition of the related part of the lattice, which is observable as weakened or missing spectral bands. It is important to note that these four stages progressively lead to mechanical changes in the affected minerals. Although the early stages are challenging to identify spectroscopically, the later stages may produce significant macroscopic consequences, as possibility partly explored in this work.

Specific results from our laboratory tests demonstrated changes induced by artificial solar wind simulations that are generally consistent with the weakening of spectral bands reported in the literature. Characteristic examples include irradiation-driven changes observed in the NWA 10580 meteorite, as described in the Methods section. The primary types of changes identified were peak shifts. For the prominent meteorite components pyroxene and feldspar, negative shifts were observed after the first and second irradiation sessions, ranging from −4 to −41 cm^{-1}, likely due to Mg loss (Lantz et al., 2017). Conversely, a positive shift occurred after the third strongest irradiation action, with values between +7 and +30 cm^{-1}, indicating general distortion of the SiO_4 tetrahedra (Sharp and De Carli, 2006; Johnson et al., 2003; 2007). Minor peaks corresponding to certain minerals were generally weakened or disappeared, following irradiation. Additionally, the olivine doublet at 849 cm^{-1} and 880 cm^{-1} merged into a single peak at 887 cm^{-1}, further supporting the conclusion of SiO_4 disordering. A representative spectral curve series is presented in Figure 1, recorded by Gyollai et al. (2024). Below, only the results related to amorphization and Mg/Fe changes are highlighted as the most prominent effects contextualized with the behavior of the weathered surface layer on grain interactions. Further specific details regarding mineral alterations can be found in the cited works.

Numerical band positions are provided in Table 1 to quantify the spectral changes observed in typical meteorite minerals from the analyzed sample. Although data for comparing band position changes are limited, especially in the IR range, few standards and FWHM measurements are available from irradiation studies in the existing literature. Earlier research predominantly focused on Raman spectroscopy rather than IR measurements. In this study, example values for peak positions and FWHM changes are listed in Table 1, 2.

The last column of Table 1 provides guidance for researchers conducting future laboratory tests, offering insights into the scale of band shifts to aid in estimating observability. The first, and to some extent, the second irradiation induced metastable states in the crystal structures of Mg-bearing minerals. Increasing fluences of irradiation led to amorphization of the crystal structure, primarily through Mg loss from MgO_6 octahedra (Lantz et al., 2015; Lantz et al., 2017). Feldspar, which was already in a less-crystallized state prior to irradiation, exhibited further distortion of SiO_4 tetrahedra during irradiation. This amorphization trend in feldspar, reflected in positive peak shifts, is consistent with the observations reported by Johnson et al. (2003) and Gyollai et al. (2024), which primarily occurred following the second irradiation. It is possible that the weakly crystallized feldspar required stronger irradiation to produce further observable distortions. FWHM changes for the major bands of feldspar exhibited an increasing trend, while olivine and pyroxene showed a decreasing trend after weaker irradiations, followed by an increasing trend after stronger irradiation sessions. The effects of irradiation-induced changes in infrared peaks partially resemble those caused by shock deformation, presenting opportunities for future synergistic studies.

Although space weathering processes primarily alter the microscopic characteristics of minerals and most ions and microscopic impact events do not penetrate deeply into the minerals, it is worth exploring whether these effects could influence larger spatial scales, for example, the mechanical behavior of grains within rubble pile asteroids (Bierhaus et al., 2023). The mechanical properties, global shape, and internal stability of such asteroids depend on the size, shape, and surface adhesion of individual grains. As asteroids undergo spin-state modifications, their global shapes may adapt to new equilibrium states through grain flow or

TABLE 1 Average peak position shift after irradiations in the reflection mode in cm^{-1}. Average original peak positions are indicated at "band" column in cm^{-1} for minerals which were observable after all of the irradiation actions.

Mineral	Band	First irr. (cm^{-1})	Deviation	Second irr. (cm^{-1})	Deviation (cm^{-1})	Third irr. (cm^{-1})	Deviation (cm^{-1})	Avg. Dev. irr. (cm^{-1})
Olivine	849.2	−11.33	6.5	2	12.8	1.8	5.7	8.3
Feldspar	1152.1	−1.58	20.4	2.16	19.9	−1.4	15.7	18.7
Pyroxene	1047.2	−7.8	14.9	7	19.6	1.4	5.6	13.4
Spinel	666.1	−3.22	5.9	0.11	1.9	3.4	2.9	3.6

TABLE 2 Average FWHM values of major mineral bands with standard deviations. At the end of the table, the average deviation after the irradiations was calculated. These data of the table contain such measurements, where the given bands appeared before and after all irradiation tests.

Mineral	Band	Before irradiation	Deviation	First irradiation	Deviation	Second irradiation	Deviation	Third irradiation	Deviation
Olivine	849.3	9.8	4.4	17.5	4.5	6.8	1	4.3	1.03
Olivine	887.6	12	3.1	8.4	2.2	6.5	2.5	12.0	13.9
Feldspar	1149.8	76.4	31.4	86.3	25.2	84.8	30.4	99.8	19.8
Pyroxene	1048.4	29.2	14	22.1	11.2	22.3	20.5	21.3	9.03
Spinel	668.5	65.8	40.7	51.4	46.3	65.6	41.9	76.6	33.09

rolling interactions (Banik et al., 2022). Since space weathering can affect the surface hardness of the grains, which is linked to mineral structure and amorphous states, the potential implications of these modifications are considered below.

3.1 Aspects of mechanical grain behavior

Ion migration and crystalline lattice destruction, as described in datasets such as those by Railsback (2006), result in decreased rigidity and mechanical properties within a very thin surface layer during various irradiation tests (Chaves et al., 2023 Harries and Langenhorst, 2014; Yang et al., 2017). A key challenge is to evaluate whether mechanical changes in this thin surface layer could influence the collective behavior of asteroid regolith grains. Alterations to amorphous structures and other mineralogical changes may reduce mechanical hardness (Zaccone, 2023) as amorphization is known to decrease the hardness of minerals (Leggett, 1991; Thorpe and Tichy, 2001). For example, the Mohs hardness of Mg-rich olivine (forsterite) decreases as its composition shifts toward Mg-poor fayalite.

In this context, hardness is considered a basic mechanical property, although it is important to note that mechanical behavior is also influenced by factors such as porosity and grain size of the crystals. For simplicity, this discussion focuses solely on mechanical hardness. The aim of this work is to explore the potential effects of irradiation-induced grain surface modifications and their implications for the temporal aspects of shape changes. However, detailed numerical calculations of the possible consequences are beyond the scope of this paper.

In rubble pile asteroids, individual grains occasionally move relative to each other during deformation caused by changes in rotational speed, such as those driven by the YORP effect. This movement allows the asteroid to achieve an equilibrium shape (Sanchez and Scheeres, 2018; Walsh et al., 2017). The timescale for YORP effect-induced shape changes ranges from 1 to 100 million years (Botke et al., 2006), depending on the size, mass, and other characteristics of the given asteroid. This range is roughly comparable to the timescale for space weathering-induced changes relevant to the main asteroid belt solar distance, estimated at 1–100 million years (Hasegawa et al., 2022; Sunho and Masateru, 2022). These estimations are based on observable amorphization using average solar wind exposure, although they are rough approximations on the exposure duration of the same surface of asteroids that do not account for mixing or fragmentation caused by impacts.

As rotational speed increases, the oblateness of the body increases (e.g., the body becomes more flattened), causing boulders and grains to roll toward lower latitudes, potentially burying previously surface-exposed weathered grains. Small, low-mass objects among asteroids strongly influenced by the YORP effect (Holsapple, 2009), such as those in the potentially hazardous asteroid (PHA) group, are particularly susceptible to these shape changes due to their low gravity (Pleasko et al., 2024; Regály et al., 2023). These objects often have diameters of a few hundred meters. During changes in oblateness, mechanical attrition and friction occur as grains interact. Grain movement and critical slope angles

depend on their shape (Jacobson and Scheeres, 2010; Kereszturi, 2023), according to the stability and spatial density of their mechanical contacts (Ferrari and Alessi, 2023; Hirabayashi, 2023).

For example, given the current obliquity of Ryugu, the asteroid is expected to be spinning down at a rate of -1.71×10^{-6} deg/day^2, corresponding to a change in the rotation period from 3.5 h to 7.6 h over approximately 2.15 million years (Kanamaru et al., 2021). In cases where hardness decreases, any grain movement, such as creeping or rolling, is facilitated by the softening of minerals. Softer minerals deform more quickly under attrition, smoothing and destroying protrusions and enabling easier movement. However, hardness changes are not well understood for all minerals under irradiation. For example, phyllosilicates may transform into oxides through OH loss, but this transformation does not necessarily result in mechanical softening.

The role of cohesion, determined by the number and characteristics of grain–grain contacts, has been studied in the context of momentum transfer-related grain movement in asteroids (Raducan et al., 2019). As cohesion decreases, the ratio of ejected momentum to impactor momentum increases. This ratio also increases, as the initial porosity and internal friction coefficient decrease. This later may be associated with reduced hardness, which allows for rounding of grains. However, this modeled aspect focuses on sudden changes affecting a relatively small volume of grains, whereas YORP-driven shape changes act over longer timescales and influence larger numbers of grains, permitting more gradual, friction-driven shape modifications. The friction coefficient between grains has been identified as an important parameter (Brisset et al., 2020), particularly under low gravity conditions (Brisset et al., 2018). Despite its importance, available data and modeling methods remain insufficient to fully evaluate the potential consequences of the processes outlined in this work.

Although the thickness of the affected grain surface layer is small, its macroscopic effects on grain behavior and regolith dynamics should not be overlooked (Kobayashi et al., 2020; Kobayashi et al., 2023; Takano et al., 2020). Grains interact primarily through this thin surface layer, and even minor changes could influence the mechanical stability of grain groups by altering their threshold angles. Surface roughness plays a key role as protrusion helps grains interlock, while smoother grains are more prone to rolling and sliding, potentially affecting the global shape of an asteroid and the manner in which it achieves equilibrium.

Global shape changes have significant implications for asteroid surfaces. Using the model proposed by Banik et al. (2022), top-shaped asteroids are made up of loose regolith lying atop a solid core (potential-related consequences are detailed below). For example, in the case of Bennu, a previously faster spin state may have been slowed by impact-induced global landslides, leading to its current spin rate. As the spin rate dropped below a critical threshold, regolith flow from higher latitudes accumulated at the equator.

Both observational data and theoretical modeling of the interior structure changes driven by the YORP effect remain poorly explored. Substantial differences are anticipated between the two theoretical end cases mentioned above: one where the entire asteroid is composed solely of grains (including the center) and another where a solid core is covered by debris. In the latter case, grains in the shallow subsurface layer are expected to exhibit greater mobility, potentially resulting in stronger mixing and more observable effects. The irradiated and slightly decreased hardness of the top surface layer of grains may further influence granular behavior in the latter scenario involving transport over a solid core.

Given the differences in the mechanical stability of grain groups within rubble pile asteroids, the considerations outlined in this work are important as they could affect the planning and implementation of mitigation strategies for hazardous NEAs. Additionally, amorphization reduces heat conduction, which could further impact asteroid regolith and grain behavior. Changes in porosity may have an even greater influence, altering mechanical contacts where heat conduction occurs.

3.2 Mechanical properties of meteorites

Several research studies have been conducted to explore the mechanical properties of meteorites and, by inference, asteroids. Moyano-Cambero et al., 2017 analyzed the highly shocked, low-porosity Chelyabinsk ordinary chondrite meteorite, which is likely similar in composition to S- or Q-type asteroids. Nanoindentation experiments revealed mechanical property variations across different regions of the meteorite that were unrelated to compositional differences. The differences were attributed to grain size as smaller mean particle sizes—produced by repetitive shocks—can increase hardness. Additionally, low-porosity sections promote higher momentum multiplication, which is defined as the ratio of the impact-induced momentum change in the target and the momentum of the projectile. Light lithology materials were found to facilitate greater momentum multiplication, while the low fracture toughness of shock veins promotes material ejection by impact and further increases momentum multiplication, potentially resembling observations from the DART impact event.

A laboratory comparison of grain physical properties between the Itokawa asteroid and the Chelyabinsk meteorite using nanoindentation (Tanbakouei et al., 2019) showed that Young's modulus for Itokawa samples was slightly higher than that for the Chelyabinsk chondrite. This difference is very small and may result from the increased compaction of Itokawa grains, suggesting that Itokawa particles are better able to absorb elastic energy during an impact than Chelyabinsk chondrite.

To date, no results in the literature have confirmed the mechanical grain surface property-related aspects hypothesized in this work. Although the mechanical effects of space-weathered grain surfaces are expected to be minor, they remain poorly understood. It may be worthwhile to explore whether space weathering-induced fragmentation and microscopic void formation could be linked to irradiation-driven alteration as these processes occur concurrently. This potential connection could offer a novel perspective for future research.

The potential effects of mechanical changes in the grain surface layer require further investigation, although this lies beyond the scope of the present work. Future studies could benefit from highly sophisticated grain surface mechanical analyses, including attrition tests, which would necessitate well-designed instruments and controlled conditions. Additionally, transmission electron

microscopy (TEM) could be used to assess amorphization levels and compare grain surface modifications across analog materials with varying hardness. Such independent inputs would enhance our understanding of the granular behavior of rubble pile asteroids and facilitate the implementation of these findings into models of small asteroids' mechanical strength and deformation.

Based on the aspects presented above, the following main research questions are proposed to evaluate the potential consequences of irradiation-induced grain-scale changes for asteroids in the near future:

1. Asteroid modeling: Improved models are needed to better understand the speed and scale of YORP effect-driven rotational modifications and their associated shape changes, with a focus on the populated and hazardous near-Earth object category of asteroids under 1 km in diameter.
2. Grain rearrangement studies: Future asteroid missions should investigate the typical movement of grains on and within rubble-pile asteroids. For example, the HERA mission for Dimorphos could provide valuable insights through surface observations and radar-based internal analyses (Michel et al., 2024).
3. Grain-size estimation: High-resolution asteroid imagery combined with Earth-based thermal inertia measurements should be jointly analyzed to estimate the typical grain sizes on small near-Earth asteroids.
4. Laboratory simulations: Artificial space weathering experiments using higher ion bombardment fluences and energies, paired with mechanical analyses of irradiated grain behavior, should be conducted in laboratories to expand the understanding of grain surface changes.

4 Conclusion

Using artificial irradiation experiments on meteorites in laboratory settings, various mineral lattice changes were observed, leading to hardness decreases through amorphization and the introduction of lattice deflects in a very thin surface layer of the target meteorites. These changes were tracked through shifts in infrared peak positions and FWHM values for minerals such as olivines, pyroxenes, and feldspars. At high fluences, these processes resulted in significant mineral lattice changes and amorphization, which corresponded to 10–100 million years of space weathering exposure, albeit confined to an extremely thin surface layer.

Despite extensive and growing mineral-based research linking meteorites and their parent asteroids through infrared spectral characteristics (Moyano-Cambero et al., 2016; Tanbakouei et al., 2019; Trigo-Rodríguez et al., 2011; 2014), including spectra recorded during meteor ablation in Earth's atmosphere (Madiedo et al., 2014), further investigations are necessary to fully understand the effects of space weathering on spectral bands. This review highlights specific infrared bands where certain minerals retain their diagnostic features despite weakening spectral signatures. Improved mineral identification, particularly for components like phyllosilicates observed on Ryugu and in meteorites (Storz et al., 2024), is critical, especially considering their metal cation-dependent band shifts and volatile content as potential sources of primordial water delivery to Earth (Trigo-Rodríguez et al., 2009).

Infrared spectral analysis also supports primordial condensation studies, which aim to reconstruct processes in the solar nebula (Trigo-Rodríguez et al., 2009). This work is particularly relevant for refractory condensates such as forsteritic olivine (Weinbruchi et al., 2000) and various isotopic and elemental analyses (Kobayashi et al., 2020). Predicting spectral alterations caused by space weathering influences the design and channel arrangement of future infrared detectors, as well as data processing schemes for upcoming missions. Such missions should prioritize identifying primordial condensates and assessing water content. Further efforts are required to clarify the changes in typical meteorite-forming minerals and their source asteroids, emphasizing the need for targeted spectral band or filter arrangements over equidistant, uniformly distributed bands.

Finally, the mechanical implications of the thin, irradiation-modified surface layer warrant consideration. Grain surface characteristics may influence joint grain group-scale mechanical processes, potentially affecting global deformation-driven shape changes in rubble-pile asteroids by facilitating the smoothing process of grain surface undulations. Although this effect is expected to be minor and likely overshadowed by other unique microgravity-driven phenomena present on small asteroids, it is nonetheless worth evaluating for its potential consequences.

Author contributions

AK: writing–original draft and writing–review and editing. IG: investigation and writing–original draft. SB: formal analysis and writing–original draft. ZJ: validation and writing–review and editing. CK: investigation and writing–original draft. BP: investigation and writing–review and editing. RR: formal analysis and writing–original draft. DR: methodology and writing–original draft. BS: conceptualization and writing–review and editing. MS: formal analysis and writing–original draft. ZS: validation and writing–review and editing. PS: formal analysis and writing–original draft.

Funding

The author(s) declare that financial support was received for the research, authorship, and/or publication of this article. This project was supported by the K_138594 Project of NKFIH. The authors acknowledge the Europlanet 2024 RI, which has been funded by the European Union's Horizon 2020 Research Innovation Program under grant agreement No. 871149. ZJ is grateful for the support of the Hungarian Academy of Sciences through the János Bolyai Research Scholarship.

Conflict of interest

The authors declare that the research was conducted in the absence of any commercial or financial relationships that could be construed as a potential conflict of interest.

Publisher's note

All claims expressed in this article are solely those of the authors and do not necessarily represent those of their affiliated organizations, or those of the publisher, the editors and the reviewers. Any product that may be evaluated in this article, or claim that may be made by its manufacturer, is not guaranteed or endorsed by the publisher.

References

Amiko, T., Naoya, S., Hideaki, M., Tomohiro, U., Takafumi, N., Pál, P., et al. (2020). *Experimental study on thermal properties of high porosity particles for understanding physical properties of Phobos surface*. JpGU-AGU Joint Meeting, PPS08–P01.

Banik, D., Gaurav, K., and Sharma, I. (2022). Regolith flow on top-shaped asteroids. *Proc. R. Soc. A* 478, 20210972. doi:10.1098/rspa.2021.0972

Bierhaus, E. B., Rossmann, F., Johnson, C., Daly, R. T., Golish, D., Nolau, J., et al. (2023). A subsurface layer on asteroid (101955) Bennu and implications for rubble pile asteroid evolution. *Icarus* 406, 115736. article id. 115736. doi:10.1016/j.icarus.2023.115736

Biri, S., Vajda, I. K., Hajdu, P., Rácz, R., Csík, A., Kormány, Z., et al. (2021). The ATOMKI accelerator centre. *Eur. Phys. J. Plus* 136, 247. doi:10.1140/epjp/s13360-021-01219-z

Brisset, J., Colwell, J., Dove, A., Abukhalil, S., Cox, C., and Mohammed, N. (2018). Regolith behavior under asteroid-level gravity conditions: low-velocity impact experiments. *Prog. Earth Planet Sci.* 5, 73. doi:10.1186/s40645-018-0222-5

Brisset, J., Cox, C., Anderson, S., Hatchitt, J., Madison, A., Mendonca, M., et al. (2020). Regolith behavior under asteroid-level gravity conditions: low-velocity impacts into mm- and cm-sized grain targets. *A&* 642, A198. doi:10.1051/0004-6361/202038665

Brucato, J. R., Strazzulla, G., Baratta, G., and Colangeli, L. (2004). Forsterite amorphisation by ion irradiation: monitoring by infrared spectroscopy. *Astronomy and Astrophysics* 413 (2), 395–401. doi:10.1051/0004-6361:20031574

Brunetto, R., Lantz, C., Ledu, D., Baklouti, D., Barucci, M., Beck, P., et al. (2014). Ion irradiation of Allende meteorite probed by visible, IR, and Raman spectroscopies. *Icarus* 237, 278–292. doi:10.1016/j.icarus.2014.04.047

Brunetto, R., Lantz, C., Nakamura, T., Baklouti, D., Le Pi vert-Joli, vet T., Kobayashi, S., et al. (2020). Characterizing irradiated surfaces using IR spectroscopy. *Icarus* 345, 113722. doi:10.1016/j.icarus.2020.113722

Campbell, B., Choudhury, W., Mainwood, A., Newton, M. E., Davies, G., and Gordon, D. (2002). Lattice damage caused by the irradiation of diamond. *Nucl. Instrum. Methods Phys. Res. Sect. A Accel. Spectrom. Detect. Assoc. Equip.* 476 (3), 680–685. doi:10.1016/s0168-9002(01)01664-3

Chapman, C. R. (2004). Space weathering of asteroid surfaces. *Annu. Rev. Earth Planet. Sci.* 32, 539–567s. doi:10.1146/annurev.earth.32.101802.120453

Chaves, L. C., Thompson, M. S., Loeffler, M. J., Dukes, C. A., Szabo, P. S., and Horgan, B. H. N. (2023). Evaluating the effects of space weathering on magnetite on airless planetary bodies. *Icarus* 402, 115634. article id. 115634. doi:10.1016/j.icarus.2023.115634

Chesser, I., Derlet, P. M., Mishra, A., Paguaga, S., Mathew, N., Dang, K., et al. (2024). Structure and migration of heavily irradiated grain boundaries and dislocations in Ni in the athermal limit. *Phys. Rev. Mater.* 8, 093606. doi:10.1103/physrevmaterials.8.093606

Clark, B. E., Hapke, B., Pieters, C., and Britt, D. (2002). "Asteroid space weathering and regolith evolution," in *Asteroids III*. Editors W. Bottke, A. Cellino, P. Paolicchi, and R. P. Binzel (Tucson, Arizona: University of Arizona Press).

Clark, B. E., Sen, A., Zou, X.-D., DellaGiustina, D. N., Sugita, S., Sakatani, N., et al. (2023). Overview of the search for signs of space weathering on the low-albedo asteroid (101955) Bennu. *Icarus* 400, 115563. doi:10.1016/j.icarus.2023.115563

Daly, R. T., Ernst, C. M., Barnouin, O. S., Chabot, N. L., Rivkin, A. S., Cheng, A. F., et al. (2023). Successful kinetic impact into an asteroid for planetary defence. *Nature* 616, 443–447. doi:10.1038/s41586-023-05810-5

De, H., and René, A. (2023). Meteor impact hazard. Biological and environmental hazards, risks, and disasters, in *Hazards and disasters series*. Second Edition. Elsevier, 499–524.

Demyk, K., d'Hendecourt, L., Leroux, H., Jones, A. P., and Borg, J. (2004). IR spectroscopic study of olivine, enstatite and diopside irradiated with low energy H and He ions. *Astronomy and Astrophysics* 420 (1), 233–243.

Dukes, C. A., Fulvio, D., and Baragiola, R. A. (2015). in *Space weathering of airless bodies: an integration of remote sensing data, laboratory experiments and sample analysis workshop*. Editor C. V. 1878 LPI, 2063.

Ferrari, F., and Alessi, E. M. (2023). A new method for identifying dynamical transitions in rubble pile asteroid scenarios. *Astronomy and Astrophysics* 672 (id.A35), A35. doi:10.1051/0004-6361/202244540

Gyollai, I., Biri, S., Juhász, Z., Király, Cs., Rácz, R., Rezes, D., et al. (2024). Raman–Infrared spectral correlation of an artificially space-weathered carbonaceous chondrite meteorite. *Minerals* 14 (3), 288. doi:10.3390/min14030288

Hapke, B. (2001). Space weathering from Mercury to the asteroid belt. *J. Geophys Res. Planet* 106 (E5), 10039–10073. doi:10.1029/2000je001338

Hapke, B., Cassidy, W., and Wells, E. (1975). Effects of vapor-phase deposition processes on the optical, chemical, and magnetic properties OE the lunar regolith. *Moon* 13, 339–353. doi:10.1007/bf00567525

Harries, D., and Langenhorst, F. (2014). The mineralogy and space weathering of a regolith grain from 25143 Itokawa and the possibility of annealed solar wind damage. *Earth, Planets Space* 66, 163. article id.163, 11. doi:10.1186/s40623-014-0163-1

Hasegawa, S., DeMeo, F. E., Marsset, M., Hanuš, J., Avdellidou, C., Delbo, M., et al. (2022). Spectral evolution of dark asteroid surfaces induced by space weathering over a decade. *Astrophysical J. Lett.* 939 (id.L9), L9–L12. doi:10.3847/2041-8213/ac92e4

Hirabayashi, M. (2023). Dynamics of a deforming planetary body. *Icarus* 389, 115258. doi:10.1016/j.icarus.2022.115258

Hiroi, T., Abe, M., Kitazato, K., Abe, S., Clark, B. E., Sasaki, S., et al. (2006). Developing space weathering on the asteroid 25143 Itokawa. *Nature* 443, 56–58. doi:10.1038/nature05073

Hiroi, T., Milliken, R. E., Robertson, K. M., Schultz, C. D., Amano, K., Nakamura, T., et al. (2023). Evidence of global space weathering by solar wind on asteroid 162173 Ryugu. *Icarus* 406, 115755. doi:10.1016/j.icarus.2023.115755

Holsapple, K. A. (2009). The deformation of asteroids from YORP spin-up, in *40th lunar and planetary science conference #2053*.

Jacobson, S. A., and Scheeres, D. J. (2010). The evolution of binary asteroids formed by spin fission.

Johnson, J. R., Hörz, F., and Staid, M. I. (2003). Thermal infrared spectroscopy and modeling of experimentally shocked plagioclase feldspars. *Am. Mineralogist* 88 (10), 1575–1582. doi:10.2138/am-2003-1020

Johnson, J. R., Staid, M. I., and Kraft, M. D. (2007). Thermal infrared spectroscopy and modeling of experimentally shocked basalts. *Am. Mineralogist* 92 (7), 1148–1157. doi:10.2138/am.2007.2356

Kanamaru, M., Sasaki, S., Morota, T., Cho, Y., Tatsumi, E., Hirabayashi, M., et al. (2021). YORP effect on asteroid 162173 Ryugu and its spin evolution. 52nd LPSC, in *Contrib*.

Kanuchova, Z., Baratta, G., Garozzo, M., and Strazzulla, G. (2010). Space weathering of asteroidal surfaces. *Astronomy Astrophysics* 517 (11), A60. doi:10.1051/0004-6361/201014061

Kaňuchová, Z., Boduch, P., Domaracka, A., Palumbo, M. E., Rothard, H., and Strazzulla, G. (2017). Thermal and energetic processing of astrophysical ice analogues rich in SO2. *A&* 604, A68. doi:10.1051/0004-6361/201730711

Kanuchova, Z., Brunetto, R., Fulvio, D., and Strazzulla, G. (2015). Near-ultraviolet bluing after space weathering of silicates and meteorites. *Icarus* 258, 289–296. doi:10.1016/j.icarus.2015.06.030

Kareta, T., Thomas, C., Li, J. Y., Knight, M. M., Moskovitz, N., Rożek, A., et al. (2023). Ejecta evolution following a planned impact into an asteroid: the first five weeks. *Astrophysical J. Lett.* 959 (1), 12. doi:10.3847/2041-8213/ad0fdd

Kereszturi, A. (2014). Surface processes in microgravity for landing and sampling site selection of asteroid missions – suggestions for MarcoPolo-R. *Planet. Space Sci.* 101, 65–76. doi:10.1016/j.pss.2014.06.005

Kereszturi, A. (2023). Meteorite irradiation to test cosmic weathering consequences on asteroid surfaces, in *Planetary research and the search for life beyond the Earth*. Ukraine: Kyiv.

Kobayashi, C., Karakas, A. I., and Lugaro, M. (2020). The origin of elements from carbon to uranium. *Astrophysical Journal* 900, 179.

Kobayashi, M., Miyamoto, H., Pál, B. D., Niihara, T., and Takemura, T. (2023). Laboratory measurements show temperature-dependent permittivity of lunar regolith simulants. *Earth Planets Space* 75 (1), 8. Paper: 8. doi:10.1186/s40623-022-01757-5

Lafuente, B., Downs, R. T., Yang, H., and Stone, N. (2016). in *The power of databases: the RRUFF project*. Editors T. Armbruster, and R. M. Danisi (Berlin, München, Boston: De Gruyter O), 1.

Lantz, C., Brunetto, R., Barucci, M. A., Dartois, E., Duprat, J., Engrand, C., et al. (2015). Ion irradiation of the Murchison meteorite: visible to mid-infrared spectroscopic results. *Astronomy and Astrophysics* 577, A41. doi:10.1051/0004-6361/201425398

Lantz, C., Brunetto, R., Barucci, M. A., Fornasier, S., Baklouti, D., Bourçois, J., et al. (2017). Ion irradiation of carbonaceous chondrites: a new view of space weathering on primitive asteroids. *Icarus* 285, 43–57. doi:10.1016/j.icarus.2016.12.019

Lauretta, D. S., Connolly, H. C., Jr, Aebersold, J. E., Alexander, C. M. O., Ballouz, R., Barnes, J. J., et al. (2024). Asteroid (101955) Bennu in the laboratory: properties of the sample collected by OSIRIS-Rex. *Meteorit. Planet. Sci.* 59, 2453–2486. doi:10.1111/maps.14227

Leggett, A. J. (1991). Amorphous materials at low temperatures: why are they so similar? *Phys. B* 169 (1–4), 322–327. doi:10.1016/0921-4526(91)90246-b

Li, J. Y., Hirabayashi, M., Farnham, T. L., Sunshine, J. M., Knight, M. M., Tancredi, G., et al. (2023). Ejecta from the DART-produced active asteroid Dimorphos. *Nature* 616, 452–456. doi:10.1038/s41586-023-05811-4

Lilienfeld, D. A., Hung, L. S., and Mayer, J. W. (1987). Ion induced metastable phases. *Nucl. Instrum. Methods Phys. Res. Sect. B Beam Interact. Mater. Atoms* 19–20, 1–7. doi:10.1016/s0168-583x(87)80004-6

Lindsley, D. H., Papike, J. J., and Bence, A. E. (1972). Pyroxferroite: breakdown at low pressure and high temperature: chemical trends due to crystal-liquid interaction. *Proc. Lunar Sci. Conf.* 3, 431.

Lubin, P., and Cohen, A. N. (2023). Asteroid interception and disruption for terminal planetary defense. *Adv. Space Res.* 71, 1827–1839. doi:10.1016/j.asr.2022.10.018

Madiedo, J. M., Trigo-Rodríguez, J. M., Zamorano, J., Izquierdo, J., Sánchez, de M. A., Ocaña, F., et al. (2014). Orbits and emission spectra from the 2014 Camelopardalids. *MNRAS* 445 (3), 3309–3314. doi:10.1093/mnras/stu1990

Michel, P., Küppers, M., Martino, P., and Carnelli, I. (2024). The ESA hera mission to the binary asteroid (65803) Didymos: ready for launch in october

Milliken, K. L. (2014). "Sediments, diagenesis and sedimentary rocks," in *Treatise on geochemistry second edition*.

Moyano-Cambero, C. E., Pellicer, E., Trigo-Rodríguez, J. M., Williams, I. P., Blum, J., Michel, P., et al. (2017). Nanoindenting the Chelyabinsk meteorite to learn about impact deflection effects in asteroids. *Astrophysical J.* 835 (2), 157. doi:10.3847/1538-4357/835/2/157

Moyano-Cambero, C. E., Trigo-Rodríguez, J. M., Llorca, J., Fornasier, S., Barucci, M. A., and Rimola, A. (2016). A plausible link between the asteroid 21 Lutetia and CH carbonaceous chondrites. *Meteorit. Planet. Sci.* 51 (10), 1795–1812.

Noble, S. K., Pieters, C. M., and Keller, L. P. (2007). An experimental approach to understanding the optical effects of space weathering. *Icarus* 192 (2), 629–642. doi:10.1016/j.icarus.2007.07.021

Noguchi, T., Kimura, M., Hashimoto, T., Konno, M., Nakamura, T., Zolensky, M. E., et al. (2014). Space weathered rims found on the surfaces of the Itokawa dust particles. *Meteorit. Planet Sci.* 49 (2), 188–214. doi:10.1111/maps.12111

Noguchi, T., Nakamura, T., Kimura, M., Zolensky, M. E., Tanaka, M., Hashimoto, T., et al. (2011). Incipient space weathering observed on the surface of Itokawa dust particles. *Science* 333 (6046), 1121–1125. doi:10.1126/science.1207794

Ott, T., Drolshagen, E., Koschny, D., Drolshagen, G., Pilger, C., Gaebler, P., et al. (2021). Infrasound signals of fireballs detected by the geostationary lightning mapper. *Astronomy and Astrophysics* 654 (id.A98), A98. doi:10.1051/0004-6361/202141106

Palomba, E., Angrisani, M., Rubino, S., Dirri, F., Longobardo, A., Pratesi, G., et al. (2024). Investigating space weathering on Ryugu by laboratory comparative analysis. *55th LPSC*, 2593.

Peña-Asensio, E., Trigo-Rodríguez, J. M., and Rimola, A. (2022). Orbital characterization of superbolides observed from space: dynamical association with near-earth objects, meteoroid streams, and identification of hyperbolic meteoroids. *Astronomical J.* 164, 76. doi:10.3847/1538-3881/ac75d2

Raducan, S. D., Davison, T. M., Luther, R., and Collins, G. S. (2019). The role of asteroid strength, porosity and internal friction in impact momentum transfer. *Icarus* 329, 282–295. doi:10.1016/j.icarus.2019.03.040

Railsback, L. B. (2006). Some fundamentals of mineralogy and geochemistry, in *Department of geology*. Athens, USA: University of Georgia.

Regály, Zs., Fröhlich, V., and Berczik, P. (2023). Mitigating potentially hazardous asteroid impacts revisited. *Astronomy and Astrophysics* 677 (6), L6. doi:10.1051/0004-6361/202347205

Sanchez, P., and Scheeres, D. J. (2018). The role of angular momentum on accreting rubble pile shapes.

Sharp, T. G., and de Carli, P. S. (2006). in *Meteorites and the early solar system II*. Editors D. S. Lauretta, and H. Y. McSween (Tucson: University of Arizona Press), 653.

Shehaj, X., Caporali, S., Palomba, E., and Pratesi, G. (2024). Textural study of vesicles in Tagish Lake (C2-ung) meteorite fusion crust: constraints on vesicle formation during their entry into the Earth's atmosphere. *Minerals* 14, 99. doi:10.3390/min14010099

Storz, J., Reitze, M. P., Stojic, A. N., Kerraouch, I., Bischoff, A., Hiesinger, H., et al. (2024). Micro-FTIR reflectance spectroscopy of Ryugu, CI chondrites and volatile-rich clasts – comparing spectral features in the Mid-IR (2.5–16.5 μm) region. *Icarus* 420, 116189. doi:10.1016/j.icarus.2024.116189

Sunho, J., and Masateru, I. (2022). Estimation of the space weathering timescale on (25143) Itokawa: implications on its rejuvenation process. *Astronomy and Astrophysics* 667, A93. doi:10.1051/0004-6361/202244326

Takano, A., Sakatani, N., Miyamoto, H., Usui, T., Niihara, T., Pál, B., et al. (2020). *Experimental study on thermal properties of high porosity particles for understanding physical properties of Phobos surface*. JpGU-AGU Joint Meeting. Paper: PPS08-P01.

Tanbakouei, S., Trigo-Rodríguez, J. M., Sort, J., Michel, P., Blum, J., Nakamura, T., et al. (2019). Mechanical properties of particles from the surface of asteroid 25143 Itokawa. *A&* 629, A119. doi:10.1051/0004-6361/201935380

Thomas, C. A., Naidu, S. P., Scheirich, P., Moskovitz, N. A., Pravec, P., Chesley, S. R., et al. (2023). Orbital period change of Dimorphos due to the DART kinetic impact. *Nature* 616, 448–451. doi:10.1038/s41586-023-05805-2

Thompson, M. S., Loeffler, M. J., Morris, R. V., Keller, L. P., and Christoffersen, R. (2019). Spectral and chemical effects of simulated space weathering of the Murchison CM2 carbonaceous chondrite. *Icarus* 319, 499–511. doi:10.1016/j.icarus.2018.09.022

Thorpe, M. F., and Tichy, L. (2001). *Properties and applications of amorphous materials*. 1st ed. Dordrecht: Springer.

Trigo-Rodríguez, J. M., García-Hernández, D. A., Lugaro, M., Karakas, A. I., van Raai, M., García, L. P., et al. (2009). The role of massive AGB stars in the early solar system composition. *Meteorit. Planet. Sci.* 44, 627–639. doi:10.1111/j.1945-5100.2009.tb00758.x

Trigo-Rodríguez, J. M., Llorca, J., Madiedo José, M., and Pinilla-Alonso, N. (2011). Precise reflectance spectra of ordinary chondrites in the visible and UV: exploring the variability of S-class asteroidal spectra. *42nd Lunar Planet. Sci. Conf. #1795*.

Trigo-Rodríguez, J. M., Moyano-Cambero, C. E., Llorca, J., Fornasier, J., Barucci, M. A., Belskaya, I., et al. (2014). UV to far-IR reflectance spectra of carbonaceous chondrites – I. Implications for remote characterization of dark primitive asteroids targeted by sample-return missions. *MNRAS* 437 (1), 227–240. doi:10.1093/mnras/stt1873

Trigo-Rodríguez, J. M., Rimola, A., Tanbakouei, S., Soto, V. C., and Lee, M. (2019). Accretion of water in carbonaceous chondrites: current evidence and implications for the delivery of water to early Earth. *Space Sci. Rev.* 215, 18. doi:10.1007/s11214-019-0583-0

Walsh, K. J., Ballouz, R. L., Durda, D. D., Richardson, D. C., Michel, P., and Jutzi, M. (2017). Preserving shape and spin in asteroid reaccumulation simulations with SSDEM. *Lunar Planet. Sci.* XLVIII (#2810).

Weinbruchi, S., Palme, H., and Spettel, B. (2000). Refractory forsterite in primitive meteorites: condensates from the solar nebula? *Meteorit. Planet. Sci.* 35, 161–171. doi:10.1111/j.1945-5100.2000.tb01983.x

Yang, Y., Zhang, H., Wang, Z., Yuan, Ye, Li, S., Hsu, W., et al. (2017). Optical spectroscopic characterizations of laser irradiated olivine grains. *Astronomy and Astrophysics* 597 (id.A50), A50–A13. doi:10.1051/0004-6361/201629327

Yesiltas, M., Glotch, T. D., Kebukawa, Y., Sava, B., Durmaz, Y. C., and Northrup, P. (2024). Nanoscale spectroscopic identification and characterization of minerals and organic matter in Ryugu particles. *J. Gephysical Res.* 129 (4), e2023JE008090. doi:10.1029/2023je008090

Zaccone, A. (2023). Theory of disordered solids, in *Lecture notes in physics*. 1015 1st ed. Springer. doi:10.1007/978-3-031-24706-4

Zhang, P., Tai, K., Li, Y., Zhang, J., Lantz, C., Hiroi, T., et al. (2022). *Diverse space weathering effects on asteroid surfaces as inferred via laser irradiation of meteorites A&A*, 659, A78.

Frontiers in
Astronomy and Space Sciences

Explores planetary science and extragalactic astronomy in all wavelengths

Advances the understanding of our universe - from planetary science to extragalactic astronomy, to high-energy and astroparticle physics.

Discover the latest Research Topics

See more →

Frontiers

Avenue du Tribunal-Fédéral 34
1005 Lausanne, Switzerland
frontiersin.org

Contact us

+41 (0)21 510 17 00
frontiersin.org/about/contact